



Production d'hydrogène issu de gazéification de biomasse : modélisation, analyse technico-économique et environnementale de solutions innovantes

Rémi Demol

► To cite this version:

Rémi Demol. Production d'hydrogène issu de gazéification de biomasse: modélisation, analyse technico-économique et environnementale de solutions innovantes. Génie des procédés. Université de Lorraine, 2021. Français. NNT: 2021LORR0322 . tel-03718121

HAL Id: tel-03718121

<https://hal.univ-lorraine.fr/tel-03718121v1>

Submitted on 8 Jul 2022

HAL is a multi-disciplinary open access archive for the deposit and dissemination of scientific research documents, whether they are published or not. The documents may come from teaching and research institutions in France or abroad, or from public or private research centers.

L'archive ouverte pluridisciplinaire **HAL**, est destinée au dépôt et à la diffusion de documents scientifiques de niveau recherche, publiés ou non, émanant des établissements d'enseignement et de recherche français ou étrangers, des laboratoires publics ou privés.



AVERTISSEMENT

Ce document est le fruit d'un long travail approuvé par le jury de soutenance et mis à disposition de l'ensemble de la communauté universitaire élargie.

Il est soumis à la propriété intellectuelle de l'auteur. Ceci implique une obligation de citation et de référencement lors de l'utilisation de ce document.

D'autre part, toute contrefaçon, plagiat, reproduction illicite encourt une poursuite pénale.

Contact : ddoc-theses-contact@univ-lorraine.fr

LIENS

Code de la Propriété Intellectuelle. articles L 122. 4

Code de la Propriété Intellectuelle. articles L 335.2- L 335.10

http://www.cfcopies.com/V2/leg/leg_droi.php

<http://www.culture.gouv.fr/culture/infos-pratiques/droits/protection.htm>



UNIVERSITÉ
DE LORRAINE



THÈSE

Présentée à l'Université de Lorraine

École doctorale SIMPPÉ :

Science et Ingénierie des Molécules, des Produits, des Procédés et de l'Énergie

Laboratoire Réactions et Génie des Procédés (UMR 7274 CNRS)

pour l'obtention du grade de

Docteur de l'Université de Lorraine
Spécialité Génie des Procédés et des Produits

par

Rémi DEMOL

**Production d'hydrogène issu de gazéification de biomasse :
modélisation, analyse technico-économique
et environnementale de solutions innovantes**

Thèse soutenue publiquement le 13 décembre 2021 à Nancy devant le jury composé de :

Rapporteurs : - Dr. Claire COURSON – Université de Strasbourg

- Prof. Diane THOMAS – Université de Mons (Présidente de jury)

Examinateurs : - Prof. Guillain MAUVIEL – Université de Lorraine (Directeur de thèse)

- Prof. Yann ROGAUME – Université de Lorraine (Co-directeur de thèse)

Invités : - Prof. Éric FAVRE – Université de Lorraine

- Dr. Anthony DUFOUR – CNRS

*« Aujourd’hui, l’utopie a changé de camp :
est utopiste celui qui croit que tout peut continuer comme avant.
L’effondrement est l’horizon de notre génération, c’est le début de son avenir. »*

*Pablo Servigne et Raphaël Stevens
Comment tout peut s’effondrer – 2015*

REMERCIEMENTS

Je tenais tout d'abord à remercier sincèrement mes directeurs de thèse, Guillain Mauviel et Yann Rogaume pour m'avoir donné l'opportunité de travailler sur cette thématique, pour leur aide et leurs conseils. Merci également à Anthony Dufour pour nos échanges et sa contribution significative à ces recherches.

Je souhaite remercier les membres du jury qui ont accepté d'évaluer ces travaux ainsi que Sylvain Caurla et Fabrice Patisson, membres de mon comité de suivi de thèse.

Je témoigne aussi de ma gratitude envers les différents collègues avec qui j'ai pu travailler directement au cours de ce doctorat : Miguel Ruiz Bailon, Erika Bartolomei, Olivier Herbinet, Roda Bounaceur, Adam Schnitzer et Anthony Biget. J'ai eu l'opportunité d'encadrer des stagiaires, merci à Aurélien Mougel, Valentin Patillon et Khadija Chafi.

Merci à Linda Bosserr pour son aide administrative efficace et réactive tout au long de ce parcours.

Bien évidemment je voulais remercier l'ensemble de l'équipe GREENER qui m'a accueilli et avec qui j'ai pu passer d'agréables moments dans nos échanges scientifiques et lors d'autres moments de convivialité. Merci à Michel Mercy, Pierre-Alann Cablé, Matteo Pietraccini, Nabil Hassibi, Mohamed Heshmi Assaoui, Eya Ghomri, Maxime Hervy, Yann Le Brech, Gabriel Wild, Thomas Di Pietro, Felipe Buendia Kandia, Akram Dahdouh, Julien Colin.

Je veux aussi remercier les participants des programmes de recherche Lorraine Université d'Excellence UIHyS et Hy-C-GREEN.

Je n'oublie pas ma famille qui a su me soutenir notamment durant la dernière ligne droite de cette thèse. Merci tout particulièrement à toi, Jérôme.

RÉSUMÉ

La minimisation des impacts causés par le changement climatique impose de substituer des énergies fossiles par des énergies faiblement émettrices de CO₂. L'hydrogène est vu comme un vecteur permettant de décarboner une partie de l'industrie et des usages de transport et de mobilité. Pourtant, l'hydrogène est produit aujourd'hui quasi-exclusivement à partir d'énergies fossiles pour des usages industriels.

Ces travaux s'intéressent à la production d'hydrogène à partir d'une ressource renouvelable, les plaquettes de bois produits secondaires de l'industrie forestière. Compte tenu de la nature du combustible utilisé, des petites unités de valorisation sont envisagées (zone d'approvisionnement limitée, transport de la ressource à courte distance). Les procédés de pyrogazéification permettent la transformation de cette ressource en un gaz de synthèse (CO, H₂, CH₄, CO₂) sous l'effet d'un apport de chaleur (pyrolyse) ou d'un agent oxydant (gazéification) constitué d'oxygène et de vapeur d'eau.

Pour juger de la pertinence de ces procédés de pyrogazéification, ils sont étudiés et modélisés avec Aspen Plus. Une attention particulière est apportée à la chaîne de traitement du gaz de synthèse produit. Ce syngaz contient des goudrons qu'il convient de réduire pour l'utilisation ultime du gaz. Dans ce but, une unité d'oxydation partielle est envisagée et modélisée à partir de mécanismes de cinétique radicalaire. Le gaz épuré peut alors être enrichi en H₂ avec des réacteurs de Reformage Catalytique et de Water Gas Shift. La séparation de l'hydrogène produit est une autre étape cruciale et les technologies classiques ne sont pas toujours adaptées au gaz produit. Quand une seule technologie n'est pas à même de réaliser la séparation, un procédé hybride combinant des technologies membranaire et d'adsorption est adopté. La chaleur produite par le procédé est valorisée dans un réseau de chaleur.

Afin de juger de la pertinence de ces options, tant d'un point de vue financier que du développement durable, une analyse technico-économique est réalisée ainsi qu'une analyse de cycle de vie. Ces procédés offrent clairement une alternative vertueuse pour la production de différents vecteurs : hydrogène, chaleur, voire biochar. Mais dans les conditions actuelles de marché, ces filières ne sont pas en mesure d'atteindre l'équilibre financier sans un soutien public.

ABSTRACT

Minimizing the impacts caused by climate change imply the replacement of fossil fuels low greenhouse gas emitting energies. The hydrogen energy vector is forecasted to contribute to decarbonizing a part of industry and the uses of transport and mobility. Yet hydrogen is produced nowadays almost exclusively from fossil fuels and is dedicated to industrial applications.

This work focuses on the production of hydrogen from a renewable resource, wood chips a by-product of the forest industry. Due to the nature of the fuel considered, small plant units are chosen (a limited supply area, short-distance transport of the resource). Pyrogasification processes transform this combustible into a synthesis gas (CO , H_2 , CH_4 , CO_2) under the effect of heat input (pyrolysis) or an oxidizing agent (gasification) consisting of oxygen and water vapor.

To evaluate the relevance of these pyrogasification processes, they are studied and modeled with Aspen Plus®. Particular attention is put on the synthesis gas cleaning process. This syngas contains tars which should be reduced for the ultimate use of the gas. For this purpose, a partial oxidation unit is envisaged and modeled from a detailed radical kinetic mechanism. The purified gas can then be enriched in H_2 with Catalytic Reforming and Water Gas Shift reactors. The separation of the hydrogen produced is another crucial step and conventional technologies are not always suited to the gas produced. When a single technology cannot achieve the separation, a hybrid process combining membrane and adsorption technologies is adopted. The heat produced by the process is recovered in a heating network.

In order to evaluate the relevance of these options, both from a financial and sustainable development point of view, a techno-economic analysis is carried out as well as a life cycle analysis. These processes clearly offer a virtuous alternative for the production of different vectors: hydrogen, heat and even bio-char. But under current market conditions, these industries are unable to reach financial equilibrium without public support.

TABLE DES MATIÈRES

REMERCIEMENTS	III
RÉSUMÉ.....	V
ABSTRACT	VII
TABLE DES MATIÈRES	IX
LISTE DES TABLEAUX.....	XV
LISTE DES FIGURES.....	XVII
LISTE DES SIGLES ET ABRÉVIATIONS	XXI
LISTE DES ANNEXES	XXIII
INTRODUCTION.....	1
1. Contexte général.....	1
2. Objectif et démarche	5
3. Plan de la thèse.....	5
4. Liste des publications	6
5. Conférences	6
6. Références	7
CHAPITRE 1 REVUE DE LA LITTÉRATURE.....	9
1.1. La ressource forestière	9
1.1.1. Produits de l'exploitation forestière	9
1.1.2. Disponibilité dans le Monde et en Europe	10
1.1.3. Disponibilité en France	12
1.1.4. Disponibilité en Grand-Est.....	13
1.1.5. Coût des produits de bois énergie	14
1.1.6. Usages énergétiques	16
1.2. État des lieux et débouchés futurs de l'hydrogène	17
1.2.1. Production d'hydrogène	17
1.2.2. L'hydrogène pour l'industrie	19
1.2.3. L'hydrogène pour l'injection dans les réseaux de gaz naturel	22
1.2.4. L'hydrogène pour la mobilité.....	23
1.2.5. L'hydrogène en France.....	25

1.3.	Valorisation thermochimique de la biomasse	28
1.3.1.	Développement de la gazéification	30
1.3.2.	Les différents types de gazéification	31
1.3.3.	Verrous technologiques	35
1.3.4.	Traitements du syngaz	35
1.1.1.1	Particules	36
1.1.1.2	Goudrons	37
1.1.1.3	Soufre	38
1.1.1.4	Azote	38
1.1.1.5	Alcalins.....	38
1.1.1.6	Chlore	38
1.3.5.	Production d'hydrogène issu de gazéification	39
1.1.1.7	Choix de la technique de gazéification	39
1.1.1.8	Chaîne de traitement.....	39
1.1.1.9	Procédés de séparation d'hydrogène	40
1.4.	Modélisation du procédé de gazéification.....	42
1.4.1.	Utilisation de solides non-conventionnels.....	42
1.4.2.	Modélisation de la gazéification	42
1.4.3.	Chaîne de traitement du syngaz	43
1.4.4.	Production d'hydrogène	45
1.5.	Analyse technico-économique	48
1.5.1.	Méthodes d'évaluation du CAPEX	48
1.5.2.	Coût des équipements.....	48
1.5.3.	Valeur de l'argent dans le temps	49
1.5.4.	Évaluation de l'investissement en capital total	50
1.5.5.	Évaluation du coût de production.....	52
1.5.6.	Flux de trésorerie et critères économiques	52
1.5.7.	Analyses technico-économiques production d'hydrogène issu de biomasse	54
1.5.8.	Prix des produits secondaires	55
1.1.1.10	Prix chaleur industrielle	56
1.1.1.11	Prix électricité	56
1.6.	Analyse de cycle de vie	58
1.6.1.	Contexte	58

1.6.2.	Principe de l'ACV	59
1.6.3.	Les étapes de l'ACV	59
1.6.4.	ACV aux filières hydrogène.....	60
1.7.	Bilan de la revue bibliographique et approche proposée	64
1.8.	Bibliographie	65
CHAPITRE 2	OXYDATION PARTIELLE D'UN SYNGAZ DE GAZÉIFICATION DE BIOMASSE	75
2.1	Introduction	75
2.2	Article 1 (reproduction intégrale).....	75
2.2.1	Abstract	75
2.2.2	Keywords	76
2.2.3	Introduction	76
2.2.4	Material and methods	80
2.2.4.1	Feedstock, experimental rig and analytical methods	80
2.2.4.2	Modeling and numerical methods	83
2.2.5	Results and discussion.....	85
2.2.5.1	Partial oxidation cracking tests	85
2.2.5.2	Modeling results	89
2.2.6	Conclusion.....	94
2.2.7	Supporting informations.....	95
2.2.8	Fundings	95
2.2.9	References	95
2.2.10	Supplementary Material	100
2.2.10.1	Experimental results	100
2.2.10.2	Validation of SYNPOX on soot formation	101
2.2.10.3	Others results.....	104
CHAPITRE 3	SIMULATION DE PROCÉDÉ	107
3.1	Introduction	107
3.2	Article 2 (reproduction intégrale).....	107
3.2.1	TOC graphic	108
3.2.2	Abstract	108
3.2.3	Introduction	109
3.2.4	Model description.....	113

3.2.4.1	Scenarios investigated	113
3.2.4.2	Description of the processes and modeling.....	113
3.2.4.3	Definition of energetic efficiency	122
3.2.5	Results and discussion.....	123
3.2.5.1	Energy & Mass balance.....	123
3.2.5.2	Fate of hydrogen along the process unit.....	127
3.2.5.3	Tar and particles	130
3.2.5.4	H ₂ separation by a hybrid process: membrane coupled to PSA	131
3.2.5.5	Comparison of the various options and recommendations	132
3.2.6	Conclusion.....	133
3.2.7	Supporting informations.....	134
3.2.8	Fundings	134
3.2.9	References	134
3.2.10	Supporting Infomation	140
3.2.10.1	Detailed Flowsheet	140
3.2.10.2	Experiments used for oxy-steam gasification	146
3.2.10.3	Pyrolyser model.....	148
3.2.10.4	Partial oxidation model	152
3.2.10.5	Determination of the minimum equivalent ratio for partial oxidation	153
3.2.10.6	Kinetics used in the reformer model	155
3.2.10.7	Hydrogen separation	157
3.2.10.8	Reference.....	161
CHAPITRE 4 ANALYSE TECHNICO-ÉCONOMIQUE ET ANALYSE DE CYCLE DE VIE		
	165	
4.1	Introduction	165
4.2	Article 3 (reproduction intégrale).....	165
4.2.1	Abstract	165
4.2.2	Keywords	166
4.2.3	Introduction	166
4.2.4	Material and methods	171
4.2.4.1	Scenarios investigated	171
4.2.4.2	Techno-Economic Model	172
4.2.4.3	Life Cycle Assessment	176

4.2.5 Results and discussion.....	177
4.2.5.1 Techno-Economic Assessment	177
4.2.5.2 Life Cycle Assessment	180
4.2.5.3 Cost of action	182
4.2.5.4 Sensitivity Analysis.....	184
4.2.6 Conclusion.....	186
4.2.7 Fundings	186
4.2.8 References	187
4.2.9 Supplementary material.....	191
4.2.9.1 Transport cost.....	191
4.2.9.2 Equipment cost.....	192
4.2.9.3 Detailed results CAPEX/OPEX	195
4.2.9.4 Life cycle inventories	200
4.2.9.5 LCA results	204
CHAPITRE 5 CONCLUSION ET PERSPECTIVES	207
5.1 Conclusions des travaux menés.....	207
5.2 Perspectives	208
ANNEXES	211

LISTE DES TABLEAUX

Tableau 1-1 : Industries utilisant de l'hydrogène (d'après [27–31]).....	21
Tableau 1-2 : Compositions typiques du syngaz de gazéification.....	34
Tableau 1-3 : Qualité syngaz [55,61,62].....	36
Tableau 1-4 : Limites d'émissions à l'environnement en France pour les unités inférieures à 50 MW [64].....	36
Tableau 1-5 : Facteur de Lang [102].....	52
Tableau 1-6 : Sélection de précédentes analyses technico-économique de procédés de production d'hydrogène issu de gazéification de biomasse.....	54
Tableau 1-7 : Evolution du prix moyen de l'électricité en France 2011-2019 selon les secteurs (reproduit de [121]).....	57
Tableau 1-8 : Liste non-exhaustive d'ACV (“berceau à la porte”) de production d'hydrogène issu de gazéification de biomasse [129].....	62
Table 2-1: Thermal cracking and POX studies.....	78
Table 2-2: Parameters of the partial oxidation unit.....	83
Table 2-3: Kinetic parameters.....	84
Table 2-4: Boundary conditions of the CHEMKIN PRO plug flow model.....	85
Table 2-5: Main operation conditions, gasification indicators and products yields in reference and partial oxidation experiments.....	86
Table 2-6: Gas residence time and soot production	91
Table 3-1: Wet scrubber efficiency.....	118
Table 3-2: Assumptions of the Aspen Plus model, utilities and material consumption.....	121
Table 3-3: Utilities consumption.....	125
Table 4-1: Non-exhaustive list of techno-economic analysis of biomass gasification in literature.....	168
Table 4-2: Non-exhaustive list of LCA on H ₂ production (cradle-to-gate) from biomass gasification in literature [16].....	170
Table 4-3: Cost of labor	173
Table 4-4: Prices of products and costs of feedstock and utilities	174
Table 4-5: Financial options.....	175
Table 4-6: Global warming potential attribution to each product.....	182

Table S2-1: Detailed results [g/kg feed (daf)].....	100
Table S3-1: Composition of the feedstock (from ²)	146
Table S3-2: Syngas composition (from ²)	146
Table S3-3: Tar composition (from ²)	147
Table S3-4: Reactions in reformer ^{12,13}	155
Table S3-5: Kinetic parameters for reformer with nickel catalyst	156
Table S3-6: Data used for specific hydrogen separation cost estimation.	159
Table S4-1: Equipment cost data.	192
Table S4-2: Detailed costs of case 1-100 MW.....	196
Table S4-3: Detailed costs of case 1-20 MW.....	197
Table S4-4: Detailed costs of case 2-20 MW.....	198
Table S4-5: Detailed costs of case 3-20 MW.....	199
Table S4-6: Life cycle inventory of thermos-chemical (TC) processes, from Demol et al. 2021.	202
Table S4-7: Life cycle inventory of steam methane reforming (SMR), from [23].....	203
Table S4-8: Detailed impacts results for case 1-20.....	204
Table S4-9: Detailed impacts results for the comparison of all cases.....	205

LISTE DES FIGURES

Figure 0-1 : Consommation d'énergie primaire dans le monde par source d'énergie et population mondiale (1800-1965 [3], 1965-2020 [4], population [5]).....	2
Figure 0-2 : Évolution historique de la température globale et sa cause [4]	3
Figure 0-3 : Évolution de la température moyenne globale de surface selon les scénarios du GIEC [4].	3
Figure 0-4: Consommation d'énergies primaires par type d'énergie en France en 2020 et production primaire d'énergies renouvelables par filière [7].	4
Figure 1-1 : Volumes aériens comptabilisés dans l'arbre par l'IGN (adapté de [1]).	9
Figure 1-2 : Aires des forêts européennes et répartition par pays en 2020 [3].....	11
Figure 1-3 : Variation annuelle de l'augmentation de la ressource par région sur la période 1990-2020 [3].	11
Figure 1-4 : Dispo BIBE BO toutes espèces et dispo supplémentaire en Grand-Est d'après [1,14].	13
Figure 1-5 : Disponibilité BIBE toutes espèces en Grand-Est (maille 20 km) selon le scénario tendanciel et la période 2015-2017 [1,14].....	14
Figure 1-6 : Prix de la différents produits transformés de bois propre 2011-2021 (prix moyens en France hors taxes, au départ du site de préparation) [15].....	15
Figure 1-7 : Relation poids total livré et taux humidité pour un camion à fond mouvant de 27 t, d'après l'ONF et Dufeu [16].	16
Figure 1-8 : Énergies spécifiques de différent combustibles [19].....	17
Figure 1-9 : Classification des procédés de production d'hydrogène d'après le département de l'énergie américain [22].	18
Figure 1-10 : Production et consommation de l'hydrogène dans le Monde en 2018 [23].....	20
Figure 1-11 : Calcul du prix de l'hydrogène pour une application mobilité [34].	24
Figure 1-12 : Exemples de véhicules hydrogène [35].....	24
Figure 1-13 : Demande d'hydrogène en France en 2019 et marché adressable [24]	27
Figure 1-14 : Voies de valorisation de la biomasse [39].....	29
Figure 1-15: Gazogène Imbert (Déglyse X.).....	30
Figure 1-16 : Technologies de gazéification [42,45–48].	33
Figure 1-17 : Capacités des différentes technologies de gazéificateurs [56,57].....	34
Figure 1-18 : Procédé d'adsorption module en pression (PSA).....	41
Figure 1-19 : Séparation membranaire [71].	41

Figure 1-20 : Modèle de lit fluidisé de Bates et al. [77].....	43
Figure 1-21 : Chaîne de traitement syngaz d'après Spath et al. [70].	45
Figure 1-22 : Modèle <i>short-cut</i> de PSA [100].....	46
Figure 1-23 : Modèles d'écoulement disponibles dans le module MEMSIC [101].....	47
Figure 1-24 : <i>Chemical Engineering Plant Cost Index</i> (CEPCI) [105].	51
Figure 1-25 : Indices <i>Marshall and Swift</i> (l'indice 100 correspond à l'année 1926).....	51
Figure 1-26 : Flux de trésorerie cumulé [102].	53
Figure 1-27 : Evolution du prix de la chaleur commercialisée en France 2011-2019 (reproduit de [121]).	56
Figure 1-28 : Evolution du prix moyen journalier sur le marché de l'électricité (SPOT) dans différents pays européens.....	57
Figure 1-29 : Modèle World3 [122].....	58
Figure 1-30 : Choix d'allocation selon l'étape pour différents systèmes de production d'hydrogène [129].	61
Figure 1-31 : Choix d'indicateurs ACV et méthodes considérées (i1 GWP, i2 : AP, i3 : CED, i4 : EP, i5 : ODL, i6 : POPH, i7 : consommation d'énergie (fossile), i8 : consommation d'énergie (non-renouvelable), i9 : AD, i10 : HT, i11 : LOP, i12 HH (dommages) [129]	62
Figure 2-1: Schema of the POX unit.....	81
Figure 2-2: Synchronous Fluorescence spectra (offset = 20 nm).....	88
Figure 2-3: Temperature profiles obtained with an overall heat transfer coefficient of 20 W/m ² /K.	90
Figure 2-4: Experimental and modelled syngas composition at the inlet and outlet of the POX unit for case 0.05-1025. Simulated composition from plug flow.....	92
Figure 2-5: Experimental and modelled syngas composition at the inlet and outlet of the POX unit for case 0.10-1100. Simulated composition from plug flow.....	93
Figure 2-6: Comparison of Tanoh's experiment and SYNPOX model (cases 1 to 4).	102
Figure 2-7: Comparison of Tanoh's experiment and SYNPOX model (cases 5 to 8).	103
Figure 2-8: Experimental and modelled syngas composition at the inlet and outlet of the POX unit for case 0.10-1034. Simulated composition from plug flow.....	105
Figure 2-9: Experimental and modelled syngas composition at the inlet and outlet of the POX unit for case 0.10-1050. Simulated composition from plug flow.....	106
Figure 3-1: Simplified process flow diagram and the various modeling approach for each units.	113
Figure 3-2: Detailed flow diagram of case 1.....	119
Figure 3-3: Sankey's type diagrams (in MW) of the 3 cases.	126

Figure 3-4: Hydrogen molar flow rate and fraction along the process. G=Gasifier, P=Pyrolyzer, POX=Partial Oxidation, R=Reformer, WGS=Water Gas Shift, M=Membrane, PSA=Pressure Swing Adsorption.....	127
Figure 3-5: Fate of atomic hydrogen along the process for each scenario (kg _H /h).....	129
Figure 3-6: Concentration of tars and tar dew point along the process. G=Gasifier, P=Pyrolyzer, POX=Partial Oxidation, R=Reformer, WS=Water Scrubber. Tars and benzene in blue, tars without benzene in green.....	130
Figure 3-7: Impact of ER on POX temperature and reduction of tars (for cases 1 and 2).....	131
Figure 3-8: Specific hydrogen separation cost for case 2 as a function of membrane area, permeate and retentate pressures.....	132
Figure 4-1: Scenarios investigated, from [8].....	172
Figure 4-2: Life cycle assessment system.....	177
Figure 4-3: Fixed capital investment of the different scenarios.....	178
Figure 4-4: Operational expenditure of the different scenarios.....	179
Figure 4-5: Minimum selling price of hydrogen for each case, black zone: range of hydrogen production cost in large-scale SMR, green zone: range of green hydrogen production cost from electrolysis [47]	180
Figure 4-6: Relative impact comparison between the different scenarios and steam methane reforming (SMR) with CML-IA baseline V3.05 method. In TC3-20, biochar is sold as a product, in TC3-20S biochar is sequestered.....	181
Figure 4-7: Case 1-20MW relative contributions of inputs & wastes for each impact.....	182
Figure 4-8: Cost of action, amount of subsidies per ton of CO ₂ avoided. In case 3-20, biochar is sold at the market price (50 €/kg) and not sequestered. In case 3-20S, biochar is sequestered and not sold.....	183
Figure 4-9: Sensitivity analysis on case 1-20 (+-50%, market price heat 30€/MWh, H ₂ 2€/kg).....	185
Figure 4-10: Sensitivity analysis on case 3-20 (+-50%, market price heat 30€/MWh, H ₂ 2€/kg).....	185
Figure S2-1: Comparison of Tanoh's experiment and SYNPOX model (cases 1 to 4).	102
Figure S2-2: Comparison of Tanoh's experiment and SYNPOX model (cases 5 to 8).....	103
Figure S2-3 : Experimental and modelled syngas composition at the inlet and outlet of the POX unit for case 0.10-1034. Simulated composition from plug flow.....	105
Figure S2-4 : Experimental and modelled syngas composition at the inlet and outlet of the POX unit for case 0.10-1050. Simulated composition from plug flow.....	106
Figure S3-1: Process flow diagram of case 1.....	142
Figure S3-2: Process flow diagram of case 2.....	143
Figure S3-3: Process flow diagram of case 3	144

Figure S3-4: Mass balance of the 3 cases in t/h: a) case 1; b) case 2; c) case 3.....	145
Figure S3-5: Principle of the model.	149
Figure S3-6: Results of the model.....	149
Figure S3-7: Products yields.	150
Figure S3-8: Carbon balance.	150
Figure S3-9: Non-condensable gases yields.....	151
Figure S3-10: Impact of oxygen (equivalence ratio) on the partial oxidation unit on the syngas temperature and composition (cases 1 & 2).	154
Figure S3-11: Architecture of H ₂ separation optimization problem.	157
Figure S3-12: Specific hydrogen separation cost for case 2.	160
Figure S3-13: Specific hydrogen separation cost for case 3.	160
Figure S4-1: Relation between biomass humidity and weight delivered in 27 t-moving floor truck [36].	191
Figure S4-2: Network of fossil carbon dioxide produced from wood chips production (from Ecoinvent).	201

LISTE DES SIGLES ET ABRÉVIATIONS

ACV	Analyse de cycle de vie (LCA)
AGR	<i>Acid gas removal</i>
AP	<i>Acidification potential</i>
ASU	<i>Air separation unit</i>
BIBE	Bois industrie bois énergie
BO	Bois d'œuvre
BTX	Benzène toluène xylène
CED	<i>Cumulative energy demand</i>
CEPCI	<i>Chemical engineering plant cost index</i>
COM	Cost of manufacturing
DAF	<i>Dissolved air flottation</i>
DC	<i>Direct costs</i>
DFB	<i>Dual fluidized bed</i>
d_k	Dépréciation à l'année k
EF	<i>Entrained flow</i>
EP	<i>Eutrophication potential</i>
FB	<i>Fluidized bed</i>
FCI	<i>Fixed capital investment</i>
GIEC	Groupe intergouvernemental pour l'étude sur le climat (IPCC)
GWP	<i>Global warming potential</i>
HAP	Hydrocarbures aromatiques polycycliques (PAH)
HT	Hors taxes

IC	<i>Indirect costs</i>
ICV	Inventaire de cycle de vie (LCI)
MB	Menu bois
NPV	<i>Net present value</i>
ODP	<i>Ozone layer depletion</i>
PCI	Pouvoir calorifique inférieur (LHV)
PCS	Pouvoir calorifique supérieur (HHV)
PEC	<i>Purchased equipment cost</i>
POX	<i>Partial oxidation</i>
PSA	<i>Pressure swing adsorption</i>
<i>R</i>	Revenus
SMR	<i>Steam methane reforming</i>
<i>t</i>	Taux d'imposition
TCI	<i>Total capital investment</i>
TTC	Toutes taxes comprises
TSA	<i>Temperature swing adsorption</i>
WC	<i>Working capital</i>
WGS	<i>Water gas-shift</i>

LISTE DES ANNEXES

Annexe A – Résultats détaillés de la simulation de procédé.....	211
Annexe B – Modélisation PSA	225

INTRODUCTION

1. Contexte général

L'énergie va de pair avec le développement de l'Humanité. Elle couvre ses besoins de chauffage, de force motrice (mobilité et machines) et ses besoins de production ou de mise en forme de matériaux (bois, plastiques, molécules...).

La Figure 0-1 présente l'évolution en série longue de la consommation d'énergie primaire par source et l'évolution de la population mondiale de 1800 à 2020. La consommation de biomasse traditionnelle (bois, déchets agriculture, *charcoal*) utilisée essentiellement pour des besoins de chauffage est restée globalement constante depuis le XIXe siècle. L'exploitation du charbon fossile a permis l'essor de la révolution industrielle qui fut rendue possible par la disponibilité de cette nouvelle énergie. Au même moment, dans les années 1850, la découverte du pétrole amène une nouvelle source d'énergie qui connaîtra un fort développement à partir des années 1950 [1]. Le gaz naturel est également exploité à partir de ce moment-là. Un peu plus tard, les filières nucléaire et hydroélectrique se sont développées. Plus récemment, les énergies renouvelables modernes (solaire, éolien) plutôt destinées à la production électrique ont émergé. Il est important de noter que la « transition » d'une source d'énergie à une autre n'annule en rien la consommation de la source d'énergie initiale, les consommations s'additionnent. Autrement dit, il n'a jamais été extrait autant de charbon fossile au cours de la dernière décennie depuis la découverte de cette source.

Ce développement de l'Humanité s'est fait essentiellement à l'aide d'énergies carbonés fossiles. Leur consommation a engendré des émissions anthropogéniques phénoménales de gaz à effet de serre responsables d'un évènement majeur : le changement du climat global. Le groupe international d'expert sur le climat (GIEC) a de nouveau tiré la sonnette d'alarme dans le 6^{ème} rapport du groupe 1 chargé de l'étude du climat [2]. En 2019, la teneur en dioxyde de carbone dans l'atmosphère atteignait les 410 ppm, niveau le plus élevé depuis au moins 2 millions d'années. Ce niveau d'augmentation des gaz à effets de serre (avec le protoxyde d'azote et le méthane) est similaire aux changements observés naturellement sur plusieurs milliers d'années entre une période glaciaire et interglaciaire.

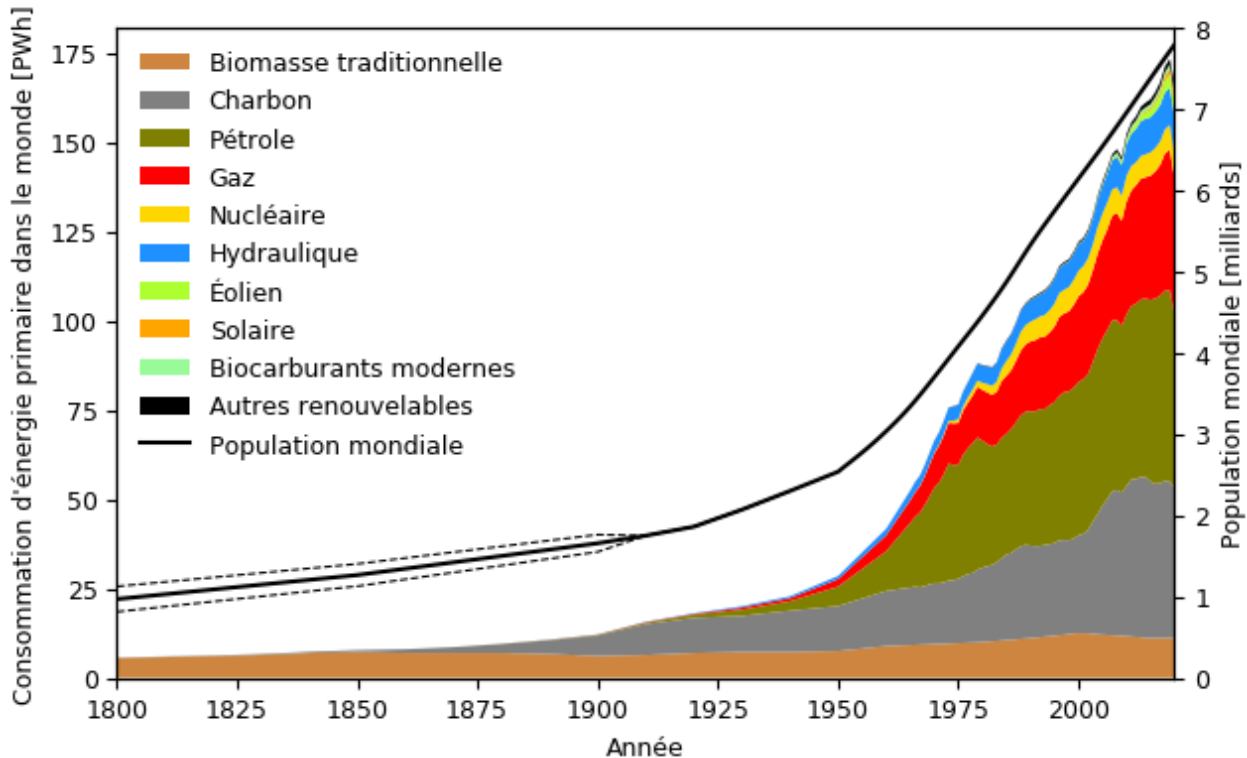


Figure 0-1 : Consommation d'énergie primaire dans le monde par source d'énergie et population mondiale (1800-1965 [3], 1965-2020 [4], population [5]).

Une conséquence immédiate est l'augmentation de la température moyenne globale à la surface qui était supérieure de 1,09°C sur la décennie 2011-2020 par rapport à la moyenne sur la période 1850-1900. Le GIEC estimait que les émissions anthropogéniques seules étaient responsables de la hausse de 1,07°C de la température globale (Figure 0-2). Les différents scénarios du GIEC (Figure 0-3) sur l'évolution du climat tablent sur une augmentation de température entre +1,5 à +5°C d'ici 2100. La cible de l'accord de Paris (+1,5°C) sera très probablement largement dépassée à moins d'une décrue rapide (SSP1-2.6) à très rapide (SSP1-1.9) des émissions suivie d'émissions nettes négatives à la moitié du siècle. Les scénarios hauts prévoient quant à eux un doublement (SSP3-7.0) et un triplement (SSP5-8.5) des émissions de gaz à effet de serre. Finalement, le scénario médian (SSP2-4.5) aux émissions constantes suivi d'une décrue à partir de 2050 pour arriver à des émissions nettes proches de zéro, conduit à un réchauffement de l'ordre de 2,8°C.

Changes in global surface temperature relative to 1850-1900

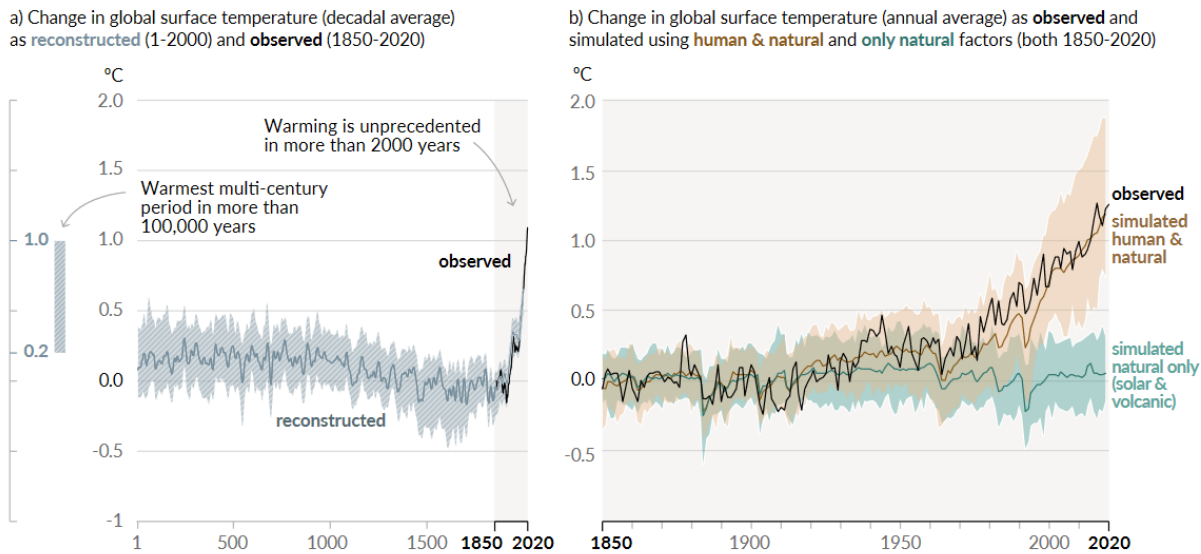


Figure 0-2 : Évolution historique de la température globale et sa cause [4].

a) Global surface temperature change relative to 1850-1900

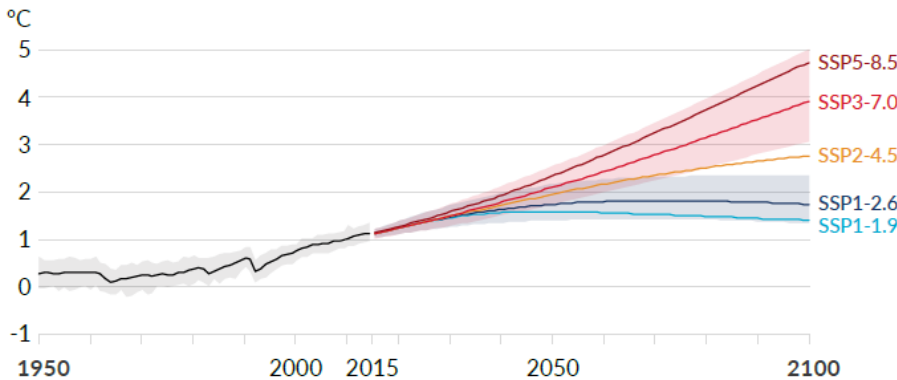


Figure 0-3 : Évolution de la température moyenne globale de surface selon les scénarios du GIEC [4].

En plus des conséquences alarmantes sur l'acidification des océans, la modification du cycle de l'eau, la perte de biodiversité [6], les tensions sur les cultures pour l'alimentation, entre autres. Ces changements climatiques auront un lourd impact sur la ressource forestière, parmi lesquels :

- La modification du régime des précipitations (pluies plus abondantes ou sécheresses),
- La salinité de surface modifiée,
- La montée des océans qui réduit ainsi la surface émergée,

- Des vagues de chaleur plus fréquentes et plus intenses (incendies de forêts), des vagues de froid moins fréquentes et moins intenses (parasites),
- La biosphère sur terre, les zones climatiques se sont élevées vers les pôles (notamment des espèces parasites).

Pour répondre à ce défi majeur, une meilleure utilisation de la ressource forestière doit être visée. En France en 2020, la biomasse représentait près de 12,9 Mtep dont 9,1 Mtep¹ de consommation primaire de bois-énergie sur 27,7 Mtep de production primaire d'énergies renouvelables et 227,9 Mtep de consommation primaire toutes énergies confondues (Figure 0-4). Le bois-énergie est utilisé à 92% pour la production de chaleur et une faible part pour produire de l'électricité (2,9% de la production brute d'électricité renouvelable) [7].

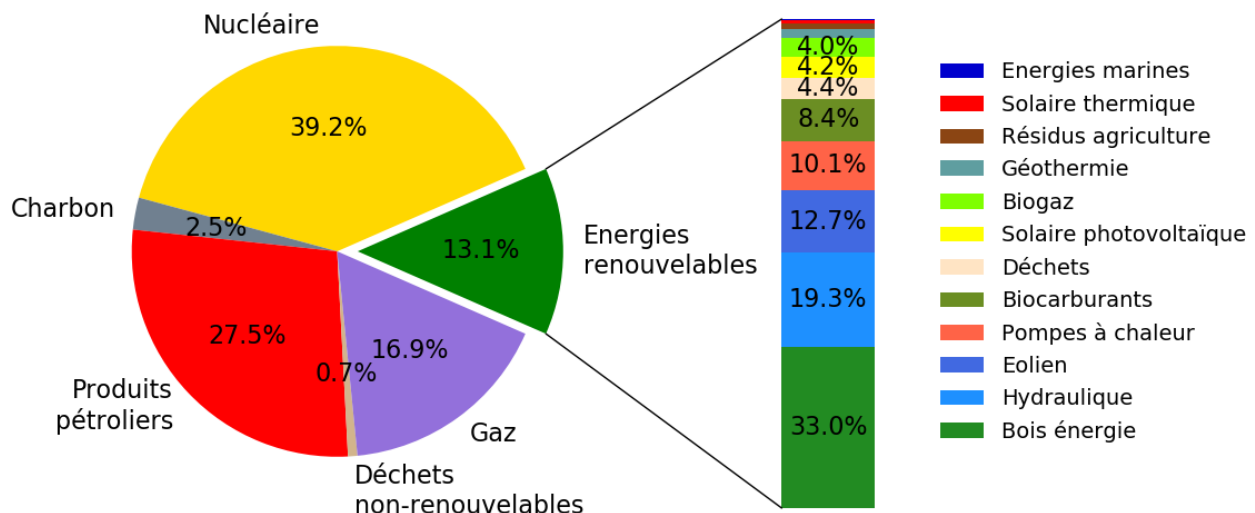


Figure 0-4: Consommation d'énergies primaires par type d'énergie en France en 2020 et production primaire d'énergies renouvelables par filière [7].

La stratégie nationale bas carbone vise à atteindre la neutralité carbone à l'horizon 2050. Dans son scénario de référence les émissions de gaz à effet de serre seraient amenées de 450 à 85 MtCO₂éq/an entre 2015 et 2050. Ces émissions seraient alors intégralement compensées par un puits de carbone constitué par le secteur des terres (forêts et terres agricoles) [8].

¹Mtep : million de tonnes équivalent pétrole (1 Mtep = 11,63 TWh = 41,868 PJ)

2. Objectif et démarche

Face aux défis énergétiques, ces travaux s'intéressent à la valorisation de produits secondaires issus de l'industrie forestière pour produire des vecteurs énergétiques d'intérêt : l'hydrogène et la chaleur. Par ailleurs, la co-production de bio-char est également envisagée.

Ces travaux s'intéressent à une production à petite échelle territoriale. Ce choix se justifie par la nature de la ressource visée pour limiter les distances de transport. De plus, il est également nécessaire de trouver un débouché à l'excédent de chaleur produite afin d'augmenter l'efficacité énergétique du procédé. Ces exutoires de chaleur sont relativement modestes.

3. Plan de la thèse

Le premier chapitre est consacré à un état de l'art en matière de gazéification de biomasse pour produire de l'hydrogène. Après un rapide état des lieux de la disponibilité de la biomasse, les voies de valorisation thermochimiques de cette ressource sont décrites. En particulier, dans le cas de la gazéification un effort important est mis pour réduire les quantités de polluants qu'il est nécessaire d'abattre avant d'envisager une valorisation subséquente.

Le deuxième chapitre s'intéresse à une technique de réduction des goudrons de gazéification par oxydation partielle. Un modèle cinétique détaillé a été bâti et validé sur un gaz de gazéification obtenu avec un pilote de gazéification en lit fluidisé.

Le troisième chapitre s'attache à présenter la modélisation de trois procédés de valorisation de biomasse par gazéification ou pyrolyse autotherme pour produire de l'hydrogène, de la chaleur et du bio-char. Ces trois voies sont modélisées avec AspenPlus® afin d'obtenir des bilans matière et énergie détaillés.

Le quatrième chapitre propose une évaluation technico-économique et une analyse de cycle de vie de ces trois scénarios.

Finalement, le chapitre 5 propose un récapitulatif de l'ensemble de ces axes de recherches ainsi que des perspectives et recommandations.

4. Liste des publications

- 1) Demol R., Ruiz M., Schnitzer A., Herbinet O., Biget A., Mauviel G., *Experimental and Modeling Investigation of Partial Oxidation Cracking of Gasification Tars*, **2022**, To be submitted.
- 2) Demol R., Dufour A., Rogaume Y., Mauviel G., *Production of purified H₂, heat and biochar from wood: comparison between gasification and autothermal pyrolysis based on advanced process modeling*, Energy & Fuels **2022**, 36 1 488-501.
<http://dx.doi.org/10.1021/acs.energyfuels.1c03528>
- 3) Demol R., Dufour A., Rogaume Y., Mauviel G., *Woodchips Pyrogasification to Produce H₂, Heat and even Bio-char: Techno-Economic and Life Cycle Assessment of Different Processes* **2022**. To be submitted.
- 4) Bartolomei E., Demol R., Buendia-Kandia F., Le Brech Y., Dufour A., *Evaluating aromatics production from lignin depolymerisation: experiments, process modelling and tech-eco assessment*. **2022**, To be submitted.

5. Conférences

- 1) *Analyse technico-économique de la production d'hydrogène issue de la gazéification de biomasse et de déchets*, Demol R., Rogaume Y., Mauviel G., XVII^{ème} congrès de la Société Française de Génie des Procédés (SFGP), Nantes, Octobre 2019.
- 2) *Production d'hydrogène issu de la gazéification de biomasse et de déchets : modélisation, analyse technico-économique et environnementale de procédés innovants*, Demol R., Rogaume Y., Mauviel G., XVII^{ème} congrès de la Société Française de Génie des Procédés (SFGP), Nantes, Octobre 2019.
- 3) *Technical-economic assessment of small scale biomass thermochemical plant producing heat, electricity and hydrogen*, Rogaume Y., Mauviel G., 29th European Biomass Conference & Exhibition (EUBCE), April 2021.

- 4) *Experimental and modelling investigation of partial oxidation cracking of gasification tars*, Demol R., Ruiz M., Schnitzer A., Herbinet O., Biget A., Mauviel G., 7th International Symposium on Gasification and its Applications (ISGA) 7, Nancy, September 2021.

6. Références

- [1] Auzanneau M. Or noir, la grande histoire du pétrole. Paris: La Découverte; 2015.
- [2] IPCC. Summary for Policymakers. In: Climate Change 2021: The Physical Science Basis. Contribution of Working Group I to the Sixth Assessment Report of the Intergovernmental Panel on Climate Change. Cambridge University Press; 2021.
- [3] Smil V. Energy Transitions: Global and National Perspectives. Second edition. Santa Barbara, California Denver, Colorado: Praeger, an imprint of ABC-CLIO, LLC; 2017.
- [4] bp Statistical Review of World Energy 2021. 2021.
- [5] United Nations, Department of Economic and Social Affairs, Population Division. World Population Prospects 2019. 2019.
- [6] Kolbert E. La 6e extinction. 2017.
- [7] Phan C, Plouhinec C. Chiffres clés des énergies renouvelables - Edition 2021. Ministère de la transition écologique; 2021.
- [8] Stratégie nationale bas-carbone. Ministère de la transition écologique et solidaire; 2020.

CHAPITRE 1 REVUE DE LA LITTÉRATURE

1.1. La ressource forestière

1.1.1. Produits de l'exploitation forestière

Différentes parties d'un arbre peuvent être distinguées (Figure 1-1). Le bois fort constitué principalement du tronc est généralement destiné à des usages matières, ce sont les parties les plus nobles de l'arbre à plus haute valeur ajoutée. On parle également de bois d'œuvre (BO) destiné le plus généralement à la construction, la fabrication de charpentes ou l'ameublement.

Les autres parties de l'arbre, les grosses branches ou les parties du tronc de trop faible diamètre, peuvent être valorisées pour des usages énergétiques ou industriels. Elles sont encore appelées bois industrie et bois énergie (BIBE). Le BO et le BIBE sont intimement liés et notamment d'un point de vue économique puisque que la vente du BIBE permet d'améliorer la rentabilité du BO. Cette valorisation complète de l'ensemble des sous-produits est profitable à l'ensemble de la filière sylvicole.

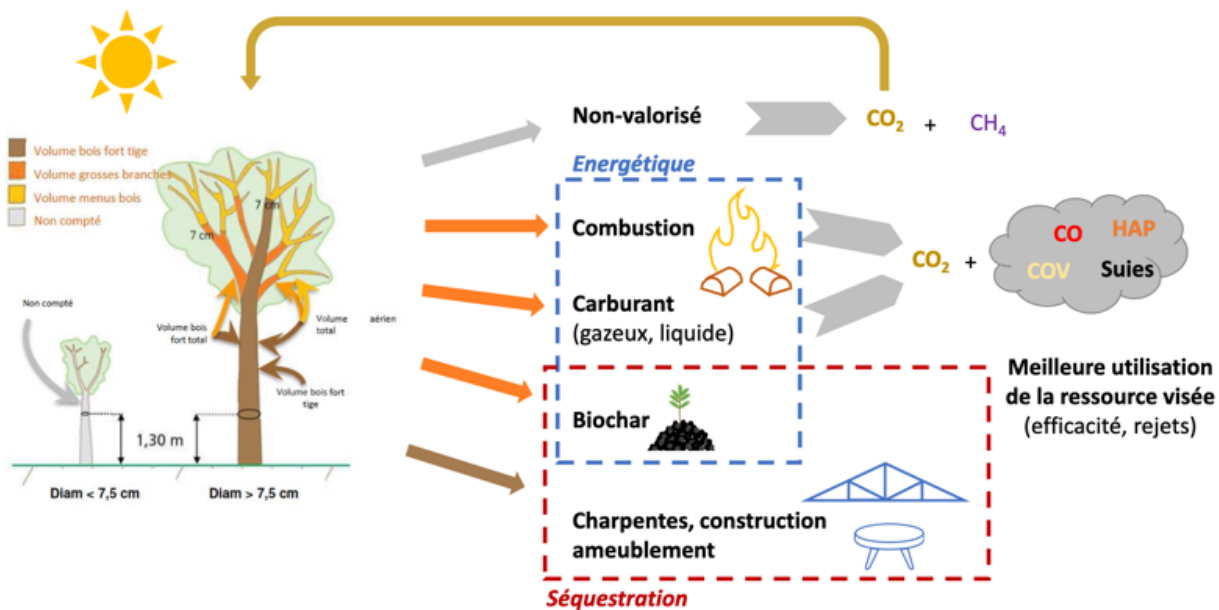


Figure 1-1 : Volumes aériens comptabilisés dans l'arbre par l'IGN (adapté de [1]).

Finalement, les plus petites branches qui constituent le menu bois (MB) ne représentent pas un intérêt économique suffisant et sont généralement laissées en forêt.

La partie du bois non valorisé est émettrice de CO₂ lors de sa dégradation naturelle. Selon les conditions, du méthane peut également être émis, ce qui s'avère problématique puisque ce gaz possède un potentiel de réchauffement global bien supérieur au CO₂.

1.1.2. Disponibilité dans le Monde et en Europe

Les forêts constituent 31% des terres émergées, reparties de manière inégale sur le Globe [2]. Plus d'un tiers sont des forêts primaires. En 2020, l'organisation des Nations unies pour l'alimentation et l'agriculture (FAO) indiquait que la déforestation se poursuivait à des niveaux alarmants, contribuant ainsi à la réduction de la biodiversité. Le taux de déforestation sur la période 2015-2020 atteignait 10 millions d'hectares par an, principalement pour répondre aux besoins en surfaces agricoles [2].

En Europe, la couverture forestière compte pour environ 35% des terres (Figure 1-2) et permet la séquestration de 10% des émissions de gaz à effet de serre de l'Union Européenne [3]. En 2020, une équipe scientifique de la commission européenne s'alertait d'une augmentation importante de la surface des parcelles de forêts européennes exploitées (+49%) et de la quantité de biomasse prélevée (+69%) sur la période 2016-2018 en comparaison de la période 2011-2015 [4]. Cet article paru dans la revue Nature a bénéficié d'une très large couverture médiatique et a suscité une vive polémique, il était jusqu'à présent admis que la forêt européenne était en expansion depuis le XIX^{ème} siècle [5].

Cette étude a été largement critiquée par de nombreux institutions chargées du suivi des inventaires forestiers nationaux. Dans ces travaux, la récolte de bois a été évaluée par télédétection en analysant des images satellites. C'est une approche nouvelle puisque les inventaires nationaux sont généralement basés sur l'extrapolation de différentes sources de données (échantillonnage sur le terrain, volumes de bois transformé et commercialisé, autoconsommation de bois des ménages...). La mesure est encore plus complexe en tenant compte d'évènements conjoncturels qui pèsent sur la forêt tels que les tempêtes ou des espèces invasives. La télédétection est aussi sujette à l'algorithme d'analyse d'image [6]. Il apparaît ainsi que l'article de Nature surestime

l'augmentation de l'exploitation forestière. Son augmentation est bien réelle mais dans des proportions moins alarmantes [7].

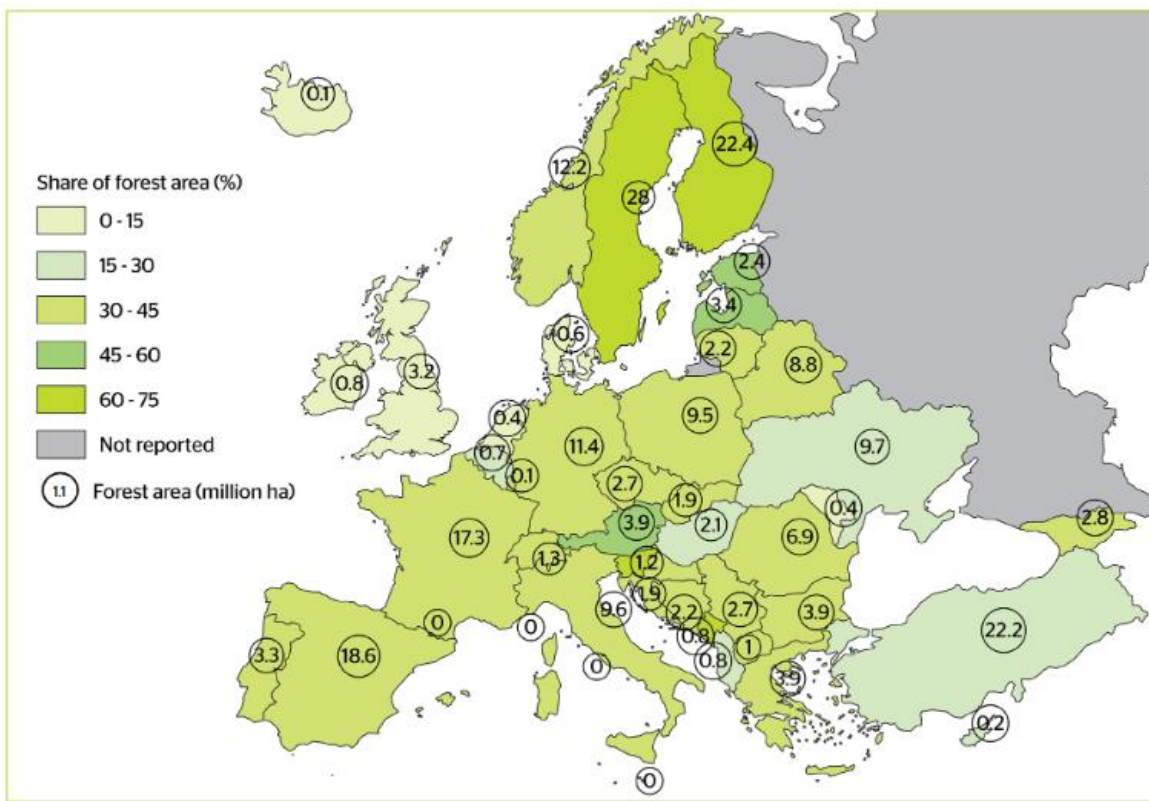


Figure 1-2 : Aires des forêts européennes et répartition par pays en 2020 [3].

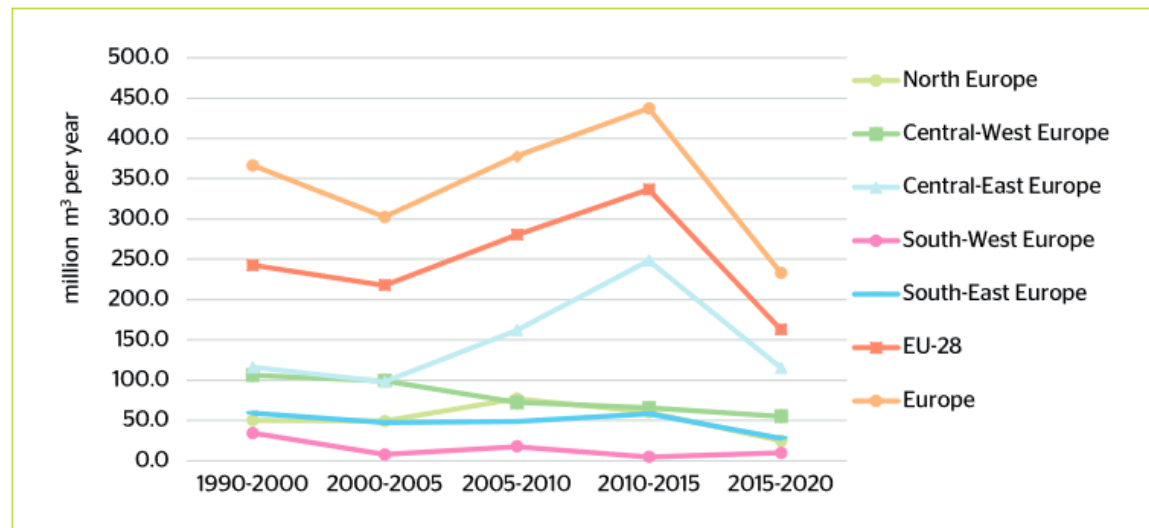


Figure 1-3 : Variation annuelle de l'augmentation de la ressource par région sur la période 1990-2020 [3].

Forest Europe, la conférence ministérielle sur la protection des forêts en Europe, note que le volume de bois sur pied a augmenté de 50% depuis 1990, même si cette croissance s'est ralentie au cours des dernières années [3]. La Figure 1-3 illustre bien cette tendance, notons que la forêt européenne connaît actuellement encore une croissance nette.

1.1.3. Disponibilité en France

Au niveau français, le volume d'arbres sur pied est évalué par l'Institut national de l'information géographique et forestière (IGN) dans son inventaire forestier national. L'IGN estime l'exploitation actuelle du bois industriel et énergie à hauteur de 23,3 Mm³/an (5,2 Mtep) sur la période 2011-2015. La disponibilité supplémentaire dans des conditions technico-économiques satisfaisantes s'élève entre 3,8 et 10,3 Mm³/an (0,9 à 2,4 Mtep) à l'horizon 2035 selon le modèle de sylviculture considéré, tendanciel ou plus dynamique [8]. Ce surplus d'énergie peut sembler modeste, mais il est à comparer avec la production intrinsèquement électrique actuelle fournie par l'éolien (3,8 Mtep) et l'énergie solaire photovoltaïque (1,3 Mtep) en 2020 [9]. Par ailleurs, un gisement additionnel est constitué de déchets de bois dont on distingue différentes qualités. Le bois A ne contient pas de pollution outre quelques pointes ou agrafes, le bois B est une classe intermédiaire et le bois C est un bois traité avec des produits plus problématiques tels que la créosote dans les traverses de chemin de fer.

Le scénario Afterres2050 proposé par SOLAGRO estime à 8,2 Mtep, à l'horizon 2050, la ressource bois énergie issue de la forêt auxquels s'ajoutent 11,9 Mtep issues des produits connexes de scierie, du bois issu de l'agroforesterie, des déchets de bois et autres dérivés du bois et des résidus de culture [10].

Outre, la recherche de nouvelles ressources, une meilleure utilisation du bois énergie mobilisé actuellement doit être envisagée. Une simple combustion mal contrôlée présente une efficacité faible et est source d'une pollution évitable (HAP, COV, poussières, CO).

Ces gisements de ressources permettent également une amélioration de l'indépendance énergétique si la ressource est nationale. La valorisation de ces ressources s'inscrit dans le cadre de l'économie circulaire et permettrait la création d'emplois locaux non-délocalisables.

Toutefois, il existe une incertitude sur la disponibilité effective de cette ressource au vue de l'évolution du climat global et de ses conséquences sur les forêts [11].

1.1.4. Disponibilité en Grand-Est

L'IGN publie régulièrement les disponibilités de la ressource biomasse à l'aide de l'inventaire forestier national. Différents scénarios de sylviculture sont envisagés : un scénario tendanciel, un scénario de gestion sylvicole évolutif et un scénario dynamique (encore plus productif). À l'échelle de la région Grand-Est, les disponibilités supplémentaires évaluées en 2016 [8] ont été revues à la baisse dans l'étude de 2018 [1]. Sur la Figure 1-4 sont présentées les disponibilités totales de bois selon les différents types de ressources et les scénarios de gestion sylvicole. La répartition des ressources est présentée à la Figure 1-5. Notons également ce fait notable, le papetier Norske Skog (Golbey) a annoncé la reconversion de son activité du bois vers le recyclage, libérant une consommation annuelle de l'ordre de 350 000 t/an [12]. Par ailleurs, les forêts du Grand-Est sont parasitées par les scolytes qui engendrent de nombreux dégâts [13].

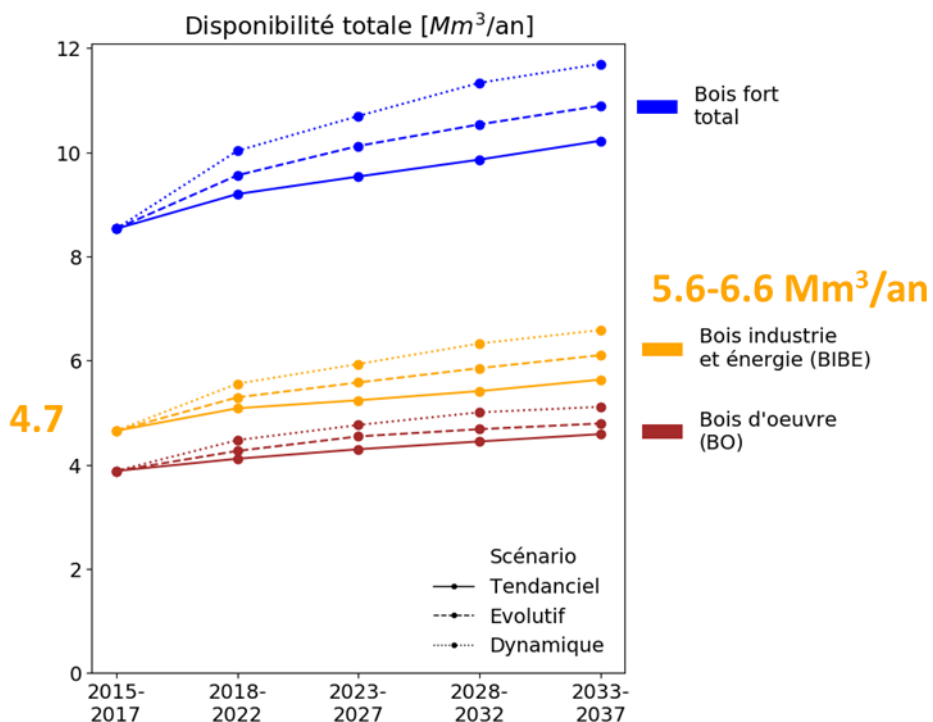


Figure 1-4 : Disponibilité en BIBE et BO toutes espèces confondues en Grand-Est d'après [1,14].

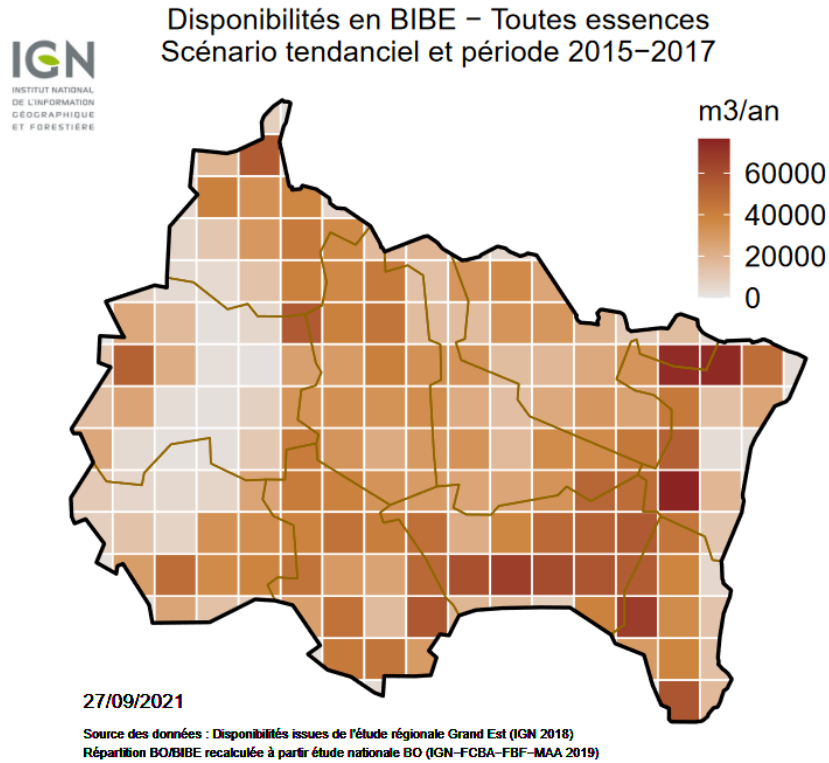


Figure 1-5 : Disponibilité BIBE toutes espèces en Grand-Est (maille 20 km) selon le scénario tendanciel et la période 2015-2017 [1,14].

1.1.5. Coût des produits de bois énergie

En France, le prix du sciage et de plusieurs produits du bois font l'objet d'un suivi par le Centre d'études de l'économie du bois (CEEB), l'INSEE et AGRESTE depuis 2011. Ces organismes publient des prix et indices de prix trimestriellement. L'évolution des prix de différents produits bois énergie est présentée à la Figure 1-6. Il s'agit de prix moyens toutes régions confondues, hors TVA et au départ des camions du site de préparation. On constate globalement une stabilité des prix des plaquettes forestières, de scierie et de mélange. Les prix de ces produits à visée énergétique s'établissaient entre 15 et 23 €/MWh au deuxième trimestre 2021 en fonction du type, de la taille et de l'humidité.

Au prix de la ressource s'ajoute le prix de son transport. D'après Yordanova et Migette (2017), pour des chaufferies supérieures à 400 kW, le bois énergie sous forme de plaquettes est transporté en majorité par des camions de 90 m³ (soit une capacité de camion de 27 t) [16].

Pour un même volume de bois livré, le poids total transporté augmente avec le taux d'humidité. Cette relation est illustrée à la Figure 1-7 pour un camion de 27 t. Ainsi la charge utile de bois sur base sèche est bien inférieure au poids transporté.

Le coût du transport du bois en camion de 27 t peut être évalué par l'équation 1.1 [16].

$$CL_{27t} = \frac{\frac{174.8}{nr} + 0.66 \cdot km + 22.3 \cdot dl}{27} \cdot f_c \quad (1.1)$$

CL_{27t} est le coût hors taxe de livraison par tonne, nr est le nombre de rotations dans la journée, km le nombre de kilomètres aller-retour, dl la durée totale de livraison et f_c le facteur spécifique pour le transport de plaquette (évalué à 1.15).

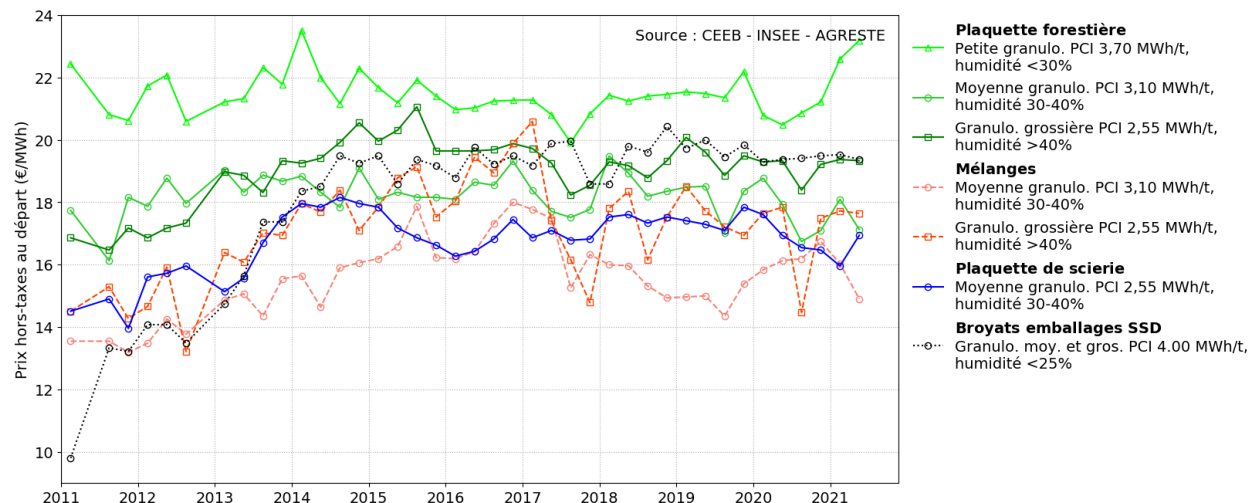


Figure 1-6 : Prix de différents produits transformés de bois propre 2011-2021 (prix moyens en France hors taxes, au départ du site de préparation) [15].

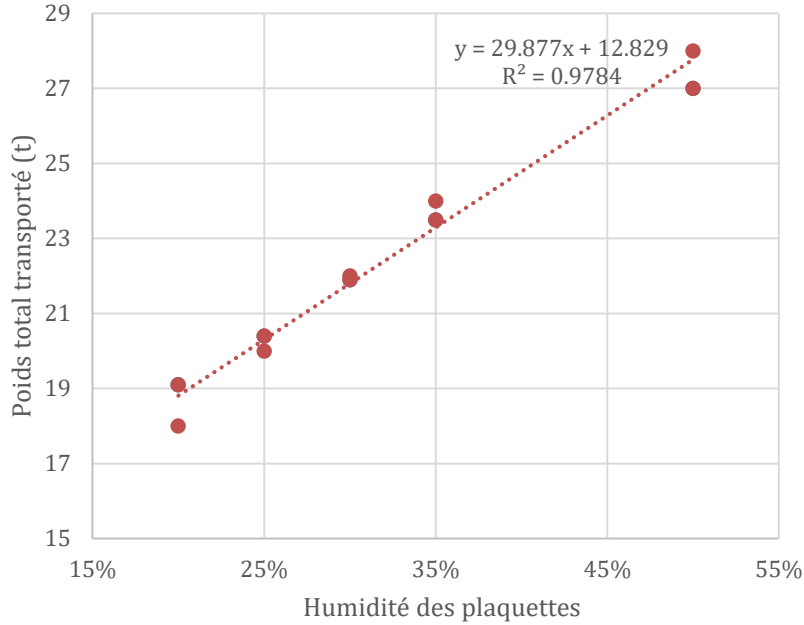


Figure 1-7 : Relation poids total livré et taux humidité pour un camion à fond mouvant de 27 t, d'après l'ONF et Dufeu [16].

1.1.6. Usages énergétiques

Le bois BIBE est généralement utilisé pour fournir de la chaleur qui alimente des réseaux de chaleur industriels ou urbains [17]. Outre cette application de chauffage, la biomasse peut aussi être valorisée sous d'autres formes.

Dans une étude, l'ADEME et GRDF envisageait la conversion du réseau de gaz naturel fossile avec des gaz renouvelables à l'horizon 2050 [18]. Trois principales filières étaient identifiées pour parvenir à cet objectif : la méthanisation, la pyro-gazéification et l'électrolyse suivie d'une méthanation (*power-to-gas*). La demande finale de gaz résultant d'une meilleure efficacité et d'une meilleure isolation des bâtiments pourrait passer de 460 TWh en 2018 à 300 TWh en 2050. D'autre part, le potentiel théorique de production s'établit à 460 TWh_{PCS} de gaz renouvelables injectables dont 40% (180 TWh_{PCS}) pourraient être issus de la filière pyrogazéification de biomasse sèche et combustibles solides de récupération (CSR).

Outre la substitution du gaz naturel par un gaz renouvelable, la pyrogazéification peut être un fournisseur d'un vecteur énergétique décarboné : l'hydrogène.

1.2. État des lieux et débouchés futurs de l'hydrogène

L'hydrogène connaît un regain d'intérêt de nos jours pour décarboner des secteurs très émetteurs de gaz à effet de serre tels que l'industrie et la mobilité. L'élément hydrogène est le plus abondant dans l'Univers, pourtant il n'est disponible sur Terre que lié à d'autres atomes (H_2O , C_xH_y). Le dihydrogène a une très importante densité énergétique massique (Figure 1-8), néanmoins sa masse volumique à l'état gazeux est très faible. Bien que son utilisation n'émette pas de carbone, la production d'hydrogène n'est pas neutre.

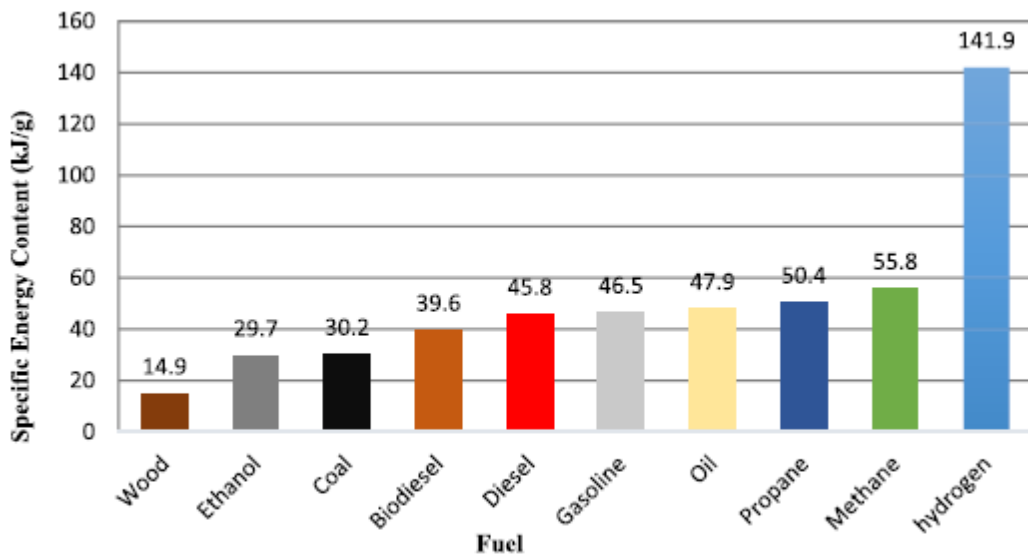


Figure 1-8 : Energies spécifiques de différent combustibles [19].

1.2.1. Production d'hydrogène

L'hydrogène peut être produit par différents procédés aux niveaux de maturité technologiques (TRL) très différents [20,21]. Quatre catégories peuvent être distinguées :

- Les procédés thermochimiques
 - o Vaporeformage du gaz naturel (SMR), procédé de référence et le plus économique actuellement,
 - o Gazéification du charbon,
 - o Gazéification de biomasse,
 - o Pyrolyse de biomasse,
 - o Reformage de liquides dérivés de la biomasse (*Biomass-derived liquid reforming*),

- Hydrogène thermochimique solaire (STCH).
- Les procédés électrolytiques
 - À basse température (<200°C) : alcaline (H_2SO_4 , KOH) ou électrolyte solide (membrane polymère conductrice de protons PEMFC)
 - À haute température (>400°C) : membrane céramique conductrice d'ions (SOFC)
- Séparation solaire directe de l'eau (*Direct Solar water splitting*)
 - Photo-électrochimique (PEC)
 - Photo-biologique
- Procédés biologiques
 - Conversion microbienne de la biomasse (*dark fermentation*)
 - Photo-biologique (biophotolyse de l'eau avec une algue)

La Figure 1-9 présente l'avancement technologique de ces différentes voies de production d'hydrogène d'après le département américain de l'énergie. La gazéification de la biomasse y est présentée comme une technologie proche d'un développement industriel.

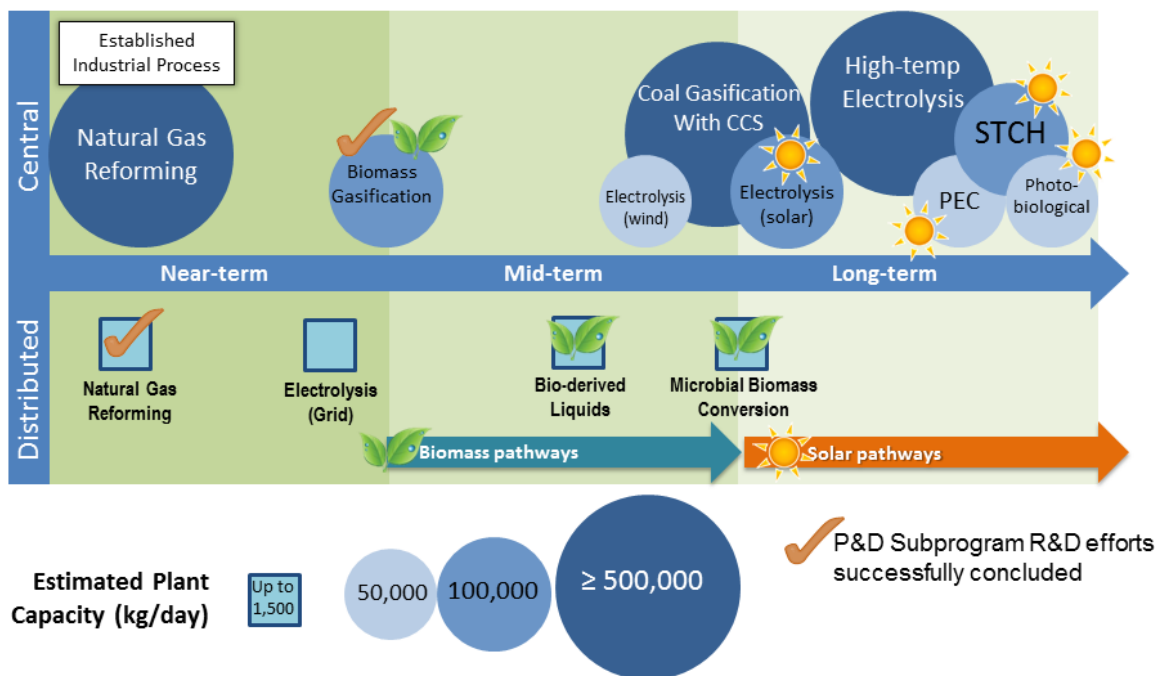


Figure 1-9 : Classification des procédés de production d'hydrogène d'après le département de l'énergie américain [22].

La production mondiale d'hydrogène était estimée à 117 Mt en 2018 [23]. Cette production est quasi exclusivement issue de combustibles fossiles (Figure 1-10). On distingue la production dédiée de la co-production d'autres industries (électrolyse de saumure, production de chlore). La production dédiée fait majoritairement appel au reformage du gaz naturel. L'hydrogène est aussi produit par la gazéification du charbon, essentiellement en Chine. Finalement, une faible partie de l'hydrogène est produite en tant que produit secondaire du raffinage et de l'électrolyse. La part de la production renouvelable était estimée à moins de 0,4 Mt, celle associant un captage du CO₂ (CCUS) inférieur à 0,4 Mt [23].

Quand il est co-produit au fil d'un procédé, l'hydrogène est réutilisé dans d'autres unités du site et quand il n'existe pas d'autre débouché, il est simplement brûlé pour récupérer de la chaleur. Notons le cas particulier des raffineries qui sont à la fois productrices et consommatrices d'hydrogène. En France métropolitaine, toutes les raffineries sont des consommateurs net d'hydrogène [24].

L'agence internationale de l'énergie constate un retard du développement de la production d'hydrogène renouvelable. À la mi-2021, les capacités de production par électrolyseurs s'élevaient à 300 MW dont 40% situées en Europe. La capacité totale pourrait atteindre 90 GW à l'horizon 2030 [25].

1.2.2. L'hydrogène pour l'industrie

La demande mondiale d'hydrogène pure s'établissait à 90 Mt en 2020 [25] dont l'usage est quasi-exclusivement destiné à l'industrie. L'hydrogène est consommé pure ou quasi pur pour le raffinage (transports) et la synthèse de l'ammoniac destinée à la production de fertilisants (Figure 1-10). Des applications beaucoup moins intensives concernent la chimie, les métaux, l'électronique ou encore l'industrie du verre. Les véhicules hydrogène dotés d'une pile à combustible ont une part extrêmement marginale (>0.009% de la consommation).

L'hydrogène est aussi consommé en mélange pour la synthèse du méthanol ou encore la réduction directe du fer dans la production d'acier. D'autres applications concernent notamment la production de chaleur. Le Tableau 1-1 présente une liste non-exhaustive d'utilisations d'hydrogène dans l'industrie.

Le prix de l'hydrogène industriel s'établi environ entre 1,50 et 2,50 €/kg_{H2} pour les gros consommateurs et peut monter à 10-20 €/kg pour les consommateurs moins intensifs (verreries, agroalimentaire, métallurgie, électronique...) [26].

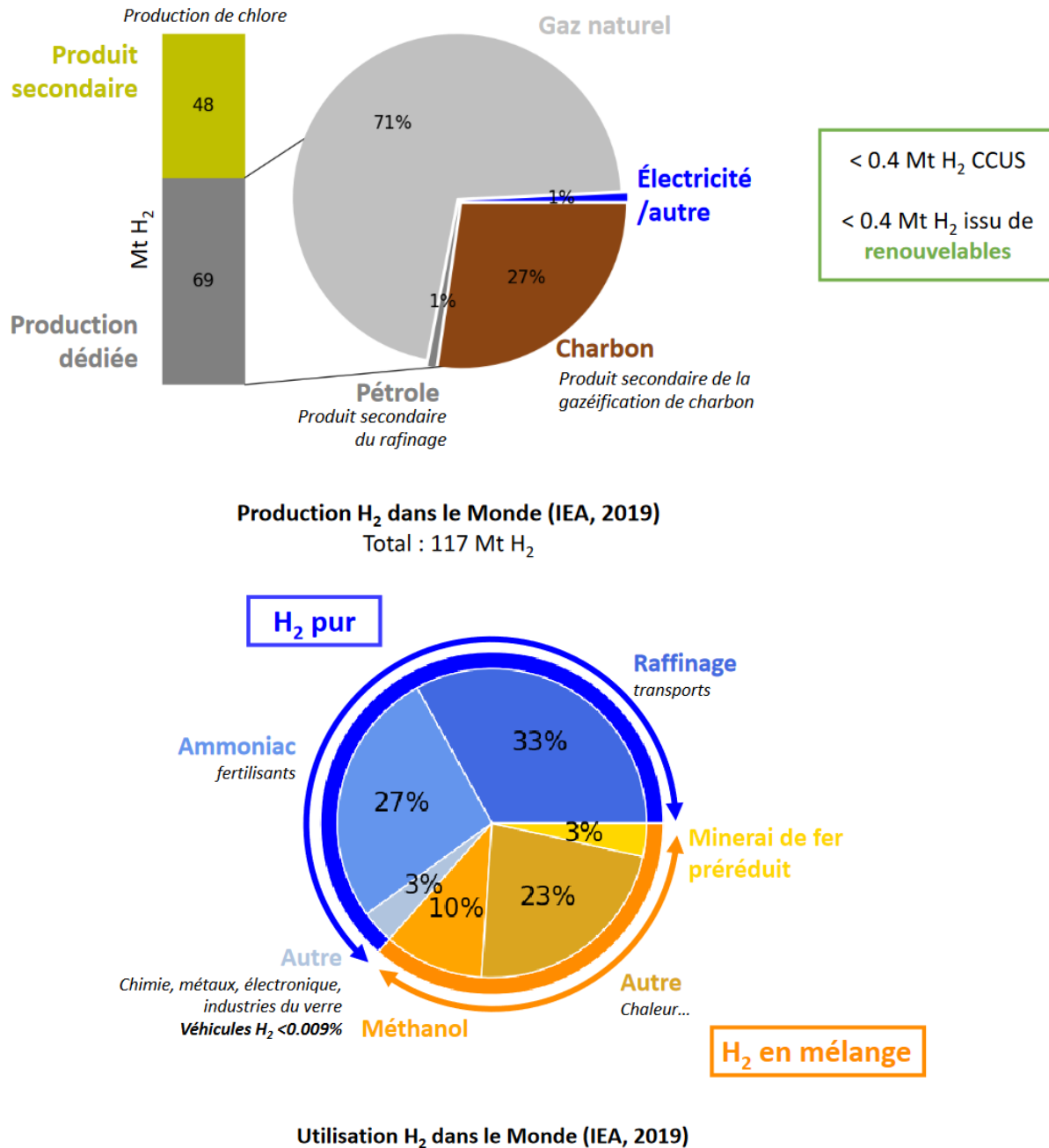


Figure 1-10 : Production et consommation de l'hydrogène dans le Monde en 2018 [23].

Tableau 1-1 : Industries utilisant de l'hydrogène (d'après [27-31]).

Secteur	Besoin*	Production H ₂	Prix (€/kg H ₂)	Applications
Raffinage pétrolier	> 10 000 Nm ³ /h	site/pipeline	1-2	Transformation du pétrole brut et des sables bitumineux : hydrocraquage des distillats (H ₂ 95% v, 25-35 kg H ₂ /t), hydrotraitement, hydrodésulfuration (HDS, H ₂ 70-85% v, 0.5-10 kg H ₂ /tonne de charge). Production de biocarburants.
Ammoniac	> 10 000 Nm ³ /h	site/pipeline	1-2	Ammoniac pour les fertilisants et les explosifs miniers (20% de la demande de NH ₃)... (180 Mt NH ₃ /an). 1 kg H ₂ permet de produire 5,6 kg NH ₃
Méthanol	> 10 000 Nm ³ /h	site/pipeline	1-2	1 500 Nm ³ H ₂ par tonne de méthanol CO + 2 H ₂ = CH ₃ OH / CO ₂ + 3 H ₂ = CH ₃ OH + H ₂ O
Métallurgie	60-480 Nm ³ /h	site/livraison	6-7	Réduction directe du fer pour la production d'acier (H ₂ + CO) (DRI : <i>Direct Reduced Iron</i>), alliages, découpage plasma
Chimie	> 1 000 Nm ³ /h	site/pipeline	2-3	Polymères (nylon), résines polyuréthane (MDI, TDI)
Huiles	> 100 Nm ³ /h	site/livraison	5-6	
Verrerie	120-360 Nm ³ /h	site/livraison	5-6	Atmosphère réductrice et protectrice de l'oxygène. Production de verre plat (procédé <i>Float</i>)
Mécanique				Frittage de pièces moulées, recuit de pièces mécaniques.
Semi-conducteurs	10-120 Nm ³ /h	site/livraison	5-6	H ₂ gaz vecteur et protection contre l'oxydation
Chimie fine	> 100 Nm ³ /h	site/livraison	6-7	
Pâtes et papiers				Biocarburants, réduction des liqueurs noires
Alimentaire	120-480 Nm ³ /h			Hydrogénéation (durcissement de graisses, margarine, beurre d'arachide, cookies, plats cuisinés), détection de fuite en ligne de l'emballage
Pharmaceutique				Production du sorbitol, des vitamines A et C.
Spatial				Carburant de fusées (Ariane 5 : 162 t O ₂ à -183°C, 28 t H ₂ à -253°C)
Énergie	10-60 Nm ³ /h	livraison		Liquide de refroidissement des rotors de générateurs électriques
Chaleur haute température				Procédés haute température > 400°C (émergent)

*100 Nm³/h = 800 kg/h

1.2.3. L'hydrogène pour l'injection dans les réseaux de gaz naturel

Afin de verdier le réseau gazier, il serait possible d'injecter directement de l'hydrogène renouvelable dans le réseau sans une étape préalable de méthanation. En effet, il est aujourd'hui possible d'injecter jusqu'à 6% en volume d'hydrogène dans les réseaux existants, à l'exception des réseaux présentant une sensibilité à la présence d'hydrogène (stations GNV puisque les réservoirs ne sont certifiés qu'à 2% pour l'hydrogène actuellement, industriels verriers...) [32]. L'injection d'hydrogène dans le réseau gazier constitue également une méthode de stockage d'énergie (équivalente en France à 130 TWh) et permettrait une amélioration de la balance commerciale [32].

Un consortium d'entreprises gestionnaires de réseaux de gaz a évalué les conditions techniques et économiques de cette potentielle injection [32]. Ces entreprises envisagent de porter de taux d'incorporation d'hydrogène à 10% puis 20% avec uniquement des adaptations limitées des installations existantes [32].

Des incertitudes sont pointées sur la garantie de l'intégrité du réseau avec l'hydrogène, ils notent cependant que l'ajout de O₂, CO ou CO₂ pourrait avoir des effets inhibiteurs et protecteurs. Des incertitudes demeurent, tout comme le comportement des stockages en réservoirs aquifères [32]. Des expérimentations devraient également être menées pour convertir des portions de réseau de gaz naturel à de l'hydrogène exclusivement.

Dans l'hypothèse d'un hydrogène pur (99,99+%) à un pouvoir calorifique de 120 MJ/kg et d'un coût de production de 2 €/kg_{H2}, le prix de l'hydrogène injecté reviendrait à 60 €/MWh. Ce prix de 2 €/kg_{H2} n'est aujourd'hui atteint en pratique pour les grosses unités de reformage de méthane. Ce cas n'est bien sûr pas pertinent puisque l'hydrogène est issu de gaz naturel. Si le prix de production d'hydrogène renouvelable atteignait 5 à 10 €/kg_{H2} ceci donnerait 150 à 300 €/MWh injectable. Ces prix sont à comparer avec les 10 à 30 €/MWh pour le méthane fossile sur le marché de gros sur la période 2015-2020. Le gaz naturel a récemment connu une brusque augmentation et frôlait les 100 €/MWh fin 2021 [33].

1.2.4. L'hydrogène pour la mobilité

Un autre secteur intéressant pour l'hydrogène est celui de la mobilité. Les voitures à hydrogène actuelles sont essentiellement des voitures électriques dont l'électricité est fournie par un réservoir d'hydrogène via une pile à combustible en lieu et place d'une batterie au lithium.

La voiture hydrogène pour les particuliers n'est probablement pas le principal débouché. Le coût d'achat d'un véhicule hydrogène est bien plus élevé qu'un véhicule électrique car la filière industrielle est moins mature que l'électrique. Par ailleurs, le réseau de distribution d'hydrogène est largement embryonnaire en comparaison du réseau actuel de stations essence conventionnelles. Les particuliers ont de plus la possibilité de recharger leurs véhicules à leur domicile sans surcoût à un prix par kilomètre plus faible que son équivalent en voiture essence. Le coût d'une station H₂ est également important et nécessite le transport du combustible quand il n'est pas produit sur place.

L'évaluation du prix de l'hydrogène mobilité n'est pas chose aisée. Afin d'estimer la cible de prix à atteindre, on peut se baser sur le coût actuel de la mobilité. À coût par kilomètre parcouru équivalent (3,54 €/km hors taxes), le prix par kilogramme d'hydrogène serait de 11,49 €/kg TTC pour un prix d'essence à 1,53 €/L TTC d'essence. En supposant le même niveau de taxation qu'actuellement, le prix de production et de distribution de l'H₂ s'établirait alors à 4,43 €/kg H₂. En effet, la TICPE représente la 4^{ème} recette budgétaire, à laquelle s'ajoute la TVA sur la TICPE et la TVA produit (Figure 1-11), il semble peu probable que ces taxes diminuent.

La cible de prix pour l'hydrogène mobilité est probablement trop faible pour rentabiliser les investissements nécessaires, en particulier pour l'acquisition d'un véhicule particulier. Cependant d'autres applications peuvent être envisagées dans le cas où l'électrification n'est pas envisageable du fait du poids des batteries telles que le transport de fret routier ou les trains circulant sur des lignes non-électrifiées (Figure 1-12).

Structuration des prix à la pompe (mai 2018)

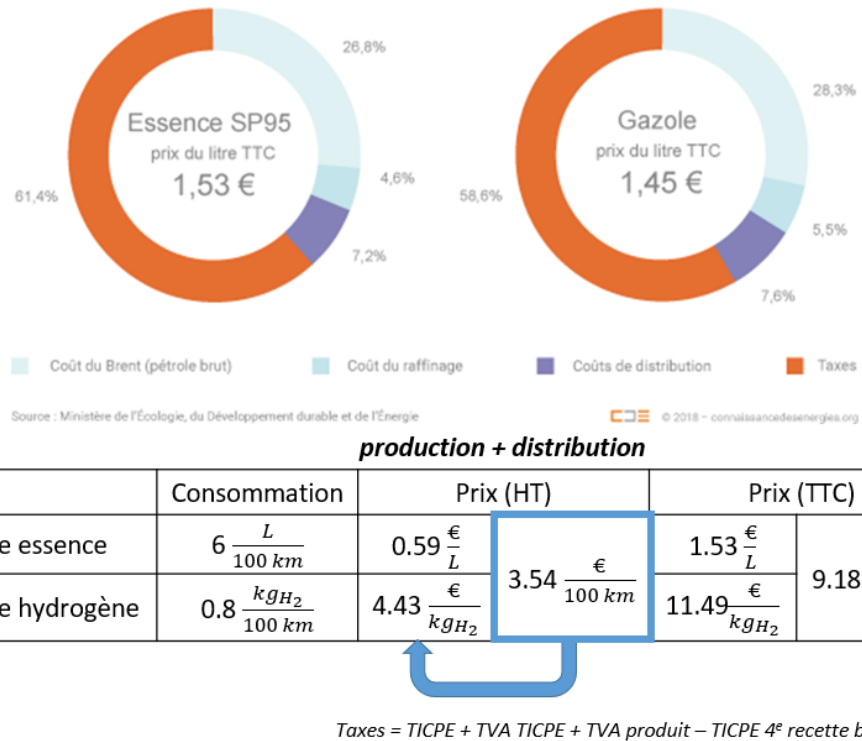


Figure 1-11 : Calcul du prix de l'hydrogène pour une application mobilité [34].



Figure 1-12 : Exemples de véhicules hydrogène [35].

1.2.5. L'hydrogène en France

La France a dévoilé en 2020 sa stratégie nationale de développement de l'hydrogène en France [36]. Elle prévoit, entre autre, une décarbonation de l'hydrogène à visée industrielle, ainsi que le développement de la mobilité lourde à l'hydrogène. La production envisagée est essentiellement d'origine électrolytique.

En 2019, la production d'hydrogène a été évaluée à 780 kt [24]. Cette production est en baisse suite à la fermeture de raffineries, d'unités de production d'ammoniac et de cokeries. Dans le détail, 390 kt d'hydrogène était co-produites et directement consommées : raffinage et pétrochimie (200 kt), cokeries (130 kt) et procédé de chlore (60 kt dont 30 kt directement brûlées pour de la chaleur ou de l'électricité) [24].

L'hydrogène issu d'une production dédiée représentait 390 kt : synthèse d'ammoniac (220 kt), raffinage consommation nette (130 kt, toutes les raffineries françaises sont en déficit sauf celle des Antilles et de la Martinique), production d'hexaméthylène diamine (HMD, 40 kt), traitement de surface de métaux (10 kt), peroxyde d'hydrogène (7 kt) [24].

Les émissions de CO₂ liées aux marchés industriels adressables de l'hydrogène en France représentaient près de 4 MtCO₂ soit plus de 1% des émissions totales, si on ajoute les émissions de la sidérurgie (20 MtCO₂) qui pourraient être neutralisées avec l'hydrogène, on atteint 8% [24].

La synthèse de l'ammoniac est l'un des principaux consommateurs d'hydrogène. Quatre sites sont encore en activité en France [37] :

- Grandpuits (Borealis) : 439 000 t_{NH₃}/an (capacité)
- Grand Quevilly (Borealis) : 400 000 t_{NH₃}/an
- Le Havre (Yara) : 400 000 t_{NH₃}/an
- Ottmarsheim (Borealis) : 260 000 t_{NH₃}/an

En 2019, 622 kt d'ammoniac ont été produites en France sur une capacité totale de 1495 kt. Les exportations représentaient 148 kt tandis que les importations s'élevaient à 654 kt.

En termes de consommation d'hydrogène cela représentait environ 99 kt H₂ pour 622 kt_{NH3} produites et potentiellement 238 kt_{H2} si la capacité totale était utilisée (1495 kt_{NH3})².

Un autre secteur consommateur d'hydrogène (en mélange avec du CO) est la synthèse du méthanol. Cependant, la France ne produit plus de méthanol depuis l'épuisement du gisement de gaz de Lacq [38].

Le marché adressable à l'hydrogène d'origine renouvelable pour les sites consommateurs nets d'hydrogène a été estimé à 420 kt/an d'après l'étude EY et Hinicio (Figure 1-13) pour l'Afhypac [24]. En 2030, la taille du marché techniquement adressable avec un hydrogène produit à 4,10 €/kg serait réparti comme suit :

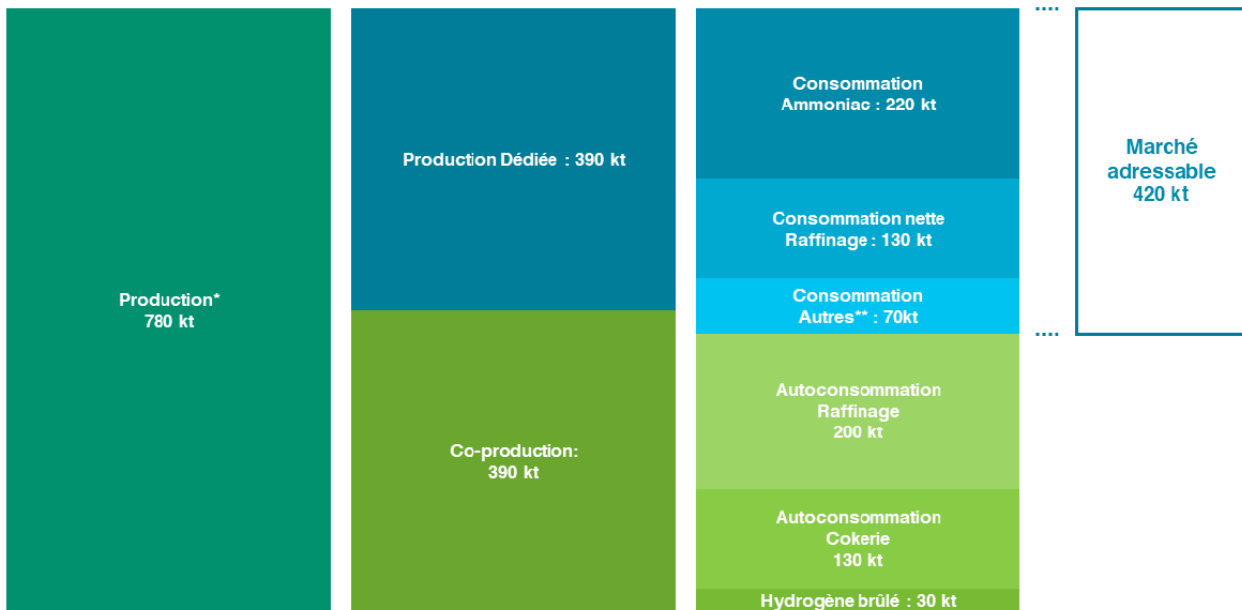
- Raffineries : 130 kt (manque 0,10 €/kg pour envisager H₂ renouvelable)
- Ammoniac : 220 kt (manque 0,40 €/kg pour envisager H₂ renouvelable)
- Métallurgie –traitement des métaux : 43 kt (une partie du marché est adressable depuis 2020, 5kt)
- Hexaméthylénediamine (HMD) : 40 kt (manque 0,20 €/kg pour envisager H₂ renouvelable)
- Peroxyde d'Hydrogène : 7 kt (économiquement adressable à partir de 2026)
- Verre : 5,2 kt (une partie du marché est adressable depuis 2020, 0.5kt)
- Microélectronique : 1,0 kt (marché est adressable depuis 2020)
- Potentiellement : 700 kt pour la production d'acier par processus DRI
- Injection dans le réseau gazier : 727 kt (manque 2,10 €/kg pour envisager H₂ renouvelable, ce marché est très loin de basculer en raison du coût trop élevé de l'hydrogène)

La quasi-totalité des politiques mises en œuvre ou prévues prévoient le développement de la production d'hydrogène issu de l'électrolyse de l'eau. Cette voie de production nécessite un surplus de consommation électrique. Pour éviter un coût environnemental contreproductif, la production électrique envisagée doit être bas carbone ou répondre à un pic de production. Ainsi, le développement de l'électrolyse devra notamment se conformer à une production électrique intermittente.

² Hypothèse 1974 m³ de H₂ pour produire 658 m³ de NH₃ à 1 bar, 25°C

Une autre source d'hydrogène possible est la valorisation thermochimique de la biomasse par gazéification ou pyrolyse. Le gaz produit qui contient de l'hydrogène peut également être séparé pour produire ce vecteur énergétique.

Estimation de la demande en hydrogène en France en 2019



Sources : HINICIO & EY, 2020 / *Production : H_2 issu de procédés générant de l' H_2 pur ou en mélange avec d'autres gaz

**Dont HMD : 40 kt, Traitement de surface du métal : 10 kt, Peroxyde d' H_2 : 7kt

Figure 1-13 : Demande d'hydrogène en France en 2019 et marché adressable [24].

1.3. Valorisation thermochimique de la biomasse

La biomasse peut être valorisée selon de multiples voies selon notamment son taux d'humidité (Figure 1-14). Lorsque la biomasse est sèche, les voies thermochimiques sont généralement privilégiées. La plus évidente est la combustion qui génère de la chaleur et conduit à la formation d'espèces gazeuses totalement oxydées (CO_2 , H_2O).

La chaleur peut être apportée par une source externe, sans agent oxydant. On parle alors de pyrolyse dont les produits sont un gaz (H_2 , CO , CH_4 et hydrocarbures légers), un résidu solide enrichi en carbone (char) et une huile (goudrons primaires séparables du gaz par condensation). Les températures atteintes sont généralement inférieures à 700°C.

Finalement, la gazéification consiste en l'oxydation partielle de la charge solide, avec l'ajout d'une quantité sous stœchiométrique d'oxygène par référence à la combustion (typiquement environ un tiers de la quantité stœchiométrique nécessaire pour une combustion). Les produits de cette transformation thermochimique sont un gaz de synthèse appelé syngaz et de la chaleur qui permet d'entretenir le procédé. Les principaux constituants du syngaz sont le monoxyde de carbone (CO), l'hydrogène (H_2), le dioxyde de carbone (CO_2), le méthane (CH_4) et d'autres hydrocarbures légers ($\text{C}_2\text{-C}_3$), de la vapeur d'eau et des hydrocarbures aromatiques polycycliques (HAP) aussi appelés goudrons. Selon que la gazéification s'effectue sous air ou sous oxygène, le syngaz est dilué dans l'azote (N_2).

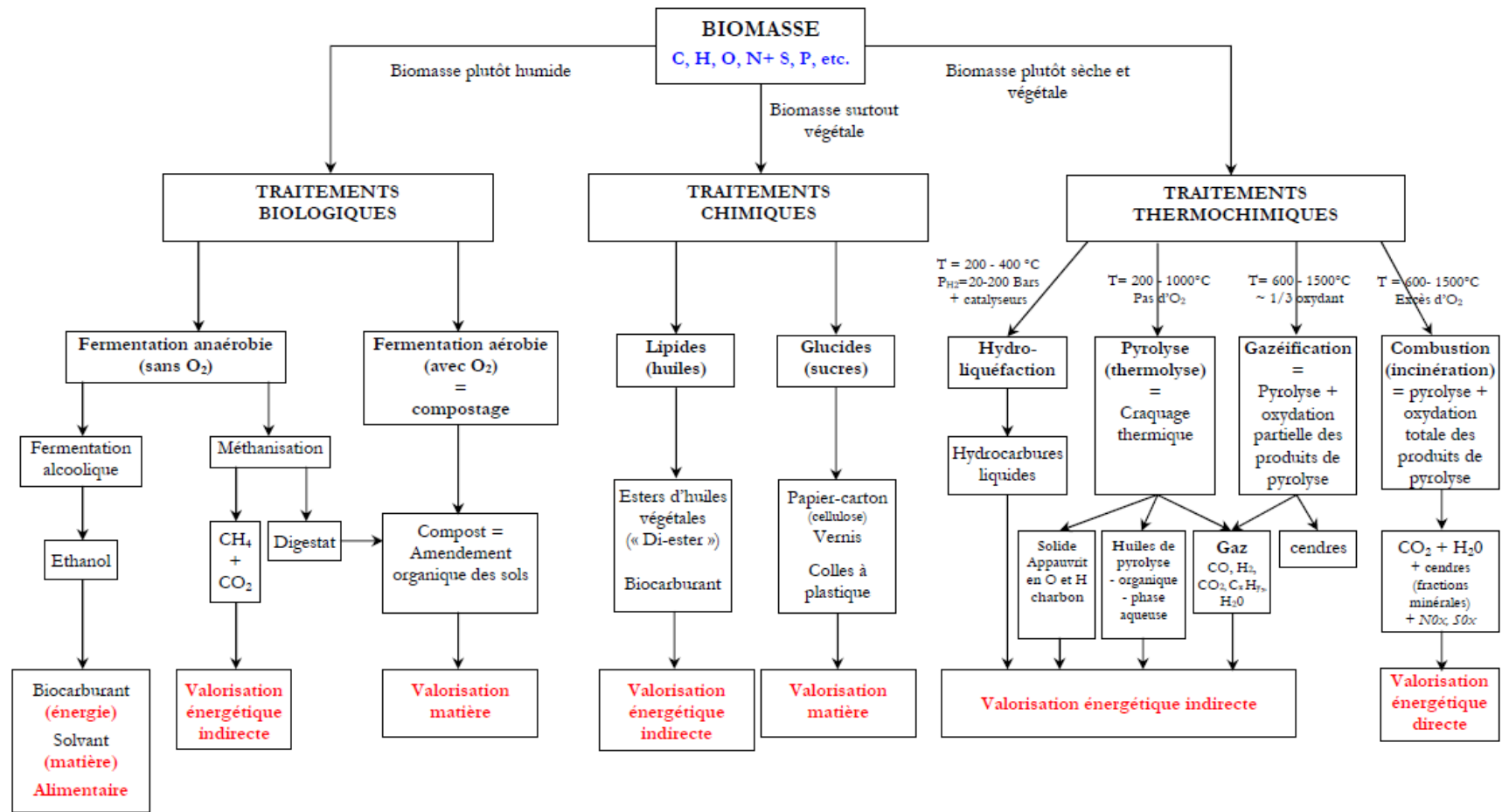


Figure 1-14 : Voies de valorisation de la biomasse [39].

1.3.1. Développement de la gazéification

La gazéification fut développée à partir de la fin du XVIII^{ème} siècle par Philippe Lebon notamment. La « distillation du bois » comme elle était appelée alors permettait de produire un gaz de bois utilisé dans les thermolampes pour le chauffage et l'éclairage, notamment de la ville de Paris. Le système est ensuite amélioré pour former un ancêtre du moteur à combustion interne [40,41]

Ce système, aussi appelé gazogène, a ensuite été modifié par Georges Imbert (1920) et utilisé pour faire face aux pénuries de carburants conventionnels (moteurs à gaz pauvres) notamment lors de la seconde guerre mondiale (Figure 1-15) [40]. Les frères Siemens mettent au point une des premières unités industrielles de gazéification de coke en 1859.

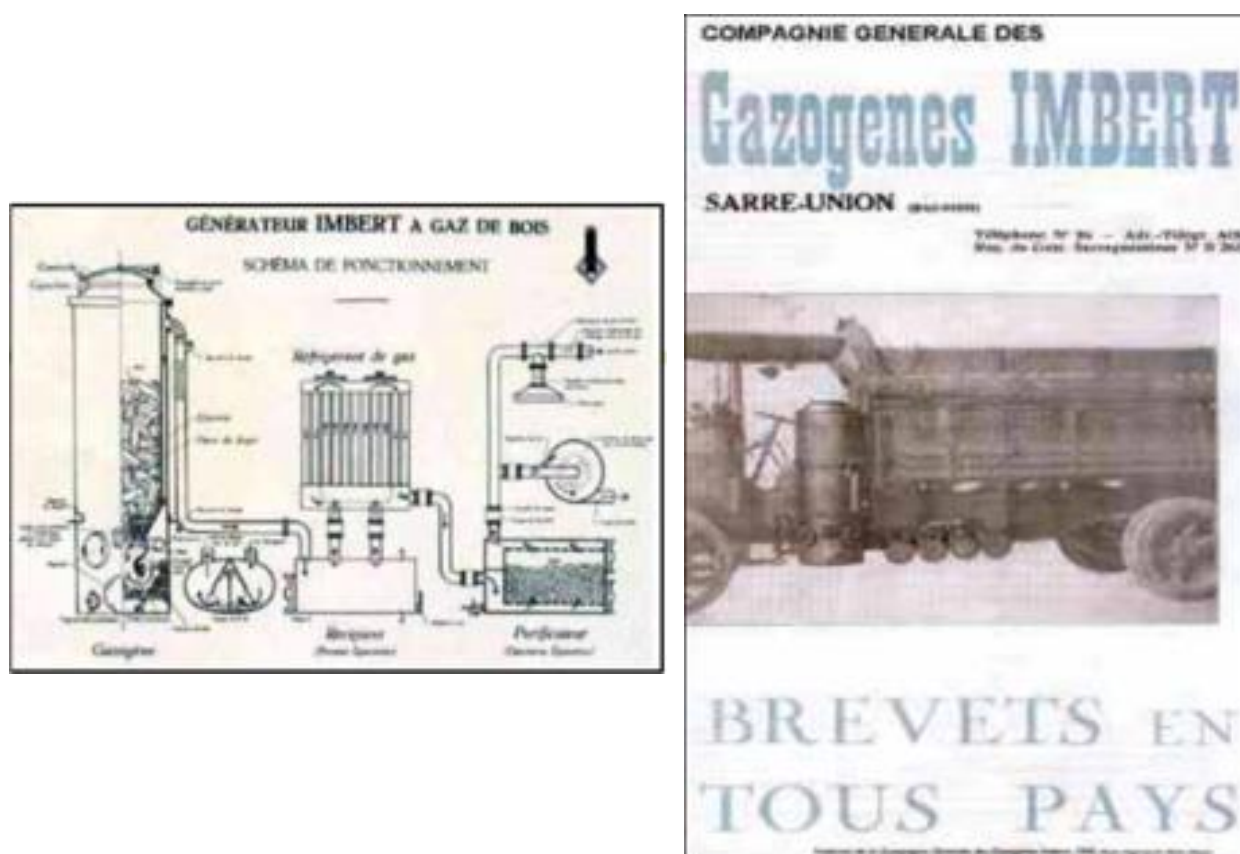


Figure 1-15: Gazogène Imbert (Déglyse X.)

1.3.2. Les différents types de gazéification

La gazéification s'effectue à une température allant de 500 à 1 600°C sous une pression variant du légèrement sous-atmosphérique à plusieurs dizaines de bars. Le gaz permettant l'oxydation partielle peut être de l'air, de l'oxygène, de la vapeur d'eau ou un mélange. Le gaz formé est constitué de gaz permanents (H_2 , CO, CO_2 , CH_4), de diazote en cas de gazéification à l'air, d'hydrocarbures légers (éthane, propane), de goudrons, de produits soufrés, chlorés et azotés (H_2S , COS, HCl, NH₃...) en fonction de la nature de la biomasse en entrée. Des solides sortent également du gazéifieur : les cendres (volantes ou sous foyer), ainsi que des particules de charbon partiellement converties et des fines de matériau du lit dans le cas d'une gazéification en lit fluidisé [9].

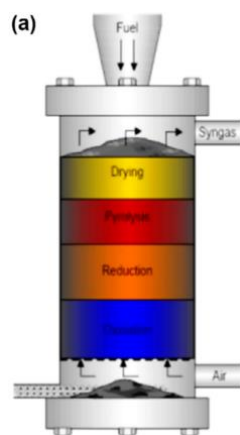
Les principales technologies de gazéification sont présentées à la Figure 1-16. On peut distinguer cinq grandes catégories de gazéification [42–44] dont les capacités sont présentées à la Figure 1-17.

- Les lits fixes présentent un temps de séjour de la biomasse de l'ordre de 1 à 3h (500–1000°C), ils engendrent une forte production de goudrons.
 - Contre-courant *updraft* (950-1150°C) : l'alimentation du combustible est réalisée par le haut du réacteur tandis que l'agent oxydant est injecté par le bas. Le gaz formé s'écoule à contre-courant de la biomasse. Cette technologie est simple et bien adaptée aux biomasses humides (jusqu'à 60%). Par contre, le gaz de synthèse obtenu contient de nombreux goudrons primaires de pyrolyse [45].
 - Co-courant *downdraft* (900-1050°C) : l'alimentation du combustible est effectuée par le haut du réacteur et l'agent oxydant est injecté par le haut ou le côté. Ici le gaz obtenu par le bas est plus propre, sa composition en goudrons est plus faible qu'à contre-courant. Cette technologie produit beaucoup de cendres, l'humidité de la biomasse ne doit pas dépasser 25%.
 - Courant-croisés *crossdraft* : cette technologie est adaptée pour l'utilisation de *charcoal*, l'alimentation est identique aux cas précédents tandis que le gaz parcourt le réacteur d'un côté à l'autre, perpendiculairement à l'écoulement de la biomasse.
- Dans les lits fluidisés, le temps de séjour de la biomasse est de l'ordre de 5 à 30 min (900 – 1000°C), la production des goudrons est plus faible.

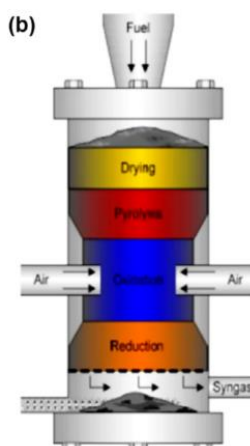
- Bouillonnant (800-900°C) : le combustible est alimenté par le haut du réacteur ou préférablement au bas du lit. L'agent oxydant est injecté par le bas et assure la fluidisation du lit.
- Circulant (750-850°C) : la vitesse de fluidisation est plus importante ici, une partie de la charge solide qui est entraînée est séparée du gaz par un cyclone. Le résidu solide est renvoyé vers le lit.
- Lit double : la gazéification du combustible est effectuée dans un premier lit fluidisé avec de la vapeur d'eau. Ces réactions sont globalement fortement endothermiques, l'apport de chaleur est assuré par le matériau du lit chaud alimenté par un second lit fluidisé. Ce second réacteur est alimenté en solide et en charbon par l'entraînement d'une partie de la charge solide du premier réacteur. Le charbon est brûlé par l'ajout d'air ce qui permet de chauffer le matériau du lit.
- Les lits entraînés (1300-1500°C) ont un temps de séjour de la biomasse de l'ordre de 1 s (900-1700°C), ils produisent une faible teneur en goudrons. Le combustible de faible taille est injecté par le haut du réacteur avec l'agent oxydant. Cette technologie est réservée pour des grosses capacités sous pression (jusqu'à 100 bars). La température atteinte est bien plus importante. Le syngaz obtenu est beaucoup plus propre.
- Les fours rotatifs sont des réacteurs cylindriques légèrement inclinés mis en rotation pour assurer le mélange du combustible et le contact avec l'agent oxydant. Ce contact est moins bon qu'avec les technologies précédentes et engendre un temps de résidence plus important.
- Les torches à plasma décomposent la charge solide en présence de l'agent oxydant. Le syngaz produit est évacué par le haut du réacteur.

Le Tableau 1-2 donne quelques compositions typiques de syngaz selon la technologie et l'agent oxydant utilisé. La gazéification à l'air induit une dilution du gaz de synthèse dans l'azote. Des gaz plus riches peuvent être obtenus en choisissant comme agent oxydant, la vapeur ou la vapeur en mélange avec de l'oxygène. La technologie des lits fluidisés doubles peut être une alternative satisfaisante.

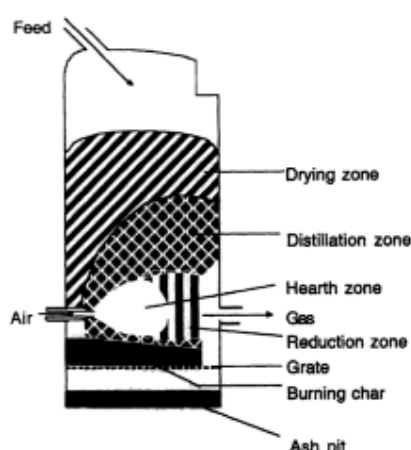
a. Contre-courant
updraft



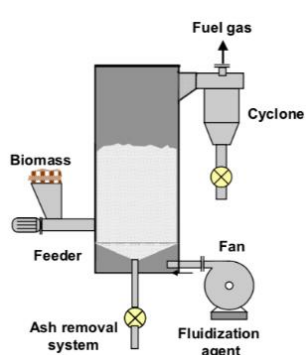
b. Co-courant downdraft



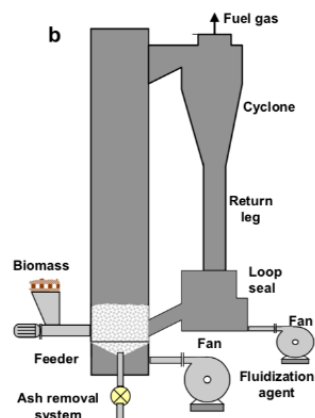
c. Courant croisés crossdraft



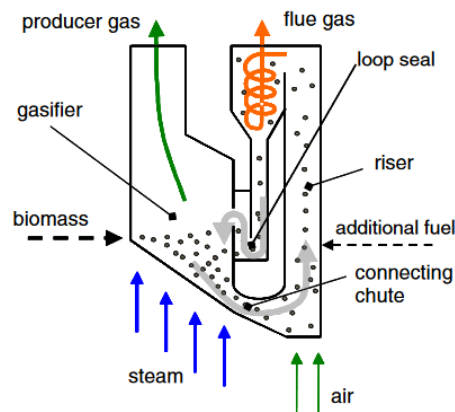
d. Lit fluidisé bouillonnant



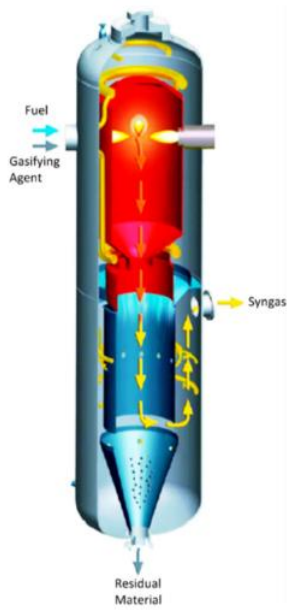
e. Lit fluidisé circulant



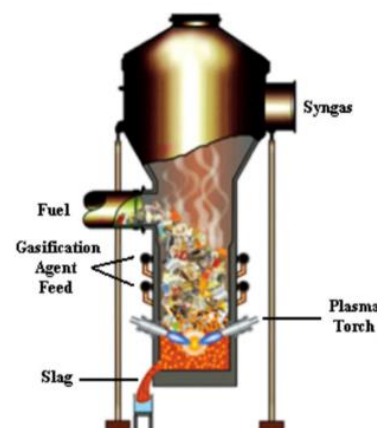
e. Lit fluidisé double



g. Lit entraîné



f. Plasma



g. Four rotatif

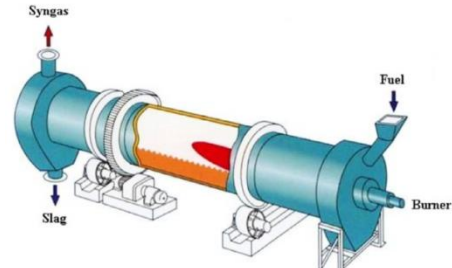


Figure 1-16 : Technologies de gazéification [42,45–48].

Tableau 1-2 : Compositions typiques du syngaz de gazéification.

	Lit fixe			Lit fluidisé			Lit entraîné	
	<i>Updraft</i>	<i>Downdraft</i>		Bouillonnant		Double		
Agent oxydant	Air [45,49]	Air [50,51]	O ₂ -H ₂ O [50]	O ₂ -H ₂ O [52,53]	Air [53]	H ₂ O [51,53]	[31,54]	O ₂ [51]
Composition syngaz [%vol, sec]								
H ₂	14-18	11-16	26-32	15-45	5-16	35-40	30-45	23-28
CO	20-29	13-18	35-43	15-50	10-22	25-30	22-25	45-55
CO ₂	6-14	12-16	22-32	25-35	9-19	20-25	20-25	10-15
CH ₄	1-3	2-6	3-6	5-7.5	2-6	9-11	10	0-1
C ₂	0.5	1	0.5-2	1-3	0.2-3		2-3	
N ₂	45-60	45-60			45-60	0-5		0-1
Goudrons [g/Nm ³] [55]	1-150	0.5-30	0.5-10	2-50	3-50	1-180	20-30	0.001-20
PCI [MJ/Nm ³]	4-6	4-6	9-12	10-14	3-8	12-14	12-17	10-12

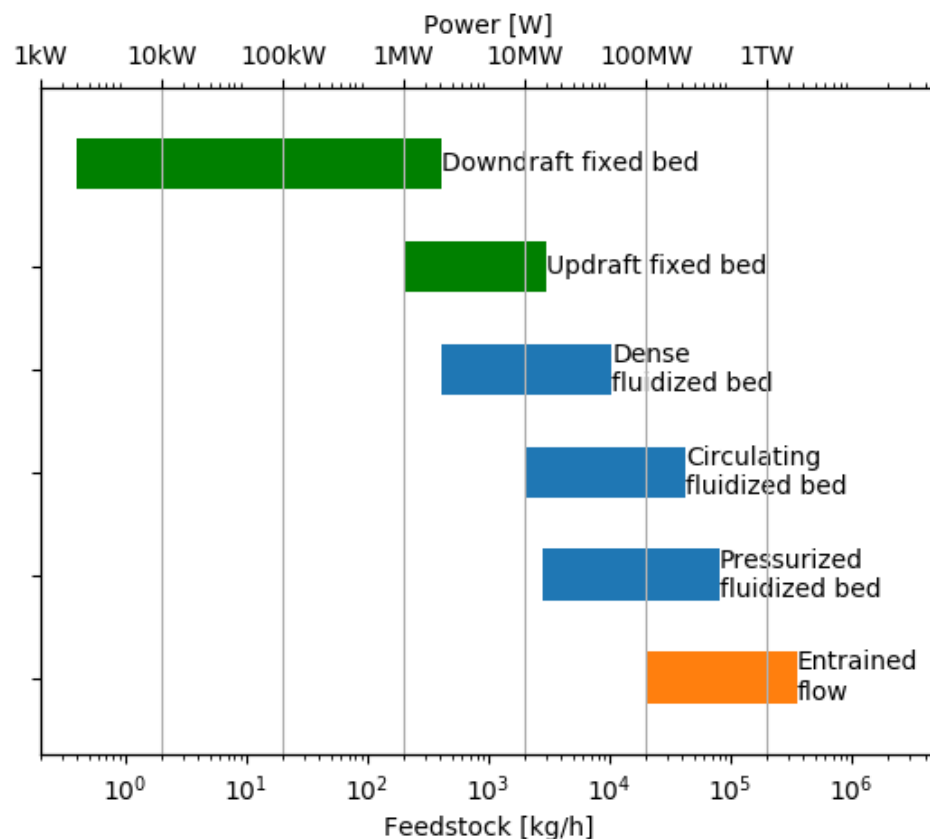


Figure 1-17 : Capacités des différentes technologies de gazéificateurs [56,57].

1.3.3. Verrous technologiques

Les forces que présentent la gazéification de la biomasse sont notamment liées à la ressource : renouvelable et locale. La gazéification permet aussi de valoriser des produits secondaires et éventuellement des déchets. De plus, le coût de la ressource est peu soumis aux effets de marché. Par ailleurs, ce type de procédés est pourvoyeur d'emplois locaux sur le site, pour le transport de la ressource et améliore plus généralement la rentabilité de la filière sylvicole. L'efficacité du procédé est élevée, néanmoins, une part importante de l'énergie peut être perdue lorsque la chaleur produite n'est pas correctement valorisée. Le traitement du gaz peut s'avérer particulièrement complexe dans le cas d'un combustible pollué [58–60]. En particulier, dans la chaîne de traitement des gaz, les goudrons peuvent poser des problèmes selon l'utilisation ultime du syngaz. Le Tableau 1-3 présente des exemples de qualités de gaz nécessaires selon les applications visées.

Les goudrons de gazéification sont des hydrocarbures aromatiques polycycliques (HAP). Selon la classification de l'ECN, on peut distinguer plusieurs classes de goudrons [63] :

- La classe 1 rassemble les goudrons les plus lourds, indétectables en chromatographie en phase gazeuse.
- La classe 2 regroupe les goudrons composés d'hétéroatomes. Ils sont généralement solubles dans l'eau (phénol, pyridine, crésol).
- La classe 3 contient les composés aromatiques à un cycle (xylène, toluène, styrène).
- La classe 4 contient les HAP légers à 2 ou 3 cycles (naphthalène, acénaphthylène, fluorène...)
- La classe 5 contient les HAP lourds à plus de 3 cycles (pyrène, chrysène, fluoranthène...).

1.3.4. Traitement du syngaz

Après formation du gaz de synthèse, il est nécessaire de le nettoyer pour son utilisation ultérieure (Tableau 1-3) et se conformer aux réglementations d'émissions à l'environnement (Tableau 1-4). On distingue trois types de technologies de lavage du gaz de synthèse en fonction des températures : à haute température ($> 300^{\circ}\text{C}$), à chaud ($100\text{--}300^{\circ}\text{C}$) ou à froid ($< 100^{\circ}\text{C}$). L'intérêt des procédés à chaud est de limiter la pénalité thermique du refroidissement, cependant ces technologies sont moins bien établies. Une bonne revue des technologies utilisées a été réalisée par Woolcock et al. [61].

Tableau 1-3 : Qualité syngaz [55,61,62].

	Moteur	Turbine à gaz	Synthèse méthanol	Synthèse Fisher-Tropsch	Compresseurs	Piles à combust.
Température	10-40°C					
Humidité relative	< 80%					
PCI syngaz	> 1,5 kWh/Nm ³					
Particules (suie, poussières, char, cendres)	< 5 mg/kWh ^a	< 30 mg/Nm ³ (PM5)	< 0.02 mg/Nm ³	n.d.		
Goudrons [mg/Nm³] Temp. de rosée Comp. inhibiteurs Classe 2, BTX	< 100 < 35°C	< 5	< 0.1	< 0.01 µL/L < 1 µL/L	50-500	< 1
Souffre (H₂S, COS)	< 20-70 mg/kWh ^a	< 20 µL/L	< 1 mg/Nm ³	< 0.01 µL/L		
Chlore (HCl)	< 2-10 mg/kWh ^a	1 µL/L		< 0.01 µL/L		
Azote NH ₃ HCN	< 5 mg/kWh ^a	< 50 µL/L	< 0.1 mg/Nm ³	< 0.02 µL/L		
Alcalins [µL/L]		< 0.024		< 0.01		

^aSyngaz

n.d. : non détectable

Tableau 1-4 : Limites d'émissions à l'environnement en France pour les unités inférieures à 50 MW [64].

Espèce	Unité	Chaudière	Moteur
SO ₂	mg/Nm ³	200	10
NOx	mg/Nm ³	400	100
Particules	mg/Nm ³	30	10
CO	mg/Nm ³	200	250
PAHs	mg/Nm ³	0.01	0.1
COV hors méthane	carbone total mg/Nm ³	50	
HCl	mg/Nm ³	10	
HF	mg/Nm ³	5	
Dioxines et furanes	ng I-TEQ/Nm ³	0.1	
NH ₃	mg/Nm ³	5	5
Formaldéhydes	mg/Nm ³		15

1.1.1.1 Particules

Les particules solides peuvent être séparées du flux gazeux par plusieurs méthodes :

- Les séparations inertielles (cyclone, séparateurs par impact, agglomérateurs de particules).
Les cyclones présentent de bonnes efficacités (90-95%) pour les particules de taille supérieure à 5 µm.

- Les filtres à manches, céramiques, rigides, en lits fixes ou mouvants, granulaires, en chadelles... présentent des efficacités encore meilleures (> 99 %).
- Les séparateurs électrostatiques peuvent être utilisés pour les cendres volantes.
- Les laveurs humides : colonne, Venturi, spray.

1.1.1.2 Goudrons

Les goudrons peuvent être évités de manière préventive (méthodes primaires) en agissant sur les conditions opératoires, l'agent oxydant ou sur le média de fluidisation dans le cas d'une gazéification en lit fluidisé [65]. Quand ils sont formés les goudrons peuvent être éliminés par des méthodes dites secondaires [55,61].

- Les méthodes à haute température :
 - Craquage thermique : sous l'effet d'un apport externe de chaleur menant à des températures supérieures à 900°C, les goudrons sont éliminés.
 - Craquage catalytique : la présence d'un catalyseur permet d'abaisser l'énergie d'activation des réactions d'élimination des goudrons et ainsi de diminuer la température requise. Il s'agit notamment de catalyseurs à base de nickel [55].
 - Oxydation partielle : l'ajout d'un peu d'oxygène permet d'augmenter la température du gaz en oxydant une partie du syngaz ce qui permet l'élimination des goudrons.
- Les plasmas non-thermiques : les goudrons sont décomposés sous l'effet d'une atmosphère réactive de radicaux libres, d'ions et d'autres molécules excitées.
- Les méthodes de séparation physique sont principalement des techniques de séparation de particules ou agissant sur la température de rosée de ces espèces.
 - Méthodes à sec (200-800°C) : cyclone, précipiteur électrostatique, filtre à manche (sur gaz refroidi), filtres, lit d'adsorbants ou de charbon actif.
 - Méthodes humides : laveur (spray, Venturi, OLGA), colonne garnie, précipiteur électrostatique humide, cyclone humide.
- Traitement biologique du gaz : ces procédés à température ambiante mettent en œuvre des biofilms capables d'absorber les composés organiques d'un flux gazeux pour les métaboliser en eau et CO₂. Ces procédés ont le désavantage d'avoir une cinétique lente.

1.1.3 Soufre

Le soufre se retrouve dans le syngaz essentiellement sous forme SO₂, H₂S ou COS. H₂S est notamment connu comme un poison pour de nombreux catalyseurs. Pour éliminer ces espèces, différentes méthodes existent [61] :

- Adsorption sur des oxydes métalliques tels que ZnO.
- Solvant chimiques : utilisation d'un solvant (amine) pour capter les espèces soufrées dans un absorbeur. Le solvant est ensuite régénéré dans un stripper. Le COS n'est pas absorbé efficacement et peut dégrader le solvant. Il faut donc préalablement l'hydrogénier en H₂S.
- Absorption physique : utilisation d'un solvant (méthanol, diméthyle éther) comme dans le procédé Rectisol. Le soufre peut être plus facilement récupéré car ce solvant est sélectif, il n'absorbe pas d'autres gaz acides tels que le CO₂.
- Procédés redox tels que le procédé LO-CAT utilisant une suspension de fer chélaté associé à un biocide.

1.1.4 Azote

Les composés azotés problématiques sont notamment l'ammoniac NH₃ et l'acide cyanhydrique HCN. Ils peuvent être simplement absorbés dans l'eau en raison de la forte solubilité de NH₃. À haute température l'oxydation de l'ammoniac forme N₂, H₂ et des oxydes d'azotes (NOx). Pour minimiser la formation de NOx, une oxydation catalytique sélective ou une décomposition catalytique peut être menée avec des catalyseurs à base de nickel, de fer ou encore de dolomite.

1.1.5 Alcalins

Les espèces alcalines peuvent être séparées par simple condensation avec les goudrons. La majorité de ces espèces en gazéification de biomasse sont, de plus, solubles dans l'eau.

1.1.6 Chlore

Les espèces chlorées (HCl ou NH₄Cl) peuvent être éliminées sur charbon actif, alumine ou oxydes d'alcalins en lit fixe. Il est également possible d'injecter directement des absorbants à base de calcium dans le gaz chaud (600-1000°C) pour abattre HCl.

1.3.5. Production d'hydrogène issu de gazéification

1.1.1.7 Choix de la technique de gazéification

Le contenu en hydrogène d'un syngaz issu de la gazéification de biomasse est relativement faible (Tableau 1-2), en raison de la faible teneur en hydrogène du combustible (de l'ordre de 5% massique). La concentration faible en hydrogène rend par ailleurs complexe et couteuse sa séparation. Afin de favoriser la production d'hydrogène, l'utilisation de vapeur d'eau comme agent oxydant permet d'augmenter le rendement en hydrogène. Cependant, la vapo-gazéification est globalement endothermique et nécessite par conséquent un apport externe de chaleur. Une alternative consiste à réaliser la gazéification en lit double pour éviter la dilution dans l'azote. Cette option peut s'avérer complexe technologiquement en raison de la circulation du média de gazéification. Finalement, la gazéification sous vapeur et oxygène pur permet d'éviter la dilution par l'azote tout en assurant un apport d'hydrogène par la vapeur d'eau. Cette option nécessite néanmoins une source d'oxygène et la production de vapeur. Selon l'option retenue une concentration en hydrogène jusqu'à 45% en volume peut être atteinte [66].

1.1.1.8 Chaîne de traitement

Pour maximiser la production d'hydrogène, deux opérations peuvent être menées : le reformage à la vapeur du syngaz et la réaction de gaz à l'eau (*water gas shift*).

Le reformage à la vapeur est effectué dans un réacteur catalytique pour convertir les hydrocarbures en hydrogène et monoxyde de carbone. Des catalyseurs à base de nickel sont couramment utilisés. L'objectif principal est de convertir le méthane mais il permet également de convertir d'autres hydrocarbures jusqu'aux goudrons [67,68].



Le CO peut ensuite être converti pour augmenter la production d'hydrogène selon la réaction de *water gas-shift* (équation 1.3). Cette réaction est également réalisée dans un réacteur catalytique.



Cette réaction est exothermique, elle est donc favorisée à basse température. Il est courant d'effectuer cette réaction dans deux réacteurs avec un refroidissement intermédiaire. La température d'entrée du premier réacteur est de l'ordre de 350°C (*high temperature shift*), et

d'environ 200°C pour le second (*low temperature shift*). Des catalyseurs à base de d'oxydes de fer et de chrome sont généralement utilisés pour le premier et à base de cuivre et d'oxyde de zinc sur alumine pour le second [66].

1.1.1.9 Procédés de séparation d'hydrogène

La purification de l'hydrogène est un point important puisque de l'hydrogène très pur est nécessaire à la synthèse de l'ammoniac (98-99,9%). Pour les applications en pile à combustible (PEM), la pureté requise est encore plus stricte avec 99,99% [44].

La technologie de référence pour réaliser la séparation de l'hydrogène lors du reformage de gaz naturel est le procédé cyclique d'adsorption modulé en pression PSA (*pressure swing adsorption*) (Figure 1-18). La composition en entrée de PSA est typiquement de l'ordre de 75% en volume. De manière analogue, le procédé d'adsorption modulée en température TSA (*temperature swing adsorption*) peut aussi être choisi [69]. Pour utiliser cette technologie avec un syngaz de gazéification, la concentration en hydrogène en entrée de PSA doit être supérieure ou égale à 70% vol pour atteindre une haute pureté (99,9% vol) [70].

La séparation peut également être effectuée avec des modules membranaires perméables à l'hydrogène (Figure 1-19). Les membranes en polyimide sont couramment utilisées mais il existe également des membranes métalliques plus sélectives. Yin et Yip ont publié une revue de la littérature des techniques de séparation d'hydrogène avec des membranes d'un gaz issu de gazéification de biomasse [71].

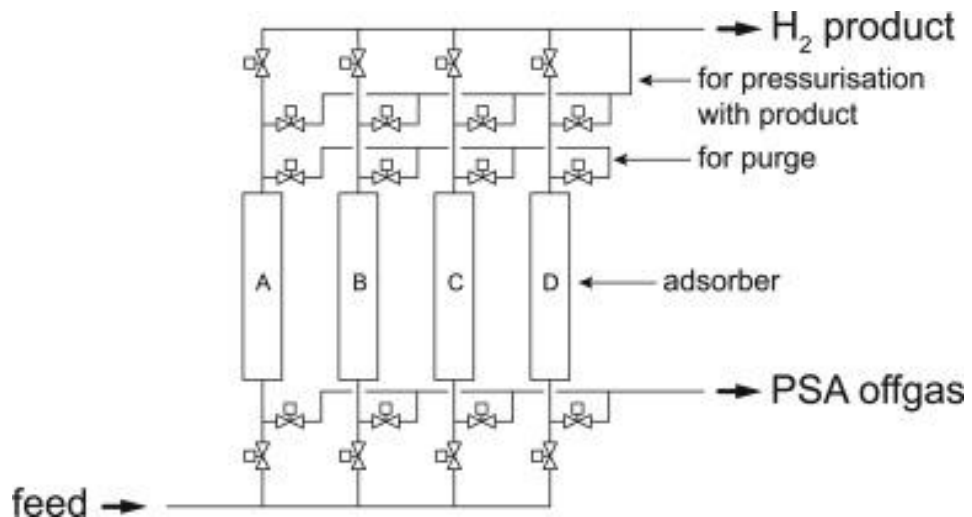


Figure 1-18 : Procédé d'adsorption module en pression (PSA).

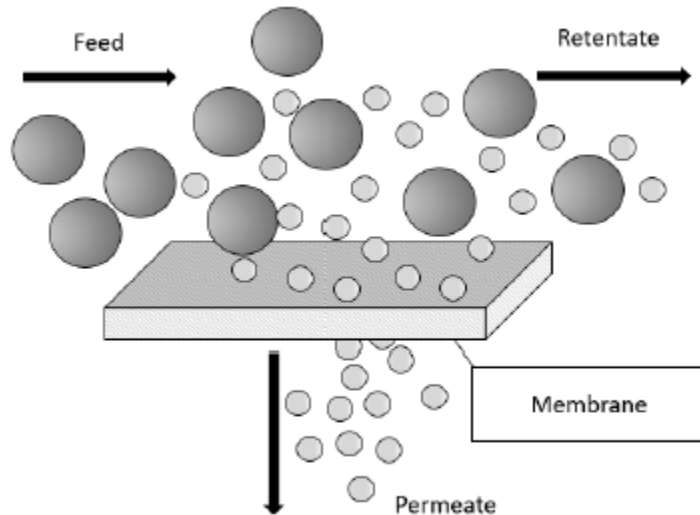


Figure 1-19 : Séparation membranaire [71].

1.4. Modélisation du procédé de gazéification

Le procédé de gazéification suivi de la valorisation du syngaz produit peut contenir de nombreuses étapes unitaires qui se succèdent. L'obtention de résultats issus de pilotes incluant la gazéification et la chaîne de traitement du syngaz s'avère couteuse en investissements, temps et en main d'œuvre qualifiée.

Afin d'évaluer la pertinence de tels procédés, la simulation numérique de procédés permet de connecter l'ensemble de ces opérations unitaires et de faciliter l'établissement des bilans de matière et d'énergie nécessaires pour l'évaluation technico-économique.

1.4.1. Utilisation de solides non-conventionnels

Une des particularités de ce type de procédés est d'utiliser comme ressource un solide non-univoque. Contrairement à des composés moléculaire, sa composition élémentaire n'est pas connue dans les bases de données thermodynamique des logiciels de simulation. Il est néanmoins possible de définir de tel composés non-conventionnel à l'aide de leur composition élémentaire (C, H, O, N, S et Cl), de leur composition en cendres, humidité, carbones volatiles et carbones fixes [72]. Ces propriétés sont ensuite utilisées pour estimer les propriétés requises (chaleur de combustion, capacité calorifique...) via différents modèles. L'essentiel de ces modèles a initialement été développé pour le charbon, il convient alors de les choisir judicieusement [73]. Il est également possible de renseigner la répartition des tailles de particules.

1.4.2. Modélisation de la gazéification

Afin de modéliser l'étape de gazéification, une première approche consiste à décomposer les éléments constitutifs de la biomasse en leurs formes stables (H_2 , C, O_2 , N_2 , H_2S , HCl). Dans un second temps, une approche à l'équilibre est utilisée pour estimer la composition du gaz de synthèse par minimisation de l'énergie de Gibbs [74]. Cette approche peut donner une estimation approximative des espèces majoritaires (gaz permanents) mais est incapable de prédire la formation des espèces minoritaires telles que les goudrons. Une approche alternative consiste à utiliser des corrélations empiriques pour estimer les compositions de syngaz et de goudrons [70]. Marcantonio et al. ont modélisé un lit fluidisé circulant par une approche de quasi-équilibre et validé ce modèle à partir de données issues d'essais sur leur pilote [75].

Afin de remédier à ce manque, plusieurs groupes se sont attelés à bâtir des modèles de lits fluidisés en tenant compte de l'hydrodynamique des réacteurs et des cinétiques en jeu (Figure 1-20) [46,76–78]. L'équipe du professeur Ranzi a mis au point un ensemble de modèles cinétiques détaillés destinés à prédire la composition des produits de la pyrolyse de la biomasse [79,80]. La biomasse est initialement décomposée en ses polymères constitutifs (cellulose, hémicellulose et lignine). Sous l'effet de la température, les produits de pyrolyse peuvent ensuite réagir en phase gazeuse avec l'oxygène notamment [81–83].

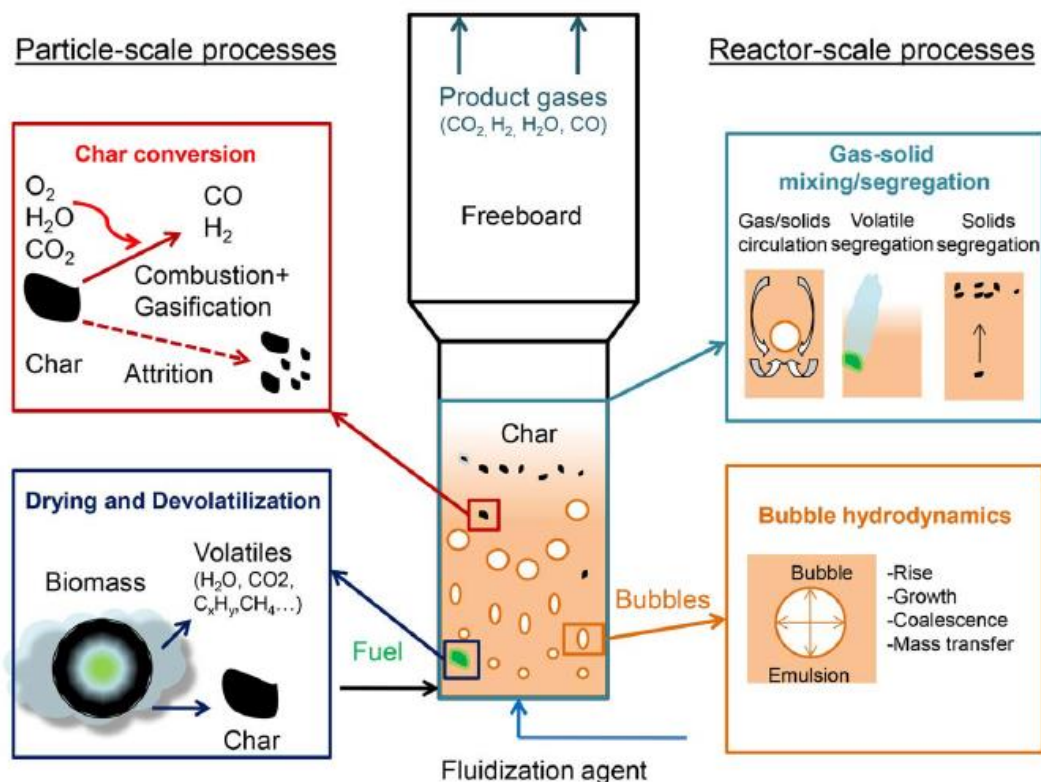


Figure 1-20 : Modèle de lit fluidisé de Bates et al. [77].

1.4.3. Chaîne de traitement du syngaz

Le procédé de gazéification a déjà été étudié dans plusieurs études avec un effort particulier pour les étapes de lavage du gaz de synthèse [84,85] ainsi que la production d'hydrogène dans des unités de grande échelle [70,86]. La prise en compte des goudrons est souvent réalisée de manière simplifiée en ne considérant que quelques espèces modèles [87].

Spath et al. ont publié l'une des premières études détaillées de modélisation sur l'ensemble du procédé de gazéification en lit double pour la production d'hydrogène (Figure 1-21). La chaîne de traitement du syngaz considérée incluait un lavage humide suivi d'un reformeur catalytique et des réacteurs de *water gas-shift* (WGS). La séparation de l'hydrogène étant assurée par un procédé PSA [70].

Notre groupe de recherche a également développé plusieurs modèles sous Aspen Plus® pour la gazéification et l'oxydation de la biomasse [76,84,85,88,89].

Les étapes de séparation des solides sont le plus souvent modélisées comme de simples séparateurs avec une efficacité globale d'abattement. Il est en outre possible de modéliser de manière plus détaillée cette étape si la répartition en tailles de particules est connue.

Pour maximiser la composition du syngaz en hydrogène des réacteurs catalytiques sont généralement utilisés (reformeur, *water gas-shift*). La simulation de ces unités est faite par des réacteurs à l'équilibre thermodynamique [90–94]. L'abattement de soufre est parfois considéré pour une valorisation en tant que produit secondaire dans des procédés à très large échelle [95]. D'autres solutions comme des filtres catalytiques ont aussi été envisagées [96]. Quand les goudrons sont considérés, seulement quelques molécules modèles sont prises en compte [90,96].

La modélisation du lavage humide des goudrons est complexe car elle nécessite de choisir un modèle thermodynamique adapté à un grand nombre d'espèces [97]. Cette unité de séparation est généralement modélisée via de simples flashes ou de manière plus fine avec des colonnes de distillation. La solution la plus convaincante à l'heure actuelle consiste à utiliser des données expérimentales d'abattement de goudrons correspondant au système étudié [85,98].

Martín et Grossmann ont proposé une optimisation du procédé de gazéification de biomasse destiné à la production de diésel par le procédé Fischer-Tropch. Ils ont bâti une superstructure simplifiée afin de déterminer le procédé optimal. La solution proposée privilégiait une gazéification indirecte suivie d'un reformage à la vapeur plutôt que d'une oxydation partielle du syngaz. Aucun autre ajustement de la composition ne s'avérait nécessaire pour obtenir le ratio CO/H₂ visé [99].

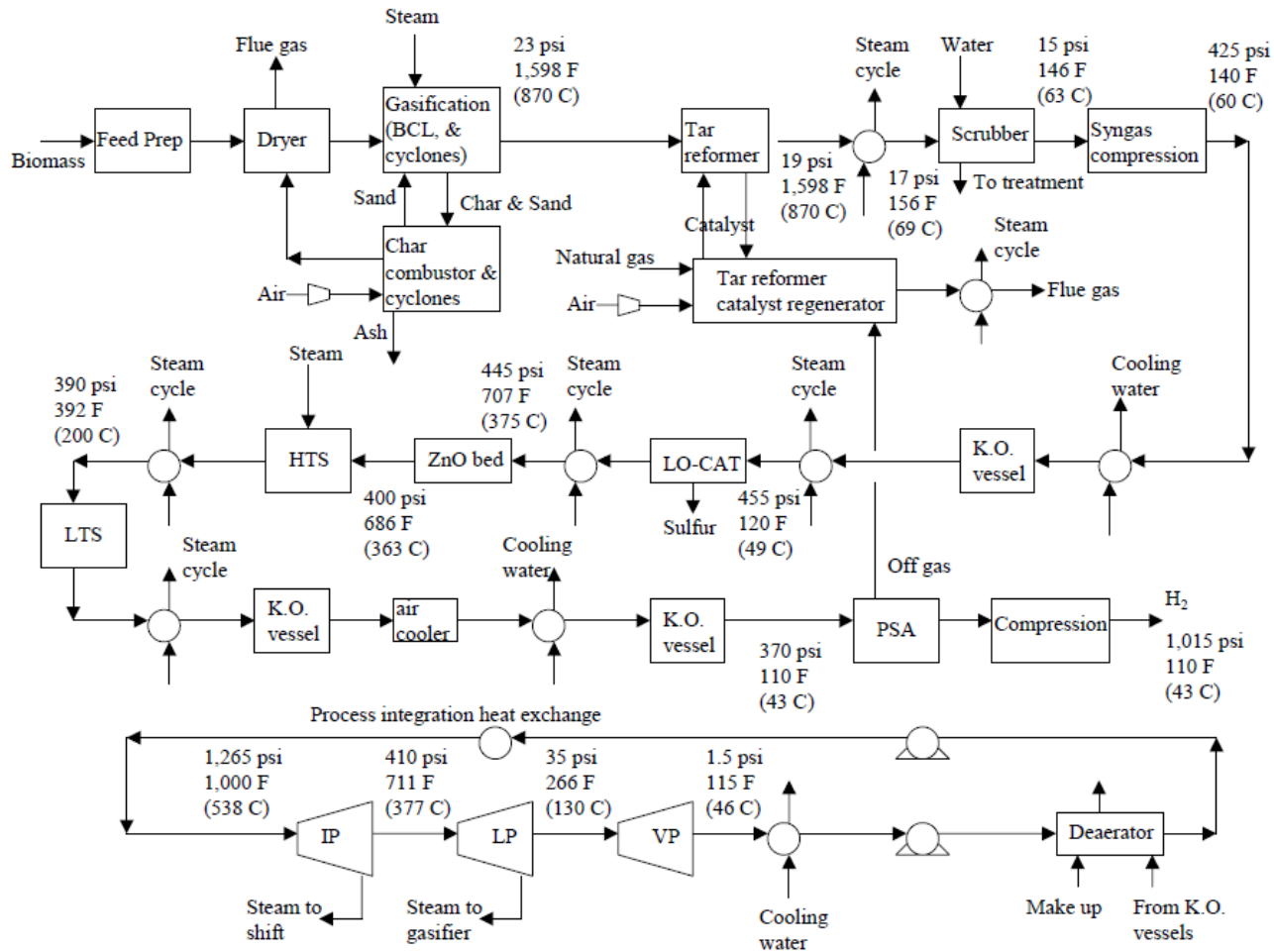


Figure 1-21 : Chaîne de traitement syngaz d'après Spath et al. [70].

1.4.4. Production d'hydrogène

La purification d'hydrogène est l'une des dernières étapes pour produire ce gaz à la pureté désirée. La technologie de référence est le procédé PSA. Il s'agit d'un procédé cyclique qui est par conséquent complexe à modéliser dans le cadre de simulation en régime permanent. Une première option consiste à fixer la récupération et la pureté obtenues en hydrogène en se basant sur des données de la littérature [70]. Cette approche nécessite de se conformer aux spécifications d'entrée pour atteindre la pureté et la récupération visées. Par exemple, il est nécessaire d'avoir un syngaz composé d'au moins 70%vol d'hydrogène pour l'obtenir à 99.9%vol en sortie avec un taux de récupération de 85% [70].

Une autre approche de la modélisation des PSA consiste à utiliser des modèles de type *short-cut* [100]. Ce modèle (Figure 1-22) prend en compte les isothermes d'adsorption de l'adsorbant

sélectionné et suppose l'atteinte de l'équilibre. Une estimation des compositions du gaz après adsorption et issu de la purge est obtenue mais celle-ci ne prend pas en compte l'avancée différenciée des différentes espèces de gaz au sein de la colonne d'adsorption.

La séparation de l'hydrogène par un module membranaire peut également être modélisée comme un simple séparateur ou de manière plus rigoureuse. Le module MEMSIC, développé au LRGP, s'inscrit parfaitement dans l'environnement Aspen Plus® et d'autres logiciels équivalents. Ce module tient compte notamment du type d'écoulement (Figure 1-23) et des perméabilités des différentes espèces pour une membrane spécifique [101].

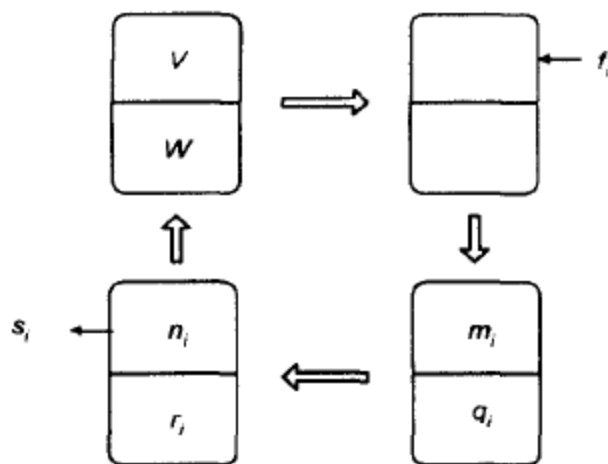


Figure 1-22 : Modèle *short-cut* de PSA [100].

La production d'hydrogène après séparation par PSA a été estimée en lit fluidisé à 76,1 g_{H2}/kg_{biomass} [90] et en lit fluidisé double à 55,0 g_{H2}/kg_{biomass} [95] et 75,2 g_{H2}/kg_{biomass} [96]. Notons également la production estimée en lit fixe à 107,4 g_{H2}/kg_{biomass} [91]. Marcantonio et al. ont également envisagé l'utilisation d'une membrane au palladium qui donne un meilleur taux de récupération de H₂ [75].

Sur le plan énergétique, Kalinci et al. ont démontré que la gazéification et la séparation de l'hydrogène par PSA avaient les plus gros impacts énergétiques et exergétiques de l'ensemble du procédé [92].

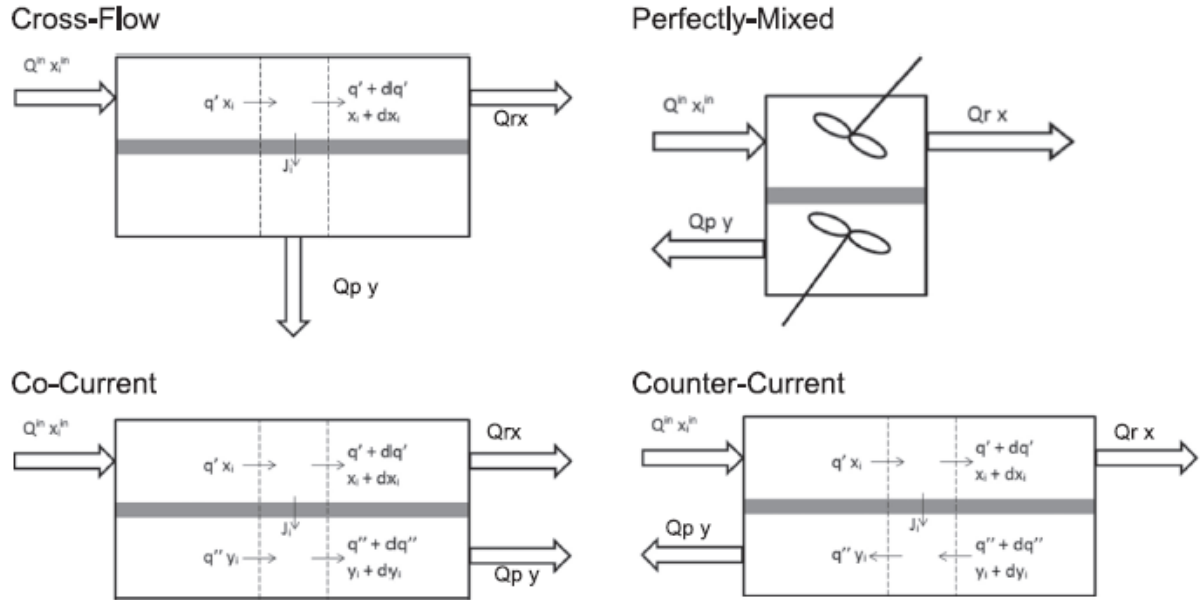


Figure 1-23 : Modèles d'écoulement disponibles dans le module MEMSIC [101].

1.5. Analyse technico-économique

Pour juger de la viabilité économique des procédés, des analyses technico-économiques sont menées. Elles permettent d'estimer l'investissement nécessaire et d'évaluer la rentabilité d'un procédé en fonction des prix d'achats des réactifs, utilités et consommables et des prix de ventes des produits.

1.5.1. Méthodes d'évaluation du CAPEX

Pour estimer le montant de l'investissement initial nécessaire à un projet, différentes méthodes sont disponibles. La précision du résultat dépend du temps alloué à l'analyse, des données disponibles et du stade d'avancement d'un projet.

On distingue cinq types d'évaluation du capital [102] :

- Ordre de grandeur (*ratio estimate*) : basé sur un ratio de production et le coût d'un procédé similaire (précision $\pm 30\%$).
- Étude (*factored estimate*) : basé sur des estimations des principaux équipements et une estimation du capital total en multipliant par des facteurs typiques ($\pm 30\%$).
- Design préliminaire (*budget authorization estimate ou scope estimate*) : basé sur des données plus précises afin d'établir un budget ($\pm 20\%$).
- Définitif (*project control estimate*) : basé sur des données complètes mais avant la fin de la réalisation des plans et du choix des spécifications finales ($\pm 10\%$).
- Détailé (*contractor's estimate*) : basé sur des devis de fournisseurs après réalisation complète des plans et choix des spécifications et études sur site ($\pm 5\%$).

1.5.2. Coût des équipements

S'il l'on dispose du coût C_0 d'un équipement existant de capacité S_0 , le coût du même équipement de capacité S_1 peut être évalué par l'équation 1.4 dans laquelle l'exposant n est propre au type d'équipement considéré et généralement compris entre 0,5 et 1. Par défaut un coefficient $n = 0,6$ est utilisé [103].

$$C_1 = C_0 \left(\frac{S_1}{S_0} \right)^n \quad (1.4)$$

Plus le procédé à évaluer contient d'équipements et plus l'erreur sur le coût global sera faible, les erreurs à la hausse et à la baisse ayant tendance à s'annuler [104].

Par ailleurs, pour estimer plus finement le coût des équipements il faut que le coût de l'équipement soit le plus récent possible et que la capacité de l'équipement à estimer soit relativement proche de l'équipement de base.

1.5.3. Valeur de l'argent dans le temps

Comme l'analyse technico-économique se base le plus souvent sur des estimations de coût d'équipements du passé et non à partir de devis actuels, il est nécessaire d'estimer le renchérissement de l'équipement.

Pour prendre en compte la valeur de l'argent dans le temps, il est possible d'utiliser un indice des prix. Il en existe plusieurs tels que le *Marshall & Swift* (M&S), le *Nelson-Farrar* pour les raffineries, le *Vatavuk* (VAPCCI) pour le contrôle de la pollution de l'air ou le *Chemical Engineering Plant Cost Index* (CEPCI). Ce dernier est généralement plus adapté pour les industries de procédé. La relation pour obtenir le coût actualisé à l'année 2020 à partir d'un coût à l'année x est la suivante.

$$C_{2020} = C_x \cdot \frac{CEPCI_{2020}}{CEPCI_x} \quad (1.5)$$

Le CEPCI utilisé est généralement un CEPCI global qui fait la synthèse des quatre indices principaux. Ils sont relatifs au :

- Coût des équipements (*Equipment*), qui est lui-même une moyenne basée sur des indices de coûts qui suivent :
 - o Échangeurs de chaleurs et cuves (*Heat exchangers and tanks*),
 - o Construction de machines et installations (*Process machinery*),
 - o Conduites, robinetterie et raccords (*Pipe, valves & fittings*),
 - o Instruments de procédé (*Process instruments*),
 - o Pompes et compresseurs (*Pumps & compressors*),
 - o Équipements électriques (*Electrical equipment*),
 - o Soutiens structurels et autres (*Structural supports & miscellaneous*)
- Bâtiments (*Buildings*)

- Ingénierie et supervision (*Engineering and supervision*)
- Main d'œuvre de construction (*Construction labor*)

Ces indices sont publiés tous les mois dans *Chemical Engineering* [105]. L'indice 100 correspond aux années 1957-1959. L'évolution du CEPCI est présenté à la Figure 1-24 et le M&S à la Figure 1-25.

1.5.4. Évaluation de l'investissement en capital total

En plus du prix d'achat de l'équipement (PEC), il faut ajouter de nombreux autres coûts pour pouvoir évaluer le coût en capital total.

On distingue [102] :

- Les coûts directs (DC) qui comprennent :
 - o L'équipement, la livraison, l'installation, l'instrumentation, les raccordements (conduites et électriques), l'isolation, la peinture (50-60% FCI)
 - o Les bâtiments de procédé et services d'appuis (10-70% PEC)
 - o L'adaptation du site et les bâtiments de service (40-100% PEC)
 - o Le terrain (1-2% FCI)
- Les coûts indirects (IC) composés de :
 - o Ingénierie et supervision (5-30% DC)
 - o Frais juridiques (1-3% FCI)
 - o Frais de constructions et honoraires d'entrepreneurs (10-20% FCI)
 - o Contingence (5-15% FCI)
- Investissement en capital fixe (FCI = DC + IC)
- Le fond de roulement (WC, 10-20% TCI)
- L'investissement en capital total (TCI = FCI + WC)

L'évaluation de l'ensemble de ces coûts est fastidieuse et source de fortes incertitudes. Il est généralement préférable d'utiliser un coefficient global permettant d'estimer l'investissement en capital fixe à partir du coût des équipements livrés (équation 1.6).

$$FCI = DC + IC = \sum LF \cdot \text{Coût d'achat d'équipement} \quad (1.6)$$

Ce coefficient est le facteur de Lang (*LF*). Sa valeur dépend du type de procédé (Tableau 1-5).

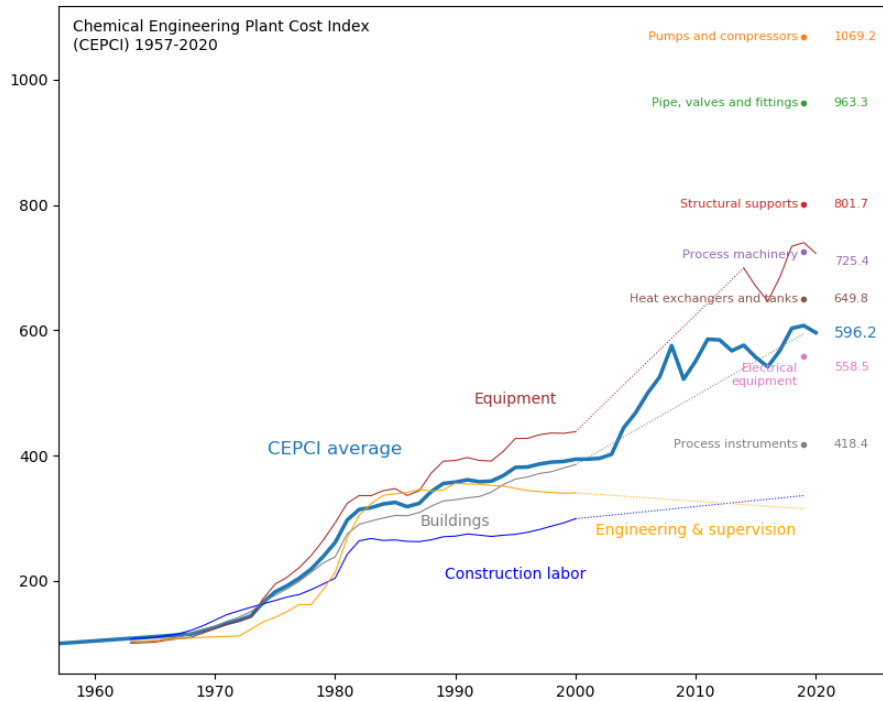


Figure 1-24 : Chemical Engineering Plant Cost Index (CEPCI) [105].

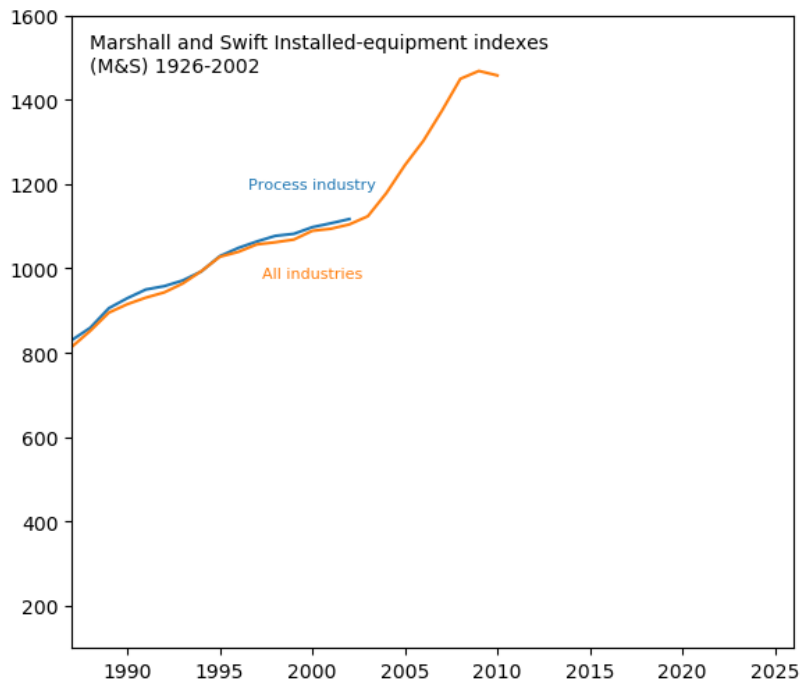


Figure 1-25 : Indices Marshall and Swift (l'indice 100 correspond à l'année 1926).

Tableau 1-5 : Facteur de Lang [102].

Type de procédé	Investissement en capital fixe (FCI)	Investissement en capital total (TCI)
Solide	4,0	4,7
Solide-fluide	4,3	5,0
Fluide	5,0	6,0

1.5.5. Évaluation du coût de production

Le coût de production dépend lui aussi de nombreux paramètres [102] :

- Le coût de fabrication incluant :
 - o Les coûts directs de production (matières premières, prix du travail et de supervision, utilités, maintenance et réparations, consommables, frais de laboratoire, brevets et royalties)
 - o Les frais fixes (dépréciation, impôts, assurances, locations, intérêts d'emprunt)
 - o Les frais indirects (entretien général et frais généraux de l'usine, frais généraux de paie, emballage, services médicaux, sécurité et protection, restaurants, loisirs, espaces de repos, laboratoires et installations de stockage)
- Les frais généraux (administratif, distribution et vente, recherche et développement)
- Coût total de production = coût de fabrication + frais généraux
- Gains bruts = revenus – coût total de production

1.5.6. Flux de trésorerie et critères économiques

Pour déterminer la viabilité économique d'une usine, il est nécessaire d'évaluer les flux de trésorerie pour la durée de vie de l'unité (Figure 1-26).

Le profit net après impôt à l'année k est calculé avec l'équation 1.7, dans laquelle R est le revenu des ventes, COM le coût de fabrication, d_k la dépréciation à l'année k et t le taux d'imposition.

$$NET\ PROFIT_k = (R - COM - d_k) \cdot (1 - t) \quad (1.7)$$

Le flux de trésorerie de l'année k est déterminé par l'équation 1.8.

$$CASH\ FLOW_k = (R - COM - d_k) \cdot (1 - t) + d_k \quad (1.8)$$

Pour estimer l'opportunité d'un investissement, la valeur actualisée nette (*net present value* NPV) peut être calculée par l'équation 1.9. Cette méthode prend en compte la valeur future de l'argent en supposant un taux d'actualisation i .

$$NPV = -TCI + \sum_n \frac{CASH FLOW_k}{(1+i)^k} \quad (1.9)$$

Le prix minimum de vente d'un produit pour assurer un retour sur investissement de 10% est le prix minimum de vente qui annule la valeur actualisée nette à la fin de la durée de vie de l'usine en prenant comme pour le taux d'actualisation 10%.

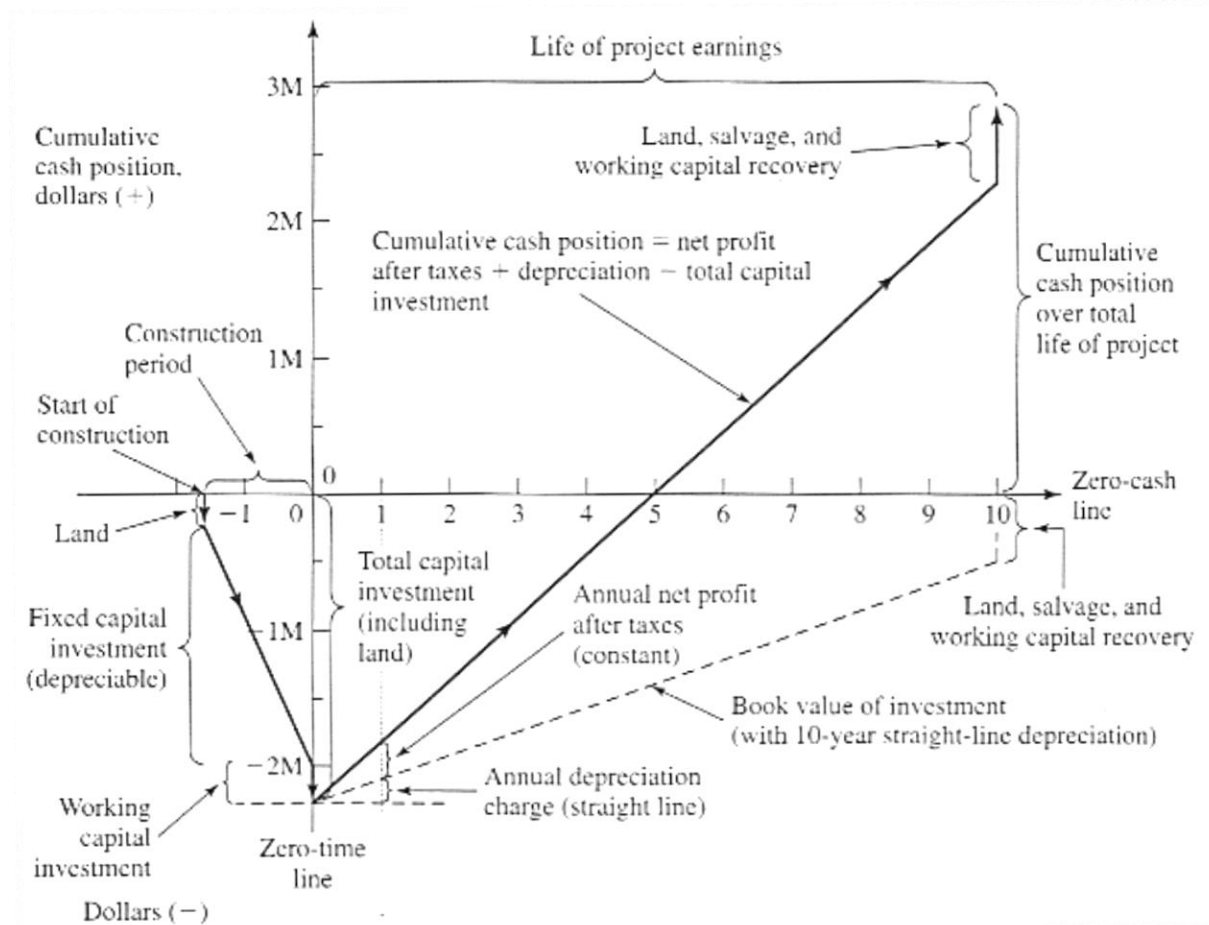


Figure 1-26 : Flux de trésorerie cumulé [102].

1.5.7. Analyses technico-économiques production d'hydrogène issu de biomasse

Dans le cas de la production d'hydrogène issu de biomasse, ces études sont généralement basées sur de grosses unités qui nécessitent des quantités très importantes de biomasse [70]. Plusieurs études, présentées dans le Tableau 1-6, ont été menées pour évaluer le coût de l'hydrogène produit à partir de biomasse. Ces études tendent à maximiser la production d'hydrogène sans nécessairement s'intéresser à la valorisation d'autres vecteurs énergétiques. Il y a pourtant beaucoup de chaleur qui est co-produite par ce type de procédé et il est préjudiciable de ne pas la valoriser. Encore faut-il que la chaleur disponible (puissance et niveau thermique) soit en adéquation avec le besoin de chaleur du site industriel ou du réseau de chaleur.

Tableau 1-6 : Sélection de précédentes analyses technico-économique de procédés de production d'hydrogène issu de gazéification de biomasse.

	Technologie	Biomasse	Taille [MW _{biomasse}]	Efficacité	Spécification H ₂ et prix	Ref.
Iwasaki, 2003	Pyrolyseur, craqueur, CO- shift, PSA ^b , moteur	Biomasse ligneuse	100 t/j 18.6 MW _{PCI}	H ₂ = 47.9% PCS (net) (5.9 t/j)	99.99% - 200 bar 4.28 \$ ₂₀₀₃ /kg ^a	[106]
Spath et al., 2005	DFB ^b , reformeur, laveur, LO- CAT ^b , lit ZnO, vaporeformeur, WGS ^b , PSA ^b	Plaquette de peuplier hybride	2000 t/j 434 MW _{PCI}	H ₂ = 49.8% PCI (net) 152 t/j	99.9% - 70 bar 1.38 \$ ₂₀₀₂ /kg	[70]
				H ₂ = 55.3% PCI (net) 163 t/j	99.9% - 70 bar 1.24 \$ ₂₀₀₂ /kg	
Lv et al., 2008	Lit fixe <i>downdraft</i> (O ₂), CO-shift, PSA ^b , moteur	Résidus forestiers	6.40 t/j 1.4 MW _{PCI}	H ₂ = 51.5% (brut) 0.52 t/j ^d	1.69 \$ ₂₀₀₈ /kg ^a	[107]
Parks et al., 2011	Première unité, gazéifieur, reformeur, WGS, PSA ^b	Biomasse ligneuse	500 t/j 109 MW _{PCI} ^c	H ₂ = 43.8% PCI (brut) 32.4 t/j	99.99% 5.40-7.70 \$ ₂₀₀₉ /kg	[108]
	N ^e me unité.			H ₂ = 45.7% PCI (brut) 135 t/j	99.99% 2.80-3.80 \$ ₂₀₀₉ /kg	
Sara et al., 2016	FB ^b indirect, chandelles catalytiques, WGS ^b , PSA ^b	Coques d'amandes	4.80 t/j ^d 1 MW	H ₂ = 46- 50% PCI ^d 0.033-0.036 t/j	9.5-13 € ₂₀₁₆ /kg ^a	[109]
			4.80 t/j ^d	H ₂ = 20% PCI ^d	6 bar	

Sentis et al., 2016	FB ^b indirect, chandelles catalytiques, WGS ^b , PSA ^b	Coques d'amandes	1 MW	Global = 30% PCI 0.14 t/j ^d	5.6-7.1 € ₂₀₁₆ /kg ^a	[110]
			48.0 t/j ^d 10 MW	H ₂ = 20% PCI ^d Global = 30% PCI 1.4 t/j ^d	6 bar 2.7-2.9 € ₂₀₁₆ /kg ^a	
Salkuyeh et al., 2018	EF ^b haute pression oxygène, ASU ^b , LO-CAT, WGS ^b , PSA ^b	Résineux canadiens	5 840 t/j 1200 MW _{PCI} ^d	H ₂ = 54% PCI ^d Global = 56% PCI 454 t/j	3.4 \$ ₂₀₁₈ /kg ^a	[111]
	Avec capture de carbone			H ₂ = 50% PCI ^d Global = 50% PCI 454 t/j	3.5 \$ ₂₀₁₈ /kg ^a	
	FB atmosph. chauffé indirect., reformeur, laveur, LO-CAT, WGS ^b , PSA ^b		7 380 t/j 1500 MW _{PCI} ^d	H ₂ = 42% PCI ^d Global = 45% PCI 454 t/j	3.1 \$ ₂₀₁₈ /kg ^a	
	Avec capture de carbone			H ₂ = 41% PCI ^d Global = 41% PCI 454 t/j	3.5 \$ ₂₀₁₈ /kg ^a	

^aAnnée supposée.

^bPSA: pressure swing adsorption, DFB: dual fluidized bed, WGS: water gas shift, FB: fluidized bed, ASU: air separation unit, EF: entrained flow.

^cHypothèse PCI 18.7 MJ/kg

^dEstimé

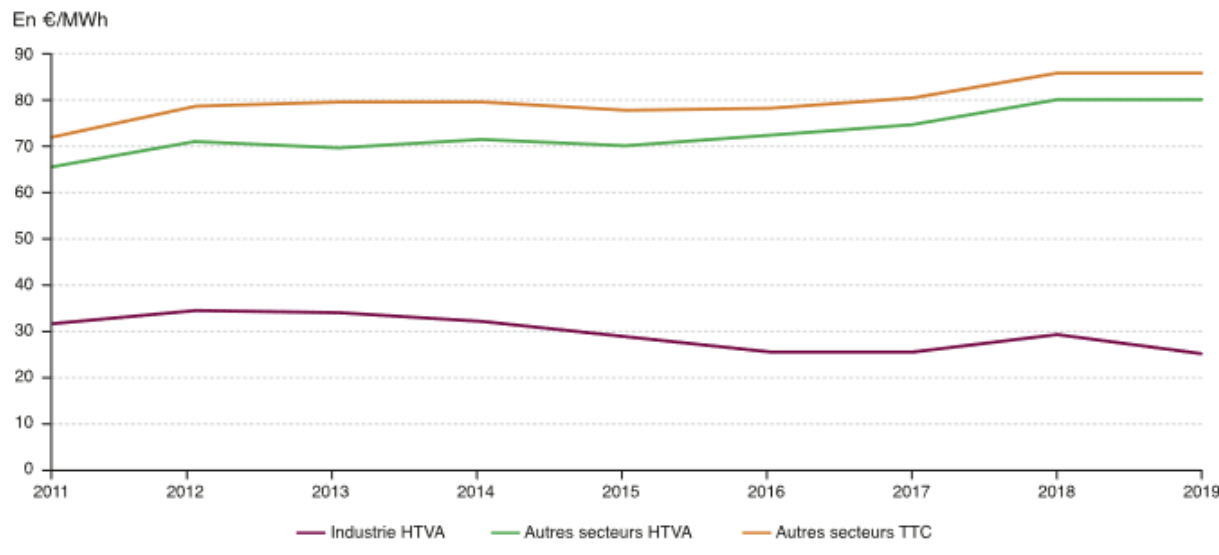
D'autres études se sont intéressées à la production d'hydrogène (et de monoxyde de carbone) pour la synthèse de carburants via le procédé Fischer-Tropsch [112-114]. De nombreuses sources de coûts d'équipements peuvent être trouvées dans les publications en référence [86,102,115,115-120]

1.5.8. Prix des produits secondaires

L'évaluation des coûts et revenus d'une unité industrielle nécessite de connaître un certain nombre de coûts tels que celui d'utilités comme l'électricité ou le prix de vente de la chaleur.

1.1.10 Prix chaleur industrielle

En France, d'après le ministère de la transition écologique, le prix de la chaleur industrielle s'établit autour de 30 €/MWh HTVA [121]. Comme l'illustre la Figure 1-27, ce prix est resté stable au cours de la dernière décennie.



Sources : EARCF ; EACEI ; calculs SDES

Figure 1-27 : Evolution du prix de la chaleur commercialisée en France 2011-2019 (reproduit de [121]).

1.1.11 Prix électricité

L'électricité est organisée comme un marché (SPOT) sur le continent européen. Tous les jours des échanges sont réalisés entre pays européens afin d'assurer la stabilité du réseau électrique. Pour arbitrer ces échanges, un prix est attribué à l'électricité en tout temps et évolue en fonction de la production et la consommation. La Figure 1-28 donne l'évolution du prix moyen journalier de l'électricité sur le marché SPOT pour différents pays européens depuis 2016. Le prix de l'électricité se situe dans la moyenne de ces pays, à moins de 50 €/MWh.

A ce prix s'ajoute le coût de l'acheminement et des taxes. En 2019, l'électricité coûtait en moyenne 115 €/MWh hors TVA pour tous les consommateurs, 80 €/MWh dans le secteur de l'énergie et 71 €/MWh dans le secteur de l'industrie (Tableau 1-7) [121].

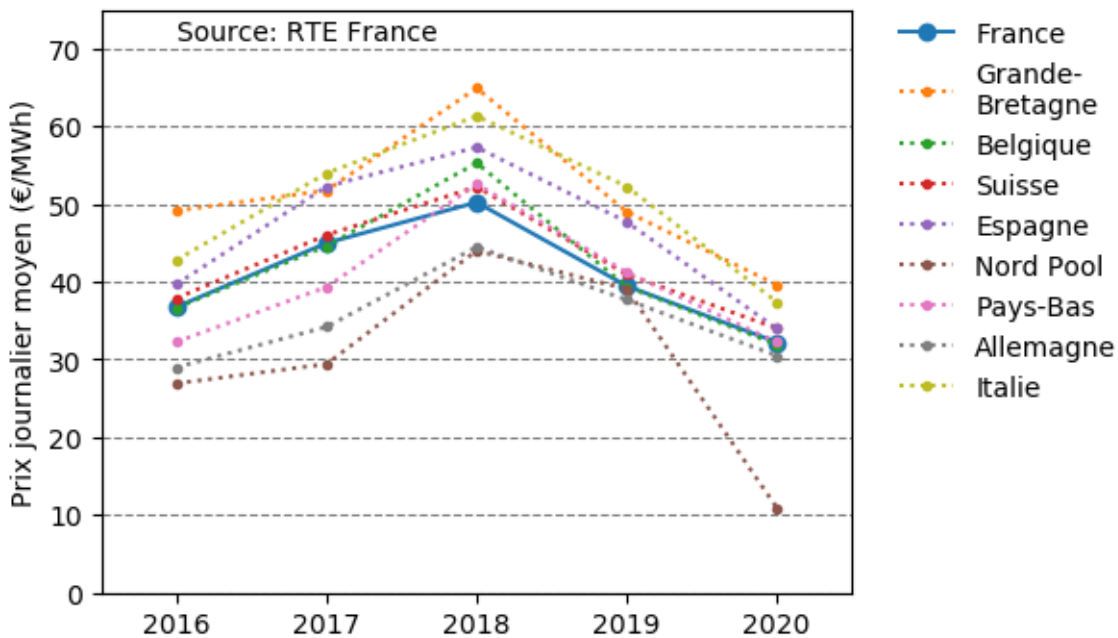


Figure 1-28 : Evolution du prix moyen journalier sur le marché de l'électricité (SPOT) dans différents pays européens.

En €/MWh

	2011	2012	2013	2014	2015	2016	2017	2018	2019
Énergie (hors électricité)	72	74	76	77	78	71	69	74	80
Consommation finale TTC*	100	104	110	114	119	116	117	120	126
Agriculture-pêche	90	90	92	105	109	112	114	122	128
Industrie	66	68	71	72	72	66	64	67	71
Transports	54	55	54	54	54	49	47	52	53
Tertiaire	95	97	103	108	112	105	107	108	115
Résidentiel HTVA	114	118	125	133	138	140	141	146	152
Résidentiel TTC	134	138	147	157	162	165	166	171	178
Tous secteurs hors TVA	92	96	101	105	109	106	107	110	115
Tous secteurs avec TVA*	99	103	109	114	118	115	116	119	125

* La TVA est incluse uniquement pour le secteur résidentiel, étant déductible par les entreprises.

Note : la branche électricité et l'autoconsommation sont exclues du champ.

Source : calculs SDES

Tableau 1-7 : Evolution du prix moyen de l'électricité en France 2011-2019 selon les secteurs (reproduit de [121]).

1.6. Analyse de cycle de vie

1.6.1. Contexte

La prise de conscience des enjeux environnementaux liés à l'activité humaine a démarré très tôt, dès les années 1970. L'une des préoccupations de l'époque concernait l'amincissement de la couche d'ozone causée par les chlorofluorocarbures (CFC). Un autre fait marquant fut la parution du rapport « Les limites à la croissance », aussi appelé « Rapport du Club de Rome ». Avec l'émergence des premiers ordinateurs, les auteurs Dennis et Donella Meadows et Jorgen Randers y exposent l'un des tous premiers modèles du Monde. Ils y exploraient les devenirs possibles du Monde selon dix scénarios [122]. Le constat est alarmant, la population mondiale sera amenée à décroître au cours du XXIème siècle dans la quasi-totalité des scénarios (Figure 1-29). Seules exceptions, les scénarios qui cherchent à stabiliser la population et la production industrielle par habitant à partir de 2002. Des technologies doivent, en outre, être capables d'améliorer l'efficacité de l'utilisation des ressources, de réduire les pollutions industrielles et l'érosion des terres tout en augmentant la production agricole.

FIGURE 4-11 – Scénario 1 : un point de repère

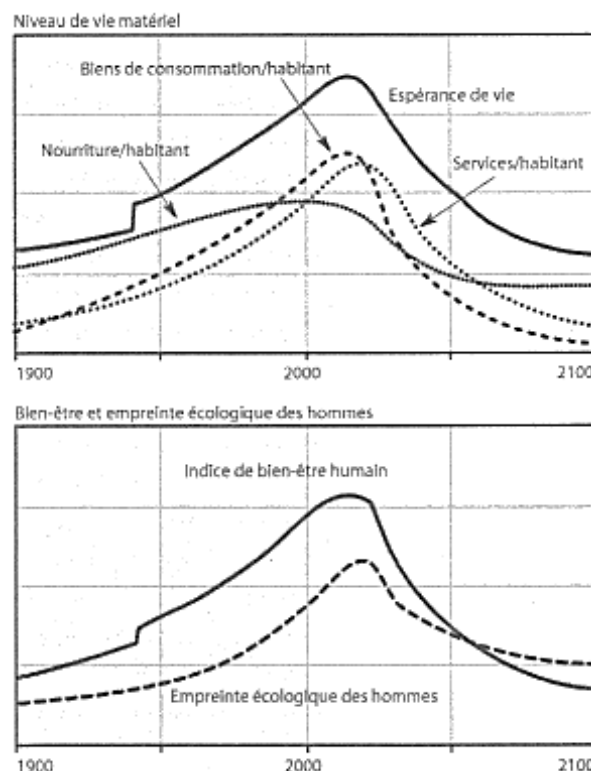
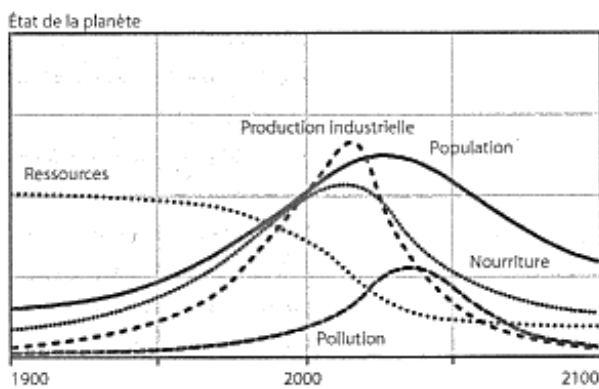


Figure 1-29 : Modèle World3 [122].

D'autres alertes ont été émises par la communauté scientifique lors du franchissement de limites planétaires [123]. Le groupe intergouvernemental pour l'étude sur le climat (GIEC) publie régulièrement des rapports sur le sujet [11].

« L'empreinte humaine sur l'environnement planétaire est devenue si vaste et intense qu'elle rivalise avec certaines des grandes forces de la Nature en termes d'impact sur le système Terre » déclarait Paul Crutzen en 2000. C'est à ce scientifique que l'on doit le terme d'Anthropocène (l'ère de l'Homme) pour nommer cette nouvelle ère géologique qui a suivi l'Holocène [124].

Face à cette prise de conscience, de nouveaux outils sont apparus pour juger de la pertinence environnementale des produits et des procédés. C'est notamment le cas de l'analyse de cycle de vie (ACV).

1.6.2. Principe de l'ACV

Cet outil permet de quantifier les performances environnementales d'un produit ou d'un procédé en tenant compte de l'ensemble de son cycle de vie depuis l'extraction des ressources initiales à la gestion ultime des déchets générés au cours de sa fabrication et de sa fin de vie.

Au niveau de la conception, l'ACV a pour objectif d'analyser la contribution de chaque étape du cycle de vie pour en diminuer ses impacts. L'ACV peut aussi être utilisée pour comparer plusieurs systèmes équivalents et choisir celui qui offre les meilleures opportunités [125].

1.6.3. Les étapes de l'ACV

L'ACV consiste en quatre étapes [125] :

- La définition des objectifs et du champ de l'étude,
- La réalisation de l'inventaire de cycle de vie,
- L'évaluation des résultats,
- L'interprétation des résultats pour répondre aux objectifs fixés.

Cette méthode est standardisée par les normes ISO 14040 et ISO 14044 [126,127]. La première définit les bases de la méthode tandis que la seconde détaille les exigences et les lignes directrices pour mener à bien l'analyse.

La définition du champ de l'étude passe par la définition de la fonction du système et de l'unité fonctionnelle. Il convient de sélectionner la méthode d'évaluation des impacts correspondant à la

motivation de l'étude. Les frontières du système doivent également être définies : les frontières physiques « du berceau à la tombe » ou « du berceau à la porte », les frontières géographiques qui auront un impact sur les émissions de différents flux tels que l'électricité qui dépend du mix électrique considéré.

La méthode d'évaluation peut évaluer les impacts (*midpoint*) ou les dommages (*endpoint*). Dans le premier cas, les résultats s'intéressent à évaluer des flux de polluants, par exemple pour le potentiel de réchauffement climatique, des émissions de CO₂ équivalentes. Dans le second cas, ce sont les effets sur l'homme ou l'environnement qui sont évalués, en terme de disparition d'espèces ou de mortalité. Cette dernière méthode donne des incertitudes supplémentaires en raison du passage des impacts aux dommages.

L'inventaire de cycle de vie consiste à répertorier l'ensemble des flux entrants et sortants du système considéré. Parmi ces flux sont distingués les flux entrants issus de l'environnement (air, eau...) et sortants (émissions à l'atmosphère, dans les eaux) des flux entrants et sortants de la technosphère.

Ces flux issus de la technosphère sont des flux de référence issus de précédentes études. Ils sont disponibles dans des bases de données telles qu'Ecoinvent [128].

Dans le cas de procédés multi produits, il convient d'associer à chaque produit ses impacts. Pour cela deux méthodes :

- ACV attributionnelle consiste à attribuer à chaque produit une part des impacts basée sur un prorata massique, volumique, énergétique ou encore économique (allocation des impacts). Dans ce cadre le produit ou procédé existe déjà.
- L'ACV conséquentielle consiste à évaluer l'impact d'un changement de système global de production de plusieurs produits par rapport à un (des) système(s) de référence (expansion du système). Cette approche permet d'évaluer les impacts de l'ajout de ce système au système actuel. Néanmoins, cette approche nécessite un plus grand nombre de données.

1.6.4. ACV aux filières hydrogène

Valente et al. [129] ont proposé une revue de la littérature des ACV portant sur les systèmes de production d'hydrogène. L'unité fonctionnelle couramment utilisée est basée sur une unité de masse ou d'énergie d'hydrogène.

La question des systèmes multi-produits se pose particulièrement pour les procédés thermochimiques (Figure 1-30). La moitié des études considérées a adopté l'extension des frontières, l'autre moitié l'allocation avec une prédominance pour l'énergie ou l'exergie

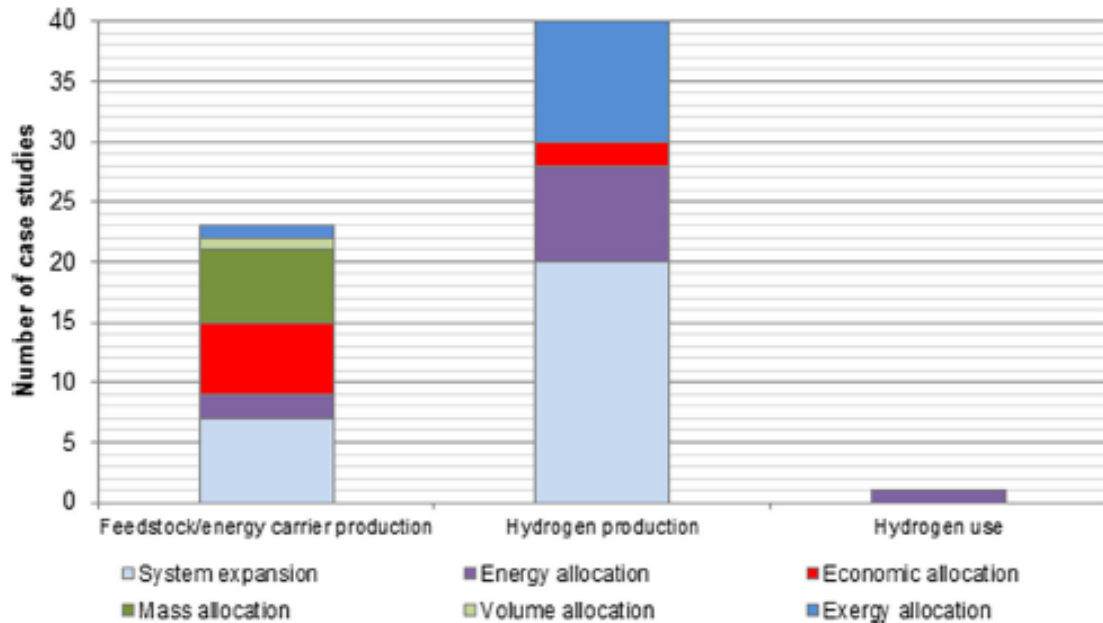


Figure 1-30 : Choix d'allocation selon l'étape pour différents systèmes de production d'hydrogène [129].

Les impacts les plus étudiés (Figure 1-31) sont par ordre d'occurrence, le potentiel de réchauffement global (GWP), l'acidification (AP), la consommation d'énergie (CED), l'eutrophisation (EP), la destruction de la couche d'ozone (ODP), la formation d'oxydants photochimiques (POFP), la consommation d'énergies fossiles. Dans moins de 20% des études, la consommation d'énergies non-renouvelables, l'épuisement des ressources naturelles (AD), la toxicité (HT), utilisation des terres (LOP) et la santé humaine (HH) sont aussi considérées.

La méthode IPCC est majoritairement utilisée pour GWP, la méthode VDI ou GREET pour CED et la méthode CML [130] pour les autres impacts.

Valente et al. ont aussi travaillé sur l'harmonisation des impacts GWP, CED et AP [131–133]. Un aspect important dans la comparaison de différents systèmes produisant de l'hydrogène est de s'assurer que l'hydrogène produit est au même niveau de pression

Le Tableau 1-8 présente les principaux paramètres utilisés pour réaliser des ACV sur les procédés de production d'hydrogène issu de la gazéification de biomasse.

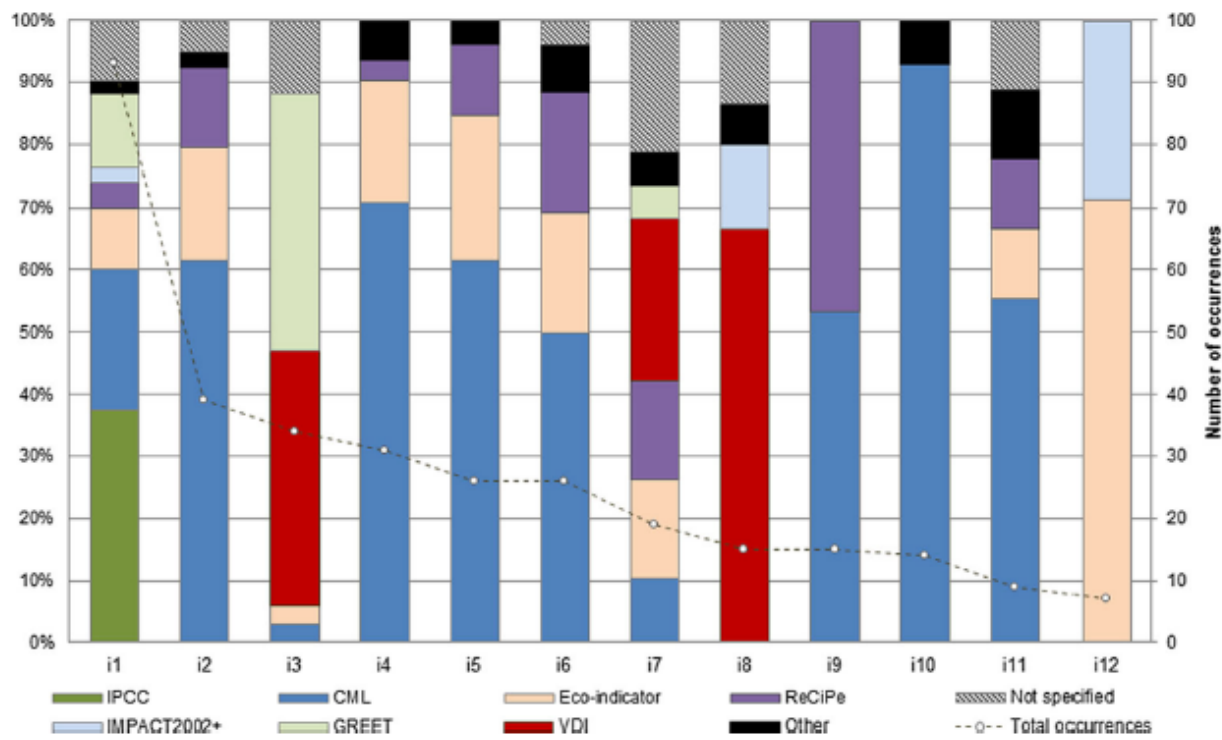


Figure 1-31 : Choix d'indicateurs ACV et méthodes considérées (i1 GWP, i2 : AP, i3 : CED, i4 : EP, i5 : ODL, i6 : POPH, i7 : consommation d'énergie (fossile), i8 : consommation d'énergie (non-renouvelable), i9 : AD, i10 : HT, i11 : LOP, i12 HH (dommages) [129]

Tableau 1-8 : Liste non-exhaustive d'ACV (“berceau à la porte”) de production d'hydrogène issu de gazéification de biomasse [129].

	Technologie ^a	Type de biomasse	Taille	Unité fonctionnelle	Autres produits	Methode & impacts ^c	Ref.
Koroneos et al. 2008	IG, laveur, reformeur, WGS, liquéfaction	Biomasse	Non spécifié	1 MJ de H ₂ liquide	Non	EcoIndicator 95 GWP, AP, EP	[94]
Tock and Maréchal, 2012	Torréfaction, FICFB, SR,	Bois	380 MW _{LHV}	1 kJ de biomasse	Non	IPCC GWP	[134]

	laveur, WGS, AGR, PSA						
Moreno and Dufour, 2013	Lit fixe, reformeur, WGS, PSA	Vigne, amandes, pin, eucalyptus	Non spécifié	1 Nm ³ de H ₂ 99.9% vol	Non	CML GWP, AP, EP	[135]
Susmozas et al., 2013	DFB, reformeur, laveur, LO-CAT, WGS, PSA, cycle vapeur	Peuplier	Non spécifié	1 kg de H ₂ 99.9% vol 28 bar	Electricité (allocation économique)	CML ADP, GWP, ODP, POFP, LC, AP, EP, CED	[136]
Iribarren et al., 2014	IG, reformeur, laveur, SR, WGS, PSA	Peuplier	Adapté de Spath et al. [70]	1 m ³ STP H ₂ 25.5 bar	Soufre (approche émissions évitées)	CML CED, GWP, ODP, POFP, LC, AP EP	[137]
Muresan et al., 2014	DFB, WGS, RME laveur, AGR, PSA, reformeur	Biomasse	70 MW _{PCI} ^b	1 MW H ₂ 99.99% vol 22.5 bar	Non	CML GWP, AP, EP, ADPF, HTP	[138]
Salkuyeh et al., 2018	Voir Tableau 1-6.			1 kg de H ₂	Electricité	GWP	[70]
Valente et al., 2019	Voir Susmozas et al. (2013)			1 kg de H ₂	Electricité	Méthode harmonisée [133] GWP, AP, CED	[139]

^aAcronymes - IG: indirect gasifier, SR: steam reformer, PSA: pressure swing adsorption, AGR: acid gas removal, DFB: dual fluidized bed, WGS: water gas-shift, FICFB: fast internally circulating fluidized bed.

^bHypothèse biomasse PCI 18 MJ/kg

^cAcronymes impacts – GWP: global warming, AP: acidification, EP: eutrophication, ODP: ozone layer depletion, POFP: photochemical oxidant formation, LC: land competition, CED: cumulative energy demand, ADPF: abiotic depletion fossil, HTTP: human toxicity.

1.7. Bilan de la revue bibliographique et approche proposée

Compte tenu de la nature du combustible, relativement peu dense énergétiquement en comparaison aux énergies fossiles, et afin de limiter les impacts associés au transport de cette ressource, une faible aire d'approvisionnement est visée (rayon de l'ordre de 100 km), ce qui limite la puissance du gazéifieur à quelques dizaines de mégawatts.

Ce projet s'intéresse à la valorisation de la biomasse et des déchets comme combustible de la gazéification. En raison de la faible taille de l'installation envisagée, la production simultanée de trois vecteurs énergétiques pourrait être envisagée : électricité, chaleur et hydrogène. La cogénération (électricité, chaleur) constitue la voie classique. Néanmoins, compte tenu des coûts de production actuels de l'électricité, la viabilité économique de telles unités est très précaire. L'hydrogène possède une plus grande valeur ajoutée, sa valorisation pourrait pallier les surcoûts liés à l'échelle.

L'objectif de ce projet est d'évaluer la pertinence économique et environnementale de petites unités de gazéification de biomasse et déchets pour produire plusieurs vecteurs énergétiques et autres produits d'intérêt.

Les objectifs spécifiques de cette thèse sont :

- La conception d'un procédé innovant de gazéification de biomasse et de déchets pour la valorisation de plusieurs vecteurs énergétiques,
- L'établissement des bilans de matière et d'énergie de ce procédé,
- L'analyse technico-économique du procédé basée sur différents critères : valeur actualisée nette, indice de profitabilité, taux de retour interne,
- Et l'évaluation environnementale du procédé au moyen d'une analyse de cycle de vie.

1.8. Bibliographie

- [1] Cuny H, Piton B. Disponibilités en bois des forêts de la région Grand-Est à l'horizon 2037. Tome 1 : rapport. IGN - DIRNE; 2018.
- [2] The State of the World's Forests 2020. FAO and UNEP; 2020. <https://doi.org/10.4060/ca8642en>.
- [3] Forest Europe. State of Europe's Forests 2020. 2020.
- [4] Ceccherini G, Duveiller G, Grassi G, Lemoine G, Avitabile V, Pilli R, et al. Abrupt increase in harvested forest area over Europe after 2015. *Nature* 2020;583:72–7. <https://doi.org/10.1038/s41586-020-2438-y>.
- [5] Polémiques sur le stock d'arbres des forêts européennes. *Le Monde.fr* 2021.
- [6] Dreyer E, Bontemps J-D, Picard N, Marty P. Comment améliorer la mesure des récoltes de bois en Europe ? *The Conversation* 2021. <http://theconversation.com/comment-ameliorer-la-mesure-des-recoltes-de-bois-en-europe-163844> (accessed October 29, 2021).
- [7] Grassi G, Cescatti A, Ceccherini G. JRC study on harvested forest area: resolving key misunderstandings. *IForest* n.d.;14:5.
- [8] Colin A, Thivolle-Cazat A. Disponibilités forestières pour l'énergie et les matériaux à l'horizon 2035. Tome 1 : Rapport. ADEME, IGN, COPACEL; 2016.
- [9] Phan C, Plouhinec C. Chiffres clés des énergies renouvelables - Edition 2021. Ministère de la transition écologique; 2021.
- [10] Couturier C, Charru M, Doublet S, Pointereau P. Le scénario Afterres2050 - version 2016. SOLAGRO; 2016.
- [11] IPCC. Summary for Policymakers. In: Climate Change 2021: The Physical Science Basis. Contribution of Working Group I to the Sixth Assessment Report of the Intergovernmental Panel on Climate Change. Cambridge University Press; 2021.
- [12] Norske Skog Golbey. Norske Skog Golbey n.d. <https://norskeskog-golbey.com/> (accessed March 6, 2022).
- [13] En forêt, la crise des scolytes s'accélère partout en France. Office national des forêts 2021. <https://www.onf.fr/onf/+/2e0::epidemie-de-scolytes-les-forestiers-de-lonf-sur-le-front.html> (accessed March 3, 2022).
- [14] Cuny H. Communication personnelle 2021.
- [15] Mercuriales trimestrielles - Centre d'Etudes de l'Economie du Bois (CEEB) 2020. <http://www.ceebois.fr/> (accessed September 16, 2020).
- [16] Yordanova S, Migette J-C. Enquête sur les prix des combustibles bois pour le chauffage industriel et collectif en 2017-2018. 2017.
- [17] Petit S, Moure G. Les réseaux de chaleur et de froid. Chiffres clés, analyses et évolution. Résultat de l'enquête annuelle - édition 2019. 2019.
- [18] Un mix de gaz à 100% renouvelable en 2050 ? ADEME; 2018.

- [19] Suleman F, Dincer I, Agelin-Chaab M. Environmental impact assessment and comparison of some hydrogen production options. International Journal of Hydrogen Energy 2015;40:6976–87. <https://doi.org/10.1016/j.ijhydene.2015.03.123>.
- [20] Hydrogen Production Processes | Department of Energy n.d. <https://www.energy.gov/eere/fuelcells/hydrogen-production-processes> (accessed April 16, 2018).
- [21] Hydrogène énergie. Connaissance des Énergies 2011. <https://www.connaissancesedesenergies.org/fiche-pedagogique/hydrogene-energie> (accessed April 9, 2018).
- [22] Hydrogen Production | Department of Energy n.d. <https://www.energy.gov/eere/fuelcells/hydrogen-production> (accessed May 23, 2018).
- [23] The Future of Hydrogen. IEA; 2019.
- [24] Etude de la demande potentielle d'hydrogène renouvelable et/ou bas carbon en France à 2030. Résumé exécutif/Synthèse. AFHYPAC; 2020.
- [25] Global Hydrogen Review 2021. IEA; 2021.
- [26] Ministère de la Transition Energétique et Solidaire. Stratégie française pour l'énergie et le climat - Programmation Pluriannuelle de l'énergie 2019-2023 2024-2028. 2018.
- [27] ADEME. Hydrogène : analyse des potentiels industriels et économiques en France. 2019.
- [28] Philibert C. Perspectives on a Hydrogen Strategy for the European Union n.d.:43.
- [29] Bessarabov D, Wang H, Li H, Zhao N. PEM Electrolysis for Hydrogen Production: Principles and Applications. CRC Press; 2016.
- [30] Surla K. Hydrogène 2019.
- [31] Binder M, Kraussler M, Kuba M, Luisser M. Hydrogen from biomass gasification 2018:85.
- [32] Conditions techniques et économiques d'injection d'hydrogène dans les réseaux de gaz naturel. 2019.
- [33] CRE. La CRE constate une nouvelle hausse du coût du gaz naturel importé entraînant une hausse des tarifs réglementés de vente de gaz naturel pour le mois d'octobre 2021. <https://www.cre.fr/Actualites/la-cre-constate-une-nouvelle-hausse-du-cout-du-gaz-naturel-importe-entraignant-une-hausse-des-tarifs-reglementes-de-vente-de-gaz-naturel-pour-le-mois-d-octobre-2021> (accessed October 29, 2021).
- [34] Composition du prix de l'essence et du gazole en France : coûts et taxes, chiffres clés. Connaissance des Énergies 2018. <https://www.connaissancesedesenergies.org/fiche-pedagogique/structuration-des-prix-de-l-essence-et-du-gazole-france> (accessed October 29, 2021).
- [35] Véhicule à hydrogène. Wikipédia 2021.
- [36] Stratégie nationale pour le développement de l'hydrogène décarboné en France 2020.
- [37] Ammoniac. L'Élémentarium n.d. <https://lelementarium.fr/product/ammoniac/> (accessed October 29, 2021).
- [38] Méthanol - Produits SCF. Société Chimique de France (SCF) n.d. <https://new.societechimiquedefrance.fr/produits/methanol/> (accessed October 29, 2021).

- [39] Dufour A. Optimisation de la production d'hydrogène par conversion du méthane dans les procédés de pyrolyse/gazéification de la biomasse. Université Henri Poincaré, 2007.
- [40] Histoire du gaz manufacturé. Wikipédia 2022.
- [41] Philippe Lebon. Wikipédia 2022.
- [42] Molino A, Chianese S, Musmarra D. Biomass gasification technology: The state of the art overview. *Journal of Energy Chemistry* 2016;25:10–25. <https://doi.org/10.1016/j.jec.2015.11.005>.
- [43] La Villetta M, Costa M, Massarotti N. Modelling approaches to biomass gasification: A review with emphasis on the stoichiometric method. *Renewable and Sustainable Energy Reviews* 2017;74:71–88. <https://doi.org/10.1016/j.rser.2017.02.027>.
- [44] Molino A, Larocca V, Chianese S, Musmarra D. Biofuels Production by Biomass Gasification: A Review. *Energies* 2018;11:811. <https://doi.org/10.3390/en11040811>.
- [45] Quaak P, Knoef H, Stassen HE. Energy from Biomass: A Review of Combustion and Gasification Technologies. World Bank Publications; 1999.
- [46] Gómez-Barea A, Leckner B. Modeling of biomass gasification in fluidized bed. *Progress in Energy and Combustion Science* 2010;36:444–509. <https://doi.org/10.1016/j.pecs.2009.12.002>.
- [47] Arora P, Hoadley AFA, Mahajani SM, Ganesh A. Compartment model for a dual fluidized bed biomass gasifier. *Chemical Engineering Research and Design* 2017;117:274–86. <https://doi.org/10.1016/j.cherd.2016.10.025>.
- [48] Pfeifer C, Koppatz S, Hofbauer H. Steam gasification of various feedstocks at a dual fluidised bed gasifier: Impacts of operation conditions and bed materials. *Biomass Conv Bioref* 2011;1:39–53. <https://doi.org/10.1007/s13399-011-0007-1>.
- [49] Kurkela E, Ståhlberg P, Simell P, Leppälähti J. Updraft gasification of peat and biomass. *Biomass* 1989;19:37–46. [https://doi.org/10.1016/0144-4565\(89\)90004-8](https://doi.org/10.1016/0144-4565(89)90004-8).
- [50] Lv P, Yuan Z, Ma L, Wu C, Chen Y, Zhu J. Hydrogen-rich gas production from biomass air and oxygen/steam gasification in a downdraft gasifier. *Renewable Energy* 2007;32:2173–85. <https://doi.org/10.1016/j.renene.2006.11.010>.
- [51] Hrbek J. Status report on thermal biomass gasification in countries participating in IEA Bioenergy Task 33. IEA Bioenergy; 2016.
- [52] Schmid M, Beirow M, Schweitzer D, Waizmann G, Spörl R, Scheffknecht G. Product gas composition for steam-oxygen fluidized bed gasification of dried sewage sludge, straw pellets and wood pellets and the influence of limestone as bed material. *Biomass and Bioenergy* 2018;117:71–7. <https://doi.org/10.1016/j.biombioe.2018.07.011>.
- [53] Gil J, Corella J. Biomass gasification in atmospheric and bubbling fluidized bed: Effect of the type of gasifying agent on the product distribution. *Biomass and Bioenergy* 1999;15.
- [54] Corella J, Toledo JM, Molina G. A Review on Dual Fluidized-Bed Biomass Gasifiers. *Industrial & Engineering Chemistry Research* 2007;46:6831–9. <https://doi.org/10.1021/ie0705507>.
- [55] Valderrama Rios ML, González AM, Lora EES, Almazán del Olmo OA. Reduction of tar generated during biomass gasification: A review. *Biomass and Bioenergy* 2018;108:345–70. <https://doi.org/10.1016/j.biombioe.2017.12.002>.

- [56] Deglise X. La gazéification thermochimique: histoire et développement de la recherche n.d.:39.
- [57] IEA BioEnergy Agreement Task 33: Thermal Gasification of Biomass n.d. <http://task33.ieabioenergy.com/> (accessed April 25, 2018).
- [58] Udomsirichakorn J, Salam PA. Review of hydrogen-enriched gas production from steam gasification of biomass: The prospect of CaO-based chemical looping gasification. *Renewable and Sustainable Energy Reviews* 2014;30:565–79. <https://doi.org/10.1016/j.rser.2013.10.013>.
- [59] da Silva Veras T, Mozer TS, da Costa Rubim Messeder dos Santos D, da Silva César A. Hydrogen: Trends, production and characterization of the main process worldwide. *International Journal of Hydrogen Energy* 2017;42:2018–33. <https://doi.org/10.1016/j.ijhydene.2016.08.219>.
- [60] Balat H, Kirtay E. Hydrogen from biomass – Present scenario and future prospects. *International Journal of Hydrogen Energy* 2010;35:7416–26. <https://doi.org/10.1016/j.ijhydene.2010.04.137>.
- [61] Woolcock PJ, Brown RC. A review of cleaning technologies for biomass-derived syngas. *Biomass and Bioenergy* 2013;52:54–84. <https://doi.org/10.1016/j.biombioe.2013.02.036>.
- [62] Jenbacher GE. Technical Instruction No.: 1000-0302. Fuel Gas Quality, Special Gases 2009.
- [63] ECN. Tar dew point - complete model 2012.
- [64] Arrêté du 26/08/13 relatif aux installations de combustion d'une puissance supérieure ou égale à 20 MW soumises à autorisation au titre de la rubrique 2910 et de la rubrique 2931 | AIDA. n.d.
- [65] Devi L, Ptasiński KJ, Janssen FJJG. A review of the primary measures for tar elimination in biomass gasification processes. *Biomass and Bioenergy* 2003;24:125–40.
- [66] Corella J, Aznar M, Caballero M, Molina G, Toledo J. 140gH₂/kg biomass d.a.f. by a CO-shift reactor downstream from a FB biomass gasifier and a catalytic steam reformer. *International Journal of Hydrogen Energy* 2008;33:1820–6. <https://doi.org/10.1016/j.ijhydene.2008.02.003>.
- [67] Caballero MA, Aznar MP, Gil J, Martín JA, France E. Commercial Steam Reforming Catalysts To Improve Biomass Gasification with Steam-Oxygen Mixtures. 1. Hot Gas Upgrading by the Catalytic Reactor. *Ind Eng Chem Res* 1997;36.
- [68] Aznar MP, Caballero MA, Gil J, Martín JA, Corella J. Commercial Steam Reforming Catalysts To Improve Biomass Gasification with Steam-Oxygen Mixtures. 2. Catalytic Tar Removal. *Industrial & Engineering Chemistry Research* 1998;37:2668–80.
- [69] Golmakani A, Fatemi S, Tamnanloo J. Investigating PSA, VSA, and TSA methods in SMR unit of refineries for hydrogen production with fuel cell specification. *Separation and Purification Technology* 2017;176:73–91. <https://doi.org/10.1016/j.seppur.2016.11.030>.
- [70] Spath P, Aden A, Eggeman T, Ringer M, Wallace B, Jechura J. Biomass to Hydrogen Production Detailed Design and Economics Utilizing the Battelle Columbus Laboratory Indirectly-Heated Gasifier. NREL; 2005. <https://doi.org/10.2172/15016221>.

- [71] Yin H, Yip ACK. A Review on the Production and Purification of Biomass-Derived Hydrogen Using Emerging Membrane Technologies. *Catalysts* 2017;7:297. <https://doi.org/10.3390/catal7100297>.
- [72] Aspentech. Getting Started Modeling Processes with Solids 2013:89.
- [73] Rönsch S, Wagner H. Calculation of heating values for the simulation of thermo-chemical conversion plants with Aspen Plus. DBFZ Germany 2012.
- [74] Puig-Arnavat M, Bruno JC, Coronas A. Review and analysis of biomass gasification models. *Renewable and Sustainable Energy Reviews* 2010;14:2841–51. <https://doi.org/10.1016/j.rser.2010.07.030>.
- [75] Marcantonio V, De Falco M, Capocelli M, Bocci E, Colantoni A, Villarini M. Process analysis of hydrogen production from biomass gasification in fluidized bed reactor with different separation systems. *International Journal of Hydrogen Energy* 2019;44:10350–60. <https://doi.org/10.1016/j.ijhydene.2019.02.121>.
- [76] Abdelouahed L, Authier O, Mauviel G, Corriou JP, Verdier G, Dufour A. Detailed Modeling of Biomass Gasification in Dual Fluidized Bed Reactors under Aspen Plus. *Energy & Fuels* 2012;26:3840–55. <https://doi.org/10.1021/ef300411k>.
- [77] Bates RB, Ghoniem AF, Jablonski WS, Carpenter DL, Altantzis C, Garg A, et al. Steam-air blown bubbling fluidized bed biomass gasification (BFBBG): Multi-scale models and experimental validation. *AICHE Journal* 2017;63:1543–65. <https://doi.org/10.1002/aic.15666>.
- [78] Bates RB, Altantzis C, Ghoniem AF. Modeling of Biomass Char Gasification, Combustion, and Attrition Kinetics in Fluidized Beds. *Energy & Fuels* 2016;30:360–76. <https://doi.org/10.1021/acs.energyfuels.5b02120>.
- [79] Debiagi PEA, Gentile G, Pelucchi M, Frassoldati A, Cuoci A, Faravelli T, et al. Detailed kinetic mechanism of gas-phase reactions of volatiles released from biomass pyrolysis. *Biomass and Bioenergy* 2016;93:60–71. <https://doi.org/10.1016/j.biombioe.2016.06.015>.
- [80] Debiagi P, Gentile G, Cuoci A, Frassoldati A, Ranzi E, Faravelli T. A predictive model of biochar formation and characterization. *Journal of Analytical and Applied Pyrolysis* 2018;134:326–35. <https://doi.org/10.1016/j.jaap.2018.06.022>.
- [81] Norinaga K, Deutschmann O, Saegusa N, Hayashi J. Analysis of pyrolysis products from light hydrocarbons and kinetic modeling for growth of polycyclic aromatic hydrocarbons with detailed chemistry. *Journal of Analytical and Applied Pyrolysis* 2009;86:148–60. <https://doi.org/10.1016/j.jaap.2009.05.001>.
- [82] Norinaga K, Shoji T, Kudo S, Hayashi J. Detailed chemical kinetic modelling of vapour-phase cracking of multi-component molecular mixtures derived from the fast pyrolysis of cellulose. *Fuel* 2013;103:141–50. <https://doi.org/10.1016/j.fuel.2011.07.045>.
- [83] Thimthong N, Appari S, Tanaka R, Iwanaga K, Kudo S, Hayashi J, et al. Kinetic modeling of non-catalytic partial oxidation of nascent volatiles derived from fast pyrolysis of woody biomass with detailed chemistry. *Fuel Processing Technology* 2015;134:159–67. <https://doi.org/10.1016/j.fuproc.2015.01.029>.

- [84] François J, Mauviel G, Feidt M, Rogaume C, Rogaume Y, Mirgaux O, et al. Modeling of a Biomass Gasification CHP Plant: Influence of Various Parameters on Energetic and Exergetic Efficiencies. *Energy & Fuels* 2013;27:7398–412. <https://doi.org/10.1021/ef4011466>.
- [85] Francois J, Abdelouahed L, Mauviel G, Patisson F, Mirgaux O, Rogaume C, et al. Detailed process modeling of a wood gasification combined heat and power plant. *Biomass and Bioenergy* 2013;51:68–82. <https://doi.org/10.1016/j.biombioe.2013.01.004>.
- [86] Swanson RM, Platon A, Satrio JA, Brown RC, Hsu DD. Techno-Economic Analysis of Biofuels Production Based on Gasification. 2010. <https://doi.org/10.2172/994017>.
- [87] Srinivas S, Field RP, Herzog HJ. Modeling Tar Handling Options in Biomass Gasification. *Energy Fuels* 2013;27:2859–73. <https://doi.org/10.1021/ef400388u>.
- [88] Pelletier C, Rogaume Y, Dieckhoff L, Bardeau G, Pons M-N, Dufour A. Effect of combustion technology and biogenic CO₂ impact factor on global warming potential of wood-to-heat chains. *Applied Energy* 2019;235:1381–8. <https://doi.org/10.1016/j.apenergy.2018.11.060>.
- [89] François J, Fortin M, Patisson F, Dufour A. Assessing the Fate of Nutrients and Carbon in the Bioenergy Chain through the Modeling of Biomass Growth and Conversion. *Environmental Science & Technology* 2014;48:14007–15. <https://doi.org/10.1021/es5032823>.
- [90] Ersöz A, DurakÇetin Y, Sarıoğlu A, Turan AZ, Mert MS, Yüksel F, et al. Investigation of a novel & integrated simulation model for hydrogen production from lignocellulosic biomass. *International Journal of Hydrogen Energy* 2018;43:1081–93. <https://doi.org/10.1016/j.ijhydene.2017.11.017>.
- [91] Gupta A, Dasappa S. Hydrogen from Biomass by Oxy-Steam Gasification - A Quantitative Analysis of Cases. Proceedings of the 26th European Biomass Conference and Exhibition 2018;14–17 May 2018:4 Pages. <https://doi.org/10.5071/26THEUBCE2018-2CV.4.22>.
- [92] Kalinci Y, Hepbasli A, Dincer I. Exergoeconomic analysis of hydrogen production from biomass gasification. *International Journal of Hydrogen Energy* 2012;37:16402–11. <https://doi.org/10.1016/j.ijhydene.2012.02.173>.
- [93] Ishaq H, Dincer I. A novel biomass gasification based cascaded hydrogen and ammonia synthesis system using Stoichiometric and Gibbs reactors. *Biomass and Bioenergy* 2021;145:105929. <https://doi.org/10.1016/j.biombioe.2020.105929>.
- [94] Koroneos C, Dompros A, Roumbas G. Hydrogen production via biomass gasification—A life cycle assessment approach. *Chemical Engineering and Processing: Process Intensification* 2008;47:1261–8. <https://doi.org/10.1016/j.cep.2007.04.003>.
- [95] Susmozas A, Iribarren D, Zapp P, Linßen J, Dufour J. Life-cycle performance of hydrogen production via indirect biomass gasification with CO₂ capture. *International Journal of Hydrogen Energy* 2016;41:19484–91. <https://doi.org/10.1016/j.ijhydene.2016.02.053>.
- [96] Pallozzi V, Di Carlo A, Bocci E, Villarini M, Foscolo PU, Carlini M. Performance evaluation at different process parameters of an innovative prototype of biomass gasification system aimed to hydrogen production. *Energy Conversion and Management* 2016;130:34–43. <https://doi.org/10.1016/j.enconman.2016.10.039>.

- [97] Masurel E, Authier O, Castel C, Roizard C. Screening method for solvent selection used in tar removal by the absorption process. *Environmental Technology* 2015;36:2556–67. <https://doi.org/10.1080/09593330.2015.1036789>.
- [98] Rabou LPLM, Zwart RWR, Vreugdenhil BJ, Bos L. Tar in Biomass Producer Gas, the Energy research Centre of The Netherlands (ECN) Experience: An Enduring Challenge. *Energy Fuels* 2009;23:6189–98. <https://doi.org/10.1021/ef9007032>.
- [99] Martín M, Grossmann IE. Process Optimization of FT-Diesel Production from Lignocellulosic Switchgrass. *Ind Eng Chem Res* 2011;50:13485–99. <https://doi.org/10.1021/ie201261t>.
- [100] Chung Y, Na B-K, Song HK. Short-cut evaluation of pressure swing adsorption systems. *Computers & Chemical Engineering* 1998;22:S637–40. [https://doi.org/10.1016/S0098-1354\(98\)00113-6](https://doi.org/10.1016/S0098-1354(98)00113-6).
- [101] Bounaceur R, Berger E, Pfister M, Ramirez Santos AA, Favre E. Rigorous variable permeability modelling and process simulation for the design of polymeric membrane gas separation units: MEMSIC simulation tool. *Journal of Membrane Science* 2017;523:77–91. <https://doi.org/10.1016/j.memsci.2016.09.011>.
- [102] Peters MS, Timmerhaus KD, West RE. Plant design and economics for chemical engineers. fifth edition. McGraw-Hill New York; 2004.
- [103] Turton R, Bailie RC, Whiting WB, Shaeiwitz JA. Analysis, Synthesis and Design of Chemical Processes. Pearson Education; 2008.
- [104] van Amsterdam MF. Factorial Techniques applied in Chemical Plant Cost Estimation: A Comparative Study based on Literature and Cases. Delft University of Technology, 2018.
- [105] 2019 Chemical Engineering Plant Cost Index Annual Average. Chemical Engineering n.d. <https://www.chemengonline.com/2019-chemical-engineering-plant-cost-index-annual-average/?printmode=1> (accessed April 8, 2020).
- [106] Iwasaki W. A consideration of the economic efficiency of hydrogen production from biomass. *International Journal of Hydrogen Energy* 2003;6.
- [107] Lv P, Wu C, Ma L, Yuan Z. A study on the economic efficiency of hydrogen production from biomass residues in China. *Renewable Energy* 2008;33:1874–9. <https://doi.org/10.1016/j.renene.2007.11.002>.
- [108] Parks GD, Curry-Nkansah M, Hughes E, Sterzinger G. Hydrogen Production Cost Estimate Using Biomass Gasification: Independent Review 2011:52.
- [109] Sara HR, Enrico B, Mauro V, Andrea DC, Vincenzo N. Techno-economic Analysis of Hydrogen Production Using Biomass Gasification -A Small Scale Power Plant Study. *Energy Procedia* 2016;101:806–13. <https://doi.org/10.1016/j.egypro.2016.11.102>.
- [110] Sentis L, Rep M, Barisano D, Bocci E, Sara Rajabi H, Pallozzi V, et al. Techno-economic analysis of UNIFHY hydrogen production system (No. SP1-JTI-FCH.2011.2.3). 2016.
- [111] Salkuyeh YK, Saville BA, MacLean HL. Techno-economic analysis and life cycle assessment of hydrogen production from different biomass gasification processes. *International Journal of Hydrogen Energy* 2018;43:9514–28. <https://doi.org/10.1016/j.ijhydene.2018.04.024>.

- [112] Tijmensen MJA, Faaij APC, Hamelinck CN. Exploration of the possibilities for production of Fischer–Tropsch liquids and power via biomass gasification. *Biomass and Bioenergy* 2002;24.
- [113] Hamelinck C, Faaij A, Denuil H, Boerrigter H. Production of FT transportation fuels from biomass: technical options, process analysis and optimisation, and development potential. *Energy* 2004;29:1743–71. <https://doi.org/10.1016/j.energy.2004.01.002>.
- [114] Im-orb K, Simasatitkul L, Arpornwichanop A. Techno-economic analysis of the biomass gasification and Fischer–Tropsch integrated process with off-gas recirculation. *Energy* 2016;94:483–96. <https://doi.org/10.1016/j.energy.2015.11.012>.
- [115] Dutta A, Talmadge M, Hensley J, Worley M, Dudgeon D, Barton D, et al. Process Design and Economics for Conversion of Lignocellulosic Biomass to Ethanol: Thermochemical Pathway by Indirect Gasification and Mixed Alcohol Synthesis. 2011. <https://doi.org/10.2172/1015885>.
- [116] Swanson RM, Platon A, Satrio JA, Brown RC. Techno-economic analysis of biomass-to-liquids production based on gasification. *Fuel* 2010;89:S11–9. <https://doi.org/10.1016/j.fuel.2010.07.027>.
- [117] Clausen LR, Elmegaard B, Houbak N. Technoeconomic analysis of a low CO₂ emission dimethyl ether (DME) plant based on gasification of torrefied biomass. *Energy* 2010;35:4831–42. <https://doi.org/10.1016/j.energy.2010.09.004>.
- [118] Meerman JC, Ramírez A, Turkenburg WC, Faaij APC. Performance of simulated flexible integrated gasification polygeneration facilities, Part B: Economic evaluation. *Renewable and Sustainable Energy Reviews* 2012;16:6083–102. <https://doi.org/10.1016/j.rser.2012.06.030>.
- [119] Holmgren KM, Andersson E, Berntsson T, Rydberg T. Gasification-based methanol production from biomass in industrial clusters: Characterisation of energy balances and greenhouse gas emissions. *Energy* 2014;69:622–37. <https://doi.org/10.1016/j.energy.2014.03.058>.
- [120] Holmgren KM, Berntsson TS, Andersson E, Rydberg T. Comparison of integration options for gasification-based biofuel production systems – Economic and greenhouse gas emission implications. *Energy* 2016;111:272–94. <https://doi.org/10.1016/j.energy.2016.05.059>.
- [121] Bilan énergétique de la France pour 2019. Le service des données et études statistiques (SDES); 2021.
- [122] Meadows D, Randers J. *The Limits to Growth: The 30-year Update*. London: Routledge; 2004. <https://doi.org/10.4324/9781849775861>.
- [123] Steffen W, Persson Å, Deutsch L, Zalasiewicz J, Williams M, Richardson K, et al. The Anthropocene: From Global Change to Planetary Stewardship. *AMBIO* 2011;40:739–61. <https://doi.org/10.1007/s13280-011-0185-x>.
- [124] Fressoz J-B, Bonneuil C. *L’Événement Anthropocène*. Seuil Editions. 2013.
- [125] Goedkoop M, Oele M, Leijting J, Ponsioen T, Meijer E. *Introduction to LCA with Simapro*. PRé; 2016.
- [126] ISO 14040:2006. 2006.
- [127] ISO 14044:2006. 2006.

- [128] Wernet G, Bauer C, Steubing B, Reinhard J, Moreno-Ruiz E, Weidema B. The ecoinvent database version 3 (part I): overview and methodology. *Int J Life Cycle Assess* 2016;21:1218–30. <https://doi.org/10.1007/s11367-016-1087-8>.
- [129] Valente A, Iribarren D, Dufour J. Life cycle assessment of hydrogen energy systems: a review of methodological choices. *The International Journal of Life Cycle Assessment* 2017;22:346–63. <https://doi.org/10.1007/s11367-016-1156-z>.
- [130] Tools and Data CML. Leiden University n.d. <https://www.universiteitleiden.nl/en/science/environmental-sciences/tools-and-data> (accessed October 19, 2021).
- [131] Valente A, Iribarren D, Dufour J. Harmonised life-cycle global warming impact of renewable hydrogen. *Journal of Cleaner Production* 2017;149:762–72. <https://doi.org/10.1016/j.jclepro.2017.02.163>.
- [132] Valente A, Iribarren D, Dufour J. Harmonising the cumulative energy demand of renewable hydrogen for robust comparative life-cycle studies. *Journal of Cleaner Production* 2018;175:384–93. <https://doi.org/10.1016/j.jclepro.2017.12.069>.
- [133] Valente A, Iribarren D, Dufour J. Harmonising methodological choices in life cycle assessment of hydrogen: A focus on acidification and renewable hydrogen. *International Journal of Hydrogen Energy* 2019;44:19426–33. <https://doi.org/10.1016/j.ijhydene.2018.03.101>.
- [134] Tock L, Maréchal F. Co-production of hydrogen and electricity from lignocellulosic biomass: Process design and thermo-economic optimization. *Energy* 2012;45:339–49. <https://doi.org/10.1016/j.energy.2012.01.056>.
- [135] Moreno J, Dufour J. Life cycle assessment of hydrogen production from biomass gasification. Evaluation of different Spanish feedstocks. *International Journal of Hydrogen Energy* 2013;38:7616–22. <https://doi.org/10.1016/j.ijhydene.2012.11.076>.
- [136] Susmozas A, Iribarren D, Dufour J. Life-cycle performance of indirect biomass gasification as a green alternative to steam methane reforming for hydrogen production. *International Journal of Hydrogen Energy* 2013;38:9961–72. <https://doi.org/10.1016/j.ijhydene.2013.06.012>.
- [137] Iribarren D, Susmozas A, Petrakopoulou F, Dufour J. Environmental and exergetic evaluation of hydrogen production via lignocellulosic biomass gasification. *Journal of Cleaner Production* 2014;69:165–75. <https://doi.org/10.1016/j.jclepro.2014.01.068>.
- [138] Muresan M, Cormos CC, Agachi PS. Comparative life cycle analysis for gasification-based hydrogen production systems. *Journal of Renewable and Sustainable Energy* 2014;6:013131. <https://doi.org/10.1063/1.4864658>.
- [139] Valente A, Iribarren D, Gálvez-Martos J-L, Dufour J. Robust eco-efficiency assessment of hydrogen from biomass gasification as an alternative to conventional hydrogen: A life-cycle study with and without external costs. *Science of The Total Environment* 2019;650:1465–75. <https://doi.org/10.1016/j.scitotenv.2018.09.089>.

CHAPITRE 2 OXYDATION PARTIELLE D'UN SYNGAZ DE GAZÉIFICATION DE BIOMASSE

2.1 Introduction

Ce chapitre s'intéresse à la réduction des goudrons issus de la gazéification biomasse à l'aide d'une unité d'oxydation partielle (POX). Des essais ont été réalisés sur une unité pilote de POX couplée à un pilote de gazéification de 5 kg/h. Afin de confronter les résultats obtenus à l'échelle pilote à des modèles de cinétique radicalaire, un modèle cinétique détaillé est mis au point en combinant différents modèles cinétiques disponibles dans la littérature.

2.2 Article 1 (reproduction intégrale)

Demol R., Ruiz M., Schnitzer A., Herbinet O., Biget A., Mauviel G., Experimental and Modeling Investigation of Partial Oxidation Cracking of Gasification Tars, to be submitted to Fuel.

2.2.1 Abstract

Among tar reduction methods, the partial oxidation (POX) of biomass gasification tars was studied experimentally at a pilot-scale and numerically. The gasification producer gas was obtained at 800°C in an air-blown fluidized bed at an equivalent ratio (ER) of 0.25. Two secondary ER were selected for the POX unit 0.05 and 0.10 with and without air pre-heating. Multiple advanced analytical methods were used to provide very detailed composition of the producer gas, tars and acid gases. 742 species and 5093 reactions. The POX unit was able to reduce the quantity of tars by 60 to 90% depending on the secondary ER (from 6.5 to 2.4 and 0.72 g tars/Nm³, excluding benzene). The lightest tars were almost fully removed. The permanent gases were barely modified whereas the lights hydrocarbons (except C₂H₂) and benzene were significantly reduced. As a result, the volumetric lower heating value was reduced. These data were compared successfully to a plug flow reactor model using a detailed radical kinetic scheme build on various sources to consider all the species measured during experiments.

2.2.2 Keywords

Biomass gasification, tar, partial oxidation, reaction kinetics, mechanism.

2.2.3 Introduction

Biomass has been dedicated for centuries for heat needs and as material [1]. This feedstock is foreseen to be used for the production of energy and chemicals as a substitute of a part of fossil fuels. Pyrogasification processes is one way to provide these bio-based products. With a limited amount of oxygen, gasification produces a synthetic gas mainly composed of H₂, CO, CO₂, CH₄ and lights hydrocarbons (C₂₊). This is a commercial readiness technology for energy production (power & heat). Yet, a part of the solid fuel is converted in the syngas as simple aromatics (BTX) and polycyclic aromatic hydrocarbons (PAHs). These secondary products are challenging for the overall process for the risk of clogging of downstream equipment. The handling of tar sludge after capture is also complex and expensive. The end use of the syngas requires also partial or complete removal (gas engine, gas turbine, Fischer-Tropsch process, H₂ recovery) [2,3]. The release in the atmosphere of these species is also harmful. Sixteen of these PAHs are considered as priority pollutants by the Environmental Protection Agency of the United States [4].

Several physical, chemical and catalytic clean-up strategies have been developed during the last decades [2]. They are classified as primary or secondary methods depending on the moment of their application. Primary methods are dedicated to avoid the tar formation inside the reactor (reactor technology, optimization of the gasification parameters, gasifying agent, bed media). Secondary methods target the elimination of tars after the gasifier at high, mild or low temperatures with dry or wet techniques [2,5]. Anyhow, a combination of primary and secondary methods is generally required to comply with quality standards.

Secondary elimination of gasification tars occurs at elevated temperature according to three modes. Thermal cracking results from external heating. It consists on the pyrolytic decomposition of tars molecules in gas phase at high temperature (>900°C) without catalyst and under inert atmosphere. Studies dealing with the thermal cracking of tars are abundant in literature but most of them concerns the mechanisms and kinetics of the decomposition of pyrolysis vapors (Table 2-1) and model molecules of primary and secondary tars derived from the pyrolysis reaction, such as: benzene, catechol, toluene. Therefore, less information is available on the thermal decomposition

of tertiary tars typically present in producer gas, in particular, in the case of refractory PAHs. Furthermore, the implementation of thermal cracking at industrial scale is hindered by the heat transfer difficulty and the negative impact of the external energy required to achieve cracking temperatures on the overall efficiency of the process.

Catalyst cracking allows to use lower temperature by decreasing the required activation energy by means of a catalytic material and is by far the most effective method to eliminate tars from the producer gas/syngas. Heterogeneous catalyst typically employed for tar elimination can consist in natural minerals generally cheaper than synthetic catalysts. However, the rapid catalyst deactivation requires the utilization of specific reactor configurations that increases the complexity of operation, such as, circulating fluid bed systems or switch reactors. Additionally, catalyst attrition and irreversible deactivation impose a substantial catalyst make-up to the system increasing thus, the operational expenditure [5–8]. Catalyst cracking for tar abatement is out of the scope of this study.

Partial oxidation (POX) increases the temperature of the syngas by oxidizing a part of it with oxygen. The reaction rates are increased allowing tar cracking and polymerization pathways different than those observed for pyrolytic thermal decomposition. According to Hoeven et al. [9], oxygen is an excellent initiator of free radicals, such as hydrogen (H), oxygen (O), hydroxyl (OH) and hydroperoxy (HO_2) and plays an eminent role in chain initiation, and proceeds in all subsequent reactions. Additionally, oxygen promotes exothermic oxidation of hydrocarbons, releasing the heat necessary for propagation reactions.

However, experimental data available is scarce for the partial oxidation of gasifier producer gas (see Table 2-1). The extrapolation of mechanisms observed with model molecules and controlled gas environments to a real gasification environment is not straightforward due to the complex chemistry of tertiary tars.

Table 2-1:Thermal cracking and POX studies.

Type ^a	Year/author	Experiments Feedstock/model molecules	Model	Pilot scale	Ref.
Producer gas/syngas					
TC	2004 Houben	Wood (willow) syngas	No	Tubular reactor L:0.7 m, d:75 mm	[10]
	2009 Valin	Modelled syngas (7-14% CH ₄ , 16-32% H ₂ , 19% CO, 14% CO ₂ , 15-30% H ₂ O, N ₂)	Plug flow, two detailed kinetic model compared (127/159 species, 1207/773 reactions)	Reactive gas total flowrate about 1-2 Nm ³ /h	[11]
POX	2005 Houben	Naphthalene (2.6 mg/Nm ³) in a simulated syngaz (22.4% H ₂ , 5% CH ₄ , 72.6% N ₂)	No	Burner	[12]
	2013 Svensson	Model validation on experimental TC data from [11]	Dynamic model (FDM): 53 species 325 reactions. Static model (series of PSR): 157 species 872 reactions.		[13]
Model molecules					
TC	1992 Blekkan	CH ₄ (with Ar and He or H ₂)	No	Tubular reactor, L:1 m, d: 9mm	[14]
	1996 Jess	Naphthalene, toluene and benzene (in N ₂)	No	Tubular reactor, L: 50 cm, d: 20 mm	[15]
	1999 Sarobe	Acenaphtho[1,2-a]acenaphthylene, Fluoranthene, Benzo[k]- and Benzo[j]fluoranthene (in N ₂)	No	Quartz tube, L: 40 cm, d: 25 mm	[16]
	2002 Winkler	Thiophene, benzo[b]thiophene, dibenzothiophene	No	Quartz tube, L: 110 cm, d: 22mm	[17]
	2016 Gai	Naphthalene, anthracene (surrogate of biomass tar)	No	Fluidized bed, d: 290 mm, L: 373 mm	[18]
	2021 Tanoh	Toluene, naphthalene	GASPAR, plug flow model, 177 species, 5988 reactions.	Tubular reactor d: 7.5 cm, L: 2.3 m	[19]
POX	2004 Liu	Hexane	No	Quartz reactor	[20]
	2007 DeCoster	Anthracene	No	Two-stage drop-tube furnace	[21]
	2008 Thomas	Catechol	No	Quartz tube, d: 2mm	[22]
	2015 Mao	Biomass tar (defined by ultimate analysis)	No	Quartz tube reactor, L: 80 mm	[23]
	2017 Zhang	2-methoxyphenol, anisole, furfural, toluene	201 species, 1100 reactions	Tube reactor, d: 8 mm, L: 350 mm	[24]
	2019 Peng	Phenanthrene	No	Quartz tube d: 30 mm, L: 500 mm	[25]
	2021 Tanoh	Toluene, naphthalene	Described above		[19]

Pyrolysis vapors (PV)					
TC	2000 Ledesma	Coal from fluidized bed reactor (600°C)	No	Tubular flow reactor d: 30 mm	[26]
	2001 McGrath	Cellulose, pectin and chlorogenic acid from quartz sample holder (300, 600°C)	No	Quartz tube, d: 0.2 to 0.8 cm, L: 20 cm	[27]
	2011 Wu	Rice straw from screw pyrolyser (500°C)	No	Tube d: 35 mm, L: 800 mm	[28]
	2013 Wongchang	Wood (600°C)	No	Tube	[29]
	2021 Tanoh	Wood pyrolysis vapors from rotary kiln (1-10 kg/h) (800°C)	Described above		[19]
POX	2000 Ledesma	Described above			[26]
	2011 Wu	Rice straw from screw pyrolyser (500°C)	No	Tube d: 35 mm, L: 800 mm	[28]
	2011 Su	Rice straw pyrolysis vapors (500°C) from screw pyrolyzer (1-10 kg/h)	2D-CFD uniform temperature 900°C, 16 reactions, 11 species.	Tube reactor d: 35 mm, L: 600mm	[30]
	2013 Ahrenfeldt	Pine wood pyrolysis vapors (600°C) from screw pyrolyzer (1.16 kg/h)	No	Tube L: 460 mm	[31]
	2014 Weston	Wood pellets (500-800°C)	No	Coanda burner d: 50 mm	[32]
	2015 Thimthong	Nascent volatiles from fast pyrolysis (700-800°C) of cedar sawdust (0.09-0.20 g/min)	Plug flow + detailed kinetics (8159 reactions, 548 species) + T inlet (700, 800°C)	Tubular vertical two-stage reactor	[33]
	2021 Tanoh	Wood pyrolysis vapors from rotary kiln (1-10 kg/h) (800°C)	Described above		[19]

^aThermal cracking (TC) or partial oxidation (POX)

To design and scale-up properly a POX unit, a kinetic model is required. Due to the number of species and the mechanism pathways involved in such system, a restricted set of reactions is not able to reproduce rigorously the detailed composition at the outlet of the setup. Radical kinetic mechanisms have been developed for thermal cracking and oxidation of biomass products. Dhahak et al. (2019) developed BioPOX-1, a model of biomass pyrolysis and oxidation including PAHs up to chrysene ($C_{18}H_{12}$) and also NOx formation mechanism (710 species and 5035 reactions) [34]. This model was revised by Darido et al. into BioPOX-2 model (634 species, 4759 reactions) [35]. Norinaga et al. (2009, 2013) developed similar models for thermal cracking in pyrolytic conditions [36,37]. The main advantage of these detailed kinetic models is to avoid the information loss of

lumping processes. Thus, the detailed composition of the gas can be known. If the computational time is reasonable, it could enhance the accuracy of the tar handling models limited with simple kinetics [38].

In this study, partial oxidation of a real producer gas stream was investigated experimentally and numerically. Partial oxidation experiments were conducted in a partial oxidation unit (POX) electrically heated and heavily isolated, coupled downstream a 5 kg/h air-blown bubbling bed gasification reactor. Results of POX experiments were compared to reference tests conducted without the POX unit to assess the impact of POX reactions on gasification indicators and pollutant contents. Numerical modeling of the POX unit was carried out with ANSYS Chemkin Pro using the composition of the producer gas experimentally measured at the exit of the gasification reactor.

The overall objective of this study is to demonstrate the reliability of advanced kinetic modelling when dealing with complex composition of real producer gas.

The novelty of this paper relies on:

- 1) A very detailed composition of gasification tars before and after a partial oxidation pilot plant coupled with a fluidized bed gasifier;
- 2) A completed detailed kinetic model for thermal cracking and oxidation of tars up to C₂₄ including soot formation validated on a real biomass gasification producer gas

2.2.4 Material and methods

2.2.4.1 Feedstock, experimental rig and analytical methods

Feedstock material used in this study corresponds to pellets of medium density fiber board (MDF). Chemical composition and other properties were fully detailed elsewhere [39]. Nitrogen content of MDF material was relatively high, 3.5 wt.% (dry basis), due to the utilization of urea-formaldehyde resins for panel fabrication. Water content was about 5 wt.%.

Gasification experimental rig consists on: (i) a double-screw feedstock alimentation system, (ii) a bubbling bed air-blow reactor externally heated, (iii) a cyclone separator and, (iv) a cooling system integrating a Venturi scrubber. The concentration of permanent gases (N₂, CO, CO₂, H₂, CH₄, C₂H₂, C₂H₆, C₃H₄ and C₃H₆) was determined every 3 minutes by µ-GC using N₂ as tracer gas. Tar

molecules were collected in a series of wet impingers with 2-propanol and quantified by GC-MS-FID and HPLC-UV. Additionally, semi-quantitative analysis of light and high tars molecules were carried out with Synchronous Fluorescence Spectroscopy (SFS). This rapid technique relies on the correlation existing between the emission spectral band and the number of the aromatic rings, in particular, for linear PAHs [40]. A comprehensive description of the experimental rig and all the analytical methods can be found elsewhere [39].

2.2.4.1.1 Partial oxidation unit

A schema of the oxidation unit (POX) developed at LRGp is depicted in Figure 2-1. The POX unit was coupled downstream a cyclone separator and consisted in a pre-heating chamber, a non-premixed gas-centered swirl coaxial burner, a reaction chamber and a cooling zone.

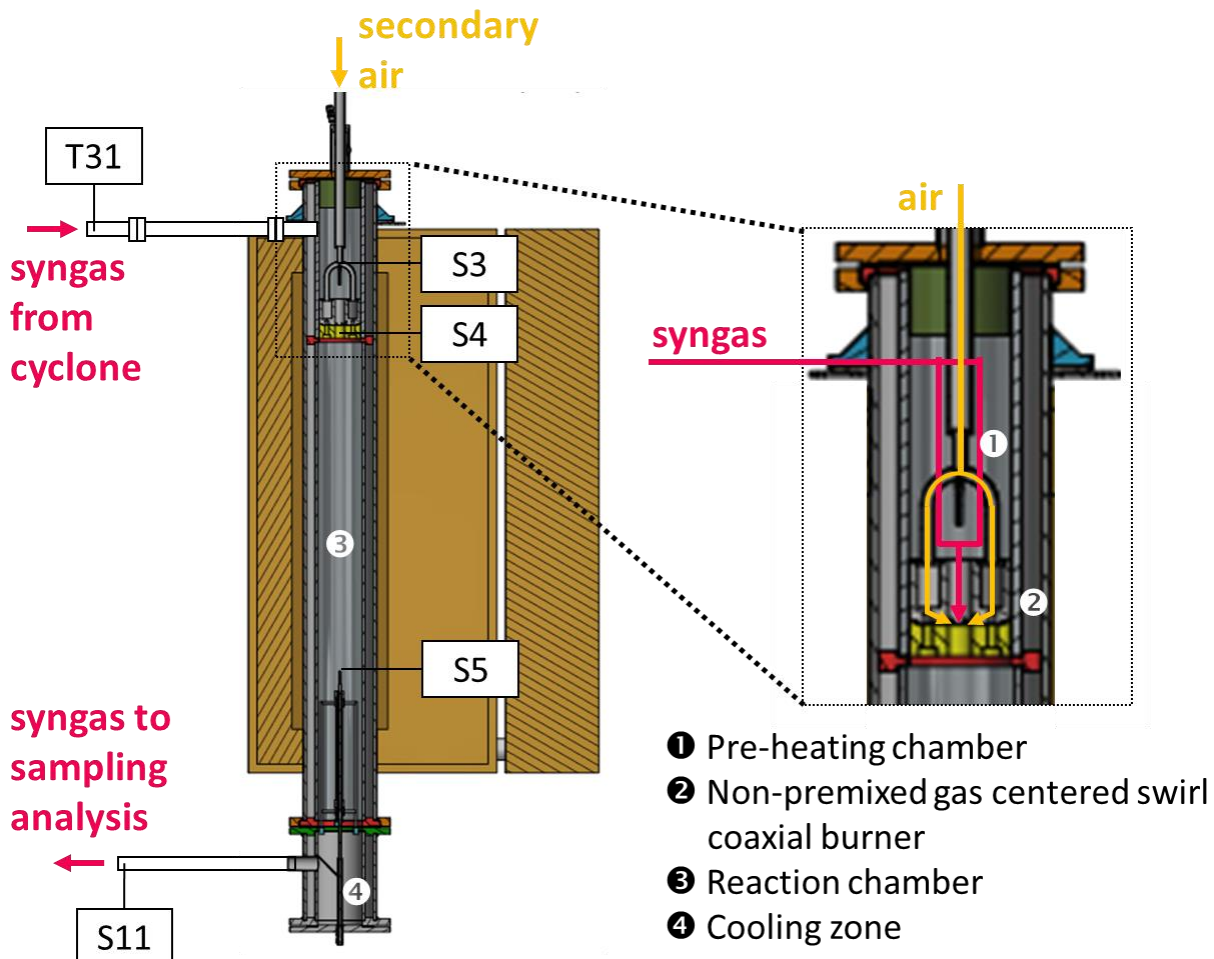


Figure 2-1: Schema of the POX unit.

The producer gas stream was directed from the cyclone to the preheating chamber of POX unit at approximately atmospheric pressure. Then, the producer gas stream passed through the center of the burner and was mixed with the airflow injected tangentially by the swirl coaxial burner. The gas-centered swirl coaxial burner consists of a pre-injection chamber where the airflow is equally distributed to the 5 injection holes with a diameter of 3.5 mm and inclined 45° respect the two axis to create a turbulent flow in order to obtain good mixing. The secondary air flow was injected at constant flow rate (Brooks 5851s) and in some cases, preheated before entering the POX unit. Preliminary design simulations revealed the development of local high temperature spots (> 2000 K) on the zone next to the injection. Therefore, to avoid the damage of reactor walls made of SYRIUS steel, the reaction chamber was confined by an inner tube of SiC of 1 cm thickness. The space between the inner SiC tube and the outer SYRIUS steel was left empty to reduce the heat transfers by conduction. The final volume of the reaction chamber inside the SiC tube was approximatively of 11.5 L (ID = 10.2 cm, length = 140 cm). The POX unit was homogeneously heated by an external oven to compensate heat loss due to the small size of the pilot plant. Finally, a cooling chamber was placed at the bottom of the POX unit.

The temperature was measured in critical points of the POX unit (see Figure 2-1) and corresponds to: the inlet of the producer gas to the swirl burner (T31), the inlet of airflow to the pre-distribution chamber (S3), the temperature of the reaction chamber (S5) and the temperature at the exit of the cooling zone (S11). The thermocouple of the reaction chamber (S5) was centered by a radial support and placed at the end of the reaction chamber. The temperature of this thermocouple was used as indicative of the temperature inside the reaction chamber.

2.2.4.1.2 Experimental conditions

To assess the impact of POX reactions on gasification indicators, gas composition, tars and acid gases, the results obtained for the POX tests were compared with the results of three repeated reference tests (REF) conducted without the POX unit and described elsewhere [39]. Main parameters of the gasification reactor, namely: the reactor temperature, the feedstock flow rate, the primary air flowrate and the test duration, were kept constant for all tests at 800°C, 4.4 kg/h, 4.5 Nm³/h and 2 h, respectively. Air-to-fuel equivalence ratio (ER) inside the reactor was constant and equals to 0.25 for all the tests. A total of four POX tests were conducted under different conditions

of temperature and secondary air flow rate. Table 2-2 summarizes the targeted values of the different parameters for the four POX tests.

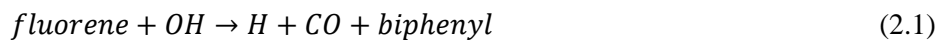
Table 2-2: Parameters of the partial oxidation unit.

Test	REF	0.05-1025	0.1-1034	0.1-1050	0.1-1100
Secondary air flow rate (NL/h)	-	1000	2000	2000	2000
Temperature set-point of secondary air preheating, °C	-	20	20	500	500
Temperature set-point of the POX unit external oven, °C	-	1100	1100	1150	1200
ER secondary	-	0.05	0.1	0.1	0.1
ER total	0.25	0.30	0.35	0.35	0.35

2.2.4.2 Modeling and numerical methods

2.2.4.2.1 Kinetic mechanism

A detailed radical kinetic mechanism was developed for the oxidation and formation of biomass tars from several literature sources [34,36,37,41]. Two main mechanisms were merged. On the one hand, BioPOX-2 from Darido et al. [35] (modified from BioPOX-1 in Dhahak et al. [34]) for biomass pyrolysis and oxidation including PAHs up to chrysene ($C_{18}H_{12}$) and also NOx formation mechanism (634 species and 4759 reactions). On the second hand, the mechanism of Norinaga et al. (2009) [36] under pyrolysis conditions was used to include other heavy HAPs (from C_{10} to C_{24}). These species were measured in the experiments but not considered in BioPOX-2 mechanism. Additionally, other reactions were included for the oxidation of these new heavy PAHs from Norinaga et al. (2013) [37]. One more reaction (2.1) was added to account for the oxidation of fluorene as no consumption reaction was considered for this important product in the resulting model. This reaction is a lumped one which was written following the methodology used by the CRECK modeling group of Politecnico di Milano [42] with kinetic parameters recommended by this group [43].



Phenanthrene and anthracene were lumped in BioPOX-2 mechanism but, since these two species were measured separately in experiments and follows different reactions paths in Norinaga's mechanisms, in this study they were considered separately.

It is generally accepted that soot is a product of POX reactions. According to Saggese et al., soot results from C₂₀ precursors [44]. In this study, the reactions 2.2 and 2.3 were then considered to roughly estimate the soot formation and soot growing from acetylene. The kinetic parameters of these reactions are presented in Table 2-3.



Table 2-3: Kinetic parameters.

Reaction	A	Ea (cal/mol)	Ref
1	$4.0 \cdot 10^{13} \text{ (s}^{-1}\text{)}$	$7.0 \cdot 10^3$	[43]
2	$5.0 \cdot 10^6 \text{ (s}^{-1}\text{)}$	$3.99 \cdot 10^4$	[41]
3	$2.5 \cdot 10^8 \text{ (cm}^3\text{mol}^{-1}\text{s}^{-1}\text{)}$	$9.99 \cdot 10^3$	[41]

The SYNPOX model, for syngas partial oxidation - contained 742 species and 5093 reactions. This kinetic model is provided in supplementary material.

2.2.4.2.2 Plug-flow reactor model

The POX pilot was modelled as an ideal plug-flow reactor of 10.2 cm-diameter and 1.10 m-length corresponding to the dimensions of the reaction chamber of the POX unit without the cooling zone. This system was simulated with ANSYS Chemkin Pro 17.0 interfaced by python software for easier results management. Syngas and air were assumed premixed and injected at the inlet. The temperature of the inlet was calculated with RK-ASPEN thermodynamic model in AspenPlus 8.8. The pressure was remained constant and equal to the inlet pressure (close to atmospheric), air composition was assumed 21%v O₂ and 79%v N₂. In this 1D-model, the gas temperature was supposed to be radially uniform and equal to the wall surface temperature.

In an industrial-scale POX unit, the thermal conditions should be close to adiabatic conditions. Due to the scale of the pilot plant, this assumption cannot be made. To take the oven surrounding the POX unit into account, the heat flux from the oven was estimated. Chemkin Pro can handle only

three heat transfer mechanisms at the walls: adiabatic (no transfer), fixed heat flux or convective heat flux. To account for the oven heat flux, the third mechanism of convective heat flux was chosen with an overall heat transfer coefficient estimated around $U = 20 \text{ W/m}^2/\text{K}$ and T_∞ equals to the oven temperature (equation 2.4). The heat transfer mechanism is far more complex: convection between the oven and the external wall through a thin layer of air, conduction in a two-layered wall, convection between the inner wall and the syngas and certainly the most difficult to quantify the heat transfer by radiation between the oven and the wall and between the wall and the solid particles of the syngas (soot) [45]. The boundary conditions are summarized in Table 2-4.

$$\dot{Q} = U(T_\infty - T) \quad (2.4)$$

Table 2-4: Boundary conditions of the CHEMKIN PRO plug flow model

Reactor model	Test	T inlet (°C)	Heat transfer coefficient U (W/m ² /K)	T _∞ (°C)
Ideal plug flow	0.05-1025	599°C	20	1100
	0.10-1034	555°C	20	1100
	0.10-1050	607°C	20	1150
	0.10-1100	674°C	20	1200

2.2.5 Results and discussion

2.2.5.1 Partial oxidation cracking tests

Table 2-5 details the values of the main POX temperatures, gas composition and product yields for reference and POX tests. For the sake of clarity, tar yields were specified according to ECN tar classification [46]. The yields of all gas and tar molecules quantified in this study were detailed in Table S2-1 (supplementary materials).

As seen from Table 2-5, targeted temperatures were successfully attained inside the POX unit thanks to the external heating and the heavy isolation. For all POX tests, the temperature inside the reaction chamber showed a slight increase during the first 30 min of the test and then, remained steady. The lower temperature measured at the inlet of the secondary air stream for the tests 0.05-1025 and 0.1-1034 results from no secondary air preheating in these cases.

Compared to the reference values (REF), the average gas concentrations measured for the four POX tests clearly showed a drop in CH₄ and C₂-C₃ hydrocarbons and, a marked raise in the values of CO and C₂H₂ (acetylene). Benzene, a major component for LHV was also consumed leading to a decrease of the volumetric LHV. The increase in the secondary air flow operated between the tests 0.05-1025 and 0.1-1034 resulted in a raise in the concentration of H₂, CO and a drop in CO₂ and C₂H₂. The increase in the temperature of the reaction chamber operated between the tests 0.1-1034, 0.1-1050 and 0.1-1100 did not lead to any notable trend (within experimental uncertainty).

Table 2-5: Main operation conditions, gasification indicators and products yields in reference and partial oxidation experiments.

Case	REF	0.05-1025	0.1-1034	0.1-1050	0.1-1100
<i>Gasifier</i>					
Test duration, h		1.43	1.73	1.61	1.38
Consumed feed, kg (as received)		6.6	7.96	8.04	6.3
Fuel feed rate, kg/h	4.5 ± 0.1	4.6	4.6	4.5	4.6
Bed temperature, °C	800 ± 2	794	789	801	796
Freeboard temperature, °C	757 ± 1	761	762	765	762
ER (reactor)	0.25 ± 0.01	0.25	0.25	0.25	0.25
<i>Partial oxidation unit</i>					
Secondary air flow rate, NL/h	-	1020	1980	1980	1980
Airflow inlet, °C	-	406 ^c	304 ^c	466	565
Producer gas inlet, °C	-	614	587	629	691
Reaction chamber, °C	-	1025	1034	1059	1100*
Cooling chamber exit, °C	-	647	601	657	668
Gas residence time, s	-	1.0	0.9	0.9	0.9
ER (total)	0.25 ± 0.01	0.30	0.36	0.37	0.36
<i>Gasification indicators</i>					
Gas Yield, Nm ³ /kg feed (daf)	1.78 ± 0.05	2.03	2.33	2.27	2.24
LHV, MJ/Nm ³	5.4 ± 0.1	4.5	4.8	4.2	4.0
%CGE	44.3 ± 0.02	42.5	53.4	45.2	42.8
%C	58.1 ± 0.02	59.5	70.6	65.5	59.9
%H	48.0 ± 0.02	42.9	52.6	44.4	42.6
<i>Gas composition, %mol (N₂ free, dry)</i>					
H ₂	17.4 ± 0.6	16.4	18.3	18.0	19.9
CO	29.3 ± 0.2	31.9	36.7	35.5	34.5
CO ₂	39.8 ± 0.4	38.1	32.5	36.7	35.8
CH ₄	9.1 ± 0.1	8.7	8.5	7.0	6.1
C ₂ H ₂	0.33 ± 0.02	1.54	1.33	1.35	1.26
C ₂ H ₄	3.0 ± 0.1	1.0	0.4	0.3	0.2

C ₂ H ₆	0.36 ± 0.01	0.01	0	0	0
C ₃ H ₄	0.04 ± 0.004	0.02	0.02	0.01	0.01
C ₃ H ₆	0.29 ± 0.04	0.01	0.01	0	0
O ₂	0.4 ± 0.2	2.3	2.3	1.1	2.4
Tar yield, g/kg feed (daf)					
benzene	6.2 ± 0.1	5.8	2.7	3.0	2.2
Class II ^a	0.61 ± 0.11	0	0	0	0
Class III ^a	5.5 ± 0.2	0.8	0.2	0.3	0.1
Class IV ^a	5.1 ± 0.4	3.6	1.2	1.5	1.1
Class V ^a	0.31 ± 0.04	0.39	0.25	0.24	0.23
Total ^b	11.6 ± 0.2	4.7	1.7	2.0	1.4
Gas dew point, °C	173	191.5	185.2	184.5	187.9
Water and acid gas yields, g/kg feed (daf)					
NH ₃	18.5 ± 4.9	19.2	25.9	27.8	18.9
HCN	2.5 ± 0.3	3.2	1.4	6.2	6.0
H ₂ O	342 ± 13	386	361	388	389

^atar groups according the ECN tar classification.

^bTotal tar yield was calculated excluding benzene.

^cNo preheating for secondary air.

In comparison to REF values, the overall tar yield dropped of 60% and 90% for the POX tests conducted with a secondary ER of 0.05 and 0.1, respectively. In terms of concentration, the POX unit led to a reduction from 6.5 g/Nm³ (dry gas, C₆H₆-free) in the case of the REF tests, to 2.4 g/Nm³ (dry gas, C₆H₆-free) for the test 0.05-1025. The increase in the secondary air flow operated in the test 0.1-1034 led to a tar concentration of 0.72 g/Nm³ (dry gas, C₆H₆-free). On the other hand, the increase in the temperature of the reaction chamber did not show any significant variation on the overall tar yield within experimental uncertainty.

The chemical composition of tars was substantially modified inside the POX unit. For example, in the case of the test 0.05-1025 and compared to REF values, yields of tar groups II, III and IV showed a drastic reduction of 100%, 86% and 30%, respectively, whereas, the yield of group V increased by 26%. A closer look on the individual tar yields, detailed in Table S2-1 (supplementary materials), revealed a significant raise of some molecules of group IV, such as: phenanthrene, fluoranthene, and, of other heavier molecules from group V present in trace concentrations, such as: benzo[b]fluoranthene, benzo[a]pyrene, dibenzo[a,h]anthracene, benzo[ghi]perylene and indeno[1,2,3-cd]pyrene. On the contrary, results indicated a reduction in the yields of some molecules of group IV, such as: naphthalene, acenaphthylene, fluorene and anthracene, explaining the 30% drop observed for the overall group. This is consistent with the production of heavier tars

from naphthalene observed by Houben et al. [12]. Moreover, the increase in the secondary air flow rate operated for the test 0.1-1034 led to a more severe reduction in the yields of groups IV and V. In this case, all molecules of the group IV showed a negative yield. These results suggest a dependence on secondary air injection i.e. the temperature reached, on the unit efficiency. The counterpart of the tar reduction is the consumption of light hydrocarbons and benzene.

Substantial modifications in the chemical composition of tars caused by the POX reactions were corroborated by SFS. Figure 2-2 shows the SFS of tars samples corresponding to reference and POX tests. These results clearly evidenced the decrease in the tar content in producer gas and shift to longer wavelength, indicating a raise in the content of heavy tars.

Finally, the yield of water increased after POX tests resulting from oxidation reactions. The ammonia composition remains approximatively constant (within the uncertainty range). A slight increase in HCN was observed up to about two times the inlet feed rate at the highest temperatures. The global nitrogen content in the syngas was then slightly increase with temperature.

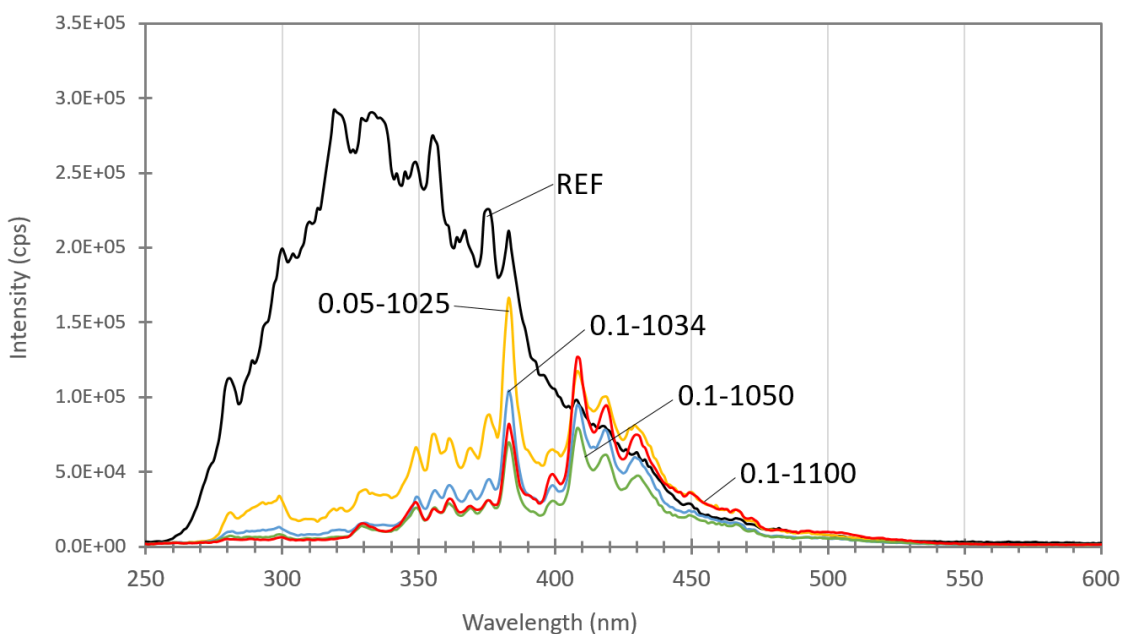


Figure 2-2: Synchronous Fluorescence spectra (offset = 20 nm).

2.2.5.2 Modeling results

The temperature profiles of the four cases are presented in Figure 2-3 for the plug flow model. The temperature profiles estimated under or over predict the experimental measurements (too low for 0.05-1025, too high for the others). An overall heat transfer coefficient estimated to 20 W/m²/K was not able to correctly reproduce the heat transfer mechanism between the oven and the reaction chamber. The definition of an overall heat transfer coefficient to model the heat transfer between the oven and the reaction chamber is highly questionable. This heat transfer is composed of heat conduction through the different layers of the walls, the heat convection through layers of air and radiative heat transfer between the oven resistances, the wall materials and the soot of the syngas. There is no reason for the overall heat transfer coefficient to be constant due to the power 4 on temperature in radiative mechanism. Moreover, the real temperature profile at the walls is not uniform contrary to the simulation profile. The real oven cannot provide such perfect behavior.

Other simulation considering isothermal conditions showed only slight differences in the gas composition compared to the heat transfer coefficient formulation. This suggested that the main impact on the composition profile was the temperature reached. All in all, these two options are questionable since they both required fitting parameters, decreasing the ability of the model to be predictable for non-adiabatic systems. In an industrial big-scale device with the adiabatic assumption, this kinetic model should be able to predict well the temperature profile without other assumption. The temperature increase rate near the injection zone suggests the potential formation of a flame at the inlet after the air injection nozzles.

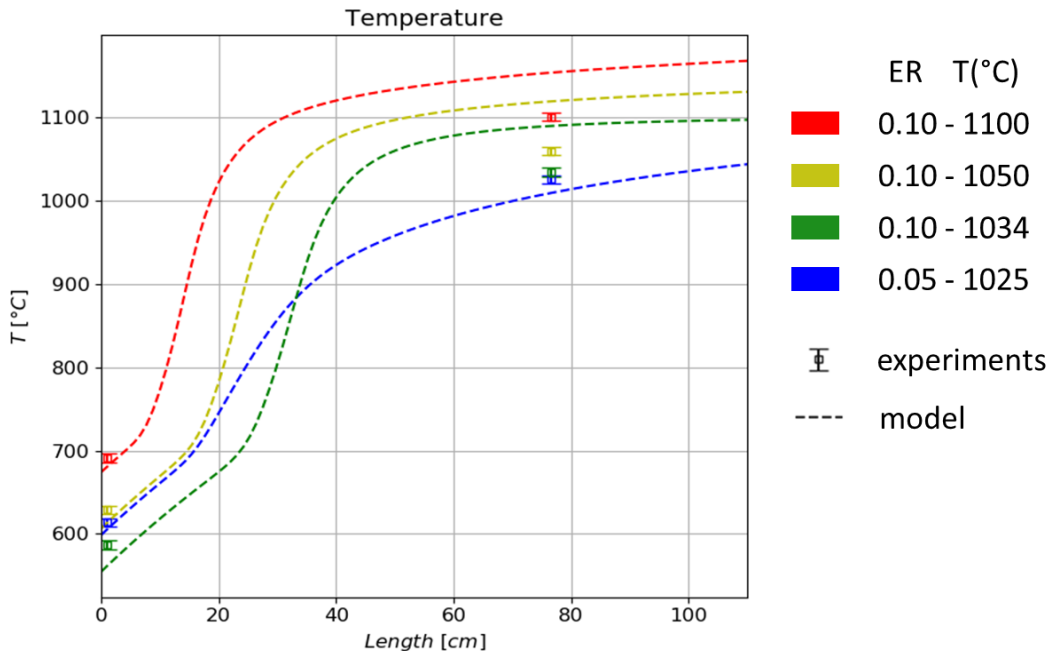


Figure 2-3: Temperature profiles obtained with an overall heat transfer coefficient of 20 W/m²/K.

In this following subsection, only two cases are presented. For the sake of concision, the two tests with the more different conditions were chosen. 0.05-1025 and 0.10-1100 present two different ER, with and without air preheating. The two other cases are presented in Supplementary Material 2.2.10.3.

The detailed composition of the syngas at the inlet and outlet are presented and compared to model results in Figure 2-4 and Figure 2-5 for ER = 0.05 and ER = 0.10, respectively. A relative good agreement was found between the experiment and the plug flow model for the permanent gases (H_2 , CO, CO_2 , CH_4) within around +/-20% difference with the experimental outlet composition. The model over predicts the consumption of O_2 . The fate of lights hydrocarbons was well reproduced within the error range showing an increase of ethylene and a decrease of all others C_2 - C_3 .

The fate of tars regrouped by ECN classes were also well reproduced. Classes 2 to 4 tars decreased in both cases whereas class 5 increased at lower temperature (0.05-1025) and slightly reduced or almost stable at higher temperature (0.10-1100). In details, for most of individual tar species the

global trend was conformed to the experimental observations. Nonetheless, some of these species were not correctly predicted for both experimental conditions: benzofuran, biphenyl and acenaphthene. Some heavy tars C₂₀₊ were over consumed in the model probably due to the soot formation mechanism.

For the acid gases the prediction of NH₃ was in the uncertainty range whereas, HCN was consumed in 0.10-1100 in contradiction with the experimental increase observation. The composition in NO and N₂O cannot be compared due to a lack of experimental data on these species.

The soot formation increased with temperature according to the model (Table 2-6). Unfortunately, the soot was not collected during the tests. To validate this model, other experimental data were used in both thermal cracking and oxidative conditions [19], although the temperature reached in those experiment was higher, around 1200°C. The results are presented in Supplementary Material (2.2.10.2).

Table 2-6: Gas residence time and soot production

Case	0.05-1025	0.10-1034	0.10-1050	0.10-1100
Residence time [s]	0.65-0.73	0.59-0.65	0.58-0.62	0.56-0.58
Soot production [g/kg biomass dry]	0.02-0.05	0.04	0.05-0.06	0.09-0.10

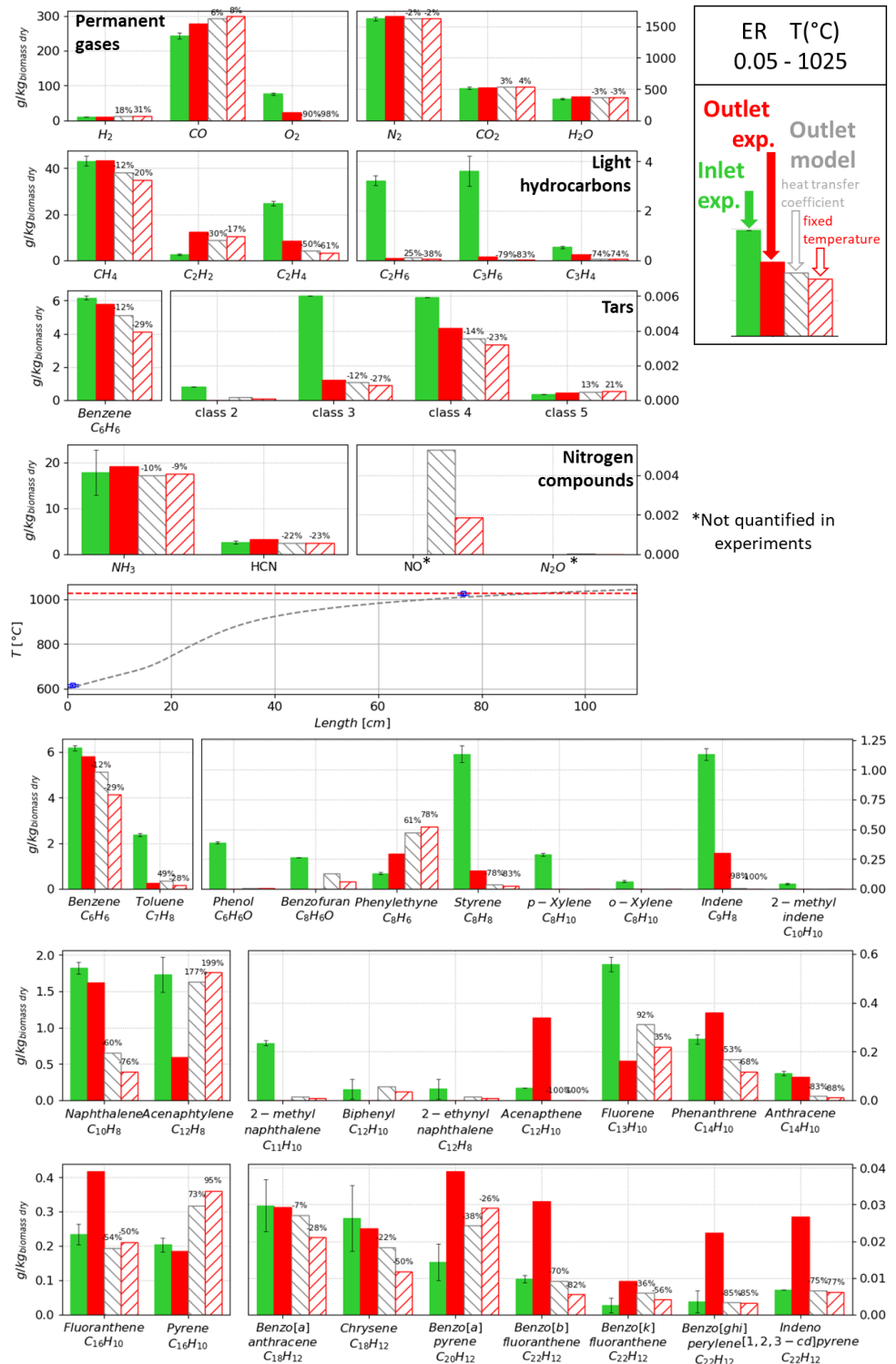


Figure 2-4: Experimental and modelled syngas composition at the inlet and outlet of the POX unit for case 0.05-1025. Simulated composition from plug flow.

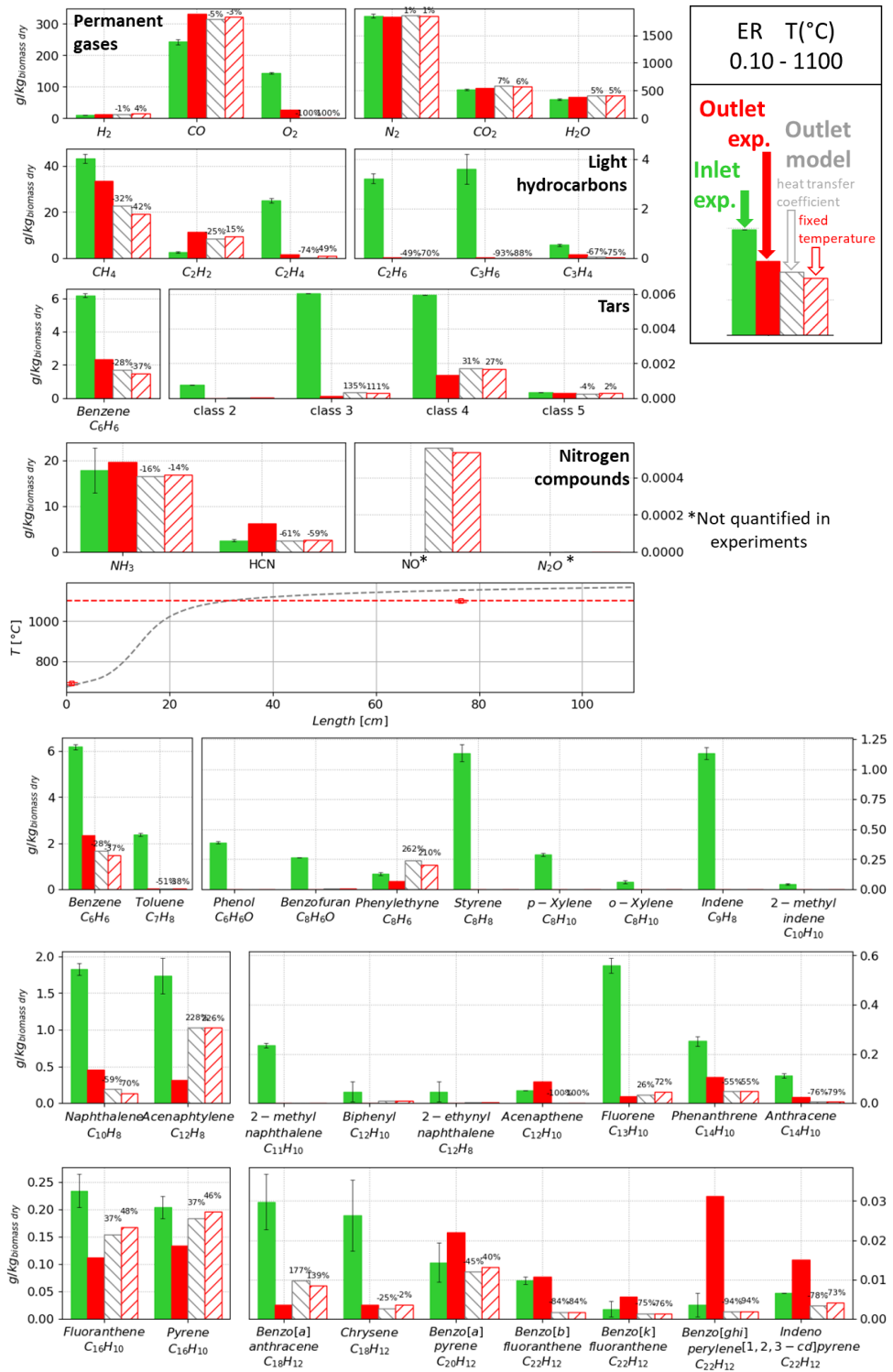


Figure 2-5: Experimental and modelled syngas composition at the inlet and outlet of the POX unit for case 0.10-1100. Simulated composition from plug flow.

Considering the results, the following recommendations could be made:

- To significantly reduce the tar content, a temperature around 1100°C must be reached.
- A balance should be made between the reduction of tars and the decrease of the lower heating value.
- The partial oxidation unit could contribute to the enrichment in CO and H₂.
- The use of pure oxygen instead of air decreases the amount of gas injected in the unit and the dilution of the syngas by nitrogen.

This kinetic mechanism gives a tool to estimate the potential reduction of tars with partial oxidation (residence time, amount of oxygen...). Despite the complexity of the kinetic model (number of species and reactions), the 1D plug flow model gives a fast solution. This model could be coupled with process modeling software (as Aspen Plus) to consider more complex systems and not only model molecules. Although all the intermediate species are not included in the global process model, they are included in the POX model and its kinetic model.

The perfect mixing assumption at the inlet of the plug flow is a big assumption. In fact, points of high oxygen concentration should be located near the air nozzles. This kinetic model could be used in CFD code to take into account the gas phase hydrodynamics to get more insights on the hot points in the mixing zone. This type of simulation could contribute to the design of such units.

2.2.6 Conclusion

This study presented detailed composition of biomass gasification syngas before and after partial oxidation unit at pilot-scale. The secondary air injected to the POX unit was varied with and without air preheating to consider the effect of temperature on the efficiency of the unit. Tars were reduced by 59 to 88% in these experiments.

These results were compared to a detailed radical kinetic model and showed a good agreement with experiments. The main components and also for most of the tar molecules were accurately modeled.

This data and model enable to simulate a partial oxidation unit without compromise on the number of species involved and the complexity of the kinetic mechanisms.

This kinetic model could be included in CFD model to consider hydrodynamics mechanisms. This should provide more insights on the crucial points to design this type of unit.

2.2.7 Supporting informations

The supporting information files 1 and 2 presents the thermodynamic properties of SYNPOX model and the kinetic model. The supporting information file 3 presents: 1) additional details on the experimental results, 2) a validation of the SYNPOX model for the soot formation, 3) the results of the cases not presented in the full-length article.

2.2.8 Fundings

This work was funded by the French PIA project “Lorraine Université d’Excellence” (reference ANR-15-IDEX-04-LUE) and by the Hy-C-GREEN project (Europe-FEDER and Grand-Est province).

2.2.9 References

- [1] Smil V. Energy Transitions: Global and National Perspectives. Second edition. Santa Barbara, California Denver, Colorado: Praeger, an imprint of ABC-CLIO, LLC; 2017.
- [2] Woolcock PJ, Brown RC. A review of cleaning technologies for biomass-derived syngas. *Biomass and Bioenergy* 2013;52:54–84. <https://doi.org/10.1016/j.biombioe.2013.02.036>.
- [3] Jenbacher GE. Technical Instruction No.: 1000-0302. Fuel Gas Quality, Special Gases 2009.
- [4] Bensabath T, Monnier H, Glaude P-A. Detailed kinetic modeling of the formation of toxic polycyclic aromatic hydrocarbons (PAHs) coming from pyrolysis in low-pressure gas carburizing conditions. *Journal of Analytical and Applied Pyrolysis* 2016;122:342–54. <https://doi.org/10.1016/j.jaat.2016.09.007>.
- [5] Valderrama Rios ML, González AM, Lora EES, Almazán del Olmo OA. Reduction of tar generated during biomass gasification: A review. *Biomass and Bioenergy* 2018;108:345–70. <https://doi.org/10.1016/j.biombioe.2017.12.002>.
- [6] Shen Y, Yoshikawa K. Recent progresses in catalytic tar elimination during biomass gasification or pyrolysis—A review. *Renewable and Sustainable Energy Reviews* 2013;21:371–92.

- [7] Ren J, Cao J-P, Zhao X-Y, Yang F-L, Wei X-Y. Recent advances in syngas production from biomass catalytic gasification: A critical review on reactors, catalysts, catalytic mechanisms and mathematical models. *Renewable and Sustainable Energy Reviews* 2019;116:109426. <https://doi.org/10.1016/j.rser.2019.109426>.
- [8] Anis S, Zainal ZA. Tar reduction in biomass producer gas via mechanical, catalytic and thermal methods: A review. *Renewable and Sustainable Energy Reviews* 2011;15:2355–77.
- [9] Hoeven TA, Der V. Partial product gas combustion for tar reduction 2007. <https://doi.org/10.6100/IR616553>.
- [10] Houben M. Analysis of tar removal in a partial oxidation burner. *Personality and Individual Differences - PERS INDIV DIFFER* 2004.
- [11] Valin S, Cances J, Castelli P, Thiery S, Dufour A, Boissonnet G, et al. Upgrading biomass pyrolysis gas by conversion of methane at high temperature: Experiments and modelling. *Fuel* 2009;88:834–42. <https://doi.org/10.1016/j.fuel.2008.11.033>.
- [12] Houben M, Delange H, Vansteenhoven A. Tar reduction through partial combustion of fuel gas. *Fuel* 2005;84:817–24. <https://doi.org/10.1016/j.fuel.2004.12.013>.
- [13] Svensson H, Tunå P, Hulteberg C, Brandin J. Modeling of soot formation during partial oxidation of producer gas. *Fuel* 2013;106:271–8. <https://doi.org/10.1016/j.fuel.2012.10.061>.
- [14] Characterization of tars and coke formed during the pyrolysis of methane in a tubular reactor. *Carbon* 1992;30:665–73. [https://doi.org/10.1016/0008-6223\(92\)90186-Z](https://doi.org/10.1016/0008-6223(92)90186-Z).
- [15] Mechanisms and kinetics of thermal reactions of aromatic hydrocarbons from pyrolysis of solid fuels. *Fuel* 1996;75:1441–8. [https://doi.org/10.1016/0016-2361\(96\)00136-6](https://doi.org/10.1016/0016-2361(96)00136-6).
- [16] Sarobe M, Kwint HC, Fleer T, Havenith RWA, Jenneskens LW, Vlietstra EJ, et al. Flash Vacuum Thermolysis of Acenaphtho[1,2-a]acenaphthylene, Fluoranthene, Benzo[k]- and Benzo[j]fluoranthene – Homolytic Scission of Carbon-Carbon Single Bonds of Internally Fused Cyclopenta Moieties at $T \geq 1100$ °C. *European Journal of Organic Chemistry* 1999;1999:1191–200. [https://doi.org/10.1002/\(SICI\)1099-0690\(199905\)1999:5<1191::AID-EJOC1191>3.0.CO;2-W](https://doi.org/10.1002/(SICI)1099-0690(199905)1999:5<1191::AID-EJOC1191>3.0.CO;2-W).
- [17] Winkler JK, Karow W, Rademacher P. Gas-phase pyrolysis of heterocyclic compounds, part 1 and 2: flow pyrolysis and annulation reactions of some sulfur heterocycles: thiophene, benzo[b]thiophene, and dibenzothiophene. A product-oriented study For part 3, see J.K. Winkler, W. Karow, P. Rademacher, ARKIVOC 1 (2000) 59. For part 4, see: J.K. Winkler, W. Karow, P. Rademacher, J. Anal. Appl. Pyrols. 57 (2000) 133. *Journal of Analytical and Applied Pyrolysis* 2002;62:123–41. [https://doi.org/10.1016/S0165-2370\(00\)00218-7](https://doi.org/10.1016/S0165-2370(00)00218-7).
- [18] Gai C, Dong Y, Yang S, Zhang Z, Liang J, Li J. Thermal decomposition kinetics of light polycyclic aromatic hydrocarbons as surrogate biomass tar. *RSC Adv* 2016;6:83154–62. <https://doi.org/10.1039/C6RA15513H>.
- [19] Tanoh TS. Production d'un syngaz par pyrogazéification de biomasse en vur d'une biométhanation. Université de Toulouse, 2021.

- [20] Liu X, Li W, Xu H, Chen Y. Production of light alkenes with low CO₂ emission from gas phase oxidative cracking (GOC) of hexane. *Reaction Kinetics and Catalysis Letters* 2004;81:203–9. <https://doi.org/10.1023/B:REAC.0000019424.06619.28>.
- [21] DeCoster J, Ergut A, Levendis YA, Richter H, Howard JB, Carlson JB. PAH emissions from high-temperature oxidation of vaporized anthracene. *Proceedings of the Combustion Institute* 2007;31:491–9. <https://doi.org/10.1016/j.proci.2006.07.211>.
- [22] Thomas S, Wornat MJ. The effects of oxygen on the yields of polycyclic aromatic hydrocarbons formed during the pyrolysis and fuel-rich oxidation of catechol. *Fuel* 2008;87:768–81. <https://doi.org/10.1016/j.fuel.2007.07.016>.
- [23] Mao Y, Dong Y, Wang B, Chang J, Yu J, Zhang Y, et al. Characteristics and kinetics of biomass tar cracking in a micro fluidized bed. *RSC Adv* 2015;5:82845–52. <https://doi.org/10.1039/C5RA13323H>.
- [24] Zhang R, Zhao S, Luo Y. Experimental and Modeling Investigation on the Effect of Intrinsic and Extrinsic Oxygen on Biomass Tar Decomposition. *Energy Fuels* 2017;31:8665–73. <https://doi.org/10.1021/acs.energyfuels.7b00989>.
- [25] Peng N, Huang C, Su J. An experimental and kinetic study of thermal decomposition of phenanthrene. *Journal of Hazardous Materials* 2019;365:565–71. <https://doi.org/10.1016/j.jhazmat.2018.11.026>.
- [26] Ledesma EB, Kalish MA, Nelson PF, Wornat MJ, Mackie JC. Formation and fate of PAH during the pyrolysis and fuel-rich combustion of coal primary tar. *Fuel* 2000;79:1801–14. [https://doi.org/10.1016/S0016-2361\(00\)00044-2](https://doi.org/10.1016/S0016-2361(00)00044-2).
- [27] McGrath T, Sharma R, Hajaligol M. An experimental investigation into the formation of polycyclic-aromatic hydrocarbons (PAH) from pyrolysis of biomass materials. *Fuel* 2001;80:1787–97. [https://doi.org/10.1016/S0016-2361\(01\)00062-X](https://doi.org/10.1016/S0016-2361(01)00062-X).
- [28] Wu W, Luo Y, Chen Y, Su Y, Zhang Y, Zhao S, et al. Experimental Investigation of Tar Conversion under Inert and Partial Oxidation Conditions in a Continuous Reactor. *Energy Fuels* 2011;25:2721–9. <https://doi.org/10.1021/ef200297s>.
- [29] Wongchang T, Patumsawad S, Fungtammasan B. An Analysis of Wood Pyrolysis Tar from High Temperature Thermal Cracking Process. *Energy Sources, Part A: Recovery, Utilization, and Environmental Effects* 2013;35:926–35. <https://doi.org/10.1080/15567036.2012.707748>.
- [30] Su Y, Luo Y, Chen Y, Wu W, Zhang Y. Experimental and numerical investigation of tar destruction under partial oxidation environment. *Fuel Processing Technology* 2011;92:1513–24. <https://doi.org/10.1016/j.fuproc.2011.03.013>.
- [31] Ahrenfeldt J, Egsgaard H, Stelte W, Thomsen T, Henriksen UB. The influence of partial oxidation mechanisms on tar destruction in TwoStage biomass gasification. *Fuel* 2013;112:662–80. <https://doi.org/10.1016/j.fuel.2012.09.048>.
- [32] Weston PM, Sharifi V, Swindenbank J. Destruction of Tar in a Novel Coandă Tar Cracking System. *Energy Fuels* 2014;28:1059–65. <https://doi.org/10.1021/ef401705g>.

- [33] Thimthong N, Appari S, Tanaka R, Iwanaga K, Kudo S, Hayashi J, et al. Kinetic modeling of non-catalytic partial oxidation of nascent volatiles derived from fast pyrolysis of woody biomass with detailed chemistry. *Fuel Processing Technology* 2015;134:159–67. <https://doi.org/10.1016/j.fuproc.2015.01.029>.
- [34] Dhahak A, Bounaceur R, Le Dreff-Lorimier C, Schmidt G, Trouve G, Battin-Leclerc F. Development of a detailed kinetic model for the combustion of biomass. *Fuel* 2019;242:756–74. <https://doi.org/10.1016/j.fuel.2019.01.093>.
- [35] Darido J, Dhahak A, Bounaceur R, Le Dreff - Lorimier C, Leyssens G, Cazier F, et al. Emissions from a Domestic Wood Heating Appliance: Experimental Measurements and Numerical Study Using an Equivalent Reactor Network (ERN) Approach Coupled with a Detailed Chemical Mechanism. *Energy Fuels* 2021;acs.energyfuels.1c01927. <https://doi.org/10.1021/acs.energyfuels.1c01927>.
- [36] Norinaga K, Deutschmann O, Saegusa N, Hayashi J. Analysis of pyrolysis products from light hydrocarbons and kinetic modeling for growth of polycyclic aromatic hydrocarbons with detailed chemistry. *Journal of Analytical and Applied Pyrolysis* 2009;86:148–60. <https://doi.org/10.1016/j.jaat.2009.05.001>.
- [37] Norinaga K, Shoji T, Kudo S, Hayashi J. Detailed chemical kinetic modelling of vapour-phase cracking of multi-component molecular mixtures derived from the fast pyrolysis of cellulose. *Fuel* 2013;103:141–50. <https://doi.org/10.1016/j.fuel.2011.07.045>.
- [38] Srinivas S, Field RP, Herzog HJ. Modeling Tar Handling Options in Biomass Gasification. *Energy Fuels* 2013;27:2859–73. <https://doi.org/10.1021/ef400388u>.
- [39] Ruiz M, Schnitzer A, Arnoux P, Mauviel G. Gasification of N-rich fibreboard in an air-blown fluidized bed reactor: A study on the fate of tars, NH₃ and HCN during oxidative mild Hot Gas Filtration. *Fuel* 2021;303:121317. <https://doi.org/10.1016/j.fuel.2021.121317>.
- [40] Kister J, Pieri N, Alvarez R, Díez MA, Pis JJ. Effects of Preheating and Oxidation on Two Bituminous Coals Assessed by Synchronous UV Fluorescence and FTIR Spectroscopy. *Energy Fuels* 1996;10:948–57. <https://doi.org/10.1021/ef950159a>.
- [41] Septien S, Valin S, Peyrot M, Spindler B, Salvador S. Influence of steam on gasification of millimetric wood particles in a drop tube reactor: Experiments and modelling. *Fuel* 2013;103:1080–9. <https://doi.org/10.1016/j.fuel.2012.09.011>.
- [42] Stagni A, Cuoci A, Frassoldati A, Faravelli T, Ranzi E. Lumping and Reduction of Detailed Kinetic Schemes: an Effective Coupling. *Ind Eng Chem Res* 2014;53:9004–16. <https://doi.org/10.1021/ie403272f>.
- [43] Pejpichertkul W, Ranzi E, Pelucchi M, Frassoldati A, Cuoci A, Parente A, et al. Examination of a soot model in premixed laminar flames at fuel-rich conditions. *Proceedings of the Combustion Institute* 2019;37:1013–21. <https://doi.org/10.1016/j.proci.2018.06.104>.
- [44] Saggesse C, Sánchez NE, Frassoldati A, Cuoci A, Faravelli T, Alzueta MU, et al. Kinetic Modeling Study of Polycyclic Aromatic Hydrocarbons and Soot Formation in Acetylene Pyrolysis. *Energy Fuels* 2014;28:1489–501. <https://doi.org/10.1021/ef402048q>.

- [45] Bird RB, Stewart WE, Lightfoot EN. Transport phenomena. second edition. 2007.
- [46] Rabou LPLM, Zwart RWR, Vreugdenhil BJ, Bos L. Tar in Biomass Producer Gas, the Energy research Centre of The Netherlands (ECN) Experience: An Enduring Challenge. Energy Fuels 2009;23:6189–98. <https://doi.org/10.1021/ef9007032>.

2.2.10 Supplementary Material

2.2.10.1 Experimental results

Table S2-1: Detailed results [g/kg feed (daf)]

Tar Class		REF	0.05-1025	0.1-1034	0.1-1050	0.1-1100
-	H ₂	10.3 ± 0.6	10.2	13.9	12.8	13.7
-	CO	242 ± 9	278	392	353	331
-	CO ₂	517 ± 18	521	546	572	540
-	CH ₄	43 ± 2	43	52	40	33
-	C ₂ H ₄	25 ± 1	8	4	3	2
-	C ₂ H ₆	3.2 ± 0.2	0.08	0.04	0.03	0.03
-	C ₂ H ₂	2.5 ± 0.2	12.4	13.2	12.4	11.3
-	C ₃ H ₆	3.6 ± 0.6	0.16	0.10	0.07	0.04
-	C ₃ H ₄	0.5 ± 0.05	0.23	0.26	0.20	0.15
-	N ₂	1387 ± 31	1659	1839	1875	1837
-	O ₂	3.4 ± 2.4	22.9	27.5	12.8	25.9
-	Benzene	6.2 ± 0.1	5.8	2.7	3.0	2.3
III	Toluene	2.37 ± 0.07	0	0.07	0.06	0.05
III	o-xylene	0.06 ± 0.01	0	0	0	0
III	p-xylene	0.29 ± 0.01	0	0	0	0
III	phenylethyne	0.13 ± 0.01	0.30	0.08	0.13	0.07
III	Styrene	1.13 ± 0.07	0.15	0	0	0
II	Phenol	0.35 ± 0.01	0	0	0	0
II	benzofuran	0.27 ± 0.00	0	0	0	0
III	Indene	1.13 ± 0.05	0.30	0.07	0.08	0.00
II	4-methyl-phenol	0	0	0	0	0
III	2-methyl-indene	0.07 ± 0.004	0	0	0	0
III	3-methyl-1H-indene	0.10 ± 0.004	0	0	0	0
III	1-ethylidene-1H-Indene	0.26 ± 0.03	0	0	0	0
IV	2-methyl-naphthalene	0.23 ± 0.01	0	0	0	0
IV	biphenyl	0.071 ± 0.04	0	0	0	0
IV	2-ethenyl-naphthalene	0.071 ± 0.04	0	0	0	0
IV	Naphthalene	1.83 ± 0.08	1.62	0.47	0.66	0.46
IV	Acenaphtylene	1.74 ± 0.24	0.59	0.25	0.38	0.32
IV	Acenaphtene	0	0.34	0.07	0.10	0.09
IV	Fluorene	0.56 ± 0.03	0.16	0.04	0.04	0.03
IV	Phenanthrene	0.25 ± 0.02	0.36	0.15	0.14	0.11
IV	Anthracene	0.11 ± 0.01	0.10	0.04	0.03	0.02
IV	Fluoranthene	0.23 ± 0.01	0.42	0.19	0.14	0.11
V	Pyrene	0.20 ± 0.02	0.19	0.13	0.13	0.13
V	Benzo[a]anthracene	0.030 ± 0.007	0.029	0.010	0.006	0.004
V	Chrysene	0.026 ± 0.009	0.024	0.011	0.006	0.004
V	Benzo[b]fluoranthene	0.010 ± 0.001	0.031	0.014	0.011	0.011
V	Benzo[k]fluoranthene	0.004 ± 0.002	0.009	0.005	0.005	0.006
V	Benzo[a]pyrene	0.014 ± 0.005	0.0391	0.0245	0.0221	0.0220
V	Dibenzo[a,h]anthracene	0.0077 ± 0.008	0.0243	0.0174	0.0176	0.0208
V	Benzo[ghi]perylene	0.0055 ± 0.0032	0.0222	0.0200	0.0205	0.0312
V	Indeno[1,2,3-cd]pyrene	0.0067 ± 0.0007	0.0266	0.0162	0.0134	0.0150
	NH ₃	18.2 ± 4.9	19.2	25.9	27.8	18.9
	HCN	2.5 ± 0.3	3.2	1.4	6.2	6.0
	H ₂ O	342 ± 13	386	361	388	389

Table S2-1 presents the detailed composition of the syngas before and after partial oxidation for all tests cases.

2.2.10.2 Validation of SYNPOX on soot formation

In order to validate the soot production, the results of the kinetic model SYNOX was compared with experimental data from Tanoh [19]. Cases 1 to 3 covered thermal cracking conditions, cases 4 to 7 steam reforming and case 8 oxy-steam-reforming. In all cases, a fixed temperature of 1200°C was considered.

Figure S2-1 and Figure S2-2 present the results of the SYNPOX model on isothermal plug flow reactor with eight different conditions. The tars injected consist in toluene and naphthalene.

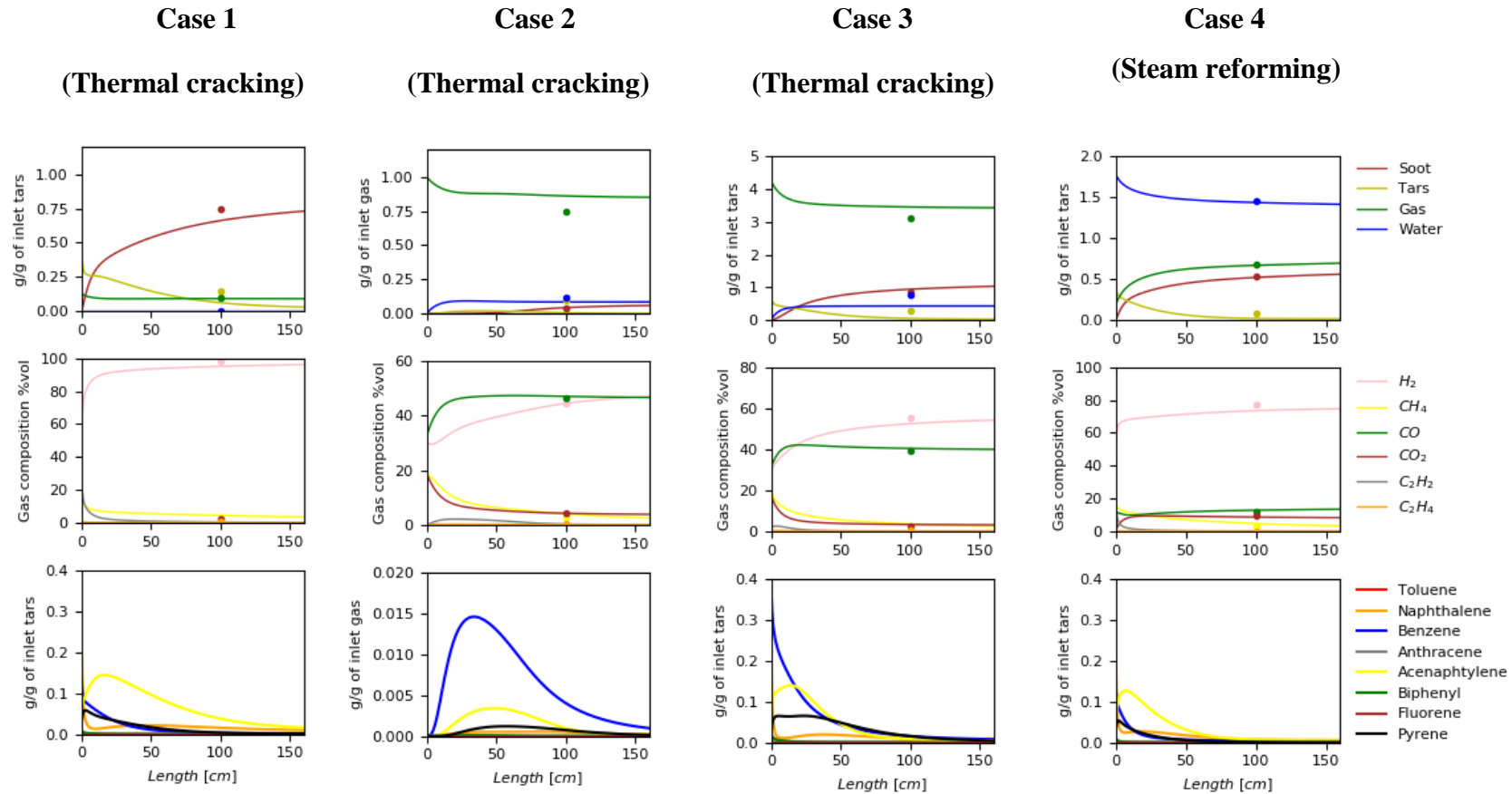


Figure S2-1: Comparison of Tanoh's experiment and SYNPOX model (cases 1 to 4).

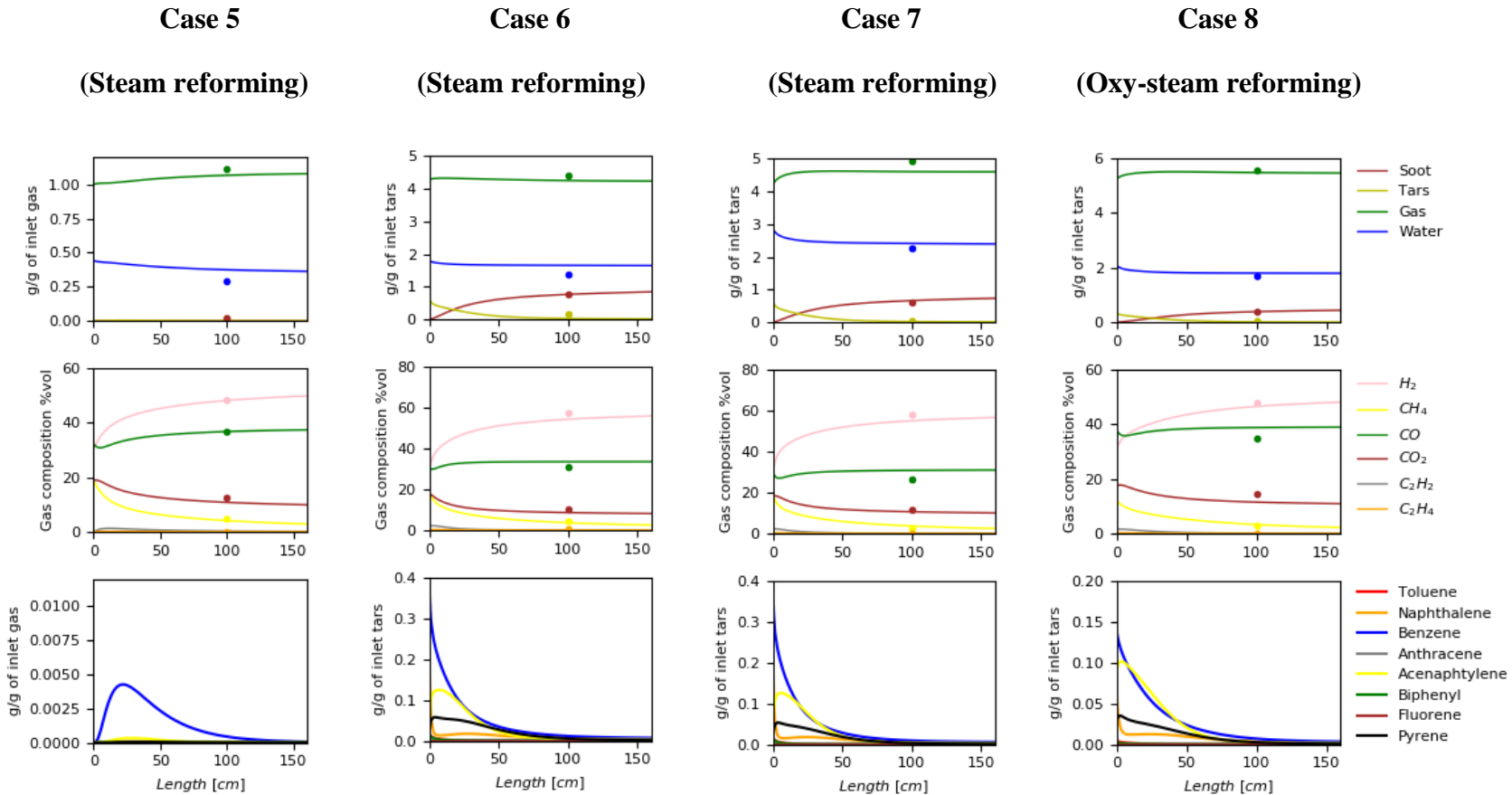


Figure S2-2: Comparison of Tanoh's experiment and SYNPOX model (cases 5 to 8).

2.2.10.3 Others results

Figure S2-3 and Figure S2-4 presents the results obtained for cases 0.10-1034 and 0.10-1050 respectively.

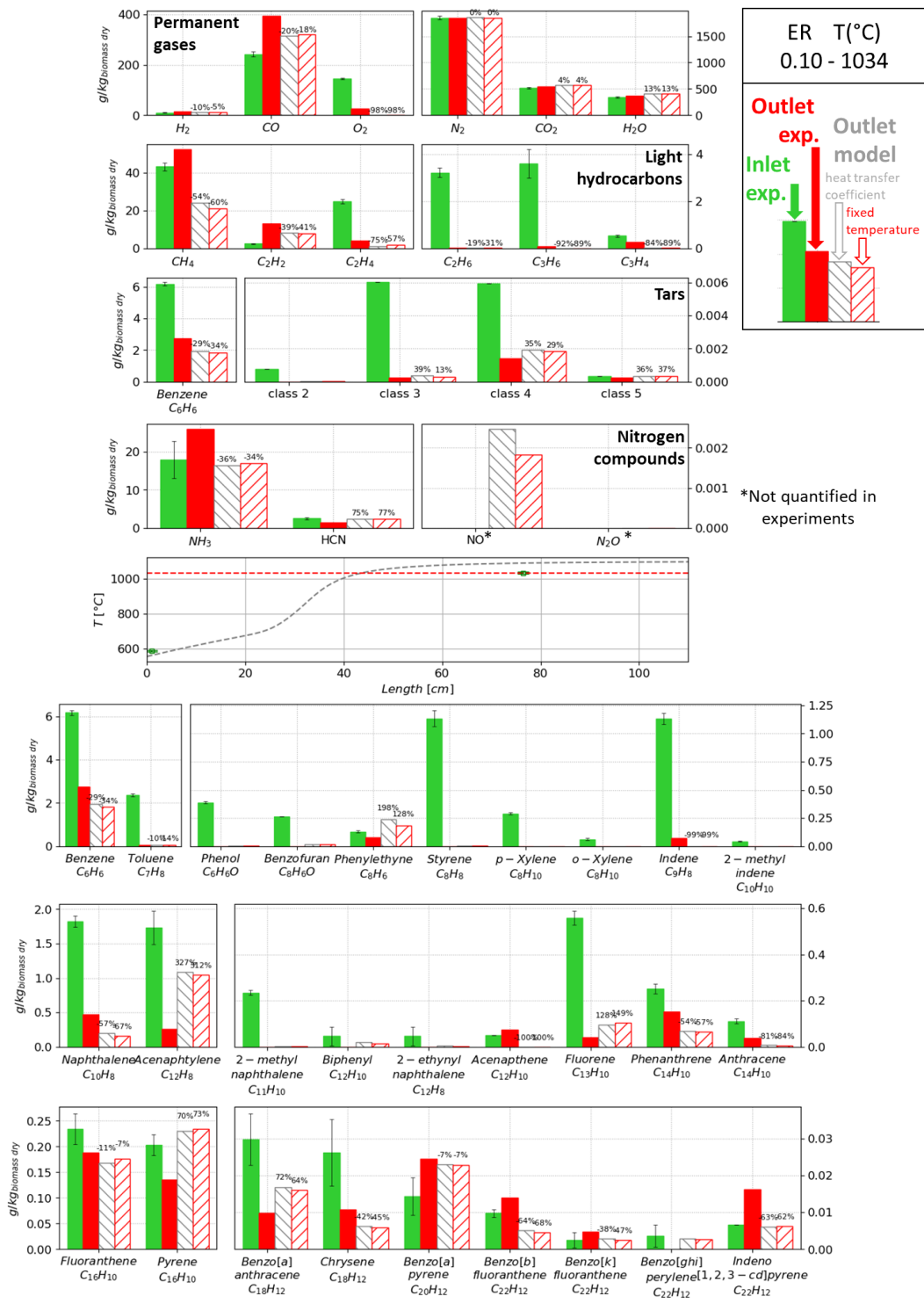


Figure S2-3 : Experimental and modelled syngas composition at the inlet and outlet of the POX unit for case 0.10-1034. Simulated composition from plug flow.

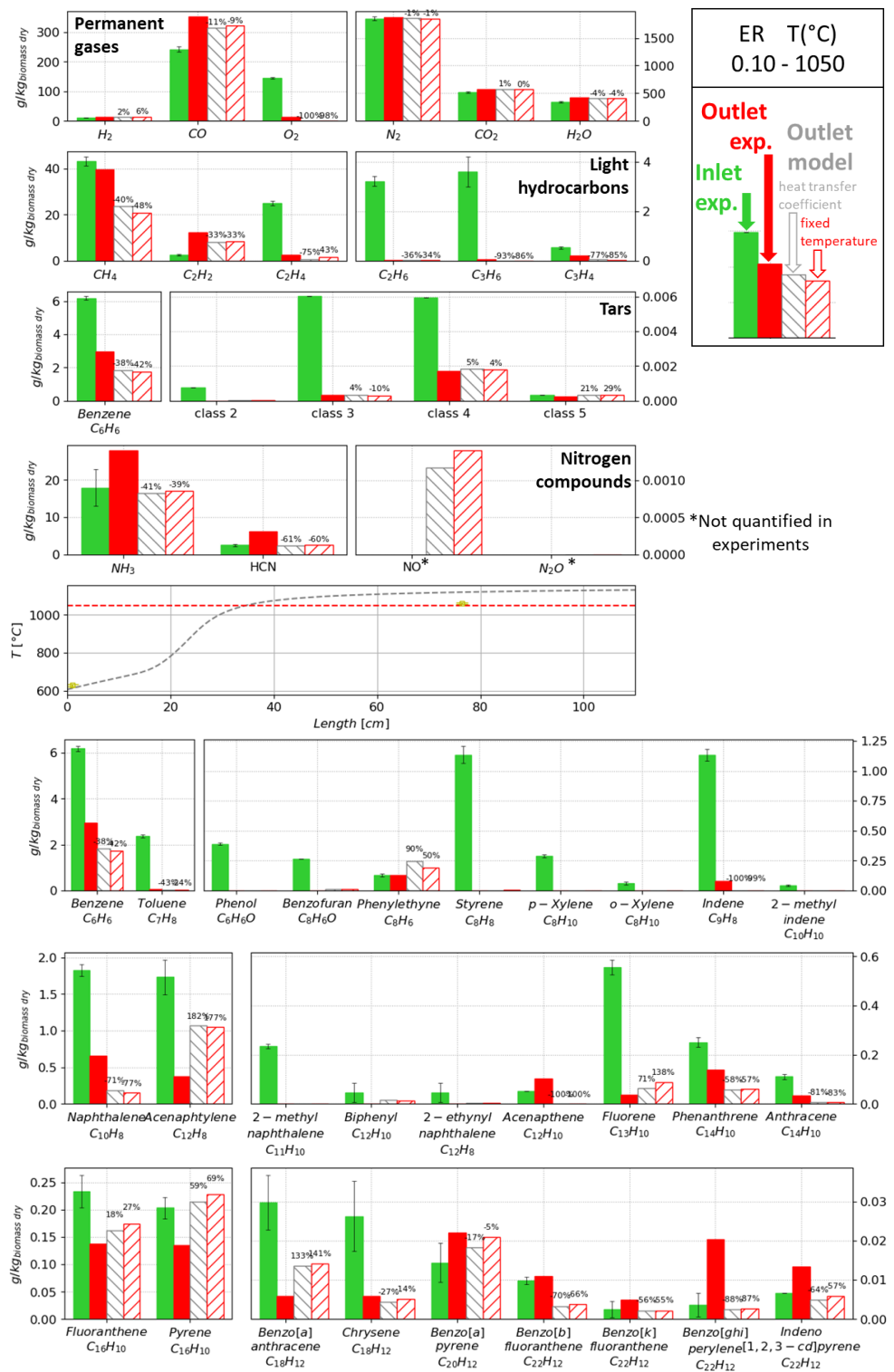


Figure S2-4 : Experimental and modelled syngas composition at the inlet and outlet of the POX unit for case 0.10-1050. Simulated composition from plug flow.

CHAPITRE 3 SIMULATION DE PROCÉDÉ

3.1 Introduction

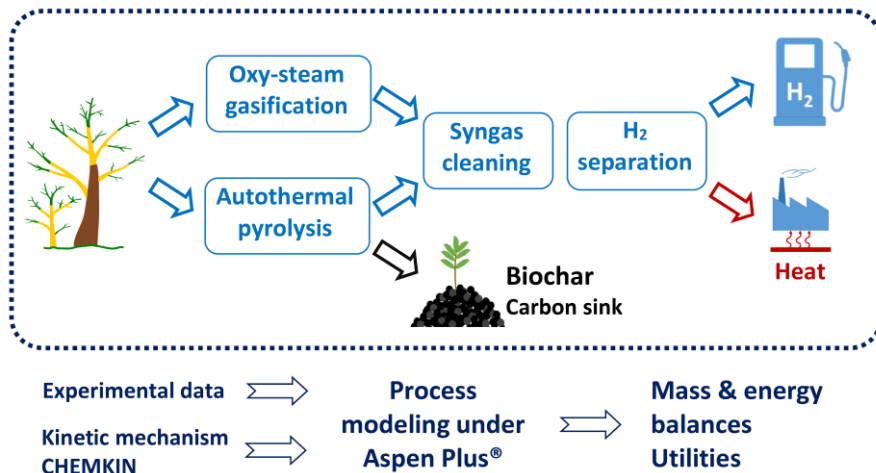
Ce chapitre propose trois voies de valorisation de la biomasse pour former de l'hydrogène. Les deux premiers scénarios consistent en une gazéification sous oxygène et vapeur d'eau suivi par une chaîne de traitement du syngaz. Le modèle de POX développé dans le chapitre précédent est repris ici. Le premier de ces scénarios vise la maximisation de la production d'hydrogène par l'intermédiaire de réacteurs catalytiques (reformeur, *water gas-shift*). La seconde option ne comprend pas ce type de réacteur. Enfin, dans un troisième scénario, une pyrolyse autotherme est envisagée suivie d'une oxydation partielle pour former un gaz riche en hydrogène. Dans les scénarios 2 et 3, la concentration d'hydrogène obtenue demeure relativement faible en amont du procédé de séparation. Une approche hybride combinant deux technologies de séparation est envisagée (PSA, membranes). Un effort est porté pour coupler les différents modèles à des données expérimentales quand elles sont disponibles.

3.2 Article 2 (reproduction intégrale)

Demol R., Dufour A., Rogaume Y., Mauviel G., Production of purified H₂, heat and biochar from wood: comparison between gasification and autothermal pyrolysis based on advanced process modeling, Energy and Fuels, 2022, 36, 1, 488–501.

<http://dx.doi.org/10.1021/acs.energyfuels.1c03528>

3.2.1 TOC graphic



3.2.2 Abstract

Biomass gasification is an interesting route for renewable hydrogen production, but it is still hampered by technical, environmental and economic issues. A first key step toward its development is the quantification of mass and energy balances of the integrated process. This work compares different processes to produce a purified H₂ from wood but also other products (heat, bio-char) at medium scale power (20 MW of biomass power inlet that corresponds to 3.7 t_{dry}/h). Three complementary processes were modeled under Aspen Plus including biomass drying, gasification-pyrolysis reactors and advanced syngas upgrading units. The first two cases are based on oxygen/steam gasification 1) with or 2) without catalytic reactors (steam reforming and water gas-shift). The third case is an autothermal oxidative pyrolysis resulting in bio-char and syngas. All the syngas cleaning process was detailed with a special focus on a partial oxidation (POX) unit to reduce the tar content. This unit was modeled by coupling Aspen Plus with Chemkin to predict tar and syngas composition by detailed elementary mechanisms. A hybrid hydrogen separation process is proposed combining membrane and pressure swing adsorption. A cape-open module for membrane modeling (called Memsic) was included in the whole process model. The global energetic efficiency is 75.4, 77.8 and 80.4% net for scenarios 1, 2 and 3, respectively. The hydrogen yields are 79, 26 and 18 g_{H₂}/kg_{biomass,dry} after separation and heat efficiencies - corresponding to hot water production - were 23.4, 60.0 and 49.0%net respectively. The option 3 produces 110 g_{biochar}/kg_{biomass,dry} which is a carbon sink. All utilities and consumables were also determined.

This model can be used for techno-economic and life cycle assessment studies. This methodology is also of interest to model all other thermochemical processes with detailed kinetics embedded in process models.

3.2.3 Introduction

Biomass is used for centuries to fulfill the heat and material demand for human activities. It is historically and even nowadays the first renewable energy^{1,2}. The growing concerns about climate change resulting from anthropogenic emissions and the forecasted peak in oil production pushes researchers to develop innovative processes for the production of energy commodities from renewables. The taxation of greenhouse gas emissions is expected to favor the development of carbon-neutral or even carbon-negative processes^{3,4}.

Among the ways to decarbonize human activities, hydrogen knows a growing interest for mobility applications and for lowering industry carbon intensity⁵. Yet, even if this fuel does not release carbon dioxide during its combustion, its production—mainly from steam methane reforming, does. If H₂ is produced from water electrolysis, the CO₂ emission problem is then related to the electricity generation processes. Different policies tend to promote renewable hydrogen. France fixed the objective to increase the share of renewable hydrogen to 20–40% in 2028 in the industry sector⁶. Besides water electrolysis from renewable electricity, the thermochemical processes also provide a potential way to produce hydrogen from biomass.

The gasification is the partial oxidation of a solid feedstock to produce a synthetic gas (syngas) made of CO, H₂, CO₂, CH₄, H₂O and light hydrocarbons. Polycyclic aromatic hydrocarbons (PAHs), NH₃, HCl, H₂S are also formed and must be removed from the syngas before its upgrading⁷. The gasifying agent could be steam in order to maximize the concentration of hydrogen but it leads to highly endothermic behavior. The use of air leads to syngas diluted with nitrogen when the gasification is direct: this option should be avoided because it hampers the H₂ purification. To overcome this problem, a dual fluidized bed can be used^{8,9} but it results in a complex technology notably due to loop seals¹⁰. Another way is to use pure oxygen and steam instead of air¹¹. In any cases, the fluidized bed temperature is typically higher than 750°C to convert the pyrolysis char into syngas¹².

Another thermochemical process can produce hydrogen: the pyrolysis, that may also be achieved in fluidized bed^{13,14}. This process produces char, tar and permanent gas. To overcome the endothermicity of pyrolysis, a small amount of oxygen can be added to reach autothermal conditions¹⁵. But this pyrolysis step alone does not lead to high H₂ yields. In this article, it is proposed to do the partial oxidation of the tar and gas produced by pyrolysis in a downstream gas-phase reactor. This second step is achieved by mixing oxygen with pyrolysis gas in a partial oxidation (POX) reactor to reach high temperature (> 1000°C), thus producing a H₂-rich syngas. Furthermore, the bio-char produced in the pyrolysis reactor enables carbon sequestration^{3,16}.

The hydrogen in the syngas is relatively diluted (even with oxy-steam gasification) in the range 30–45% vol on a dry basis^{11,17,18}. The production of hydrogen at high purity is difficult at this concentration for standard separation unit. Pressure swing adsorption (PSA H₂) is the classical technology. More than 70% vol of H₂ are required at the inlet¹⁹. To increase the content of H₂, a reformer and water-gas-shift catalytic reactors should be added^{11,20–22}. These reactors can be positioned after cold syngas cleaning^{4,20,23}, or rather, downstream the gasifier to promote heat integration. The use of catalytic reactors after a gasifier has been demonstrated with catalytic reformers^{24,25,11} and CO-shift catalytic reactors^{11,21,22,26}. The tar content must be reduced below 2 g/Nm³ dry basis (including benzene) at high temperature to avoid catalyst deactivation²⁵. No deactivation from H₂S was observed below 100 ppm¹¹.

The harvesting area of the biomass should be limited to minimize the economic and environmental impacts of its transport. Besides another argument for relatively small-scale biomass conversion process is linked to the fact that heat produced by the process should be valorized locally in order to increase the global efficiency²⁷. It is clearly easier to find a location for biomass gasifiers with a small heat demand (few MW) than a large one (dozens of MW). Finally, a local production of H₂ might be preferred for more direct and decentralized H₂ station for transport or industrial sectors, instead of a centralized production with H₂ transport by trucks²⁸.

The whole pyrogasification process must be modeled, from biomass drying to hydrogen separation, in order to assess the potential of the production of hydrogen from biomass. The study must also include co-products recovery and waste treatment. The modeling of pyrogasification processes has already been conducted, especially for the cleaning and conditioning of the syngas^{27,29} and also for hydrogen production at large-scale facilities^{19,20}. Gasification is often modeled as a combination of

RYIELD and RGIBBS reactors. Firstly, the biomass is decomposed into its elemental stable components (H_2 , C, O_2 , N_2 , H_2S , HCl). Then the RGIBBS reactor estimates the equilibrium composition at a given temperature³⁰. This model can give a rough estimate of the main components but it is unable to predict the yields of minor products (tars) which are the bottleneck of gasification. The tar formation and up-grading has been modeled but the chosen models are frequently overly simplistic³¹. Some research groups developed a fluidized bed model to predict the main products and some secondary products^{32–34}.

To the best of our knowledge, advanced models of the complete process, from biomass to purified H_2 , are still scarce, notably if one considers tar formation and upgrading.

Spath et al. has studied in a pioneering work the modeling of the complete process of hydrogen production from biomass gasification in an indirectly-heated gasifier. The steam reformer and water gas-shift reactors was positioned after wet scrubbing of tars inducing a heat penalty on the process²⁰. The scale (2000 dry ton/day) of this process makes possible the use of catalytic reactors but it requires long-distance collection of biomass. They used empirical correlations to model syngas and tar composition.

Martín and Grossmann presented the basis of a superstructure optimization for the production of Fischer-Tropsch diesel from biomass³⁵. The optimal solution to reach the targeted CO/ H_2 ratio was composed of an indirect gasifier and a steam reformer instead of direct gasification coupled to partial oxidation. No further composition adjustment (waster gas-shift, PSA H_2) was necessary for this application³⁵.

Syngas cleaning and upgrading processes usually consist in tar reformer, water gas-shift reactor and PSA H_2 ^{36–40}, possibly with Sulphur removal with a chelated iron solution (LO-CAT process)⁴¹. The tar reformer can be replaced by catalytic filter candles⁴². When tars species were considered, only few surrogate molecules were included^{36,42}. The purified H_2 yield was estimated to 76.1³⁶, 55.0⁴¹, 75.2⁴² or 107.4³⁷ g H_2 /kgbiomass. On an energetic basis, Kalinci et al. showed that gasifier and PSA exhibit the most energy and exergy losses along the process³⁸.

Marcantonio et al. modeled a circulating bubbling fluidized bed with a quasi-equilibrium approach model validated on experimental data from a pilot plant. They also investigated the use of a palladium membrane that gave a better H_2 recovery⁴³.

The purification of the syngas was investigated in more details with Ribeiro et al. by modeling the detailed PSA cycle to remove CO₂ from the syngas. H₂ and CO were dedicated for Fischer-Tropsch fuels production⁴⁴. To the best of our knowledge, no model was published on membrane combined with PSA for H₂ separation.

Our research group has developed previous Aspen Plus® models about biomass gasification and oxidation^{27,29,32,45,46} for heat or power production. Here, we complete our previous work on different pyro-gasification processes dedicated to the production of purified hydrogen and bio-char, with different gasification reactors and syngas refining units. We have also improved our modeling approach by including detailed kinetic mechanisms embedded under Aspen Plus.

The aim of this work is to provide detailed mass and energy balances for three processes along with utilities and consumables. These data are essential for further techno-economic and environmental assessment.

The first scenario considers the maximization of hydrogen production and a residual heat production. The second one is a simpler and probably cheaper process with lower hydrogen production but higher heat production. The third case is based on oxidative pyrolysis to produce bio-char (carbon sink), hydrogen and heat. All these options were modeled in Aspen Plus® associated with experimental data obtained from the literature and from a semi-industrial pilot plant (University of Lorraine, Epinal, France)⁴⁷.

Therefore, the novelty of this work can be outlined by these three main aspects:

- 1) To the best of our knowledge, these three processes were not yet modeled with the proposed detailed approach under the Aspen Plus framework, including elementary reactions for gas-phase reactions, hydrodynamic of fluidized bed, and advanced purification of H₂ (membrane permeation and PSA adsorption).
- 2) Novel results on gas cleaning in a Venturi scrubber on a gasification pilot plant are presented and embedded in the Aspen Plus model.
- 3) These three main routes of H₂, heat and bio-char production are compared and discussed based on their energy, mass and hydrogen balance.

3.2.4 Model description

3.2.4.1 Scenarios investigated

Three scenarios of hydrogen production from biomass were investigated (Figure 3-1). The three scenarios were designed for a territorial scale of 20 MW LHV-basis (30 kt dry biomass/year). The gasifier is a single fluidized bed reactor, which is cheaper and simpler to manage at territorial scale in comparison to dual fluidized bed technology. The gasifying agent is a mixture of oxygen and steam. Case 1 aims at maximizing the production of H₂ by implementing a steam reformer and water-gas shift catalytic reactors downstream the fluidized bed. It is based on experimental results of Corella et al.¹¹. Case 2 considers a simpler process without catalytic reactors, targeting a lower production of H₂ and a higher production of heat. The last case investigates the autothermal pyrolysis of biomass to produce bio-char and a H₂-rich gas obtained after the partial oxidation of the pyrolysis gas.

3.2.4.2 Description of the processes and modeling

The modeling approach is presented in Figure 3-1.

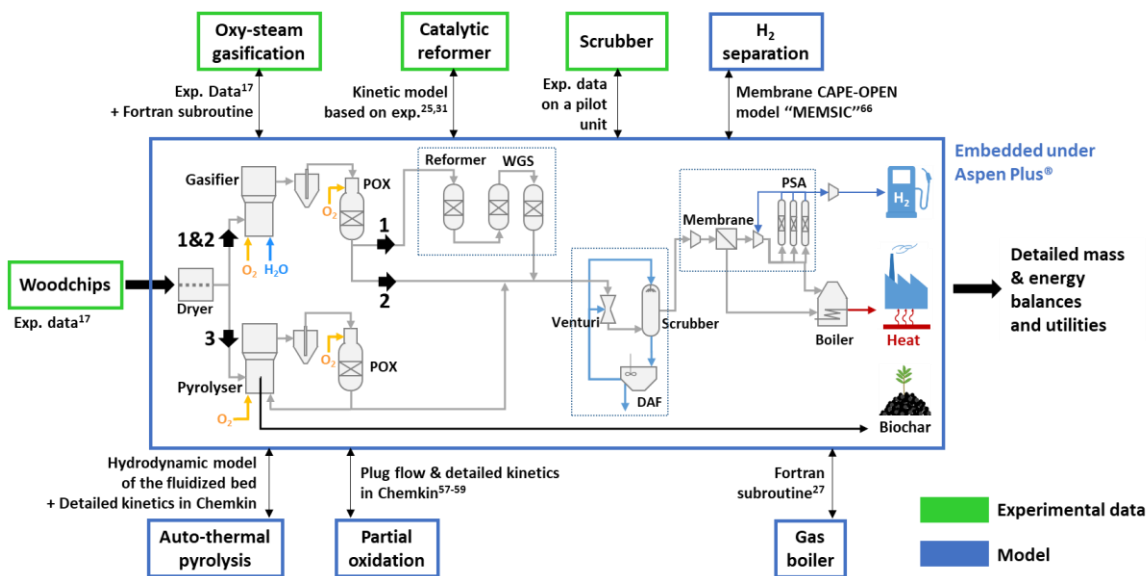


Figure 3-1: Simplified process flow diagram and the various modeling approach for each units.

Our model under Aspen Plus 8.8® handles a combination of experimental data, which were preferred when available, and of more fundamental modeling based on kinetics (for gas-phase or catalytic reactions) or on mass transfers (membrane) when experimental results on biomass real syngas were not available.

Figure 3-1 presents a simplified flow sheet of the 3 cases and Figure 3-2 the detailed flow sheet for case 1. The main assumptions of each process units are summarized in Table 3-2 and discussed here after.

The feedstock considered was woodchips, a by-product of the forest harvesting and wood industry. This biomass was supposed to be crushed directly in the forest or in dedicated platforms. The humidity was fixed to 40%wt after delivery. Table S1 provides the detailed composition of the feedstock.

The detailed flow sheets of the three options are presented in supporting information (SI) (Figure S1-S3). The equation of state RK-Aspen was used as it is recommended for hydrocarbon mixtures and light gases⁴⁸. The species BIOMASS and CHAR were modeled as non-conventional solids with their proximate and elemental composition. The heat of combustion was estimated with Mott and Spooner model, which is tailored for biomass and its high oxygen content⁴⁹.

3.2.4.2.1 Biomass drying

The biomass was considered dried down to 20%wt with the low-temperature heat contained in the boiler exhaust gas in order to increase energy efficiency and to limit the amount of tars produced by the gasifier⁵⁰. The dryer model was taken from François et al.²⁷. It estimates the VOCs emissions during the drying.

3.2.4.2.2 Oxygen production

Concerning the production of oxygen as gasifying agent, the VSA O₂ (vacuum swing adsorption) process is the most adapted one for small-scale production in the range of 10 to 200 tons of O₂ per day and if very highly pure O₂ is not required (93-95% v, the rest is mainly argon)⁵¹. The VSA O₂ was modeled as a simple separator to reach a purity of 93% v and a recovery rate of 55%⁵². Air was compressed at 1.5 bar before the columns. The purge pressure was set to 0.6 bar obtained with a

vacuum pump. An adsorbent commonly used consists of lithium-doped zeolites. The required adsorbent quantity was estimated from ref.⁵³.

3.2.4.2.3 Gasifier

The gasification and the pyrolysis were conducted in a bubbling fluidized bed, which is the most adapted technology for the targeted scale⁵⁴.

For cases 1 and 2, a real syngas composition from literature data was used in order to have a detailed and accurate composition of tars. Among few detailed results available in literature^{17,18}, the experimental results obtained by Schmid et al.¹⁷ in a steam/oxygen fluidized bed were selected (see SI S2). Their operating conditions were tailored to the production of hydrogen with an equivalent ratio (ER) of 0.25 and a molar steam to carbon ratio of 1 for a bed temperature at 850°C. The solid organic residue (char) yield was estimated to 10 g daf/kg of dry biomass. Gil et al. mentioned 5-20 g/kg daf as char yield for a steam-oxygen bubbling fluidized bed⁵⁵. Therefore, 10 g daf/kg dry biomass of char is an average common value for char yield produced by this technology. The elemental composition of char was assumed as: 85% C, 2% H and 13% O daf. The global solid residue recovered is made up of char and ash. An external Fortran subroutine linked to RYIELD model was used to compute the gas and tar composition according to the experimental results and to the biomass flow rate. Atomic balances in C, H, O, Cl and S were ensured by adjusting the CO₂, H₂O, O₂, HCl and H₂S flows, respectively. The heat balance was used in the RYIELD model to calculate the temperature of the syngas at the outlet assuming an adiabatic reactor.

3.2.4.2.4 Pyrolyser

In the case 3, an adiabatic fluidized bed pyrolyser was used. A small amount of oxygen was injected (auto-thermal conditions) to provide heat internally¹⁵. As a consequence, its behavior was very close to the auto-thermal fluidized bed gasifier used in the first scenarios. The main difference was the bed temperature below 600°C instead of 850°C. In this condition, pyrolysis char was an important product to be recovered. To the best of the author's knowledge, no detailed data on the auto-thermal pyrolysis presenting gas molecular composition (gas and tar) is available in the literature. Therefore, in order to model this auto-thermal pyrolysis, a model was developed to estimate the yield and detailed composition of pyrolysis products (char, gas, water and tars). Ranzi's model of biomass pyrolysis⁵⁶ and radical kinetic mechanisms⁵⁷⁻⁵⁹ were used. The ER used

was set to 0.10, slightly higher than the minimum ER of 0.08 estimated by Brown for autothermal pyrolysis at around 500°C to compensate heat losses¹⁵. The heat balance showed that an ER equals to 0.10 was able to reach a mean temperature in the fluidized bed of 565°C. Additional information on the pyrolysis model and a comparison with experimental results can be found in SI S3. A part of the syngas was recycled to the fluidized bed to maintain a fluidization velocity consistent to the gasification cases. An external Fortran subroutine was used to ensure mass balance similarly to the gasification reactor.

3.2.4.2.5 Partial oxidation, steam reformer and water-gas shift

When the production of H₂ is maximized (case 1), the process includes catalytic steam reformer and water gas shift units. These two steps were conducted at high temperature after the gasifier in order to promote heat integration and according to the experiments of Corella et al.¹¹. Unfortunately, the catalysts are sensitive to the concentration of tars which may cause their deactivation. 2 g/Nm³ (including benzene, dry basis) was recommended by Corella et al. as the targeted tar content for maintaining the stability of the catalytic reformer²⁵. Therefore, a partial oxidizing unit was used after the gasifier to reduce the tar content down to 2 g/Nm³. This limit can also be obtained by an optimized design and operation of the gasifier even if it was not the case with the experimental data used here for syngas composition since olivine was used as bed material. A better catalyst (dolomite, nickel-olivine) can contribute to the reduction of tar content, but it would also increase the operating costs. The addition of a small amount of oxygen in the syngas leads to the oxidation and cracking of tars at high temperature (over 1000°C). This POX unit was modeled by detailed kinetic models^{57–59} which were implemented by coupling Aspen Plus with ANSYS Chemkin Pro 17.0 (SI S4). For the gasification scenarios (1-2), the oxygen was adjusted to an equivalent ratio of 0.12 to reach the target of 2 g/Nm³ of tars. More details on the impact of this ER are given in SI, section S5.

Experiments on steam reforming and water-gas-shift with a real syngas were conducted in the literature^{25,60}. The reformer reactor was modeled with RPLUG and the kinetics of Corella's team²⁵ with a nickel-based catalyst (reactions and kinetics presented in SI S6). The dimensions of the reactor were adjusted to reach 95% conversion of methane according to Caballero et al.²⁴. This kinetic approach allowed to predict the remaining tars after the catalytic reformer.

Then, two stages of water gas shift were used, first at high temperature (350°C), second at a lower temperature (200°C) to promote CO conversion. The catalysts commonly used are iron/chromium oxide and Cu/ZnO/Al₂O₃ for high and low temperature respectively¹¹. The water-gas-shift reactors were modeled with RGIBBS model and a temperature approach of 20°C²⁰. A steam to CO ratio of 3 was used to maximize the H₂ production.

3.2.4.2.6 Wet scrubbing of syngas

As a final syngas polishing, water scrubber was chosen to remove residual tars and other contaminants (NH₃, HCl, H₂S). Even if this operation was not required for tar removal in case 1, the wet scrubber has another purpose: the condensation of the syngas water content. Table 3-1 presents the tar removal efficiency found in literature and based on a pilot system experiment with Venturi and wet scrubbers in series. This pilot plant at University of Lorraine (Epinal, France) can operate 50 kg biomass/h. The scrubbing water flow rate is about 1 m³/h.

This step was modeled as a FLASH unit and the composition of tars adjusted accordingly to the experimental results (of Table 3-1). The removal of NH₃, H₂S and HCl was modeled with ELECNRTL model²⁷.

3.2.4.2.7 Wastewater treatment

The species removed from the syngas and present in the scrubbing water were separated by coagulation and flotation in a dissolved air flotation unit (DAF) with the addition of soda to increase the pH along with flocculants and coagulant. The excess of water resulting from condensing water from the syngas was removed and sent to district water system after a fixed bed of activated carbon to remove the residual contaminants^{61,62}. The amount of activated carbon was estimated with ref.⁶².

3.2.4.2.8 Hydrogen separation

The standard process for H₂ separation is the pressure swing adsorption unit (PSA). Yet, the inlet concentration of H₂ should be at least 70%v to reach a high purity separation (99.99%v)²⁰. To achieve such high concentration at the inlet, a part of the pure hydrogen produced can be recycled at the inlet of the PSA²⁰. However, when the concentration of H₂ was too low (cases 2 and 3), a polyimide membrane permeable to H₂ was used before the PSA. The membrane plays the role of a H₂ pre-concentrator (more details are given in SI S7).

Table 3-1: Wet scrubber efficiency.

	Pilot plant, this work (Venturi + wet scrubber)^a	Rabou et al. (2009)⁶³ Water absorber
Benzene	0%	35%
Class 2^b	44% (global^c)	72%
o-Xylene	9%	
Phenol	99%	
o-Cresol	33%	
m,p-Cresol	100%	
Class 3^b	4% (global^c)	28%
Toluene	4%	
Class 4^b	70% (global^c)	69%
Indene	37%	
Naphthalene	58%	
2-methylNaphthalene	80%	
1-methylNaphthalene	82%	
Acenaphthylene	91%	
Acenaphthene	97%	
Fluorene	100%	
Phenanthrene	95%	
Anthracene	100%	
Fluoranthene	100%	
Class 5^b	100% (global^c)	50%
Pyrene	100%	

^aSyngas temperature around 150°C and 30°C at the inlet and outlet respectively, scrubbing water between 25 and 35°C at the inlet and outlet respectively.

^bECN classification⁶⁴.

^cThis value is an average that takes into account the relative yields of tars in this class.

The PSA was modeled as a SEP block with fixed recovery and purity, a part of the product was recycled to reach 70% v content in H₂²⁰. The recovery rate was assumed to be 85%. The amount of adsorbent (zeolite and activated carbon) was estimated based on NREL calculation⁶⁵. The membrane permeable to H₂ was modeled with the cape-open model called “MEMSIC” developed in our laboratory⁶⁶.

The optimal design of the hybrid H₂ separation unit was determined based on the specific separation cost. The method used for the determination of the optimal architecture (membrane surface, pressure on the retentate and permeate of the membrane) is described in SI S7. The goal was to achieve 99.99% vol hydrogen purity of hydrogen provided at 70 bar.

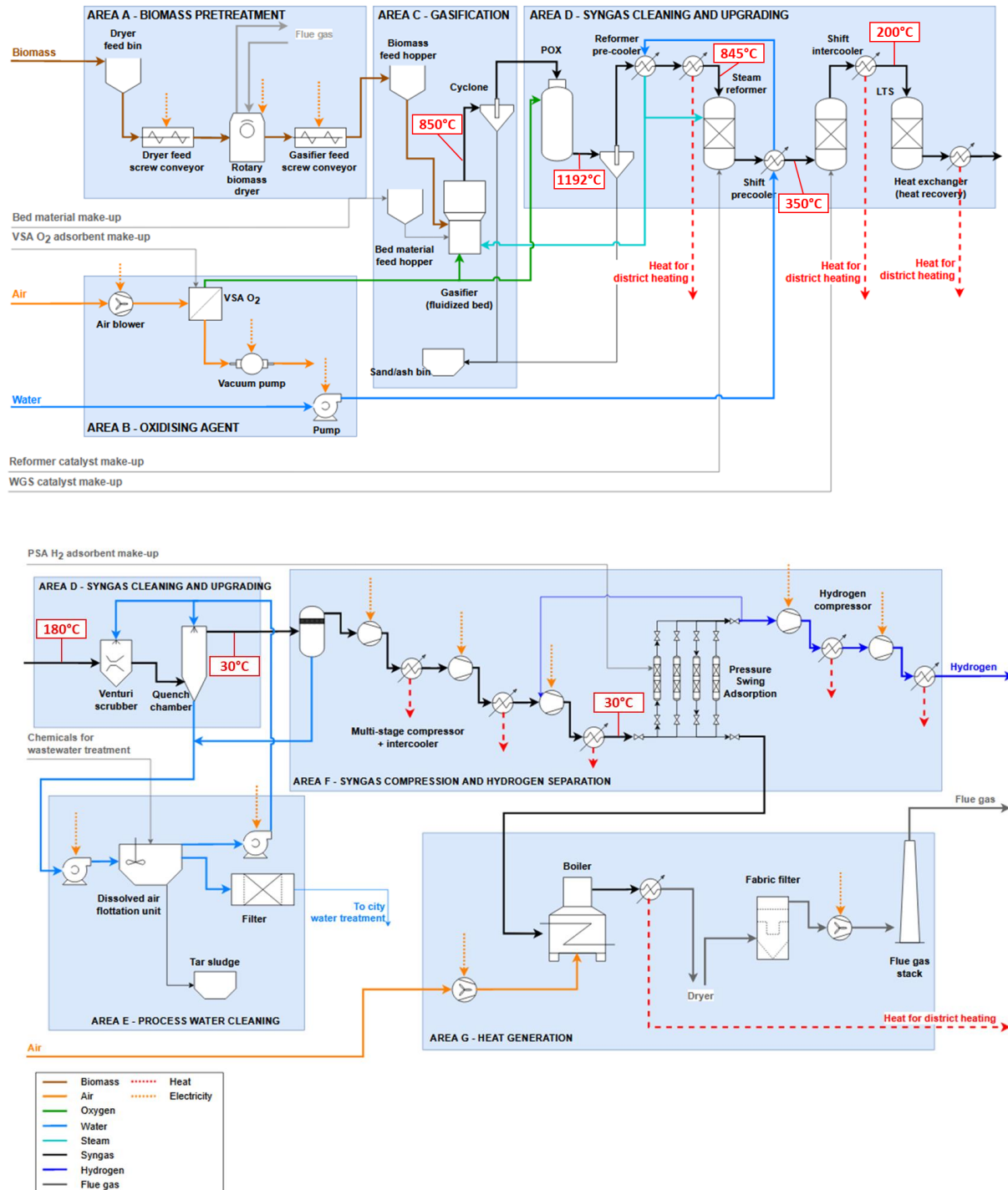


Figure 3-2: Detailed flow diagram of case 1.

3.2.4.2.9 Heat generation

The tail gas of the hydrogen separation unit still contains some H₂, CO, CH₄ and C₂. Its lower heating value was too low for using it in an internal combustion engine for electricity production. Therefore, this gas was burnt in a gas boiler to produce heat for a heating network. The temperature range of the water network was 40/80°C.

The gas boiler model was adapted from François et al.²⁷. We have implemented a Fortran subroutine fixing the pollutants yields based on the exhaust gas concentration of an industrial gas boiler. The atomic mass balance was computed with the same procedure as for the gasifier model.

3.2.4.2.10 Thermal integration

A pinch analysis was performed to build the heat exchanger network. The steam required for gasification was obtained with heat exchangers cooling the syngas before the reformer and the water-gas shift (case 1) or before the wet scrubber (case 2). The excess of heat was recovered for the heating network. Syngas and hydrogen compression requires multistage compression with intercooler. A part of this heat was used for preheating steam flow to feed the gasifier and the steam reformer, another part was recovered for the heat network. A small amount of cold water (15°C) was required as cooling utility to reach the lowest temperatures level in the process (30°C, between two compression stages).

Table 3-2: Assumptions of the Aspen Plus model, utilities and material consumption.

Unit	Methods	Results
Drier ^b	Adapted from François et al. ²⁷	Heat required, VOCs emissions
VSA O ₂ ^{a,c}	SEP, O ₂ recovery rate 55%	Air input
Gasifier ^d	RYIELD with external Fortran subroutine (experimental data ¹⁷ and atoms balances)	Composition of the syngas, temperature reached
Auto-thermal pyrolyser	RYIELD with external Fortran subroutine (ChemkinPro)	Composition of the syngas and bio-char, temperature reached
Cyclone	SEP, ΔP = 0.5 kPa	
POX	Fortran subroutine, CHEMKIN-PRO simulation with adiabatic plug-flow reactor and radical kinetic mechanism ⁵⁷⁻⁵⁹	Composition of the syngas after POX unit, temperature reached
Steam reformer ^e	RPLUG, kinetics in SI S6, T _{inlet} 845°C	Composition and temperature of the syngas after reformer, amount of catalyst.
Water-gas-shift ^f	RGIBBS, temperature approach 20°C, ΔP = 0.4 kPa, HTS (T _{inlet} 350°C), LTS (T _{inlet} 200°C)	Composition and temperature of the syngas after WGS, amount of catalyst.
Water scrubber ^g	FLASH with experimental data, ΔP = 0.15 kPa water flow rate adjusted to reach a syngas at 30°C at the outlet.	Composition of the syngas after scrubber
Compressor ^a	Multi-stage compressor with intercooler (30°C), GPSA method, polytropic efficiency 0.80 and mechanical efficiency 0.98	Power required and outlet temperature.
Membrane H ₂ ⁱ	Cape-open MEMSIC ⁶⁶ , countercurrent flow pattern and permeance for UBE B-H membrane from ⁶⁷ .	Compositions of the outlets and the corresponding membrane surface area
PSA H ₂ ^h	SEP, recovery efficiency 85%, ΔP = 5 kPa	Flow of hydrogen produced, composition of the tail gas, amount of adsorbent.
Air booster ^a	GPSA method, polytropic efficiency 0.80 and mechanical efficiency 0.98	Power required and outlet temperature.
Gas boiler	RYIELD with external Fortran subroutine adapted from François et al. ²⁷ - excess of air λ=1.5 - CO: 0.006 kg/Nm ³ - C ₁₀ H ₈ : 4 10 ⁻⁹ kg/Nm ³ - Other PAHs: 1.5 10 ⁻⁹ kg/Nm ³ (acenaphthylene, anthracene, phenanthrene, pyrene) mole fraction 0.25 each.	Heat generated by the boiler, exhaust gas composition.

	- NO mass fraction from oxidation of atmospheric N ₂ 7 10 ⁻⁵ - Soot 3 10 ⁻⁵ kg/Nm ³ - VOC 0.25 g/Nm ³	
Heat exchanger	ΔP = 2 kPa, minimum temperature approach 5°C	Surface area

^aEstimated from Aspen Plus model assuming 80% polytropic efficiency and 98% mechanical efficiency for compressors and boosters.

^bRef ²⁰ is used for conveyor and dryer consumption.

^cMass of fresh adsorbent per year estimated from Peters et al. and Swanson et al.^{19,68}, adsorption isotherms for lithium doped adsorbent⁵³ assuming a 1-year lifetime (7500 hours of operations).

^dAssuming 2.6 kg/h of fresh bed material for a 20 MW gasifier.

^eAssuming SV 14 000 h⁻¹ and density 1025 kg/m³ ²⁴, catalyst replacement 33% per year.

^fAssuming SV 2 700 h⁻¹ for HTS (iron and chromium oxide BASF K6-11 in¹⁰) and SV 5100 h⁻¹ for LTS (Cu/ZnO/Al₂O₃ BASF K3-110 in¹¹) and catalyst density 897.0 kg/m³, catalyst replacement 33% per year.

^gChemicals required for Dissolve Air Flotation unit and activated carbon guard bed for residual tars. Amount of activated carbon estimated assuming 3.25 g PAH adsorbed per g of activated carbon⁶².

^hMass of fresh adsorbent per year estimated from Peters et al. and Swanson et al.^{19,68}, adsorption isotherms for activated carbon and zeolite adsorbent⁶⁵ assuming a 4-year lifetime (7500 hours of operations).

ⁱSince membrane module lifetime is expected to last 5 years, it assumed 20% of membrane surface replacement per year.

3.2.4.3 Definition of energetic efficiency

The energetic efficiency is defined with reference to the lower heating value of woodchips on dry basis. The net η_{net} and gross η_{gross} energetic efficiencies are linked to heat η_{hn} , hydrogen η_{H_2} and bio-char $\eta_{biochar}$ efficiency.

$$\eta_{net} = \eta_{hn} + \eta_{H_2} + \eta_{biochar} - \eta_{power\ consumption} \quad (1)$$

$$\eta_{gross} = \eta_{hn} + \eta_{H_2} + \eta_{biochar} \quad (2)$$

$$\eta_{hn} = \frac{\dot{Q}_{hn}}{\dot{m}_{wood,dry} \cdot LHV_{wood,dry}} \quad (3)$$

$$\eta_{H_2} = \frac{\dot{m}_{H_2} \cdot LHV_{H_2}}{\dot{m}_{wood,dry} \cdot LHV_{wood,dry}} \quad (4)$$

$$\eta_{biochar} = \frac{\dot{m}_{biochar} \cdot LHV_{biochar,dry}}{\dot{m}_{wood,dry} \cdot LHV_{wood,dry}} \quad (5)$$

$$\eta_{power\ consumption} = \frac{\dot{W}_{consumption}}{\dot{m}_{wood,dry} \cdot LHV_{wood,dry}} \quad (6)$$

\dot{Q}_{hn} is the heat power sent to the heat network, $\dot{m}_{wood,dry}$, \dot{m}_{H_2} and $\dot{m}_{biochar}$ the mass flowrate of biomass, hydrogen and biochar. $\dot{W}_{consumption}$ is the electrical power consumption. $LHV_{biochar,dry}$ and $LHV_{wood,dry}$ are the lower heating value of biochar and wood.

3.2.5 Results and discussion

3.2.5.1 Energy & Mass balance

The energy balances of each option are presented in Figure 3-3. The mass balance and the detailed composition of the main streams are available in SI S1. The main utilities consumptions including catalysts and adsorbents (Activated carbon AC and zeolite Ze) are given in Table 3-3. The electricity consumption was mainly driven by the hydrogen separation step and its compressors. The first option was the most electricity consuming because the entire syngas was compressed to 25 bar whereas the first stage of separation in cases 2 and 3 required a lower pressure (5 bar) (see supporting information S7). The electricity demand was also higher because of the final compression of H₂ on a bigger flow rate. The estimated amount of activated carbon to clean the excess water of residual PAHs and other contaminants was lower in the case 1 since the steam reformer reactor exhibits a catalytic effect on the tar reduction. The worst case for activated carbon consumption was the third case due to a higher quantity of tars in the syngas before wet scrubbing.

Spath et al. studied a similar process with indirectly heated biomass gasifier on a larger scale (434 MW LHV-basis). They determined a gross efficiency of 49.8% and a net efficiency of 45.6% for the production of hydrogen²⁰. We found in this work a higher H₂ efficiency (57.6% gross and 52.0% net in case 1). This is mainly due to a better conversion of biomass into H₂ and CO in our

case. At the exit of the gasifier, the yields were $24.8 \text{ mol}_{\text{H}_2}/\text{kg}_{\text{biomass dry}}$ and $11.7 \text{ mol}_{\text{CO}}/\text{kg}_{\text{biomass dry}}$ ($\text{O}_2/\text{H}_2\text{O}$ bubbling fluidized bed¹⁷) compared to $8.4 \text{ mol}_{\text{H}_2}/\text{kg}_{\text{biomass dry}}$ and $14.8 \text{ mol}_{\text{CO}}/\text{kg}_{\text{biomass dry}}$ in Spath et al.²⁰ (a dual fluidized bed).

The second case without catalytic reactors gives a similar global efficiency (77.8% net) but the production of heat was higher (60.0% instead of 23.4%) and the production of H_2 smaller (17.9% instead of 52.0%). The second case is less interesting based on H_2 production, but its CAPEX and OPEX are probably significantly lower (two catalytic reactors were removed). Furthermore, this process can present an interest for the co-production of H_2 and heat for sites with higher heat demands.

The third case of autothermal pyrolysis and its three products (hydrogen, heat and bio-char) gives a higher efficiency (80.4% net) when the bio-char is considered as an energy product. The two energy vectors (hydrogen and heat) represent a 51.2% net efficiency. A large amount of syngas was recycled to the pyrolyser to maintain its fluidization.

In the autothermal pyrolysis option (case 3), 408 kg/h of bio-char are produced corresponding to a char yield around 11.0% daf and a carbon yield of 16.6%. This bio-char yield should be considered with caution because it is estimated from Ranzi's model of biomass pyrolysis and not validated in a pilot plant. Yet, this model gives a rough estimate of the bio-char composition and the gas and tar detailed composition. As a comparison, Polin et al. conducted autothermal pyrolysis at 500°C in a fluidized bed of two biomasses: Red Oak and corn stover with an ER of 0.10 and 0.068, respectively. The biochar yields were 9.5%wt for Red Oak and 20.1%wt for corn stover. The corresponding carbon yields were estimated to 14.5% for Red Oak and 26.7% for corn stover^{69,70}. The Red Oak experiments are compared with the results of this model in SI 3. The model predicts nicely the overall permanent gas mass yield but over-predicts the char yield (see SI 3 for more details).

Table 3-3: Utilities consumption.

	Case 1	Case 2	Case 3
Electrical consumption [MWe]	2.08	1.66	1.36
Fresh water for steam generation [thousands of m ³ /y]	25.9	9.4	0
Adsorbent VSA O ₂ [t/y]	0.96	0.96	0.63
Bed material [t/y]	19.5	19.5	19.5
Reformer catalyst [t/y]	0.25		
WGS catalyst [t/y]	HTS: 1.26 LTS: 0.68		
Chemicals for water treatment	NaOH: 210 t/y Flocculant: 23 m ³ /y Coagulant: 23 m ³ /y AC: 0.37 t/y	NaOH: 210 t/y Flocculant: 23 m ³ /y Coagulant: 23 m ³ /y AC: 11.7 t/y	NaOH: 210 t/y Flocculant: 23 m ³ /y Coagulant: 23 m ³ /y AC: 24.8 t/y
Adsorbent PSA H ₂ [t/y]	AC: 0.465 Ze: 0.371	AC: 0.090 Ze: 0.071	AC: 0.063 Ze: 0.049
Membrane H ₂ area [m ² /y]		300	300
Natural gas ^a [Nm ³ /y]	3600	3600	3600
Nitrogen ^b [Nm ³ /y]	3600	3600	3600

^aEstimate for two start-ups per year and auxiliary fuel for flare.

^bEstimate for the nitrogen safety system.

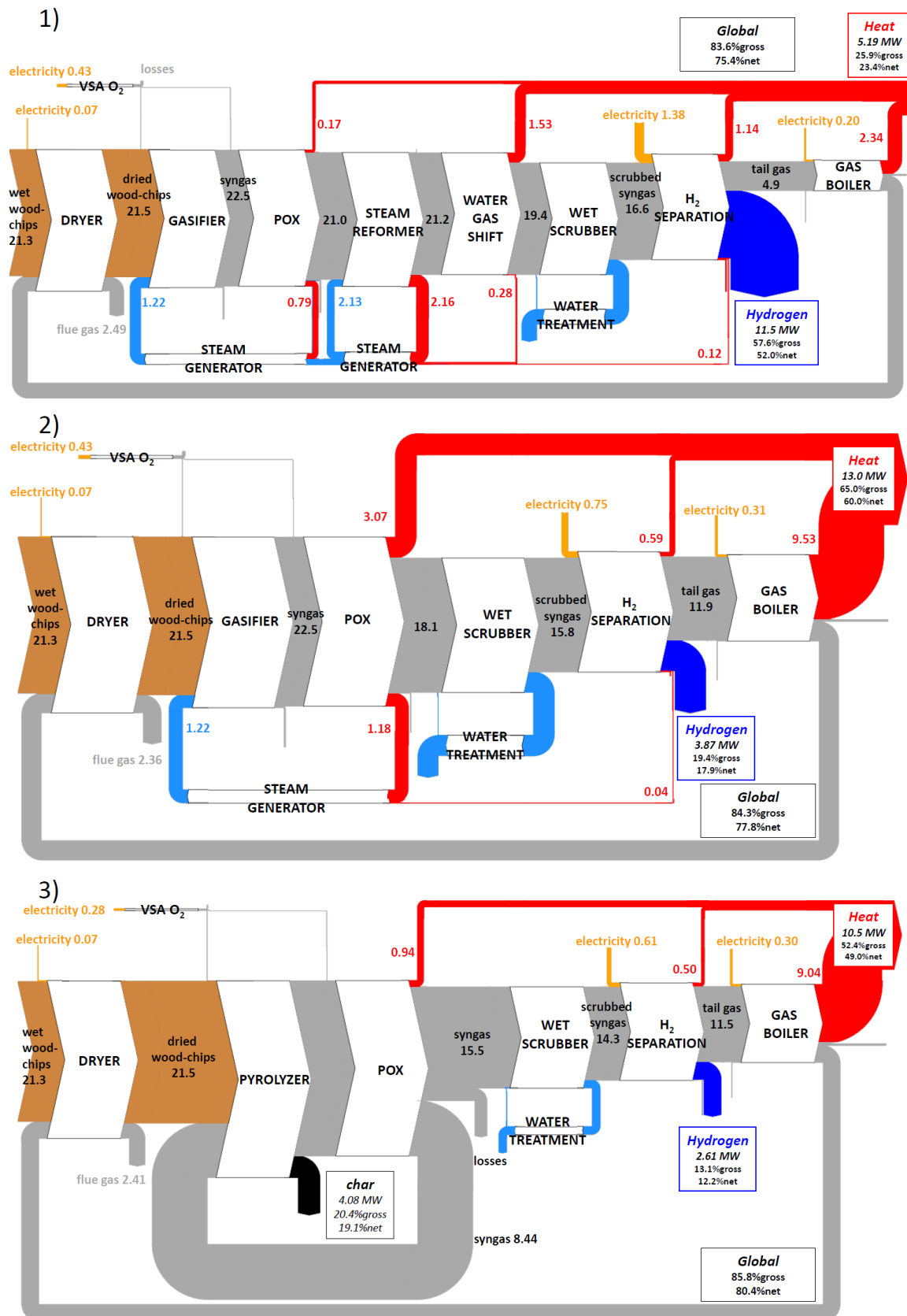


Figure 3-3: Sankey's type diagrams (in MW) of the 3 cases.

3.2.5.2 Fate of hydrogen along the process unit

Figure 3-4 shows the molar flow rate and fraction of hydrogen along the process for each option.

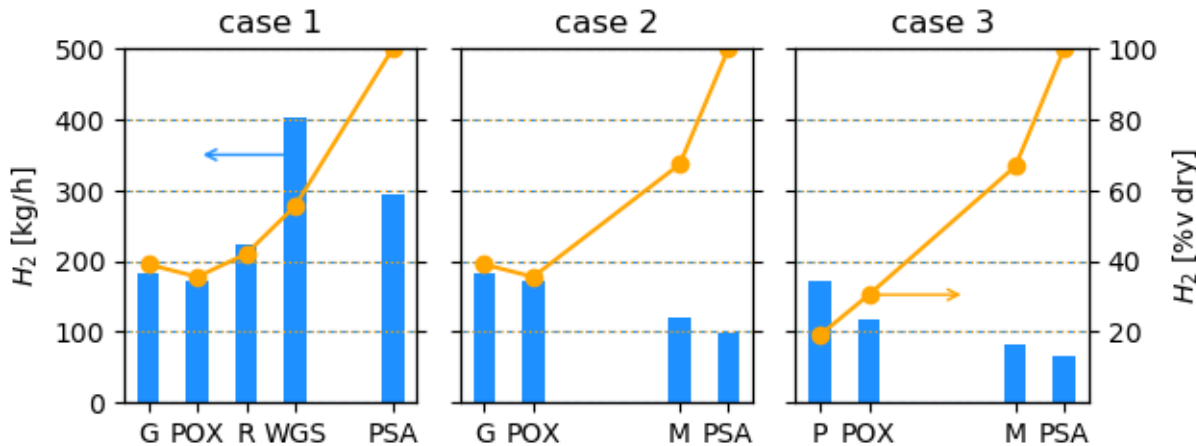


Figure 3-4: Hydrogen molar flow rate and fraction along the process. G=Gasifier, P=Pyrolyzer, POX=Partial Oxidation, R=Reformer, WGS=Water Gas Shift, M=Membrane, PSA=Pressure Swing Adsorption.

The objective was to reach 70% vol of H_2 before the PSA to produce quasi-pure hydrogen with the PSA H_2 . The flow rate of hydrogen is doubled when catalytic reformer and water-gas shift reactors are used (Figure 3-4). Its molar fraction is increased from 35.5% to 55.5% db. This concentration is reached in case 2 and 3 with a membrane module (67.3 and 66.8%db respectively for cases 2 and 3). The 70% vol concentration is achieved by recirculating a part of the hydrogen produced.

In the best case (1), $107 \text{ g}_{H_2}/\text{kg}_{\text{biomass,dry}}$ could be produced in which 79 g are effectively separated (76% recovery). This result compares well with the $140 \text{ g}_{H_2}/\text{kg}_{\text{biomass,dry}}$ produced claimed by Corella et al.¹¹ for oxy-steam gasification followed by reformer and shift reactors. This lower yield of hydrogen can be explained by the partial oxidation of a part of the hydrogen in the POX unit. This reactor is necessary because the syngas produced by Schmid et al.¹⁷ contains more tars than Corella et al.¹¹ with dolomite as bed material. Indeed the syngas produced by Corella et al. contains less than 2 g/Nm^3 of tars whereas, the syngas produced by Schmid et al. contains 38 g/Nm^3 ¹⁷.

When catalytic reactors are removed, the hydrogen production is divided by a factor of 2 or 3. In case 2, $47 \text{ g}_{H_2}/\text{kg}_{\text{biomass,dry}}$ could be produced in which 26 g are effectively separated. In the case

3, 31 g_{H₂}/kg_{biomass,dry} could be produced and 18 g are separated. These two cases present smaller hydrogen production but they could be more suitable for a territorial level: the processes are simpler and more robust than with catalytic reactors. The separation process of hydrogen was chosen to minimize the hydrogen specific separation cost but this architecture did not lead necessarily to the maximum hydrogen recovery rate. A higher production of H₂ would lead to higher specific separation cost. In case 3, char is produced and may be used to create a carbon sink.

The final H₂ yield of case 1 (79 g_{H₂}/kg_{biomass,dry}) is in good agreement with previous studies. In bubbling fluidized bed, Ersöz et al. evaluated a yield of 76.1 g_{H₂}/kg_{biomass,dry} after PSA³⁶. Susmozas et al. found a lower value in a steam dual fluidized bed: 55.0 g_{H₂}/kg_{biomass,dry}⁴¹ whereas Pallozzi et al. found 75.2 g_{H₂}/kg_{biomass,dry}⁴² for the same technology. Gupta and Dasappa determined 107.4 g_{H₂}/kg_{biomass,dry}³⁷ with a fixed bed downdraft. The values obtained for case 2 and 3 of this study cannot be compared because our separation process had never been previously proposed.

In order to better understand the H atoms transfer from wood and water to H₂, Figure 3-5 shows the fate of H along the process units. In the first scenario, 42.7% of the produced H₂ comes from the oxy-steam gasification of biomass after the POX unit, 13.2% results from steam reforming and 44.2% from water gas-shift reactors. As a consequence of catalytic reactors, almost all the hydrogen content in the syngas before the separation process is attributed to the H₂ molecule. In the second case, all the H₂ comes from biomass and steam during gasification. As in case 1, after the partial oxidation of the syngas to reduce the amount of tars, the hydrogen yield was slightly reduced by 6%. The temperature in the POX unit was too high to promote the conversion of CO by the water gas-shift. In the third case, the POX unit increases the hydrogen yield from 19.4% v after pyrolysis to 31% v on a dry basis. The H₂ content in case 3 is lower than in case 2. First, a part of hydrogen is kept in bio-char. In addition, the carbon in biochar which is not converted into syngas as CO could not contribute to the H₂ formation by the water-gas shift reaction. To increase the amount of hydrogen after POX unit, we tried to add steam in the POX. This addition has no effect on H₂ formation. Indeed, as shown by our group⁷¹, OH radicals mainly result from CO₂ conversion during syngas thermal conversion and H₂O is poorly reactive under such conditions.

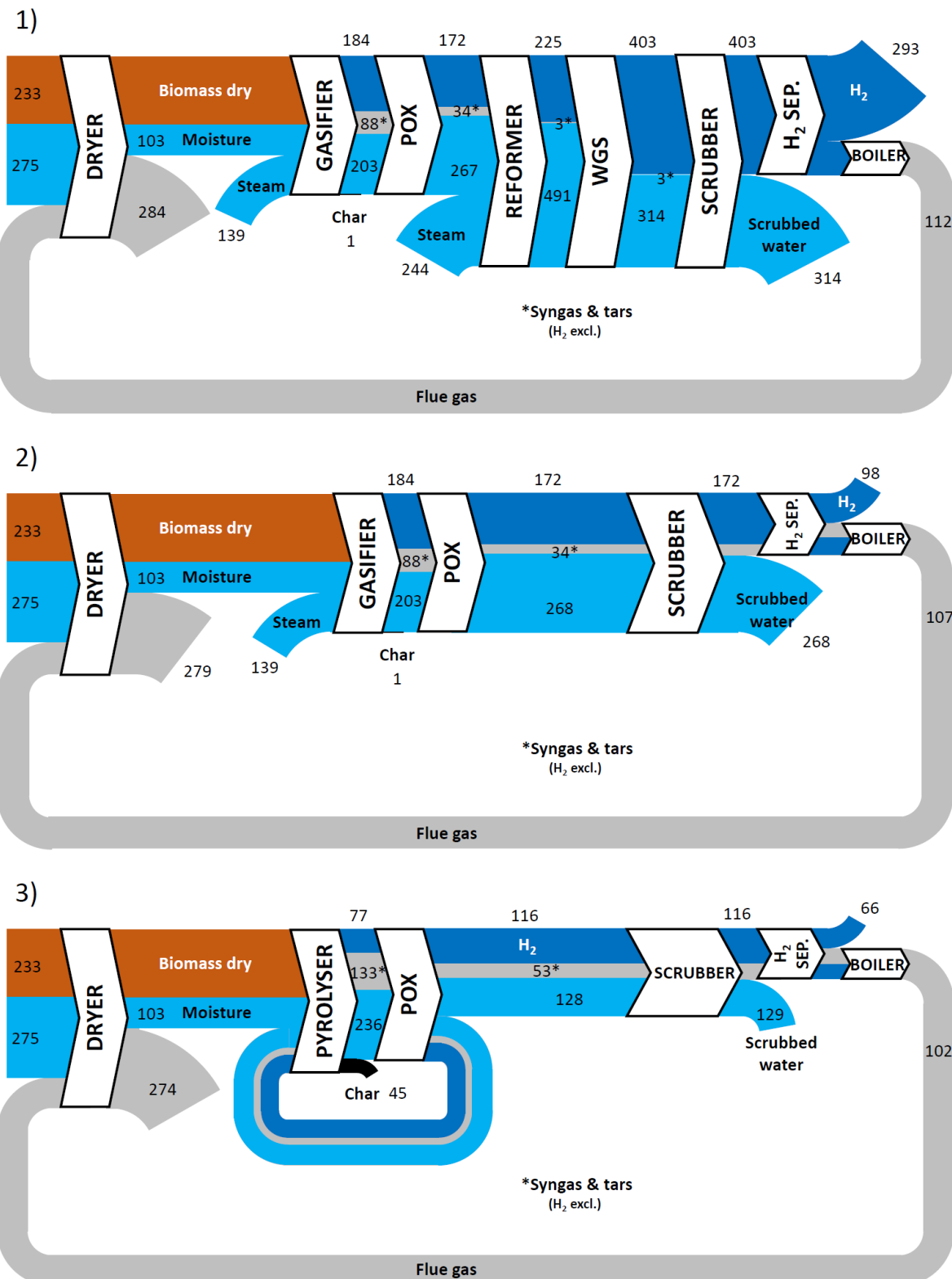


Figure 3-5: Fate of atomic hydrogen along the process for each scenario (kgH/h).

3.2.5.3 Tar and particles

The Figure 3-6 shows the tar dew point and the tar concentration in the syngas along the process. The POX unit seems to have no effect on tar dew point. In fact, tars are effectively converted but the heaviest tars mainly control the dew point value even at very low concentration. A higher amount of oxygen would increase the efficiency of the POX unit. Unfortunately, the temperature rise would have been too high for the refractory material of the reactor. The addition of oxygen was then limited by the temperature reached in the POX unit (Figure 3-7) (more details presented in SI S5). The temperature limit was set to 1300°C for a classical refractory material of the POX unit. The peak temperature corresponds to the maximum temperature reached in the POX unit.

The reduction of global tar concentration is relatively small after the wet scrubber for case 1, but this equipment is required for water condensation from syngas. It also plays the role of extra dust/soot removal. The heaviest PAHs are removed by the wet scrubber, thus reducing the tar dew point.

In case 3, the POX unit is not able to reduce the amount of tars below 2 g/Nm³ as for gasification scenarios, even with higher gas-phase residence times. The addition of oxygen was limited by the temperature reached (max 1300°C). The initial content of tars is higher after pyrolysis than after gasification. Its composition is also different with more primary and secondary tars. However, the tar dew point is reduced to around 25°C after the wet scrubber.

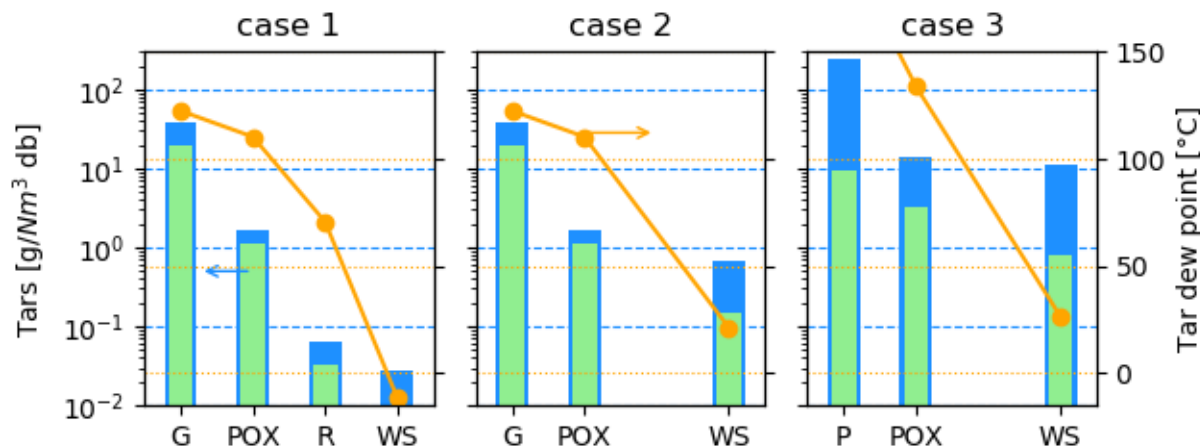


Figure 3-6: Concentration of tars and tar dew point along the process. G=Gasifier, P=Pyrolyzer, POX=Partial Oxidation, R=Reformer, WS=Water Scrubber. Tars and benzene in blue, tars without benzene in green.

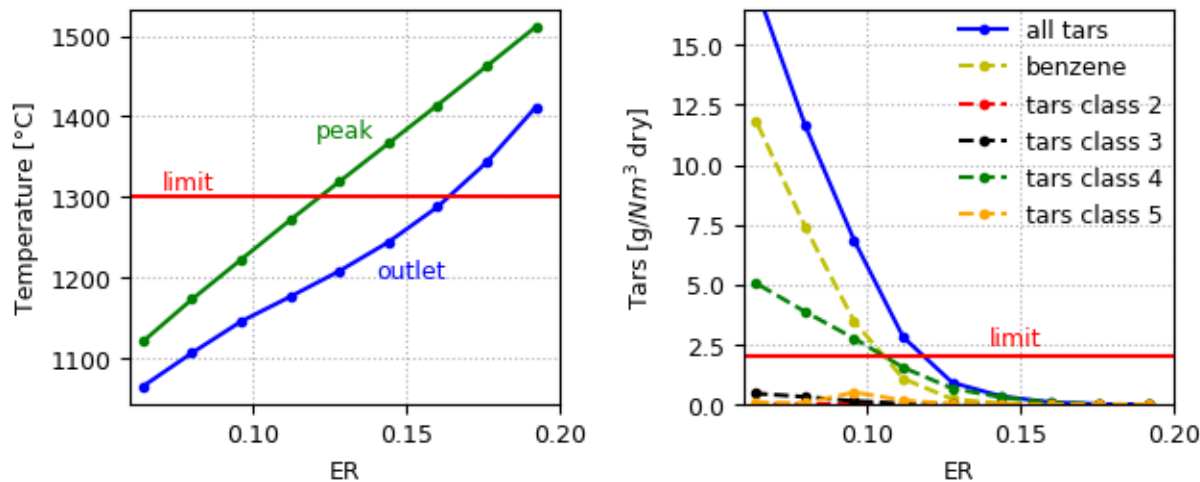


Figure 3-7: Impact of ER on POX temperature and reduction of tars (for cases 1 and 2).

3.2.5.4 H₂ separation by a hybrid process: membrane coupled to PSA

Two stages of separation were required (membrane and PSA) when the H₂ concentration in the syngas was too low, since a single PSA would require a very large product recycling to reach 70% v at the inlet²⁰. The membrane as a first stage plays the role of a pre-concentrator before the PSA (see supplementary material S7). To the best of our knowledge, this architecture of hydrogen separation from a biomass syngas is proposed for the first time. No data is available on the membrane lifetime using syngas with a residual amount of tars. If necessary, a guard bed filled with activated carbon could be added to remove these tars before the separation stage.

The minimum specific separation costs were estimated at 0.91 and 1.08 €/kg_{H2} for case 2 (Figure 3-8) and 3 respectively (SI S7). The first stage of separation with the membrane module requires a syngas pressure of around 5 bar, which is lower than the pressure required for PSA H₂ (around 25 bar). Only a part of the syngas enriched in hydrogen is compressed to this higher pressure in the second stage. As a result, the required energy is lowered with these two levels of pressure. The operational expenditure is decreased for the power consumption, but the H₂ recovery rate is lower. This explains why the specific separation cost is only 0.59 €/kg_{H2} in the case 1 with one stage PSA.

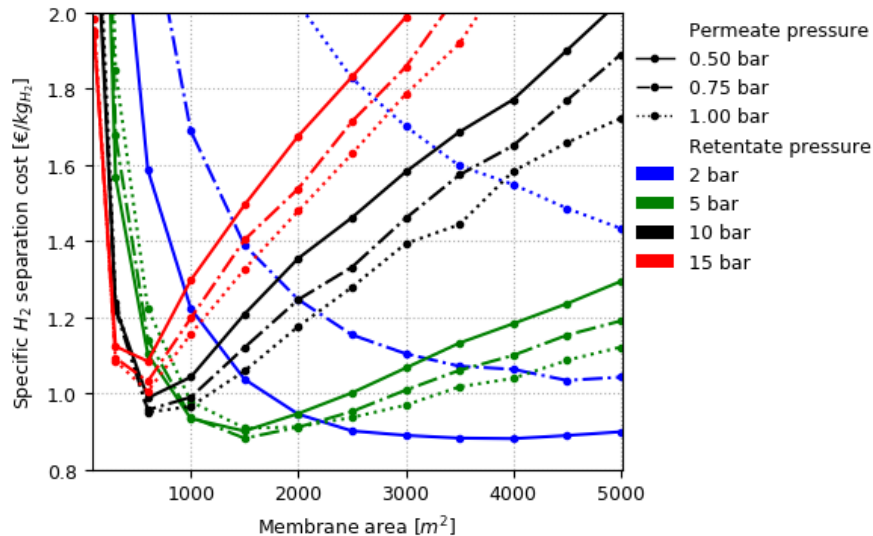


Figure 3-8: Specific hydrogen separation cost for case 2 as a function of membrane area, permeate and retentate pressures.

3.2.5.5 Comparison of the various options and recommendations

The choice between these scenarios is dependent on various criteria. The heat represents roughly between one third and more than half of energy outputs. Therefore, the choice may depend on the valorization of heat on the selected locations (like industrial sites). In any case, it would be far better if the heat demand of the site is relatively constant during the year. The availability of the feedstock is another criterion on the scale that is linked to the location of the plant. Finally, this location should avoid the transport of hydrogen on large distance by trucks. The bio-char can be more easily transported than hydrogen, but its production supposes a demand nearby since its density is quite low. This bio-char could also be stored or sequestered to create a carbon sink³.

Case 1 could fulfill hydrogen demand at 293 kg_{H₂}/h and it produces 5.2 MW_{th} of heat that must be valorized. Case 2 and 3 are simpler from a technology point of view: fewer unit operations, no catalytic reactor. This gain in robustness has to be counterbalanced with the hydrogen separation process that is more complex. The production of hydrogen is also far lower 98 kg_{H₂}/h in case 2 and only 66 kg_{H₂}/h in case 3.

From these results, we could expect the capital costs of case 1 to be much higher than cases 2 and 3 due to the catalytic reactors and the additional cost of catalysts. However, for cases 2 and 3, the hydrogen separation was achieved in two stages, increasing the specific cost of hydrogen separation. This point should be quantified properly with a further techno-economic assessment.

The third case can be chosen for its carbon sequestration potential through bio-char production. This option leads to a net negative CO₂ emission process as it may lead to a stable sink of carbon³.

Furthermore, in the context of bioenergy with carbon capture and storage (BECCS) processes, the PSA tail gas has a high concentration of CO₂ (between 60 to 70% v according to the cases). This high concentration favors the capture of CO₂ for carbon sequestration.

3.2.6 Conclusion

The aim of this work was to provide a detailed mass and energy balance of three scenarios of production of hydrogen from biomass: a first case dedicated to produce the maximum of hydrogen, a simpler option without catalyst reactors and a carbon-negative process that also produced bio-char.

The model covered the whole process from drying of the biomass to the production of H₂, heat and bio-char. All these operation units were modeled with Aspen Plus® with a detailed composition of tars. The accuracy of the model was ensured with experimental data when they were available. Chemkin Pro was coupled to Aspen Plus® to model the partial oxidation unit with a detailed radical kinetic mechanism. A hybrid hydrogen separation process was proposed using two technologies, namely membrane and PSA. The high-temperature heat was recovered for steam generation used for the gasification. The low-grade heat was used for woodchips drying whereas the rest of the heat was valorized in a heating network.

Global energetic efficiencies are 75.4, 77.8 and 80.4% net for scenarios 1 to 3, respectively. The hydrogen yields were 79, 26 and 18 g_{H₂}/kg_{biomass,dry} after separation. The excess of heat dedicated to a heating network leads to heat efficiencies of 23.4, 60.0 and 49.0% net for the same three options respectively. 110 g_{biochar}/kg_{biomass,dry} was produced in the third option. The needs of utilities and commodities are also quantified.

These data will be used in a techno-economic assessment and a life cycle assessment to consider all the aspects: profitability and environmental impacts.

The production of renewable hydrogen from biomass represents an alternative path to electrolysis processes when the available electricity production is too low or too carbon intensive.

3.2.7 Supporting informations

The supporting information file 1 presents: 1) details flowsheets of each scenarios and mass balance results, 2) the composition of the syngas and tars used as experimental data for oxy-steam gasification, 3) the presentation and the results of the auto-thermal pyrolyser model, 4) few details about the partial oxidation model, 5) the influence of the equivalent ratio on the efficiency of the partial oxidation unit, 6) the kinetic model used for the steam reformer model, 7) the methods and results used to define the architecture of the hydrogen separation. The supporting information file 2 presents the detailed composition of each flow from Aspen Plus.

3.2.8 Fundings

This work was funded by the French PIA project “Lorraine Université d’Excellence” (reference ANR-15-IDEX-04-LUE) and by the Hy-C-GREEN project (Europe-FEDER and Grand-Est province).

3.2.9 References

- (1) Smil, V. *Energy Transitions: Global and National Perspectives*, Second edition.; Praeger, an imprint of ABC-CLIO, LLC: Santa Barbara, California Denver, Colorado, 2017.
- (2) *Bp Statistical Review of World Energy 2021*; 2021.
- (3) Dufour, A. Geological Sequestration of Biomass Char to Mitigate Climate Change. *Environmental Science & Technology* **2013**, 130829114030003. <https://doi.org/10.1021/es4036418>.
- (4) Williams, R. H.; Larson, E. D.; Katofsky, R. E.; Chen, J. Methanol and Hydrogen from Biomass for Transportation. *Energy for Sustainable Development* **1995**, 1 (5), 18–34. [https://doi.org/10.1016/S0973-0826\(08\)60083-6](https://doi.org/10.1016/S0973-0826(08)60083-6).
- (5) *The Future of Hydrogen*; IEA, 2019; p 203.
- (6) Ministère de la Transition Energétique et Solidaire. *Stratégie Française Pour l’énergie et Le Climat - Programmation Pluriannuelle de l’énergie 2019-2023 2024-2028*; 2018.
- (7) Woolcock, P. J.; Brown, R. C. A Review of Cleaning Technologies for Biomass-Derived Syngas. *Biomass and Bioenergy* **2013**, 52, 54–84. <https://doi.org/10.1016/j.biombioe.2013.02.036>.

- (8) Xu, G.; Murakami, T.; Suda, T.; Matsuzawa, Y.; Tani, H. The Superior Technical Choice for Dual Fluidized Bed Gasification. *Ind. Eng. Chem. Res.* **2006**, *45* (7), 2281–2286. <https://doi.org/10.1021/ie051099r>.
- (9) Corella, J.; Toledo, J. M.; Molina, G. A Review on Dual Fluidized-Bed Biomass Gasifiers. *Industrial & Engineering Chemistry Research* **2007**, *46* (21), 6831–6839. <https://doi.org/10.1021/ie0705507>.
- (10) Larsson, A.; Thunman, H.; Ström, H.; Sasic, S. Experimental and Numerical Investigation of the Dynamics of Loop Seals in a Large-Scale DFB System under Hot Conditions. *AICHE Journal* **2015**, *61* (11), 3580–3593. <https://doi.org/10.1002/aic.14887>.
- (11) Corella, J.; Aznar, M.; Caballero, M.; Molina, G.; Toledo, J. 140gH₂/Kg Biomass d.a.f. by a CO-Shift Reactor Downstream from a FB Biomass Gasifier and a Catalytic Steam Reformer. *International Journal of Hydrogen Energy* **2008**, *33* (7), 1820–1826. <https://doi.org/10.1016/j.ijhydene.2008.02.003>.
- (12) Bates, R. B.; Altantzis, C.; Ghoniem, A. F. Modeling of Biomass Char Gasification, Combustion, and Attrition Kinetics in Fluidized Beds. *Energy Fuels* **2016**, *30* (1), 360–376. <https://doi.org/10.1021/acs.energyfuels.5b02120>.
- (13) Kersten, S. R. A.; Wang, X.; Prins, W.; van Swaaij, W. P. M. Biomass Pyrolysis in a Fluidized Bed Reactor. Part 1: Literature Review and Model Simulations. *Ind. Eng. Chem. Res.* **2005**, *44* (23), 8773–8785. <https://doi.org/10.1021/ie0504856>.
- (14) Bruchmüller, J.; van Wachem, B. G. M.; Gu, S.; Luo, K. H.; Brown, R. C. Modeling the Thermochemical Degradation of Biomass inside a Fast Pyrolysis Fluidized Bed Reactor. *AICHE Journal* **2012**, *58* (10), 3030–3042. <https://doi.org/10.1002/aic.13705>.
- (15) Brown, R. C. Heterodoxy in Fast Pyrolysis of Biomass. *Energy Fuels* **2021**, *35* (2), 987–1010. <https://doi.org/10.1021/acs.energyfuels.0c03512>.
- (16) Lehmann, J. A Handful of Carbon. *Nature* **2007**, *447* (7141), 143–144. <https://doi.org/10.1038/447143a>.
- (17) Schmid, M.; Beirow, M.; Schweitzer, D.; Waizmann, G.; Spörl, R.; Scheffknecht, G. Product Gas Composition for Steam-Oxygen Fluidized Bed Gasification of Dried Sewage Sludge, Straw Pellets and Wood Pellets and the Influence of Limestone as Bed Material. *Biomass and Bioenergy* **2018**, *117*, 71–77. <https://doi.org/10.1016/j.biombioe.2018.07.011>.
- (18) Barisano, D.; Canneto, G.; Nanna, F.; Alvino, E.; Pinto, G.; Villone, A.; Carnevale, M.; Valerio, V.; Battafarano, A.; Braccio, G. Steam/Oxygen Biomass Gasification at Pilot Scale in an Internally Circulating Bubbling Fluidized Bed Reactor. *Fuel Processing Technology* **2016**, *141*, 74–81. <https://doi.org/10.1016/j.fuproc.2015.06.008>.
- (19) Swanson, R. M.; Platon, A.; Satrio, J. A.; Brown, R. C.; Hsu, D. D. *Techno-Economic Analysis of Biofuels Production Based on Gasification*; NREL/TP-6A20-46587, 994017; 2010. <https://doi.org/10.2172/994017>.
- (20) Spath, P.; Aden, A.; Eggeman, T.; Ringer, M.; Wallace, B.; Jechura, J. *Biomass to Hydrogen Production Detailed Design and Economics Utilizing the Battelle Columbus Laboratory Indirectly-Heated Gasifier*; NREL/TP-510-37408, 15016221; 2005. <https://doi.org/10.2172/15016221>.

- (21) Fail, S.; Diaz, N.; Benedikt, F.; Kraussler, M.; Hinteregger, J.; Bosch, K.; Hackel, M.; Rauch, R.; Hofbauer, H. Wood Gas Processing To Generate Pure Hydrogen Suitable for PEM Fuel Cells. *ACS Sustainable Chemistry & Engineering* **2014**, *2* (12), 2690–2698. <https://doi.org/10.1021/sc500436m>.
- (22) Kraussler, M.; Binder, M.; Hofbauer, H. 2250-h Long Term Operation of a Water Gas Shift Pilot Plant Processing Tar-Rich Product Gas from an Industrial Scale Dual Fluidized Bed Biomass Steam Gasification Plant. *International Journal of Hydrogen Energy* **2016**, *41* (15), 6247–6258. <https://doi.org/10.1016/j.ijhydene.2016.02.137>.
- (23) Hamelinck, C. N.; Faaij, A. P. C. Future Prospects for Production of Methanol and Hydrogen from Biomass. *Journal of Power Sources* **2002**, *22*.
- (24) Caballero, M. A.; Aznar, M. P.; Gil, J.; Martín, J. A.; France, E. Commercial Steam Reforming Catalysts To Improve Biomass Gasification with Steam-Oxygen Mixtures. 1. Hot Gas Upgrading by the Catalytic Reactor. *Ind. Eng. Chem. Res.* **1997**, *36* (5227–5239).
- (25) Aznar, M. P.; Caballero, M. A.; Gil, J.; Martín, J. A.; Corella, J. Commercial Steam Reforming Catalysts To Improve Biomass Gasification with Steam-Oxygen Mixtures. 2. Catalytic Tar Removal. *Industrial & Engineering Chemistry Research* **1998**, *37*, 2668–2680.
- (26) Chianese, S.; Fail, S.; Binder, M.; Rauch, R.; Hofbauer, H.; Molino, A.; Blasi, A.; Musmarra, D. Experimental Investigations of Hydrogen Production from CO Catalytic Conversion of Tar Rich Syngas by Biomass Gasification. *Catalysis Today* **2016**, *277*, 182–191. <https://doi.org/10.1016/j.cattod.2016.04.005>.
- (27) François, J.; Mauviel, G.; Feidt, M.; Rogaume, C.; Rogaume, Y.; Mirgaux, O.; Patisson, F.; Dufour, A. Modeling of a Biomass Gasification CHP Plant: Influence of Various Parameters on Energetic and Exergetic Efficiencies. *Energy & Fuels* **2013**, *27* (12), 7398–7412. <https://doi.org/10.1021/ef4011466>.
- (28) Emonts, B.; Reuß, M.; Stenzel, P.; Welder, L.; Knicker, F.; Grube, T.; Görner, K.; Robinius, M.; Stolten, D. Flexible Sector Coupling with Hydrogen: A Climate-Friendly Fuel Supply for Road Transport. *International Journal of Hydrogen Energy* **2019**, *44* (12918–12930), *13*. <https://doi.org/10.1016/j.ijhydene.2019.03.1>.
- (29) Francois, J.; Abdelouahed, L.; Mauviel, G.; Patisson, F.; Mirgaux, O.; Rogaume, C.; Rogaume, Y.; Feidt, M.; Dufour, A. Detailed Process Modeling of a Wood Gasification Combined Heat and Power Plant. *Biomass and Bioenergy* **2013**, *51*, 68–82. <https://doi.org/10.1016/j.biombioe.2013.01.004>.
- (30) Puig-Arnavat, M.; Bruno, J. C.; Coronas, A. Review and Analysis of Biomass Gasification Models. *Renewable and Sustainable Energy Reviews* **2010**, *14* (9), 2841–2851. <https://doi.org/10.1016/j.rser.2010.07.030>.
- (31) Srinivas, S.; Field, R. P.; Herzog, H. J. Modeling Tar Handling Options in Biomass Gasification. *Energy Fuels* **2013**, *27* (6), 2859–2873. <https://doi.org/10.1021/ef400388u>.
- (32) Abdelouahed, L.; Authier, O.; Mauviel, G.; Corriou, J. P.; Verdier, G.; Dufour, A. Detailed Modeling of Biomass Gasification in Dual Fluidized Bed Reactors under Aspen Plus. *Energy & Fuels* **2012**, *26* (6), 3840–3855. <https://doi.org/10.1021/ef300411k>.

- (33) Gómez-Barea, A.; Leckner, B. Modeling of Biomass Gasification in Fluidized Bed. *Progress in Energy and Combustion Science* **2010**, *36* (4), 444–509. <https://doi.org/10.1016/j.pecs.2009.12.002>.
- (34) Bates, R. B.; Ghoniem, A. F.; Jablonski, W. S.; Carpenter, D. L.; Altantzis, C.; Garg, A.; Barton, J. L.; Chen, R.; Field, R. P. Steam-Air Blown Bubbling Fluidized Bed Biomass Gasification (BFBBG): Multi-Scale Models and Experimental Validation. *AICHE Journal* **2017**, *63* (5), 1543–1565. <https://doi.org/10.1002/aic.15666>.
- (35) Martín, M.; Grossmann, I. E. Process Optimization of FT-Diesel Production from Lignocellulosic Switchgrass. *Ind. Eng. Chem. Res.* **2011**, *50* (23), 13485–13499. <https://doi.org/10.1021/ie201261t>.
- (36) Ersöz, A.; DurakÇetin, Y.; Sarıoglan, A.; Turan, A. Z.; Mert, M. S.; Yüksel, F.; Figen, H. E.; Güldal, N. Ö.; Karaismailoğlu, M.; Baykara, S. Z. Investigation of a Novel & Integrated Simulation Model for Hydrogen Production from Lignocellulosic Biomass. *International Journal of Hydrogen Energy* **2018**, *43* (2), 1081–1093. <https://doi.org/10.1016/j.ijhydene.2017.11.017>.
- (37) Gupta, A.; Dasappa, S. Hydrogen from Biomass by Oxy-Steam Gasification - A Quantitative Analysis of Cases. *Proceedings of the 26th European Biomass Conference and Exhibition* **2018**, 14-17 May 2018, 4 Pages. <https://doi.org/10.5071/26THEUBCE2018-2CV.4.22>.
- (38) Kalinci, Y.; Hepbasli, A.; Dincer, I. Exergoeconomic Analysis of Hydrogen Production from Biomass Gasification. *International Journal of Hydrogen Energy* **2012**, *37* (21), 16402–16411. <https://doi.org/10.1016/j.ijhydene.2012.02.173>.
- (39) Ishaq, H.; Dincer, I. A Novel Biomass Gasification Based Cascaded Hydrogen and Ammonia Synthesis System Using Stoichiometric and Gibbs Reactors. *Biomass and Bioenergy* **2021**, *145*, 105929. <https://doi.org/10.1016/j.biombioe.2020.105929>.
- (40) Koroneos, C.; Dompros, A.; Roumbas, G. Hydrogen Production via Biomass Gasification—A Life Cycle Assessment Approach. *Chemical Engineering and Processing: Process Intensification* **2008**, *47* (8), 1261–1268. <https://doi.org/10.1016/j.cep.2007.04.003>.
- (41) Susmozas, A.; Iribarren, D.; Zapp, P.; Linßen, J.; Dufour, J. Life-Cycle Performance of Hydrogen Production via Indirect Biomass Gasification with CO₂ Capture. *International Journal of Hydrogen Energy* **2016**, *41* (42), 19484–19491. <https://doi.org/10.1016/j.ijhydene.2016.02.053>.
- (42) Pallozzi, V.; Di Carlo, A.; Bocci, E.; Villarini, M.; Foscolo, P. U.; Carlini, M. Performance Evaluation at Different Process Parameters of an Innovative Prototype of Biomass Gasification System Aimed to Hydrogen Production. *Energy Conversion and Management* **2016**, *130*, 34–43. <https://doi.org/10.1016/j.enconman.2016.10.039>.
- (43) Marcantonio, V.; De Falco, M.; Capocelli, M.; Bocci, E.; Colantoni, A.; Villarini, M. Process Analysis of Hydrogen Production from Biomass Gasification in Fluidized Bed Reactor with Different Separation Systems. *International Journal of Hydrogen Energy* **2019**, *44* (21), 10350–10360. <https://doi.org/10.1016/j.ijhydene.2019.02.121>.

- (44) Ribeiro, A. M.; Santos, J. C.; Rodrigues, A. E. Pressure Swing Adsorption for CO₂ Capture in Fischer-Tropsch Fuels Production from Biomass. *Adsorption* **2011**, *17* (3), 443–452. <https://doi.org/10.1007/s10450-010-9280-8>.
- (45) Pelletier, C.; Rogaume, Y.; Dieckhoff, L.; Bardeau, G.; Pons, M.-N.; Dufour, A. Effect of Combustion Technology and Biogenic CO₂ Impact Factor on Global Warming Potential of Wood-to-Heat Chains. *Applied Energy* **2019**, *235*, 1381–1388. <https://doi.org/10.1016/j.apenergy.2018.11.060>.
- (46) François, J.; Fortin, M.; Patisson, F.; Dufour, A. Assessing the Fate of Nutrients and Carbon in the Bioenergy Chain through the Modeling of Biomass Growth and Conversion. *Environmental Science & Technology* **2014**, *48* (23), 14007–14015. <https://doi.org/10.1021/es5032823>.
- (47) Debal, M.; Girods, P.; Rogaume, Y. Wood Gasification in a Semi-Industrial Bubbling Fluidized Bed Gasifier. In *7th international symposium on gasification and its applications*; Nancy, 2021.
- (48) Aspentech. *Aspen Physical Property Methods*; 2013; p 250.
- (49) Rönsch, S.; Wagner, H. Calculation of Heating Values for the Simulation of Thermo-Chemical Conversion Plants with Aspen Plus. *DBFZ Germany* **2012**.
- (50) Corella, J.; Toledo, J. M.; Molina, G. Calculation of the Conditions to Get Less than 2 g Tar/Mn3 in a Fluidized Bed Biomass Gasifier. *Fuel Processing Technology* **2006**, *87* (9), 841–846. <https://doi.org/10.1016/j.fuproc.2006.05.002>.
- (51) Smith, A. R.; Klosek, J. A Review of Air Separation Technologies and Their Integration with Energy Conversion Processes. *Fuel Processing Technology* **2001**, *70* (2), 115–134. [https://doi.org/10.1016/S0378-3820\(01\)00131-X](https://doi.org/10.1016/S0378-3820(01)00131-X).
- (52) Ding, Z.; Han, Z.; Qiang, F.; Shen, Y.; Tian, C.; Zhang, D. Optimization and Analysis of the VPSA Process for Industrial-Scale Oxygen Production. *Adsorption* **2018**, *24*, 499–516. <https://doi.org/10.1007/s10450-018-9956-z>.
- (53) Santos Silva Ferreira, D. A. High-Purity Oxygen Production by VPSA. Ph.D. Dissertation, University of Porto, 2016.
- (54) Dufour, A. Optimisation de la production d'hydrogène par conversion du méthane dans les procédés de pyrolyse/gazéification de la biomasse, Université Henri Poincaré, Nancy, 2007.
- (55) Gil, J.; Corella, J. Biomass Gasification in Atmospheric and Bubbling Fluidized Bed: Effect of the Type of Gasifying Agent on the Product Distribution. *Biomass and Bioenergy* **1999**, *15*.
- (56) Debiagi, P. E. A.; Gentile, G.; Pelucchi, M.; Frassoldati, A.; Cuoci, A.; Faravelli, T.; Ranzi, E. Detailed Kinetic Mechanism of Gas-Phase Reactions of Volatiles Released from Biomass Pyrolysis. *Biomass and Bioenergy* **2016**, *93*, 60–71. <https://doi.org/10.1016/j.biombioe.2016.06.015>.
- (57) Dhahak, A.; Bounaceur, R.; Le Dreff-Lorimier, C.; Schmidt, G.; Trouve, G.; Battin-Leclerc, F. Development of a Detailed Kinetic Model for the Combustion of Biomass. *Fuel* **2019**, *242*, 756–774. <https://doi.org/10.1016/j.fuel.2019.01.093>.
- (58) Norinaga, K.; Deutschmann, O.; Saegusa, N.; Hayashi, J. Analysis of Pyrolysis Products from Light Hydrocarbons and Kinetic Modeling for Growth of Polycyclic Aromatic

- Hydrocarbons with Detailed Chemistry. *Journal of Analytical and Applied Pyrolysis* **2009**, *86* (1), 148–160. <https://doi.org/10.1016/j.jaap.2009.05.001>.
- (59) Norinaga, K.; Shoji, T.; Kudo, S.; Hayashi, J. Detailed Chemical Kinetic Modelling of Vapour-Phase Cracking of Multi-Component Molecular Mixtures Derived from the Fast Pyrolysis of Cellulose. *Fuel* **2013**, *103*, 141–150. <https://doi.org/10.1016/j.fuel.2011.07.045>.
- (60) Kraussler, M.; Binder, M.; Fail, S.; Bosch, K.; Hackel, M.; Hofbauer, H. Performance of a Water Gas Shift Pilot Plant Processing Product Gas from an Industrial Scale Biomass Steam Gasification Plant. *Biomass and Bioenergy* **2016**, *89*, 50–57. <https://doi.org/10.1016/j.biombioe.2015.12.001>.
- (61) Yousef, R.; Qiblawey, H.; El-Naas, M. H. Adsorption as a Process for Produced Water Treatment: A Review. *Processes* **2020**, *8* (12), 1657. <https://doi.org/10.3390/pr8121657>.
- (62) Yuan, M.; Tong, S.; Zhao, S.; Jia, C. Q. Adsorption of Polycyclic Aromatic Hydrocarbons from Water Using Petroleum Coke-Derived Porous Carbon. *Journal of Hazardous Materials* **2010**, *181* (1–3), 1115–1120. <https://doi.org/10.1016/j.jhazmat.2010.05.130>.
- (63) Rabou, L. P. L. M.; Zwart, R. W. R.; Vreugdenhil, B. J.; Bos, L. Tar in Biomass Producer Gas, the Energy Research Centre of The Netherlands (ECN) Experience: An Enduring Challenge. *Energy Fuels* **2009**, *23* (12), 6189–6198. <https://doi.org/10.1021/ef9007032>.
- (64) ECN. Tar Dew Point - Complete Model. 2012.
- (65) Golmakani, A.; Fatemi, S.; Tamnanloo, J. Investigating PSA, VSA, and TSA Methods in SMR Unit of Refineries for Hydrogen Production with Fuel Cell Specification. *Separation and Purification Technology* **2017**, *176*, 73–91. <https://doi.org/10.1016/j.seppur.2016.11.030>.
- (66) Bounaceur, R.; Berger, E.; Pfister, M.; Ramirez Santos, A. A.; Favre, E. Rigorous Variable Permeability Modelling and Process Simulation for the Design of Polymeric Membrane Gas Separation Units: MEMSIC Simulation Tool. *Journal of Membrane Science* **2017**, *523*, 77–91. <https://doi.org/10.1016/j.memsci.2016.09.011>.
- (67) Ramírez-Santos, Á. A.; Castel, C.; Favre, E. Utilization of Blast Furnace Flue Gas: Opportunities and Challenges for Polymeric Membrane Gas Separation Processes. *Journal of Membrane Science* **2017**, *526*, 191–204. <https://doi.org/10.1016/j.memsci.2016.12.033>.
- (68) Peters, M. S.; Timmerhaus, K. D.; West, R. E. *Plant Design and Economics for Chemical Engineers*, fifth edition.; McGraw-Hill New York, 2004.
- (69) Polin, J. P.; Peterson, C. A.; Whitmer, L. E.; Smith, R. G.; Brown, R. C. Process Intensification of Biomass Fast Pyrolysis through Autothermal Operation of a Fluidized Bed Reactor. *Applied Energy* **2019**, *249*, 276–285. <https://doi.org/10.1016/j.apenergy.2019.04.154>.
- (70) Polin, J. P.; Carr, H. D.; Whitmer, L. E.; Smith, R. G.; Brown, R. C. Conventional and Autothermal Pyrolysis of Corn Stover: Overcoming the Processing Challenges of High-Ash Agricultural Residues. *Journal of Analytical and Applied Pyrolysis* **2019**, *143*, 104679. <https://doi.org/10.1016/j.jaap.2019.104679>.
- (71) Dufour, A.; Valin, S.; Castelli, P.; Thiery, S.; Boissonnet, G.; Zoulalian, A.; Glaude, P.-A. Mechanisms and Kinetics of Methane Thermal Conversion in a Syngas. *Ind. Eng. Chem. Res.* **2009**, *48* (14), 6564–6572. <https://doi.org/10.1021/ie900343b>.

3.2.10 Supporting Information

3.2.10.1 Detailed Flowsheet

An excel file is provided as a supplementary material with all streams mass flow rate, composition and properties for the three cases.

3.2.10.1.1 Case 1

In this first case (Figure S3-1), the wet woodchips (40%) is fed in a rotary dryer. The heat required for drying is provided by the process exhaust gas from the gas boiler. The dried feedstock (20%) is directed to the fluidized bed for its oxy-steam gasification. The oxygen is produced by air separation in a VSA O₂ unit. The steam is formed by heating water with heat sources along the process.

The syngas tar content is reduced in a partial oxidation (POX) unit by adding some oxygen. Then, the syngas is cooled down to 850°C before entering the steam reforming reactor. The syngas is cooled to 350°C to promote water-gas shift in the high-temperature shift (HTS) reactor, and to 250°C before the low-temperature shift (LTS) reactor. The hydrogen-enriched syngas is cleaned in a Venturi and a wet scrubber to remove residual NH₃, HCl and potential solids and condense the water content of the syngas. This scrubbing water is cleaned in a dissolve air flotation (DAF) unit and recycled to the scrubber. The excess of water exited the process after an activated carbon bed to remove residual PAHs and other contaminants in the water.

The purified syngas is then compressed to 25 bar, prior the PSA H₂, a part of the product is recycled to reach the minimum hydrogen concentration before the PSA (70% vol¹). The tail gas at 1.3 bar is burnt in a gas boiler to provide additional heat to the heat network. The exhaust gas is used for woodchips drying.

Figure S3-4 a presents the sankey mass flow diagram.

3.2.10.1.2 Case 2

This second case (Figure S3-1) is similar to the first scenario without reformer and water-gas shift reactors. Because the hydrogen content is lower in this case, the separation of hydrogen is done in two stages to reduce the specific separation cost. The syngas is pre-concentrated with a membrane

permeable to hydrogen before entering the PSA. As the PSA tail gas, the syngas of the membrane retentate is burnt in the gas boiler.

Figure S3-4b presents the sankey mass flow diagram.

3.2.10.1.3 Case 3

The third case (Figure S3-1) differs from the case 2 in the pyrogasification step. The woodchips are pyrolyzed in a fluidized bed to produce gas and tars in the gas phase and biochar. The heat is provided by adding some oxygen in the pyrolyser. The biochar is removed from the process, and the gas phase with a high content of tars was partially oxidized in the POX unit.

Figure S3-4c presents the sankey mass flow diagram.

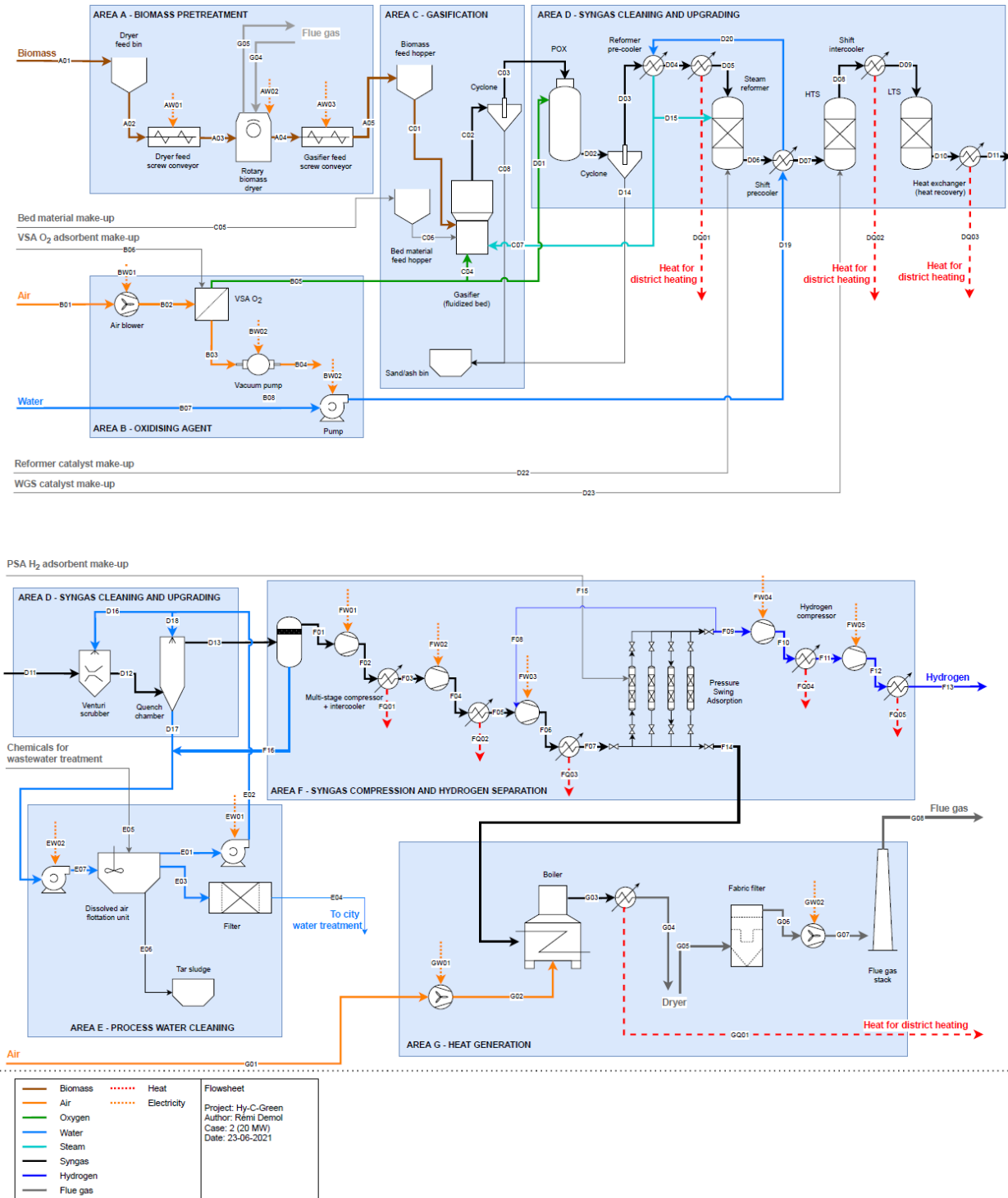


Figure S3-1: Process flow diagram of case 1.

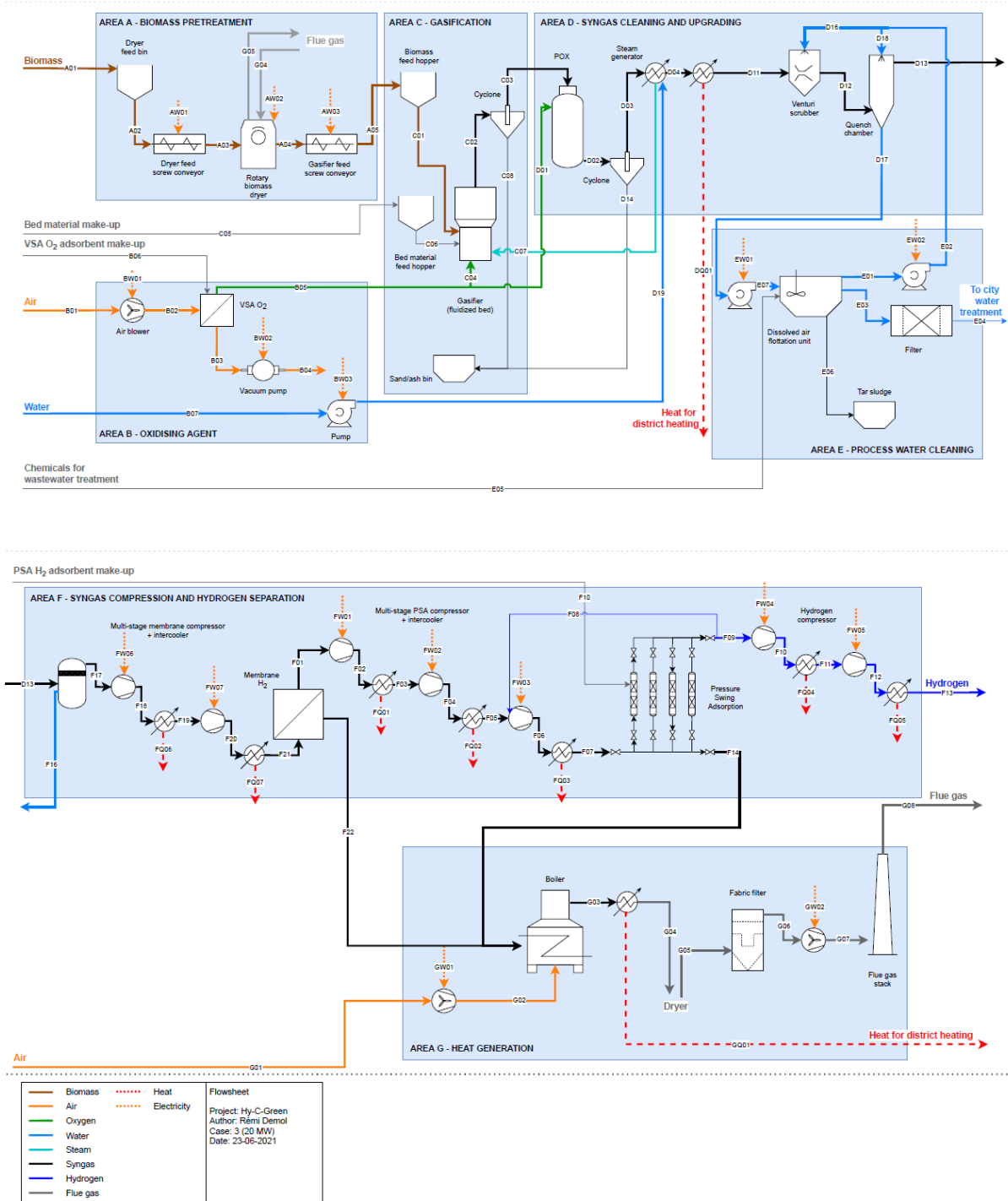


Figure S3-2: Process flow diagram of case 2.

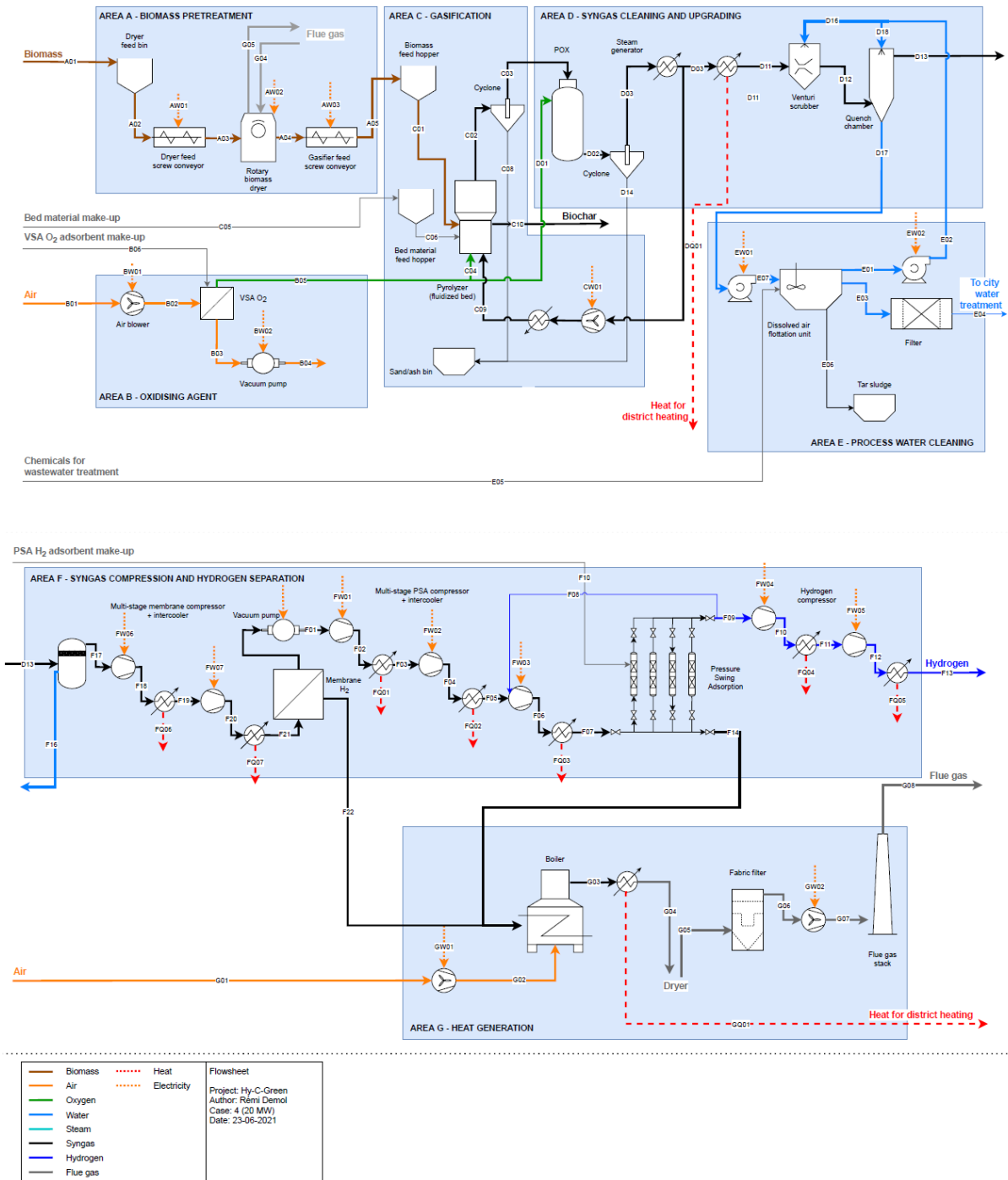


Figure S3-3: Process flow diagram of case 3

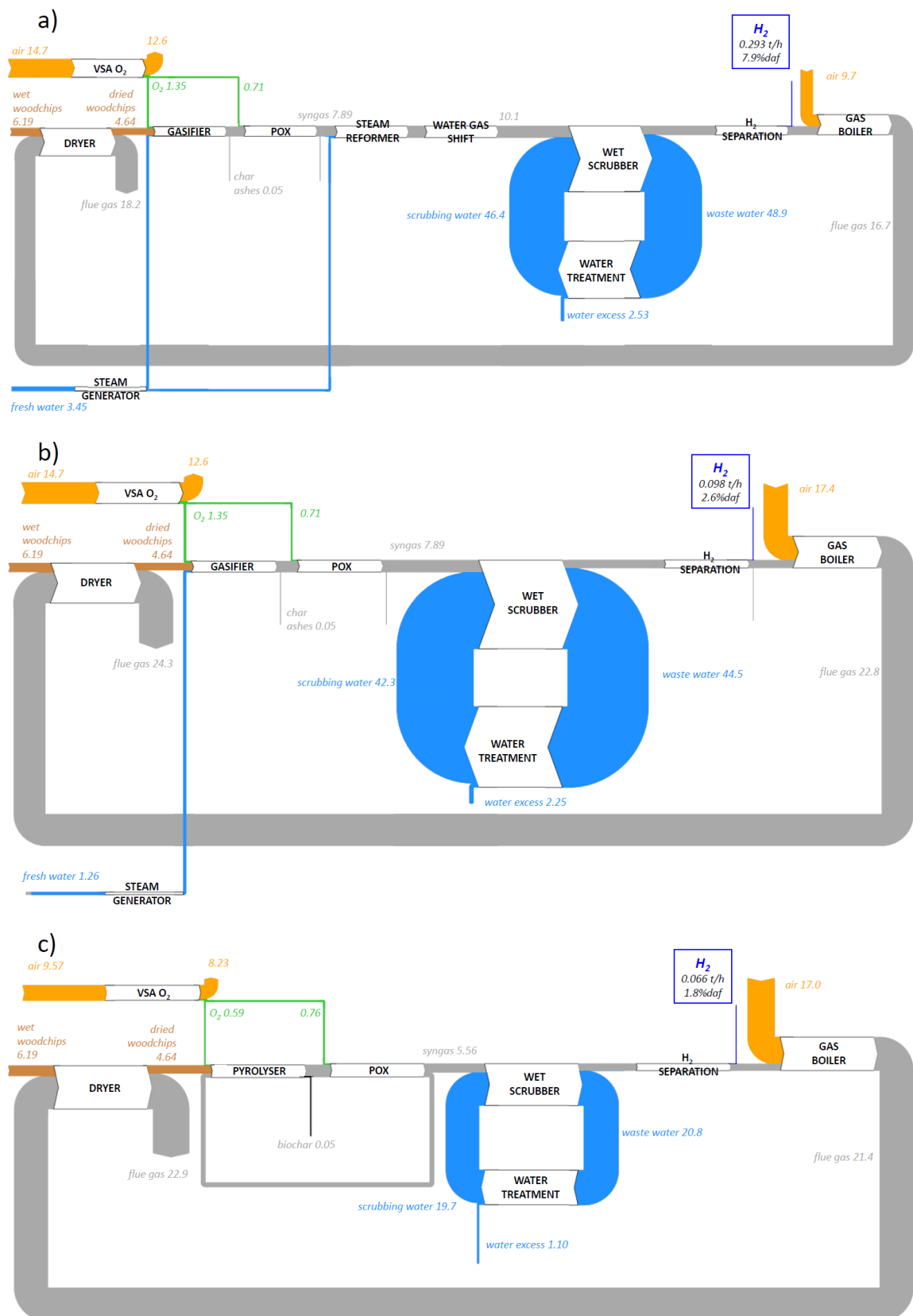


Figure S3-4: Mass balance of the 3 cases in t/h: a) case 1; b) case 2; c) case 3.

3.2.10.2 Experiments used for oxy-steam gasification

The composition of the feedstock and the syngas from oxygen/steam gasification is provided in Table S3-1, S2 and S3. It is based on the experimental data of Schmid et al.². These experiments were conducted in an oxygen-steam bubbling fluidized bed, with a fluidization velocity 0.4 m/s, a feeding rate of 4 kg/h of wood chips. The bed temperature was adjusted to 850°C with an equivalent ratio ER = 0.25±0.02 and a molar S/C=1.

Table S3-1: Composition of the feedstock (from ²).

Biomass woodchips					
Proximate Analysis				LHV	dry basis
Moisture 40%wt	Ash 0.40%db	Fixed carbon 17.50%db	Volatile matter 77.80%db	19.4 MJ/kg	
Ultimate analysis (water and ash free)					
C 51.0%	H 6.30%	O 42.4%	N 0.20%	S 0.02%	Cl 0.02%

Table S3-2: Syngas composition (from ²).

Syngas composition (%dry)				
H ₂ 40.4%	CO 19.2%	CH ₄ 6.6%	CO ₂ 32.4%	C _n H _m 1.4%

Table S3-3: Tar composition (from ²).

Tars (g/Nm ³ dry, N ₂ free)	
Benzene	18.46
Cresol	0.140
Xylenol	0.090
Toluene	3.840
Xylene	0.220
Indane	0.020
Indene	2.090
Phenol	1.320
Naphthalene	6.290
Methylnaphthalene	0.950
Biphenyl	0.440
Acenaphthylene	1.590
Acenaphthene	0.050
Fluorene	0.570
Phenanthrene	1.300
Anthracene	0.520
Fluoranthene	0.480
Pyrene	0.420

3.2.10.3 Pyrolyser model

No similar detailed composition of pyrolysis products, as those for gasification, were available in the literature, notably concerning a detailed tar composition. For this reason, we have modeled the auto-thermal pyrolysis reactor by the Ranzi's team kinetic mechanism of biomass pyrolysis³.

The biomass was decomposed into cellulose (CELL), lignin (LIG-C, LIG-O, LIG-H) and hemicelluloses (HCE) to match its elemental composition. Oxygen was added to solid reactors and reacted with char molecule (C) to form CO and CO₂. The gas-phase products released by pyrolysis can afterward react in homogeneous phase according to the radical kinetic model described for partial oxidation (Table S3-5).

The kinetic model was coupled with a hydrodynamic model of the fluidized bed. The dense zone of the fluidized bed was modeled as 14 perfectly stirred reactors (Figure S3-6) with fixed temperature, seven for the solid phase and the seven others for gas phase. The freeboard of the fluidized bed was modeled as an adiabatic plug flow reactor. The gas produced from the freeboard was sent to a partial oxidation unit with a small flow of oxygen. The POX unit was also assimilated to an adiabatic plug flow reactor. The results are presented on Figure S3-6 for a feed flow of 1 g/s of dry biomass but can be extrapolated to any feed flow.

A script written in Python is used to launch the CHEMKIN PRO calculation. As this software is dedicated to gas phase, it does not include phase separator. The gas and solid species were separated with a python subroutine.

The amount of oxygen injected was equivalent to an ER=0.10 in the fluidized bed and ER=0.129 in the POX unit to decrease the amount of tars but staying below the temperature limit for the material (assumed 1300°C).

The temperature of the dense bed and the recycled syngas composition were adjusted to ensure mass balance and energy conservation (the dense bed should be globally autothermal). The heat was generated by the partial oxidation of char and gases. The biochar composition was assumed to be the elemental composition of solid species including solid intermediates in Ranzi's mechanism². Figure S3-6 presents the results of the model.

The total residence time of gas was about 1s in the dense bed, 0.65s in the freeboard and 3.15 s in the POX. Solid residence time 55 s was in good agreement with Agu et al.⁴.

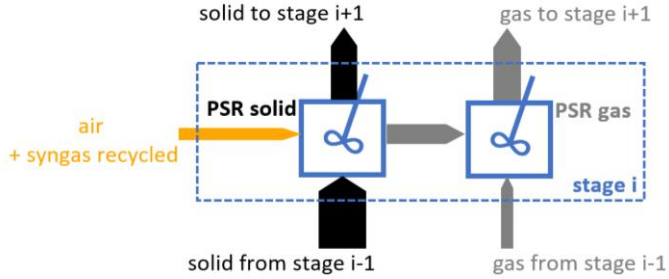


Figure S3-5: Principle of the model.

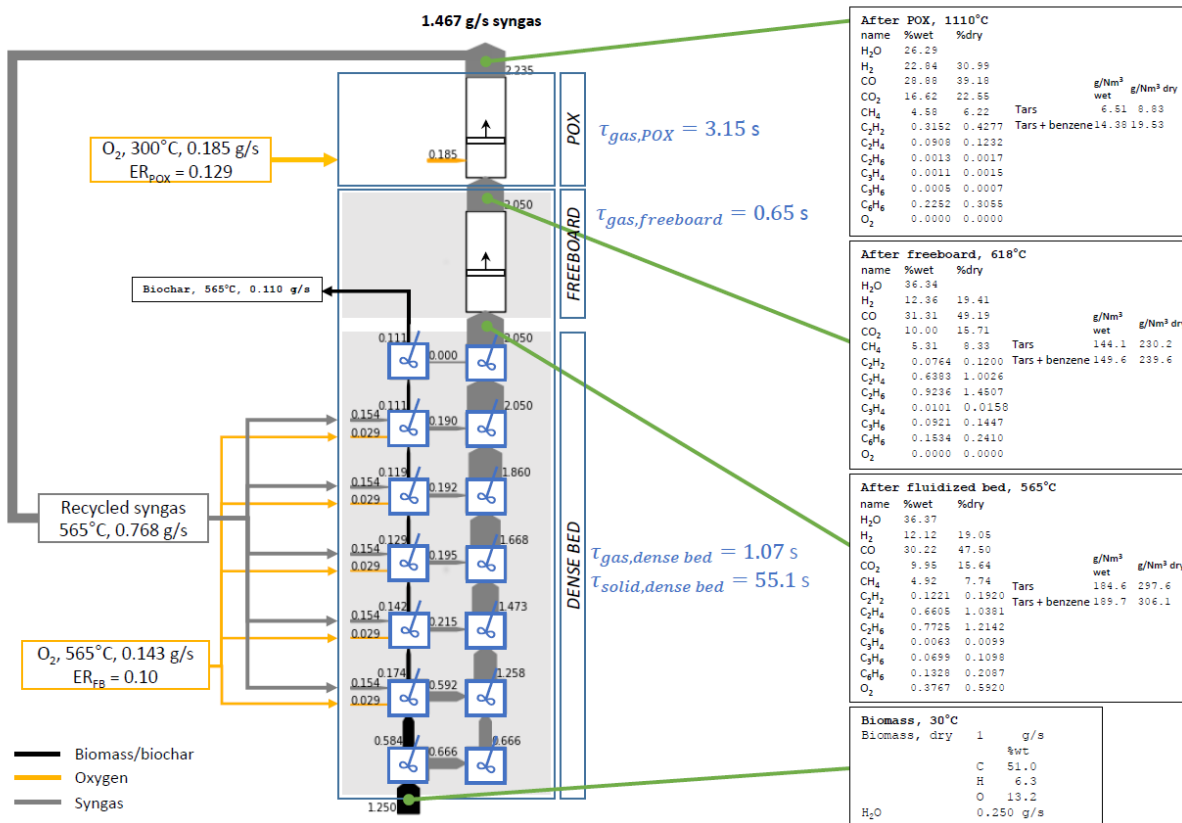


Figure S3-6: Results of the model

In order to evaluate the accuracy of the approach proposed, the model predictions were compared to the experiments of Polin et al. (2019)⁵ on autothermal pyrolysis of Red Oak in a fluidized bed at 500°C with air at ER = 0.10. The composition of Red Oak was adjusted to CELL 45.5%mol, HCE 40.5%mol, LIG-C 8.8%mol, LIG-H 0.5% and LIG-O 4.7%mol to match the elemental composition (C 49.26%wt, H 4.99%wt and O 45.57%wt). The products yields, carbon balance and non-condensable gases (NCGs) yields are presented in Figure S3-7, Figure S3-8 and Figure S3-9 respectively.

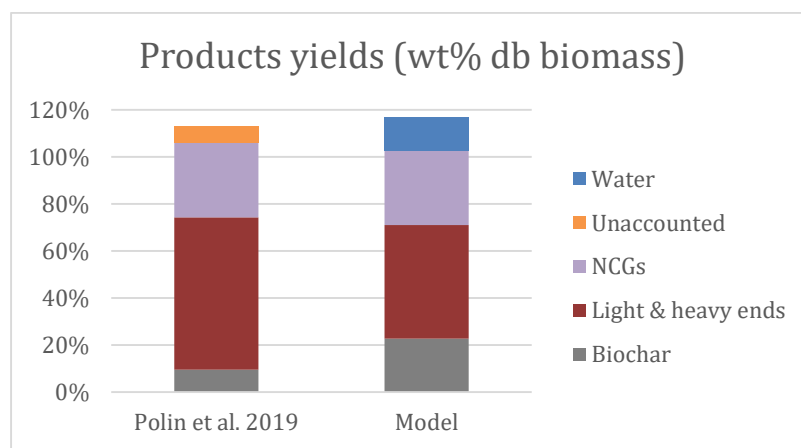


Figure S3-7: Products yields.

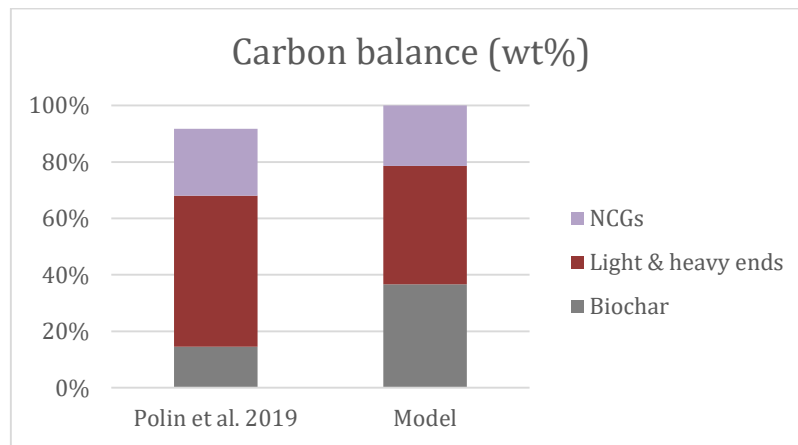


Figure S3-8: Carbon balance.

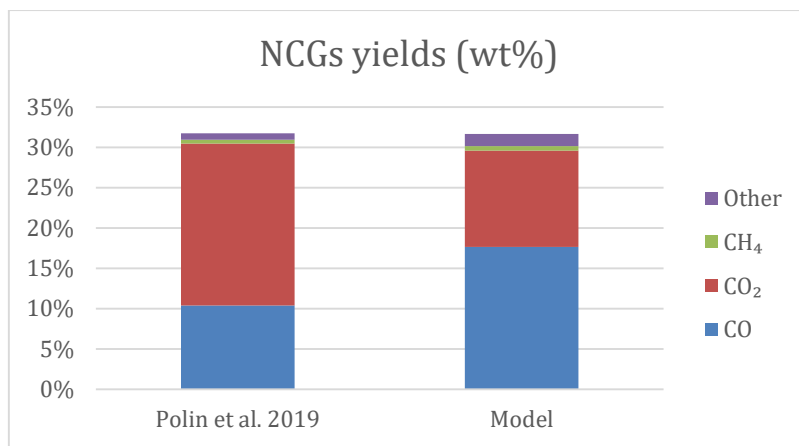


Figure S3-9: Non-condensable gases yields.

The model predicts the same non-condensable gas yields as the experiments but it over predicts the formation of biochar. The resulting biochar carbon yield is then higher than in experiments. The model predicts a higher formation of CO than CO₂. The experiments showed the opposite trend.

In conclusions, the kinetic model of Ranzi et al.³ is not fully accurate for those oxidative fast pyrolysis conditions. Our group had previously shown some discrepancies of this model notably for fast pyrolysis conditions⁶. Nevertheless, this model is still the best one (to the best of our knowledge) to model the molecular composition of the gas phase (including tar) which is not provided in details in the experimental results of Polin et al.⁵.

With a molecular composition of the organic compounds contained in this pyrolysis gas, this approach enables to determine the effect of POX reactor on the autothermal pyrolysis gas phase. The other interest of this pyrolyzer simulator is its ability to estimate the effect of some operating variables (air to biomass flow rates for instance).

3.2.10.4 Partial oxidation model

The partial oxidation unit was modeled with a plug flow model under Chemkin Pro 17.0.

The kinetic mechanism was adapted from Dhahak et al.⁷ for pyrolysis and oxidation of unsaturated light hydrocarbons leading to polycyclic aromatic hydrocarbons (PAHs). This model was completed with Norinaga et al.^{8,9} mechanisms of PAHs pyrolysis and oxidation to account for the PAHs omitted in the initial model. C₂₀ and higher PAHs were considered as soot precursors¹⁰ and the equations of soot formation were written according to Septien et al.¹¹:



3.2.10.5 Determination of the minimum equivalent ratio for partial oxidation

The main objective of the POX unit was the reduction of the tar content to 2 g/Nm³. The Figure S3-10 presents a sensitivity analysis of the impact of oxygen addition to the tar reduction and syngas outlet composition and temperature. The syngas at the inlet corresponded to cases 1 and 2.

The minimum ER to reach 2 g/Nm³ was around 0.12. To the best of our knowledge, no experiment was yet conducted on such a POX unit. The gas temperature (peak and outlet) stays below 1300°C which is the estimated limit in temperature for a common refractory material. At this ER, part of the hydrogen is consumed with a noticeable decrease of hydrogen content (-6%). At the same time, the content of CO increases (+97%) leading to a global H₂+CO content increased by 27%.

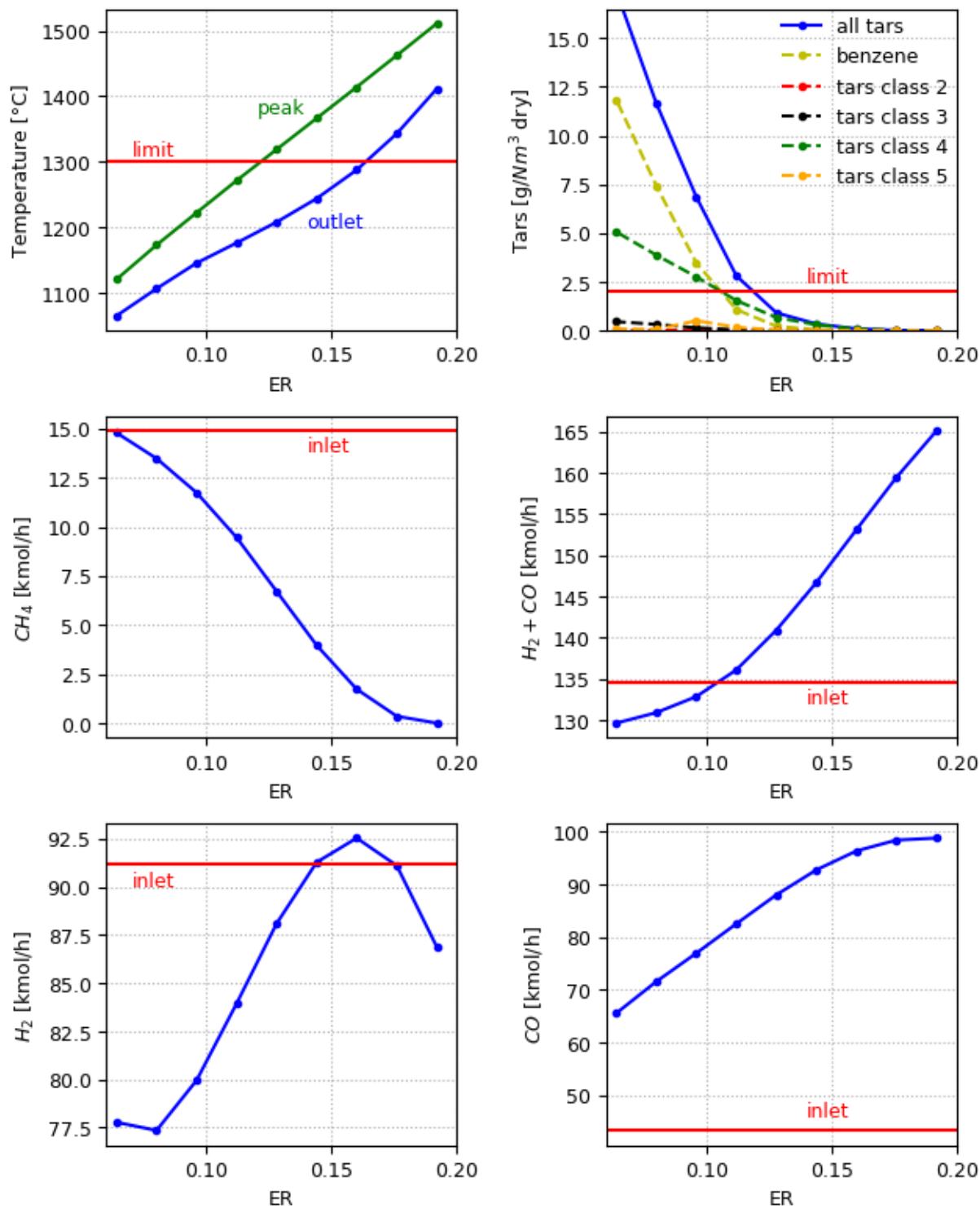


Figure S3-10: Impact of oxygen (equivalence ratio) on the partial oxidation unit on the syngas temperature and composition (cases 1 & 2).

3.2.10.6 Kinetics used in the reformer model

To estimate the products after the steam reformer, a PLUG model associated with kinetics was used instead of a hypothetical equilibrium reactor. Equations 1 to 10 in Table S3-4 were used by Srivanas et al.¹². They considered only benzene, phenol, toluene and naphthalene as tar products. To consider the other tar species, a steam reforming equation was written for each tars according to equation 11. The kinetics parameters are presented in Table S3-5. The missing kinetic parameters were calculated from Aznar et al. for global tar reduction on nickel catalyst¹³. As detailed by Srinivas et al., the reaction rate in the original source was converted from kg of tar per kg of catalyst per h into kmol of tar per m³ of catalyst per h according to the following equation.

$$k'_{app} = k_{app} \cdot \frac{\rho_{cat}}{MW(1 - \varepsilon)}$$

$k_{app} = 250\,000 \text{ m}^3/\text{kg/h}$ ¹³, the bed porosity was assumed $\varepsilon = 0.5$, the catalyst density $\rho_{cat} = 900 \text{ kg/m}^3$ and MW the molar weight of the tar considered. The activation energy for these additional reaction is $5.8 \cdot 10^7 \text{ J/kmol}$ ¹³.

Table S3-4: Reactions in reformer^{12,13}

Steam reforming	$2C_7H_8 + 21H_2O \rightarrow 7CO_2 + 29H_2 + 7CO$	1
Hydrodealkylation	$C_7H_8 + H_2 \rightarrow CH_4 + C_6H_6$	2
Water-gas shift (WGS)	$CO + H_2O \rightarrow H_2 + CO_2$	3
Reverse WGS	$CO_2 + H_2 \rightarrow CO + H_2O$	3r
Steam reforming	$CH_4 + H_2O \rightarrow CO + 3H_2$	4
Thermal cracking	$C_6H_5OH \rightarrow CO + 0.4C_{10}H_8 + 0.15C_6H_6 + 0.1CH_4 + 0.75H_2$	5
Steam reforming	$C_6H_5OH + 3H_2O \rightarrow 2CO + CO_2 + 2.95CH_4 + 0.05C + 0.1H_2$	6
Thermal cracking	$C_{10}H_8 \rightarrow 7.38C + 0.275C_6H_6 + 0.97CH_4 + 1.235H_2$	7
Steam reforming	$C_6H_6 + 2H_2O \rightarrow 1.5C + 2.5CH_4 + 2CO$	8
Steam gasification	$C + H_2O \rightarrow CO + H_2$	9
Steam reforming	$C_{10}H_8 + 4H_2O \rightarrow C_6H_6 + 4CO + 5H_2$	10
Steam reforming	$C_nH_m + nH_2O \rightarrow nCO + \left(n + \frac{m}{2}\right)H_2$	11- ...

Table S3-5: Kinetic parameters for reformer with nickel catalyst.

	Pre-exponential factor k'_{app}	Activation energy (J/kmol)	Rate expression	Ref.
1	$1.36 \cdot 10^3$	$5.8 \cdot 10^7$	$Cm_{C_7H_8}$	13
2	$3.3 \cdot 10^5$	$2.47 \cdot 10^8$	$C_{C_7H_8} C_{H_2}^{0.5}$	14
3	$1.39 \cdot 10^3$	$1.26 \cdot 10^7$	$C_{CO} C_{H_2O}$	14
3r	$2.21 \cdot 10^5$	$5.37 \cdot 10^7$	$C_{CO_2} C_{H_2}$	
4	$1.04 \cdot 10^4$	$6.2 \cdot 10^7$	Cm_{CH_4}	13
5	$1 \cdot 10^7$	$1 \cdot 10^8$	$C_{C_6H_5OH}$	14
6	$1.33 \cdot 10^3$	$5.8 \cdot 10^7$	$Cm_{C_6H_5OH}$	13
7	$3.39 \cdot 10^{14}$	$3.5 \cdot 10^8$	$C_{C_{10}H_8}^{1.6} C_{H_2}^{-0.5}$	14
8	$1.60 \cdot 10^3$	$5.8 \cdot 10^7$	$Cm_{C_6H_6}$	13
9	$3.6 \cdot 10^{12}$	$3.1 \cdot 10^8$	$C_C C_{H_2O}$	14
10	$9.78 \cdot 10^2$	$5.8 \cdot 10^7$	$Cm_{C_{10}H_8}$	13

Cm stands for mass concentration

3.2.10.7 Hydrogen separation

When the production of hydrogen was not maximized by catalytic reactors (cases 2 and 3), the content of hydrogen in the syngas was too low to be separated from the syngas in only one separation stage with high purity. In this work, we propose to use a membrane permeable to hydrogen as a first step of separation based on UBE B-H polyimide membrane¹⁵. The pre-concentrated syngas was then sent to a second stage with a PSA (Figure S3-11). Many parameters can be varied to make this separation in two stages. The architecture was optimized by varying the membrane surface, pressure of the retentate and the pressure at the permeate. The optimal architecture was determined by minimizing the specific hydrogen separation cost.

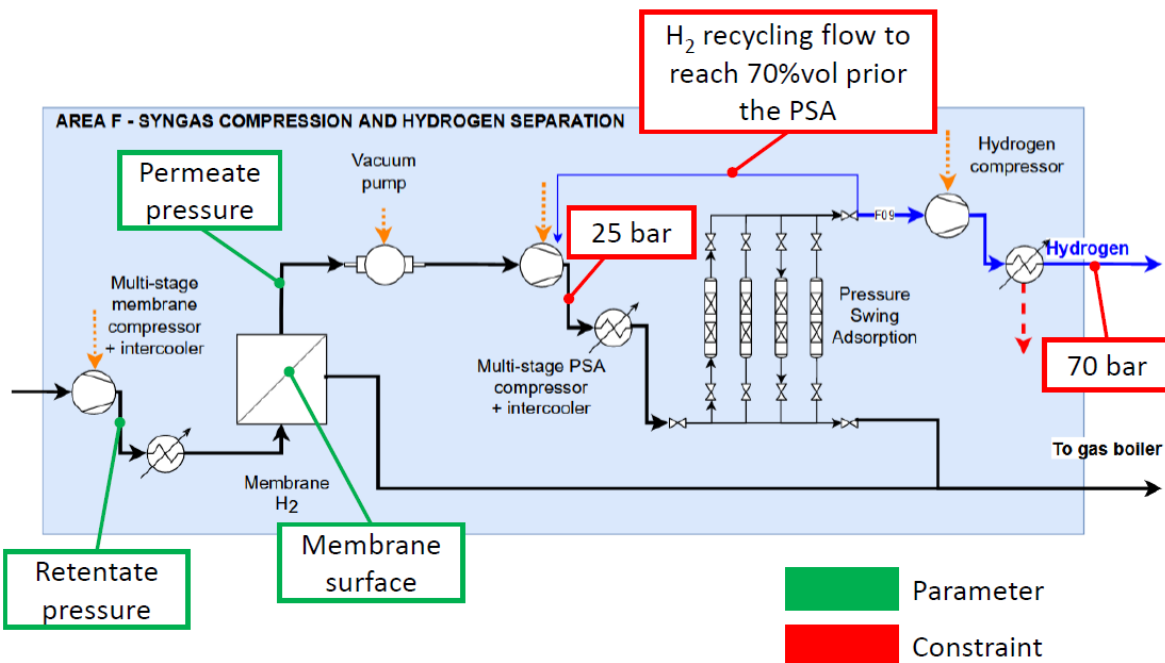


Figure S3-11: Architecture of H₂ separation optimization problem.

The operating conditions for the PSA H₂ with 85% H₂ recovery and 99.99% purity led to an adsorption pressure around 25 bar¹. The purge pressure was set to 1.3 bar, the minimum pressure required to inject the tail gas in a burner. The membrane unit was simulated with ‘MEMSIC’, a CAPE-OPEN module embedded inside Aspen Plus, with counter-current pattern¹⁶.

The fixed capital investment was estimated based on base equipment cost from Table S3-6 and updated to the year 2020 with the chemical engineering plant cost index (CEPCI)¹⁷.

$$I_{actual,2020} = I_{base,y} \cdot \left(\frac{Actual\ capacity}{Base\ capacity} \right)^n \cdot FCIF \cdot \frac{CEPCI_{2020}}{CEPCI_y} DTE$$

FCIF is the fixed capital investment factor to include all direct and indirect costs related to the equipment. DTE is the dollar to euro conversion coefficient (0.877 €/\$2020). The cost of compressors and PSA H₂ were estimated with four different sources, the average values were used.

The fixed capital investment is:

$$CAPEX = I_{Feed\ compressor} + I_{Membrane\ module} + I_{Vacuum\ pump} + I_{Stage\ compressor} + I_{PSA}$$

The cost of the membrane module is¹⁵:

$$I_{Membrane\ module} = I_{Membrane} + I_{Frame}$$

$$I_{Membrane} = Area \cdot 40[\text{€}/m^2]$$

$$I_{Frame} = 2.86 \cdot 10^5 \cdot \left(\frac{Area[m^2]}{2000} \right)^{0.7} \cdot \left(\frac{P_{feed}[bar]}{55} \right)^{0.875}$$

The operating cost of the whole system (membrane + PSA) is the sum of power consumption C_{elec} and the operating and maintenance cost C_{om} :

$$OPEX = C_{elec} + C_{om}$$

The replacement cost of the membrane was assumed as 25 €/m², the cost of replacement and repairs was assumed to be 3% of the CAPEX and the adsorbent 20 €/kg with a lifetime of 4 years.

The mass of the adsorbent for the PSA was estimated with adsorption isotherms¹⁸ assuming equilibrium according to Peters et al. and Swanson et al.^{19,20}.

The plant is assumed to run 7500 h per year. The cost of electricity was set to 50 €/MWh.

$$C_{om} = 20\% \cdot Area \cdot 25[\text{€}/m^2] + 0.03 \cdot CAPEX + 25\% \cdot Mass\ adsorbent \cdot 20[\text{€}/kg]$$

$$C_{elec} = (W_{feed\ compressor} + W_{vacuum\ pump} + W_{stage\ compressor}) \cdot 7500[h/year] \cdot 50[\text{€}/MWh]$$

The specific hydrogen separation cost was calculated with the following relation.

$$C_{H_2,spec}[\text{€}/kg] = \frac{0.854 \cdot CAPEX[\text{€}] + OPEX[\text{€}/year]}{F_{H_2}[kg/h] \cdot 7500[h/year]}$$

Table S3-6: Data used for specific hydrogen separation cost estimation.

	Base cost		Base scale		n	FCIF
Syngas compressor						
Liu et al. 2011 ²¹	6.31	M\$2007	10 MWe		0.67	1.32
Kreutz et al. 2008 ²²	6.0	M\$2007	10 MWe		0.67	1.52
Hamelinck et al. 2004 ²³	0.7	k\$1993	1 kWe		1	2.1
Tijmensen et al. 2002 ²⁴	12	M\$2000	13.2 MWe		0.85	2.11
Vacuum pump						
Ramirez-Santos et al. 2017 ¹⁵	1.5	k€2020	1 kWe		1	1
PSA H2						
Hamelinck, 2004 ²³	23	M\$1993	9600 kmol/h (syngas inlet)		0.7	1.69
Kreutz et al., 2008 ²²	7.1	M\$2002	1058.4 kmol/h (purge)		0.74	1
Spath et al., 2005 ¹	4.86	M\$2002	6468 kg/h (H ₂ produced)		0.6	2.47
Meerman et al., 2012 ²⁵	12	M\$2008	16616 kmol/h (H ₂ produced)		0.65	2.28

The results of this cost optimization for case 2 and 3 are presented in Figure S3-12 and Figure S3-13.

In the case 2, the pressure selected was 5 bar at the retentate and 1 bar at the permeate (meaning no vacuum pump needed). The resulting membrane area was estimated to 1 500 m² for a specific hydrogen separation cost around 0.91 €/kg H₂. These conditions give a lower cost of H₂ with a smaller membrane area and no vacuum pump.

In the case 3, the upstream pressure was 5 bars and the downstream pressure 0.75 bar (a vacuum pump is required). The membrane area was estimated to 1 500 m² for a specific hydrogen separation cost around 1.08 €/kg H₂. These conditions lead to a smaller membrane area and a lower vacuum demand.

The use of two stage separation was also tested for case 1, but it did not decrease the specific separation cost evaluated to 0.59€/kg H₂ in one stage PSA.

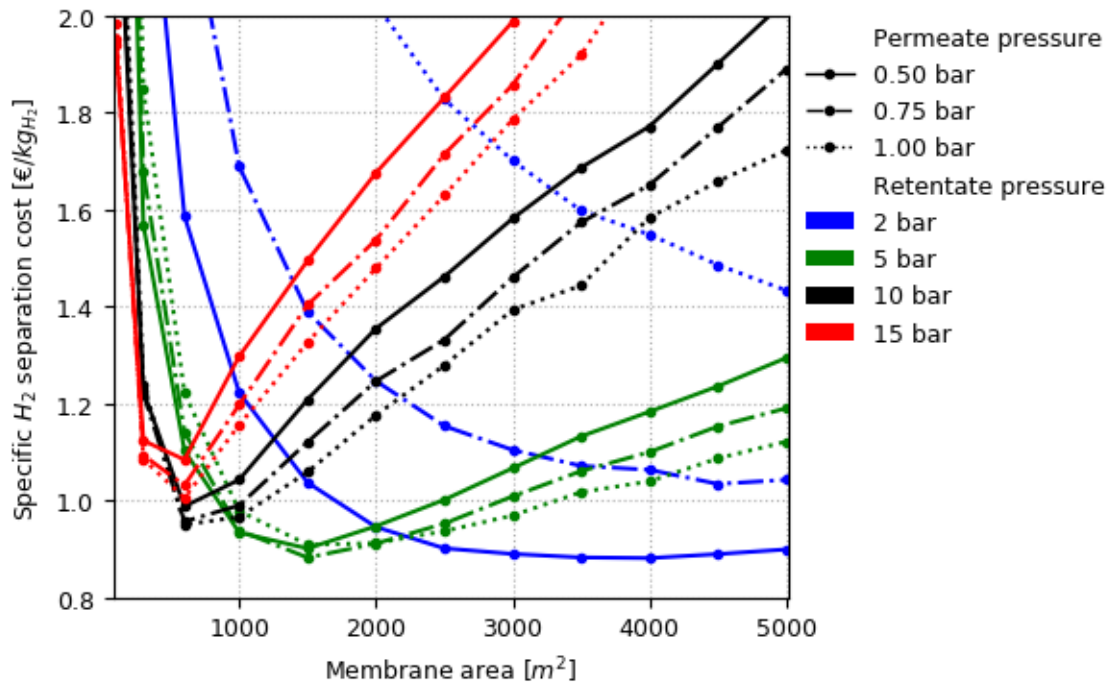


Figure S3-12: Specific hydrogen separation cost for case 2.

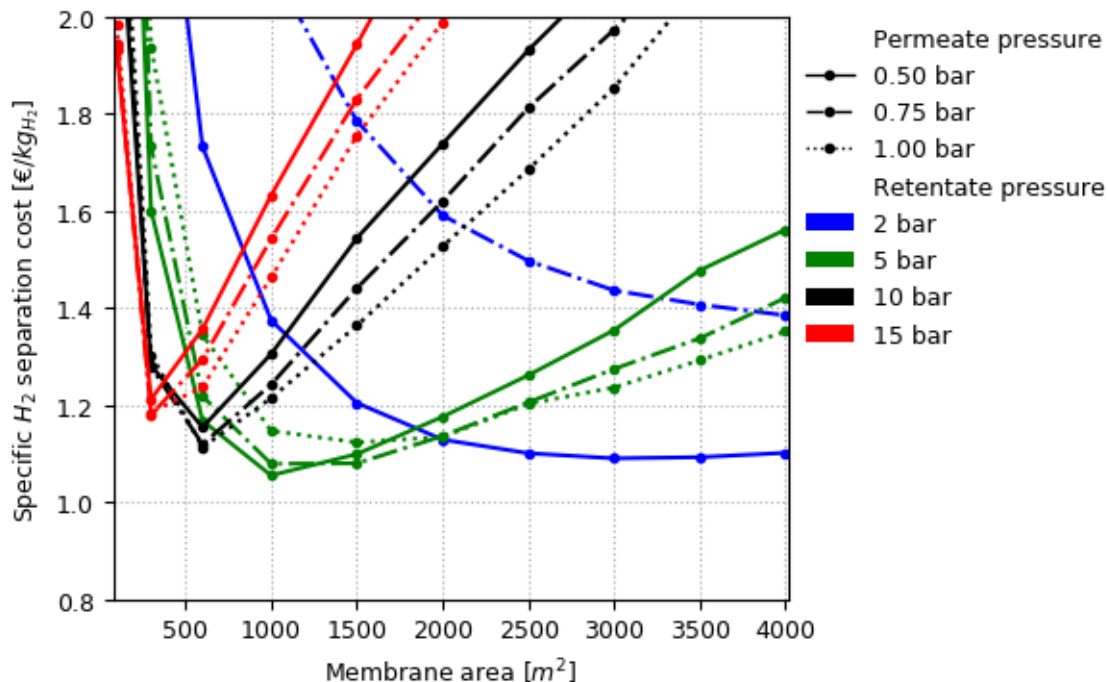


Figure S3-13: Specific hydrogen separation cost for case 3.

3.2.10.8 Reference

- (1) Spath, P.; Aden, A.; Eggeman, T.; Ringer, M.; Wallace, B.; Jechura, J. *Biomass to Hydrogen Production Detailed Design and Economics Utilizing the Battelle Columbus Laboratory Indirectly-Heated Gasifier*; NREL/TP-510-37408, 15016221; NREL, 2005. <https://doi.org/10.2172/15016221>.
- (2) Schmid, M.; Beirow, M.; Schweitzer, D.; Waizmann, G.; Spörl, R.; Scheffknecht, G. Product Gas Composition for Steam-Oxygen Fluidized Bed Gasification of Dried Sewage Sludge, Straw Pellets and Wood Pellets and the Influence of Limestone as Bed Material. *Biomass and Bioenergy* **2018**, 117, 71–77. <https://doi.org/10.1016/j.biombioe.2018.07.011>.
- (3) Debiagi, P. E. A.; Gentile, G.; Pelucchi, M.; Frassoldati, A.; Cuoci, A.; Faravelli, T.; Ranzi, E. Detailed Kinetic Mechanism of Gas-Phase Reactions of Volatiles Released from Biomass Pyrolysis. *Biomass and Bioenergy* **2016**, 93, 60–71. <https://doi.org/10.1016/j.biombioe.2016.06.015>.
- (4) Agu, C. E.; Pfeifer, C.; Eikeland, M.; Tokheim, L.-A.; Moldestad, B. M. E. Measurement and Characterization of Biomass Mean Residence Time in an Air-Blown Bubbling Fluidized Bed Gasification Reactor. *Fuel* **2019**, 253, 1414–1423. <https://doi.org/10.1016/j.fuel.2019.05.103>.
- (5) Polin, J. P.; Peterson, C. A.; Whitmer, L. E.; Smith, R. G.; Brown, R. C. Process Intensification of Biomass Fast Pyrolysis through Autothermal Operation of a Fluidized Bed Reactor. *Applied Energy* **2019**, 249, 276–285. <https://doi.org/10.1016/j.apenergy.2019.04.154>.
- (6) Jia, L.; Dufour, A.; Le Brech, Y.; Authier, O.; Mauviel, G. On-Line Analysis of Primary Tars from Biomass Pyrolysis by Single Photoionization Mass Spectrometry: Experiments and Detailed Modelling. *Chemical Engineering Journal* **2017**, 313, 270–282. <https://doi.org/10.1016/j.cej.2016.12.021>.
- (7) Dhahak, A.; Bounaceur, R.; Le Dreff-Lorimier, C.; Schmidt, G.; Trouve, G.; Battin-Leclerc, F. Development of a Detailed Kinetic Model for the Combustion of Biomass. *Fuel* **2019**, 242, 756–774. <https://doi.org/10.1016/j.fuel.2019.01.093>.
- (8) Norinaga, K.; Deutschmann, O.; Saegusa, N.; Hayashi, J. Analysis of Pyrolysis Products from Light Hydrocarbons and Kinetic Modeling for Growth of Polycyclic Aromatic Hydrocarbons with Detailed Chemistry. *Journal of Analytical and Applied Pyrolysis* **2009**, 86 (1), 148–160. <https://doi.org/10.1016/j.jaat.2009.05.001>.
- (9) Norinaga, K.; Shoji, T.; Kudo, S.; Hayashi, J. Detailed Chemical Kinetic Modelling of Vapour-Phase Cracking of Multi-Component Molecular Mixtures Derived from the Fast Pyrolysis of Cellulose. *Fuel* **2013**, 103, 141–150. <https://doi.org/10.1016/j.fuel.2011.07.045>.
- (10) Saggese, C.; Sánchez, N. E.; Frassoldati, A.; Cuoci, A.; Faravelli, T.; Alzueta, M. U.; Ranzi, E. Kinetic Modeling Study of Polycyclic Aromatic Hydrocarbons and Soot Formation in Acetylene Pyrolysis. *Energy Fuels* **2014**, 28 (2), 1489–1501. <https://doi.org/10.1021/ef402048q>.
- (11) Septien, S.; Valin, S.; Peyrot, M.; Spindler, B.; Salvador, S. Influence of Steam on Gasification of Millimetric Wood Particles in a Drop Tube Reactor: Experiments and Modelling. *Fuel* **2013**, 103, 1080–1089. <https://doi.org/10.1016/j.fuel.2012.09.011>.

- (12) Srinivas, S.; Field, R. P.; Herzog, H. J. Modeling Tar Handling Options in Biomass Gasification. *Energy Fuels* **2013**, *27* (6), 2859–2873. <https://doi.org/10.1021/ef400388u>.
- (13) Aznar, M. P.; Caballero, M. A.; Gil, J.; Martín, J. A.; Corella, J. Commercial Steam Reforming Catalysts To Improve Biomass Gasification with Steam-Oxygen Mixtures. 2. Catalytic Tar Removal. *Industrial & Engineering Chemistry Research* **1998**, *37*, 2668–2680.
- (14) Su, Y.; Luo, Y.; Chen, Y.; Wu, W.; Zhang, Y. Experimental and Numerical Investigation of Tar Destruction under Partial Oxidation Environment. *Fuel Processing Technology* **2011**, *92* (8), 1513–1524. <https://doi.org/10.1016/j.fuproc.2011.03.013>.
- (15) Ramírez-Santos, Á. A.; Castel, C.; Favre, E. Utilization of Blast Furnace Flue Gas: Opportunities and Challenges for Polymeric Membrane Gas Separation Processes. *Journal of Membrane Science* **2017**, *526*, 191–204. <https://doi.org/10.1016/j.memsci.2016.12.033>.
- (16) Bounaceur, R.; Berger, E.; Pfister, M.; Ramirez Santos, A. A.; Favre, E. Rigorous Variable Permeability Modelling and Process Simulation for the Design of Polymeric Membrane Gas Separation Units: MEMSIC Simulation Tool. *Journal of Membrane Science* **2017**, *523*, 77–91. <https://doi.org/10.1016/j.memsci.2016.09.011>.
- (17) 2019 Chemical Engineering Plant Cost Index Annual Average <https://www.chemengonline.com/2019-chemical-engineering-plant-cost-index-annual-average/?printmode=1> (accessed 2020 -04 -08).
- (18) Golmakani, A.; Fatemi, S.; Tamnanloo, J. Investigating PSA, VSA, and TSA Methods in SMR Unit of Refineries for Hydrogen Production with Fuel Cell Specification. *Separation and Purification Technology* **2017**, *176*, 73–91. <https://doi.org/10.1016/j.seppur.2016.11.030>.
- (19) Peters, M. S.; Timmerhaus, K. D.; West, R. E. *Plant Design and Economics for Chemical Engineers*, fifth edition.; McGraw-Hill New York, 2004.
- (20) Swanson, R. M.; Platon, A.; Satrio, J. A.; Brown, R. C.; Hsu, D. D. *Techno-Economic Analysis of Biofuels Production Based on Gasification*; NREL/TP-6A20-46587, 994017; 2010. <https://doi.org/10.2172/994017>.
- (21) Liu, G.; Larson, E. D.; Williams, R. H.; Kreutz, T. G.; Guo, X. Making Fischer-Tropsch Fuels and Electricity from Coal and Biomass: Performance and Cost Analysis. *Energy Fuels* **2011**, *25* (1), 415–437. <https://doi.org/10.1021/ef101184e>.
- (22) Kreutz, T.; Williams, R.; Consonni, S.; Chiesa, P. Co-Production of Hydrogen, Electricity and CO from Coal with Commercially Ready Technology. Part B: Economic Analysis. *International Journal of Hydrogen Energy* **2005**, *30* (7), 769–784. <https://doi.org/10.1016/j.ijhydene.2004.08.001>.
- (23) Hamelinck, C.; Faaij, A.; Denuil, H.; Boerrigter, H. Production of FT Transportation Fuels from Biomass; Technical Options, Process Analysis and Optimisation, and Development Potential. *Energy* **2004**, *29* (11), 1743–1771. <https://doi.org/10.1016/j.energy.2004.01.002>.
- (24) Tijmensen, M. J. A.; Faaij, A. P. C.; Hamelinck, C. N. Exploration of the Possibilities for Production of Fischer Tropsch Liquids and Power via Biomass Gasification. *Biomass and Bioenergy* **2002**, *24*.

- (25) Meerman, J. C.; Ramírez, A.; Turkenburg, W. C.; Faaij, A. P. C. Performance of Simulated Flexible Integrated Gasification Polygeneration Facilities, Part B: Economic Evaluation. *Renewable and Sustainable Energy Reviews* **2012**, *16* (8), 6083–6102. <https://doi.org/10.1016/j.rser.2012.06.030>.

CHAPITRE 4 ANALYSE TECHNICO-ÉCONOMIQUE ET ANALYSE DE CYCLE DE VIE

4.1 Introduction

Suite à l'obtention des bilans matière et énergie dans le chapitre précédent, la viabilité de ces procédés est évaluée avec une analyse technico-économique. Par ailleurs, pour évaluer la pertinence environnementale de ces trois voies de valorisation, une analyse de cycle de vie comparative est également réalisée.

4.2 Article 3 (reproduction intégrale)

Demol R., Dufour A., Rogaume Y., Mauviel G., Woodchips Pyrogasification to Produce H₂, Heat and even Bio-char: Techno-Economic and Life Cycle Assessment of Different Processes. To be submitted.

4.2.1 Abstract

The mitigation of the climate change effects calls for carbon neutral or negative processes to produce energy commodities. Hydrogen is forecasted to play a major role in the energy transition, if its production becomes less carbon-based. This article presents a renewable alternative production of hydrogen from woodchips through three pyrogasification processes. These processes can also co-produce heat and biochar. To evaluate the economic and environmental potential of these processes, a comparative techno-economic analysis and a life cycle assessment were conducted. These show that the market prices of hydrogen (2 €/kg), heat (30 €/MWh) and biochar are not sufficient to reach profitability, as it is the case for other renewable H₂ pathways. The extra-cost required to make the plant profitable was divided by the CO₂ emissions avoided from traditional production processes (steam methane reforming and carbon content in heat networks). The resulting costs were evaluated between 120 and 210 € per ton of CO₂ avoided. If a higher selling price of hydrogen is considered (4 €/kg instead of 2 €/kg), the extra-cost could be significantly reduced. Thus such processes could be considered to reach the targets of international

agreements. The pyrogasification processes are found better than steam reforming regarding global warming potential, ozone depletion layer and fossil fuel consumption impacts. On the opposite, acidification, eutrophication, ecotoxicity and toxicity potential impacts are higher because of the electricity consumption or wastes generated by pyrogasification processes.

4.2.2 Keywords

Gasification, Hydrogen, Techno-economic analysis, Life cycle assessment.

4.2.3 Introduction

The intergovernmental panel on climate change (IPCC), in his sixth assessment report, sounded once again the alarm on the consequences of the anthropogenic emissions of greenhouse gases [1]. To mitigate global warming, carbon-neutral or even carbon-negative processes in the energy sector could contribute to the reduction of these emissions. As an energy vector, hydrogen knows a growing interest for its ability to decarbonize the industry sector and future mobility applications. Yet, the production of hydrogen mainly relies nowadays on fossil fuels: natural gas steam reforming (71%) or coal gasification (27%) [2]. Other ways of production are investigated, especially water electrolysis. The CO₂ emission problem is then transferred to the electricity production. As an example, in France, the electric mix contains 34 gCO₂/kWh in 2020 [3]. As a result of its low energetic efficiency (40 to 70%), electrolysis produces H₂ that “contains” between 48 and 85 gCO₂/kWh (lower if a part of the heat produced is valorized). This is clearly better than H₂ from CH₄ (560 gCO₂/kWh) or coal (410 gCO₂/kWh) [4] but it is still far to be carbon-neutral. In countries where the electric mix is carbon-rich (over 300 gCO₂/kWh), electrolytic H₂ is clearly not a good idea to reduce the GHG emissions [5,6].

Hydrogen can also be produced from other renewable resources as woody biomass. This gas can be produced by thermochemical processes through pyrolysis and gasification [7,8]. In this case, the hydrogen efficiency is around 35-50% [5] or even lower when the goal of the plant is not to maximize the hydrogen production [8]. These processes are by nature multi-products, excess of heat produced along the process could be recovered to feed a heat network. Considering all these energy products, the global efficiency can reach 70-80% [8].

Due to the nature of the feedstock, small units were investigated to use local resources and minimize the transport distance and the truck concentration near the plant. These processes come with other products such as heat and biochar. The main issue relies on the economic feasibility of such processes at relatively small scale.

Shahabuddin reviewed some techno-economic assessment of biomass and waste gasification to produce hydrogen [9]. Table 4-1 presents previous techno-economic analysis of the literature. The final cost of hydrogen could vary a lot from one study to another. All these studies do not give the same details on the hypothesis considered. For instance, the feedstock price chosen has a major impact on the cost of hydrogen. Besides, the hydrogen produced is not at the same purity or pressure.

Spath et al. [7] produced a fundamental work on the economic evaluation of large-scale production of hydrogen (434 MW_{biomass,LHV}). They concluded to a very low price of 1.64-1.82€_{2020/kgH₂}, this price was reviewed by Park et al. to 2.67-3.60€_{2020/kgH₂}. Salkuyeh et al. on a even larger scale (1200-1500 MW_{biomass,LHV}) evaluated this price at 2.86-3.22€_{2020/kgH₂} without and with CO₂ capture [15]. Such large scale does not really correspond to the availability of the feedstock considered (wood based). Sentis et al. evaluated the hydrogen cost on smaller scales (0.1 to 10 MW) and concluded to 3.19 to 13.31€_{2020/kgH₂} [14].

The production price of hydrogen should not be the only criteria to evaluate the interest of a process. The impacts generated by such processes can be evaluated through a life cycle assessment (LCA) framework. Table 4-2 provides a non-exhaustive list of previous LCA studies made on biomass gasification.

Valente et al. [16] reviewed LCA done on hydrogen energy production systems. The functional unit frequently chosen is energy or mass-based. Particularly for thermochemical processes, the production of multi-products put the problem of the attribution of the impacts on the various products. A first option consists of the system expansion. A second option is to allocate the impacts on the products of a mass, energy, exergy, volume or economic basis. Half of the studies reviewed chose the system expansion, the other half the allocation with a predominance on energy/exergy allocation. The impacts the most studied are by order of occurrence: the global warming potential (GWP), the acidification potential (AP), the cumulative energy demand (CED), the ozone layer depletion (ODP), the photochemical oxidant formation (POFP), the energy consumption (fossil).

In less than 20% of the studied reviewed, the energy consumption (nonrenewable), the abiotic depletion, the human toxicity and the land use were also considered. The methods used are IPCC for GWP, VDI or GREET for CED and CML for all other indicators.

Valente et al. worked on the harmonization of GWP, CED and AP [17–19]. One important point in comparing hydrogen production system is the purity and the compression of hydrogen at the same level.

Our group worked previously on the global warming potential of combustion technologies [27] and on gasification processes to produce heat and electricity [28]. To continue, we investigate the economic and impact potential of pyrogasification units at small scale to produce hydrogen, heat and biochar. From a detailed mass and energy balance done in a previous study [8], we propose a detailed techno-economic analysis and a life cycle assessment.

The aim of this work is to evaluate the economic conditions to produce H₂ from biomass at small scale and evaluate the impacts resulting in this production.

The novelty of this work relies on:

- 1) Techno-economic assessment of three small-scale scenarios of production of hydrogen, heat and bio-char from biomass from a detailed heat and mass balance (Demol et al., 2021).
- 2) A life cycle assessment of these scenarios compared with steam methane reforming (SMR) since it is now the most common technology in Europe to produce H₂.

Table 4-1: Non-exhaustive list of techno-economic analysis of biomass gasification in literature.

	Technology	Biomass	Size [MW_{biomass}]	Efficiencies	H₂ specification and price	Ref.
Iwasaki, 2003	Pyrolyser, cracker, CO-shift, PSA ^b , engine	Woody biomass	100 t/d 18.6 MW _{LHV}	H ₂ = 47.9% _{HHV} (net) (5.9 t/d)	99.99% - 200 bar 4.28 \$ _{2003/kg^a}	[10]
Spath et al., 2005	DFB ^b , reformer, wet scrubber, LO-CAT ^b , ZnO bed, steam	Hybrid poplar wood chips	2000 t/d 434 MW _{LHV}	H ₂ = 49.8% _{LHV} (net) 152 t/d	99.9% - 70 bar 1.38 \$ _{2002/kg}	[7]
				H ₂ = 55.3% _{LHV} (net)	99.9% - 70 bar 1.24 \$ _{2002/kg}	

	reformer, WGS ^b , PSA ^b			163 t/d		
Lv et al., 2008	Downdraft gasifier (O ₂), CO-shift, PSA ^b , engine	Forest residues	6.40 t/d 1.4 MW _{LHV}	H ₂ = 51.5% (gross) 0.52 t/d ^d	% 1.69 \$ _{2008/kg^a}	[11]
Parks et al., 2011	First unit, gasifier, reformer, WGS, PSA ^b	Woody biomass	500 t/d 109 MW _{LHV^c}	H ₂ = 43.8% LHV (gross) 32.4 t/d	99.99% 5.40-7.70 \$ _{2009/kg}	[12]
	N th unit.		2000 t/d 434 MW _{LHV^c}	H ₂ = 45.7% LHV (gross) 135 t/d	99.99% 2.80-3.80 \$ _{2009/kg}	
Sara et al., 2016	Indirect FB ^b , catalytic candles, WGS ^b , PSA ^b	Almond shells	4.80 t/d ^d 1 MW	H ₂ = 46- 50% LHV ^d 0.033-0.036 t/d	9.5-13 € _{2016/kg^a}	[13]
Sentis et al., 2016	Indirect FB ^b , catalytic candles, WGS ^b , PSA ^b	Almond shells	4.80 t/d ^d 1 MW	H ₂ = 20% LHV ^d Global = 30% LHV 0.14 t/d ^d	6 bar 5.6-7.1 € _{2016/kg^a}	[14]
			48.0 t/d ^d 10 MW	H ₂ = 20% LHV ^d Global = 30% LHV 1.4 t/d ^d	6 bar 2.7-2.9 € _{2016/kg^a}	
Salkuyeh et al., 2018	High-pressure EF ^b oxygen- blown, ASU ^b , LO-CAT, WGS ^b , PSA ^b	Canadian pine wood	5 840 t/d 1200 MW _{LHV^d}	H ₂ = 54% LHV ^d Global = 56% LHV 454 t/d	3.4 \$ _{2018/kg^a}	[15]
	With carbon capture			H ₂ = 50% LHV ^d Global = 50% LHV 454 t/d	3.5 \$ _{2018/kg^a}	
	Atmospheric indirectly- heated FB, tar reformer, scrubber, LO- CAT, WGS ^b , PSA ^b		7 380 t/d 1500 MW _{LHV^d}	H ₂ = 42% LHV ^d Global = 45% LHV 454 t/d	3.1 \$ _{2018/kg^a}	
	With carbon capture			H ₂ = 41% LHV ^d Global = 41% LHV 454 t/d	3.5 \$ _{2018/kg^a}	

^aYear cost assumed.

^bPSA: pressure swing adsorption, DFB: dual fluidized bed, WGS: water gas shift, FB: fluidized bed, ASU: air separation unit, EF: entrained flow.

^cAssuming a LHV of 18.7 MJ/kg

^dEstimate

Table 4-2: Non-exhaustive list of LCA on H₂ production (cradle-to-gate) from biomass gasification in literature [16].

	Technology ^a	Type of biomass	Size	Functional Unit	Other product	Method & impacts ^c	Ref.
Koroneos et al. 2008	IG, scrubber, reformer, WGS, liquefaction	Biomass	Not specified	1 MJ of H ₂ liquid	No	EcoIndicator 95 method GWP, AP, EP	[20]
Tock and Maréchal, 2012	Torrefaction, FICFB, SR, scrubber, WGS, AGR, PSA	Wood	380 MW _{LHV}	1 kJ of biomass	No	IPCC method GWP	[21]
Moreno and Dufour, 2013	Fixed bed gasifier, reformer, WGS, PSA	Vine, almond, pine, eucalyptus	Not specified	1 Nm ³ of H ₂ 99.9% vol	No	CML method GWP, AP, EP	[22]
Susmozas et al., 2013	DFB, tar reformer, scrubber, LO-CAT, WGS, PSA, steam cycle	Poplar biomass	Not specified	1 kg of H ₂ 99.9% vol 28 bar	Electricity (economic allocation)	CML method ADP, GWP, ODP, POFP, LC, AP, EP, CED	[23]
Iribarren et al., 2014	IG, tar reformer, scrubber, SR, WGS, PSA	Poplar biomass	Adapted from Spath et al. [7]	1 m ³ STP of H ₂ 25.5 bar	Sulphur (avoided burden approach)	CML method CED, GWP, ODP, POFP, LC, AP EP	[24]
Muresan et al., 2014	DFB, WGS, RME scrubber , AGR, PSA, reformer	Biomass	70 MW _{LHV} ^b	1 MW H ₂ 99.99% vol 22.5 bar	No	CML method GWP, AP, EP, ADPF, HTP	[25]
Salkuyeh et al., 2018	See Table 4-1.			1 kg of H ₂	Electricity	GWP	[7]
Valente et al., 2019	See Susmozas et al. (2013)			1 kg of H ₂	Electricity	Harmonized method [19] GWP, AP, CED	[26]

^aAcronyms - IG: indirect gasifier, SR: steam reformer, PSA: pressure swing adsorption, AGR: acid gas removal, DFB: dual fluidized bed, WGS: water gas-shift, FICFB: fast internally circulating fluidized bed.

^bAssuming biomass LHV 18 MJ/kg

^cImpacts acronyms – GWP: global warming, AP: acidification, EP: eutrophication, ODP: ozone layer depletion, POFP: photochemical oxidant formation, LC: land competition, CED: cumulative energy demand, ADFP: abiotic depletion fossil, HTTP: human toxicity.

4.2.4 Material and methods

4.2.4.1 Scenarios investigated

Three scenarios were investigated corresponding to the scenarios in [8]. The mass and energy balance were estimated from the processes presented in Figure 4-1 and the result of our previous study [8]. Case 1 corresponds to a steam-oxygen gasification combined with a reformer and water gas-shift reactor to promote the production of hydrogen. After a wet scrubber, the hydrogen is separated from syngas by a pressure swing adsorption (PSA), the usual separation technology. The tail gas is burnt in a gas boiler. Two scales were considered: 100 MW for a large-scale production unit referred as 1-100 and 20 MW for a local production named 1-20. The second case was a similar process but without catalytic reactors, at 20 MW scale (2-20). Because the hydrogen is more diluted in syngas than in case 1, a two-stage separation process is used. The first step consists of a membrane separation and the second step uses a PSA. The third case (3-20) consists in an autothermal pyrolysis to produce biochar and a gas phase. This gas phase is oxidized in a partial oxidation (POX) unit. The syngas produced from the POX follows the same treatment as in case 2.

In all cases, heat is recovered along the process and in the gas boiler to provide the heat required in the process. The heat surplus is valorized as a product of the process. The products of these cases are hydrogen at 70 bars and 99.99% purity, heat dedicated to a heat network and biochar in the third case.

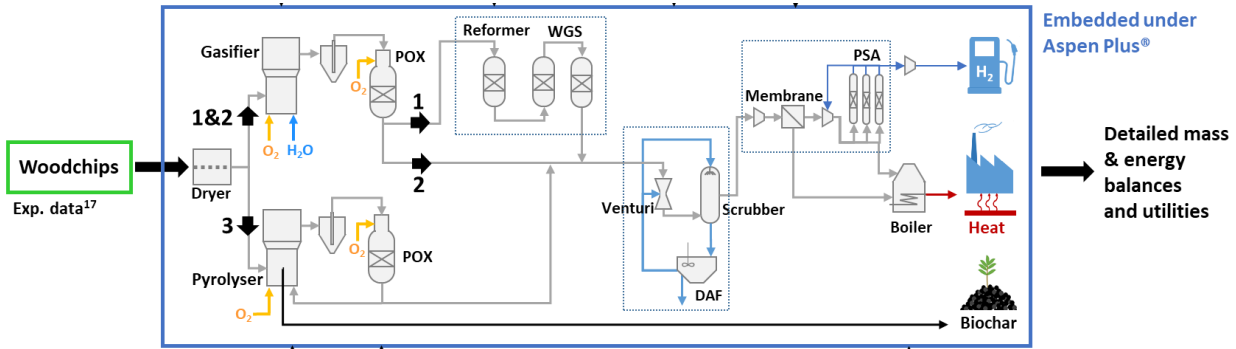


Figure 4-1: Scenarios investigated, from [8].

4.2.4.2 Techno-Economic Model

In order to compare these scenarios on an economic basis, few figures need to be estimated: the fixed capital cost, the manufacturing cost and the revenues from product sales. In the following, all prices are given in €2020.

4.2.4.2.1 Fixed Capital Investment

The fixed capital investment (FCI) can be estimated from the equipment cost. The individual costs of equipment were estimated with abacus [29,30] or scale-up power law based on capacity according to equation (4.1). The prices were adjusted to the year 2020 with equation (4.2) using the chemical engineering price cost index CEPCI, its value for 2020 was $CEPCI_{2020} = 596.2$ [31]. Prices in US dollars were also converted to euro with the mean value of exchange rate 0.877 in 2020 [32].

$$C_{new} = C_0 \cdot \left(\frac{Q_{new}}{Q_0} \right)^n \quad (4.1)$$

$$C_{2020} = C_y \cdot \left(\frac{CEPCI_{2020}}{CEPCI_y} \right) \quad (4.2)$$

C_{new} is the equipment cost for a capacity of Q_{new} estimated from a reference unit costing C_0 for a Q_0 capacity. n is the exponent factor specific to the equipment. C_{2020} and C_y are the cost updated to 2020 and the reference cost of year y .

To account for all direct costs (DC i.e., equipment purchase, installation, instrumentation, piping, electrical, insulation, painting & buildings, process, auxiliary & service facilities, yard improvement) and indirect costs (IC i.e., engineering, supervision, construction expenses, legal expenses, contractor fee and contingency) this cost was multiplied by a fixed capital investment factor FCIF. This coefficient depends on the original reference cost.

$$FCI = DC + IC = \sum FCIF \cdot Purchased\ equipment\ cost \quad (4.3)$$

The costs of all major equipment can be found in supplementary material. When available, abacus estimations were preferred because these estimations come with domains of validity. This is usually not the case with scale-up power law, the potential error on the cost is then bigger, especially when the scale ratio between the estimate and the reference unit is far from 1.

4.2.4.2.2 Cost of manufacturing

The cost of manufacturing takes into account the cost of the raw material, the utilities, the labor, the maintenance and repairs and other costs related to the unit operation.

The cost of labor was estimated by the number of workers required and the mean wages in France. More details can be found in Table 4-3. Relevant hypotheses on the feedstock, utilities and consumables costs and price products are gathered in Table 4-4.

Table 4-3: Cost of labor

	Full cost of salary ¹	1-100	1-20	2-20	3-20
Operators	27.9 k€/year	24	12	12	12
Chief of maintenance	55.4 k€/year	2	1	1	1
Reformer-shift engineer	55.4 k€/year	2	1		
H2 separation engineer	55.4 k€/year	2	1	1	1
Head of plant	65.0 k€/year	1	1	1	1
Trucks drivers	Included in biomass cost ²	21	2	2	2

¹Sources for salaries [33] and [34].

²See supplementary material. The averaged distance is three time less in 20 MW cases (50 km vs 150 km), thus the number of rotation per day is higher and the number of drivers required much lower.

The cost of biomass was supposed 17 €/MWh on a LHV-basis corresponding to an average market price for woodchips in 2021 in France [35]. This price does not include the transport cost; it was

evaluated by assuming a 150 km distance for the case 1-100 and 50 km for the other scenarios [36]. More details can be found in supplementary material. The overall cost of biomass was estimated to 26.9 and 22.0 €/MWh at the entrance of the pyrogasification facility considering transport and taxes for the 100 MW and 20 MW cases, respectively. In the case 100MW, there are 30 trucks that arrive each day at the plant in comparison with only 6 in the 20MW-cases. The neighbors might complain about such a truck traffic.

The price of H₂ can vary from 1-3 €/kg_{H₂} for large-scale consumer delivered with pipeline (ammonia, petrochemical, methanol, chemical processes) to 5-7 €/kg_{H₂} for smaller consumers delivered by truck [37–40]. In the following, we assumed a market production cost of 2 €/kg_{H₂} without transport (equivalent to 51 €/MWh_{H₂}).

Table 4-4: Prices of products and costs of feedstock and utilities.

Feedstock cost		Ref
woodchip (40% humidity)	22.0-26.9 €/MWh LHV-basis	[35,36]
Product market prices		
Heat (water at 80°C)	40 €/MWh	[41]
Hydrogen (99.99%, large scale)	2 €/kg	[37–40]
Bio-char	0.50 €/kg	
Utility costs		
Electricity (taxes included)	80 €/MWh	[41]
Natural gas (startup)	40 €/MWh (value in 2019)	[41]
Propane (forklifts)	40 €/MWh	assumed
Fresh water	2 €/m ³	
Bed material	200 €/t	assumed
Catalyst reformer (Ni-based)	50 €/kg	[42]
Catalyst HTS	50 €/kg	assumed
Catalyst LTS	50 €/kg	assumed
Membrane cost	40 €/m ²	[43]
Membrane replacement	25 €/m ²	[43]
Adsorbent	20 €/kg	assumed
Waste disposal		
Landfill	90 €/t	
Ash under cyclone and fabric filter	250 €/t	

4.2.4.2.3 Financial options and economical criterion

The economic hypothesis are presented in Table 4-5.

Table 4-5: Financial options.

Options	
Operation time	7500 h/year
Discounting rate i	7%
Taxation rate t	30%
Project life	20 years
Construction period	1 year
Depreciation period	15 years (linear)
Loan	50% of total capital investment Interest rate 2% per year
CAPEX estimation	
Working capital WC	$WC = 15\% \cdot FCI$ [44]
Total capital investment	$TCI = FCI + WC$
OPEX estimation	
Raw materials & utilities	From process simulation
Operating labor	See Table 4-3.

The net profit after taxes of year k is calculated from equation 4.4, in which R is the revenue from sales, COM the cost of manufacturing, d_k the depreciation cost and t the taxation rate.

$$NET\ PROFIT_k = (R - COM - d_k) \cdot (1 - t) \quad (4.4)$$

The resulting cash flow at the year k is deduced with equation 4.5.

$$CASH\ FLOW_k = (R - COM - d_k) \cdot (1 - t) + d_k \quad (4.5)$$

To estimate the opportunity of the investment, the net present value (NPV) can be determined with equation 4.6. This method considers the time value of money, assuming a discounting rate i.

$$NPV = -TCI + \sum_{k=1,n} \frac{CASH\ FLOW_k}{(1 + i)^k} \quad (4.6)$$

The minimum selling price of H₂ to get a given internal rate of return (IRR) is the minimum price of hydrogen that gives a NPV equal zero at the end of the plant life considering the discounting rate equal to the IRR. The IRR expected is estimated to 7% [45].

4.2.4.3 Life Cycle Assessment

The four thermochemical options were compared to the reference steam methane reforming (SMR) process for the production of hydrogen. The life cycle inventory (LCI) was taken from Susmozas et al. for SMR [23]. The LCI of the thermochemical processes were calculated from [8]. The detailed LCI are presented in supplementary material.

The carbon content of biomass before logging/hauling was considered carbon-neutral and the CO₂ from biomass as biogenic emissions. The different inputs and outputs were evaluated from Ecoinvent database (woodchips, transport, electricity, natural gas...). The calculations were conducted with Simapro 9.

For all these options, the cradle-to-gate system boundaries were set to cover the biomass production or extraction of natural gas to the final product hydrogen (Figure 4-2). The functional unit consists in 1 kg of hydrogen with 99.9 vol% purity at 70 bars. Hydrogen is the only product of SMR, this process requires extra methane for heat requirements. In Susmozas et al. the hydrogen was produced at 28 bars [23], the additional electrical consumption to increase the pressure to 70 bars was evaluated with AspenPlus® and included in its LCI. For the thermochemical processes, heat and biochar are two other products sold. The relative impacts were allocated on an energy basis.

The method chosen for the evaluation of the impacts was the midpoint method CML-IA baseline V3.05 [46]. This method evaluates abiotic depletion (ADP), abiotic depletion (fossil fuels) (ADPf), global warming potential for 100 years (GWP100), ozone layer depletion (ODP), human toxicity (HTTP), fresh water and marine aquatic ecotoxicity (FAETP, MAETP), terrestrial ecotoxicity (TETP), photochemical oxidation (POFP), acidification (AP) and eutrophication (EP).

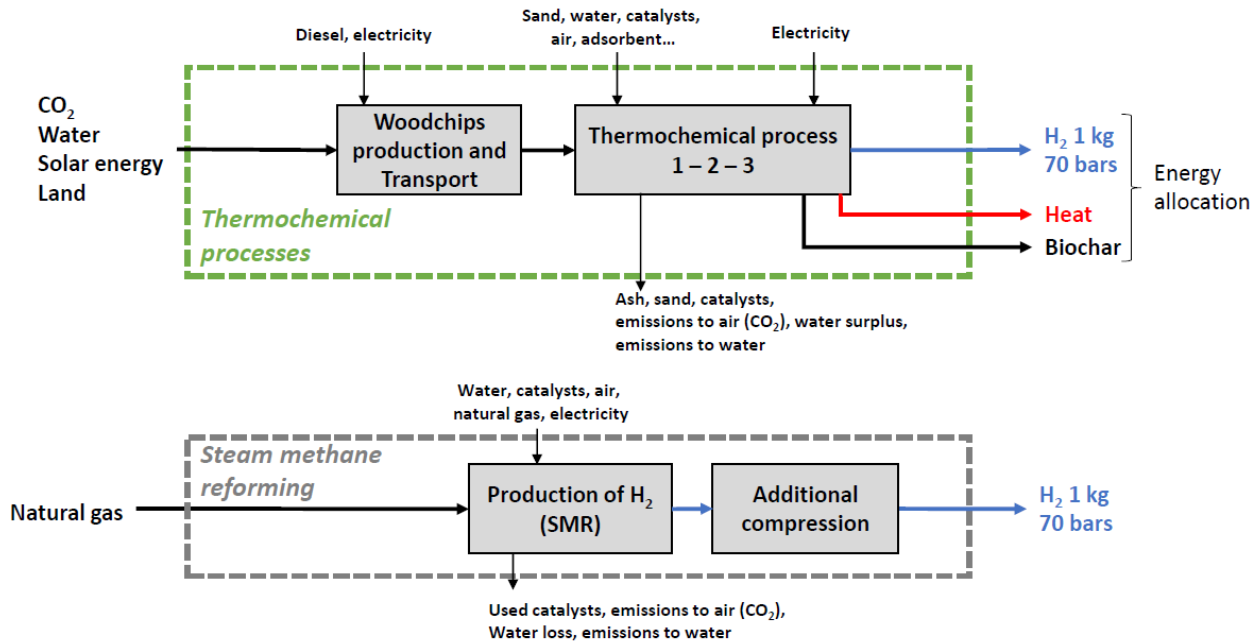


Figure 4-2: Life cycle assessment system.

4.2.5 Results and discussion

4.2.5.1 Techno-Economic Assessment

Figure 4-3 presents the fixed capital investment for each case and each sub process. The detailed equipment cost of each case is presented in supplementary material.

The case 1-100 presents an economy of scale in comparison with 1-20. The capital required for 100 MW scale is less than 5 times those of 20 MW scale, the size ratio between the two options.

Cases 2 and 3 have lower capital requirements due to the absence of catalytic reactors in the syngas cleaning and upgrading sub-process. In the hydrogen separation sub-process, the first stage separation unit (membrane) is used at lower pressure (5 bars) than PSA (27 bars). The PSA unit is also smaller. The cost of compressors and the PSA unit is then reduced in comparison with case 1. At the heat generation stage, the amount of tail gas dedicated to the boiler is bigger, increasing the cost of the gas boiler.

The case 3-20 is the cheapest of all options due to a lower gas production of the process that reduce the cost of gas cleaning and syngas compression.

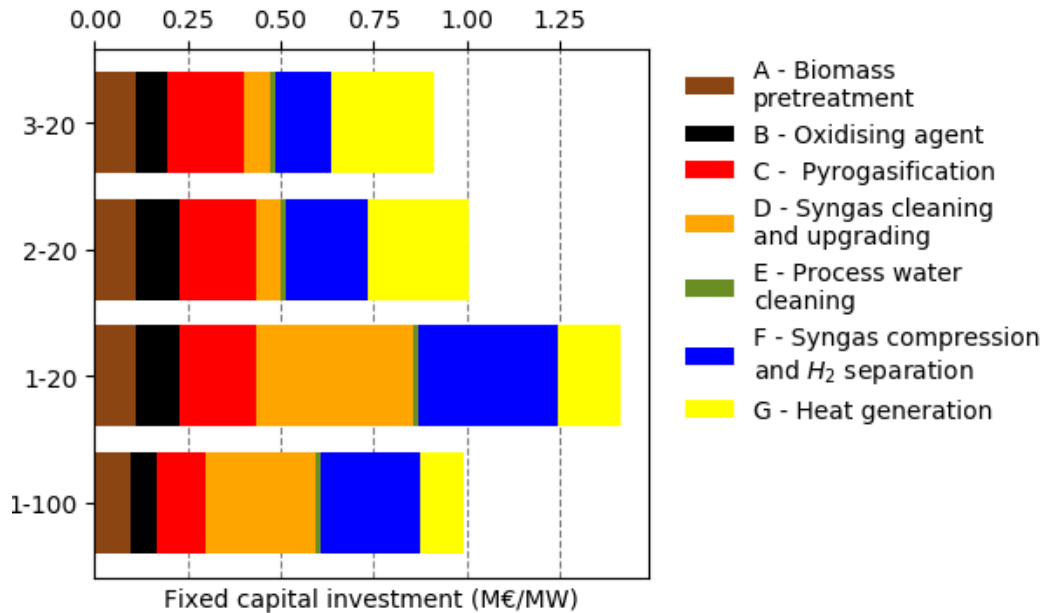


Figure 4-3: Fixed capital investment of the different scenarios.

Figure 4-4 presents the operational expenditure of each cases. The main operational cost of these processes are driven by the cost of biomass feedstock. The biomass specific cost was supposed higher at larger scale (1-100) due to a bigger transport distance. The second main cost was due to the consumption of electricity mainly for syngas compression in the hydrogen separation subprocess. The relative contribution of labor was estimated higher at the small scale (20 MW) compared to bigger scale (100 MW). Finally, the OPEX of case 1-100 (34 M€/year) is 5.1 times higher than the case 1-20 (6.7 M€/year), whereas cases 2-20 and 3-20 yield lower operating costs (6.0 M€/year and 5.7 M€/year respectively).

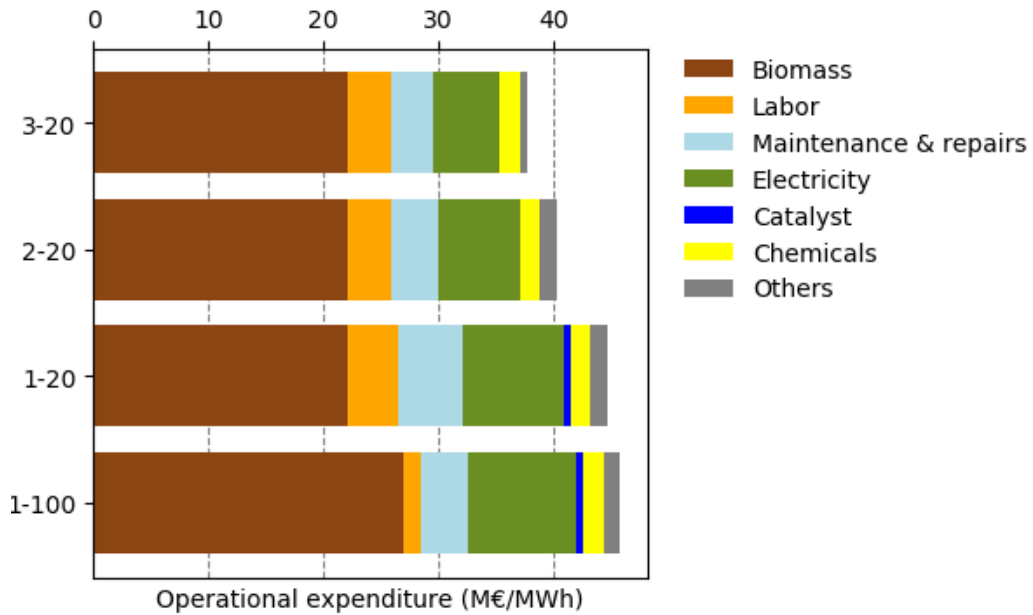


Figure 4-4: Operational expenditure of the different scenarios.

Figure 4-5 presents the minimum selling price of hydrogen to reach an internal rate of return of 7% considering a market price for heat (40 €/MWh) and biochar (0.50 €/kg). The results show small difference between case 1 at two scales (3.28 and 3.61 €/kg_{H2} for 100 MW and 20 MW respectively). The economy done at bigger scale is counterbalanced by the higher biomass cost. Cases 2 and 3 presents higher hydrogen costs: 4.98 and 5.56 €/kg_{H2} for cases 2 and 3 respectively. With this method, all the extra-cost required to reach market prices is attributed to hydrogen, even this is not the only product. The yield of hydrogen is also smaller in cases 2 and 3. The reduction of the costs for these scenarios and the increase of the revenues related to heat and bio-char do not compensate the large reduction of H₂ yield. This might be different if the price of heat and bio-char are supposed higher (see sensitivity analysis).

The minimum selling price of hydrogen at large scale (case 1-100) is close to the value mentioned by Park et al. (2.67-3.60 €₂₀₂₀/kg_{H2}) [12]. Salkuyeh et al. mentioned 2.86-3.22 €₂₀₂₀/kg_{H2} on a scale more than ten times bigger without and with CO₂ capture [15]. On a smaller scale (10 MW), Sentis et al. evaluated the hydrogen cost equal to 3.19 €₂₀₂₀/kg_{H2} [14].

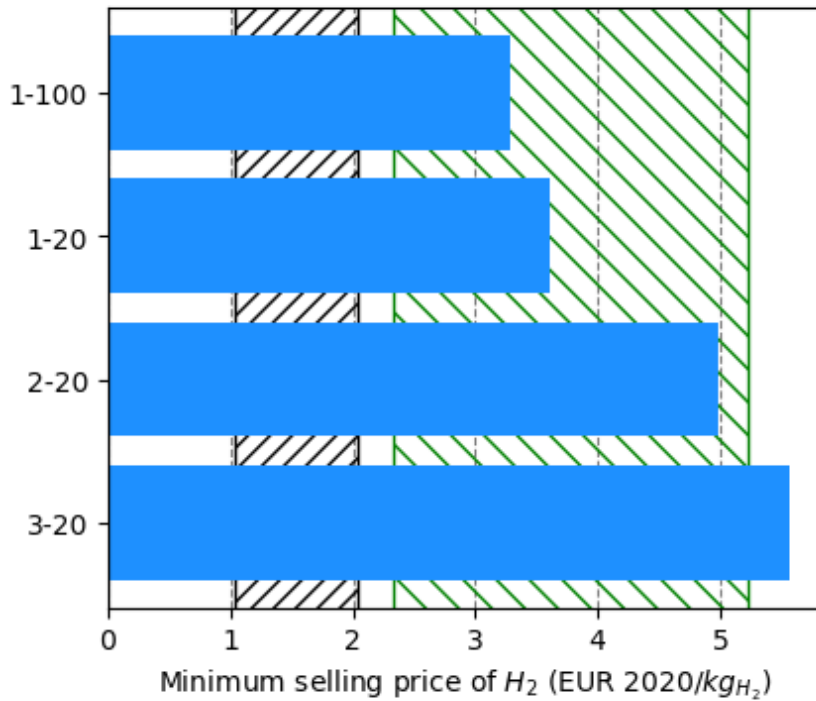


Figure 4-5: Minimum selling price of hydrogen for each case, black zone: range of hydrogen production cost in large-scale SMR, green zone: range of green hydrogen production cost from electrolysis [47].

4.2.5.2 Life Cycle Assessment

4.2.5.2.1 LCA results on impact factor of the different options

Figure 4-6 presents the impacts of the four thermochemical (TC) processes (1-100, 1-20, 2-20 and 3-20) and the reference system: steam methane reforming (SMR) process. An additional case is considered 3-20S to investigate the sequestration of the biochar formed in case 3-20 in a former mine [48]. In this case, the biochar can be considered as a stable carbon sink. Figure 4-7 presents the relative contribution of inputs and waste to the impacts. Electricity, woodchips and waste are the main impacting factors.

The slight differences in the numerical values for each impact category between case 1-100 and case 1-20 are only resulting from the transport distance (150 km and 50 km).

The GWP of 1 kg of H₂ in the thermo-chemical processes are more than ten times smaller than in the reference system. If biochar can be sequestered in a long-term, the GWP become negative. Table 4-6 presents the GWP value in each case with energy allocation and 100% allocation to H₂.AP is higher for the TC processes, contrary to SMR process the Sulphur capture is not considered in the TC cases. These impacts factor are in good agreement with Valente et al. [19].

ADPf is much smaller in TC processes because fossil fuels are mainly required for biomass preparation, starting-up and transport. Yet, ADP is higher due to a higher mineral demand (electricity demand, woodchips and water treatment). ODP is smaller and mainly driven by electricity demand.

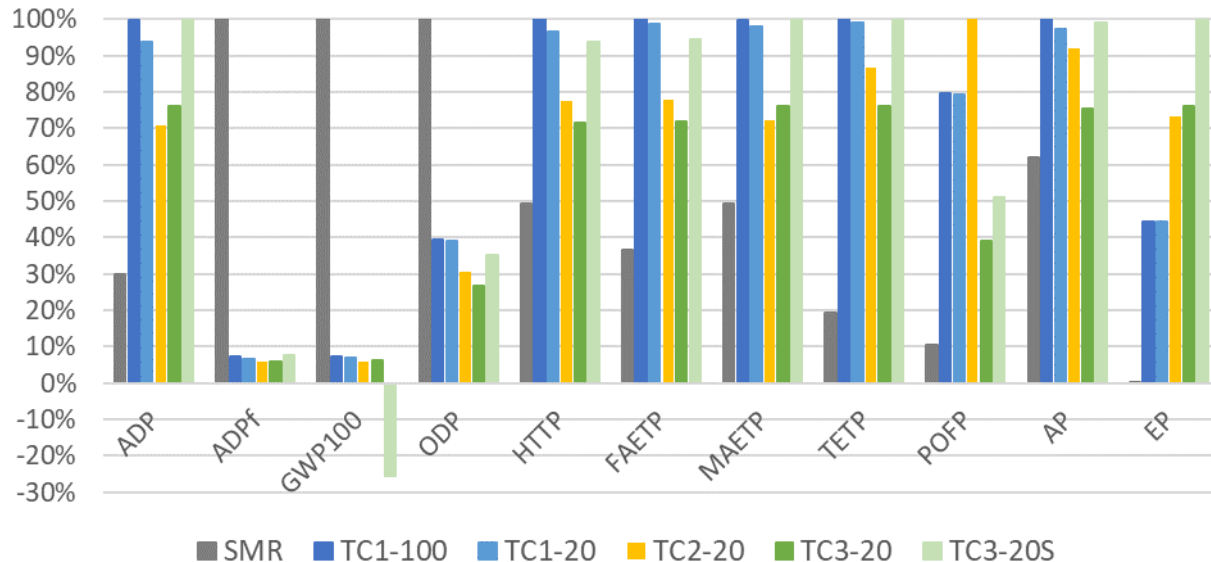


Figure 4-6: Relative impact comparison between the different scenarios and steam methane reforming (SMR) with CML-IA baseline V3.05 method. In TC3-20, biochar is sold as a product, in TC3-20S biochar is sequestered.

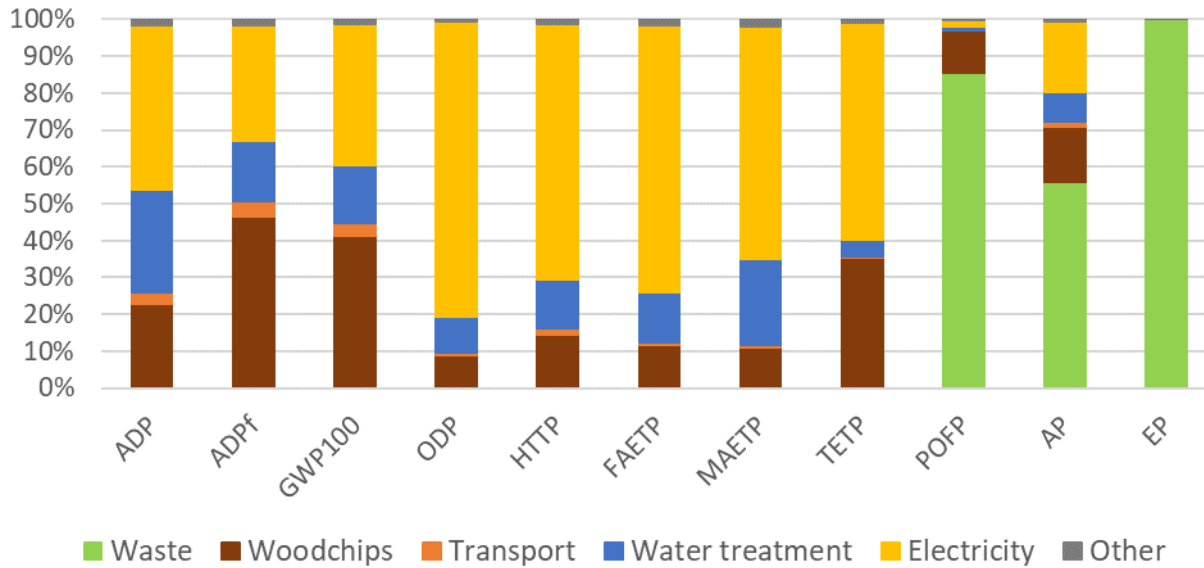


Figure 4-7: Case 1-20MW relative contributions of inputs & wastes for each impact.

Table 4-6: Global warming potential attribution to each product.

Product		1-100	1-20	2-20	3-20	3-20S	SMR
H ₂	kg CO ₂ eq/FU	0.77	0.73	0.62	0.63	-2.63	10.3
Heat	kg CO ₂ eq/FU	0.39	0.37	1.60	2.53	-10.6	
Bio-char	kg CO ₂ eq/FU				0.99		
Total	kg CO ₂ eq/FU	1.16	1.09	2.22	4.15	-13.2	10.3

4.2.5.3 Cost of action

The production of hydrogen in 20 MW-scale units is dedicated to feed with pipelines small consumer industry, thus avoiding the cost of transport. Considering an estimated production price of hydrogen in small-scale SMR (around 3 €/kg_{H2}), this price is too low to find economic profitability for small-scale TC processes. All the more so with a hydrogen production cost at 2 €/kg_{H2}. Yet, these scenarios have a beneficial impact by providing renewable hydrogen and heat. An over-cost can be calculated to reach profitability that considers the avoided CO₂ emissions in comparison with standard means of production. This “cost of action” can be calculated as the ratio of extra-cost (subsidies) divided by the emissions avoided by a classical production process. The avoided emissions are related to the hydrogen production and the heat production. The GWP for

heat dedicated to heat network was estimates to 116 kgCO₂/MWh as the average value for 2018 [49].

To estimate the potential of a process, this cost must be under 250 €/t CO₂ avoided in 2030 and 500 €/t CO₂ avoided in 2050 in France according to a report prepared for the government [50].

The results are presented in Figure 4-8. Two sets of market prices were considered: 40€/MWh of heat and 3 €/kg of hydrogen (higher market price) or 30 €/MWh of heat and 2 €/kg of hydrogen (closer to actual market price and large scale production). All scenarios gave result below 250 €/t CO₂ avoided. Although cases 2 and 3 were not as efficient as case 1. Case 2 and 3 produce more heat, less hydrogen. It requires fewer investments because the technologies are simpler. It should be stressed out that the cost of action is quite the same between scenario 3-20 and 3-20S: it means that the carbon sequestration instead of carbon selling is possible from an economic standpoint.

The energy market price increase would definitively improve the profitability. This increase could be driven by an increase of the carbon emissions taxation. On the other hand, the cost of action, i.e. the need for subsidies, would decrease.

a) Market prices: heat 40 €/MWh, H₂ 3 €/kg b) Market prices: heat 30 €/MWh, H₂ 2 €/kg

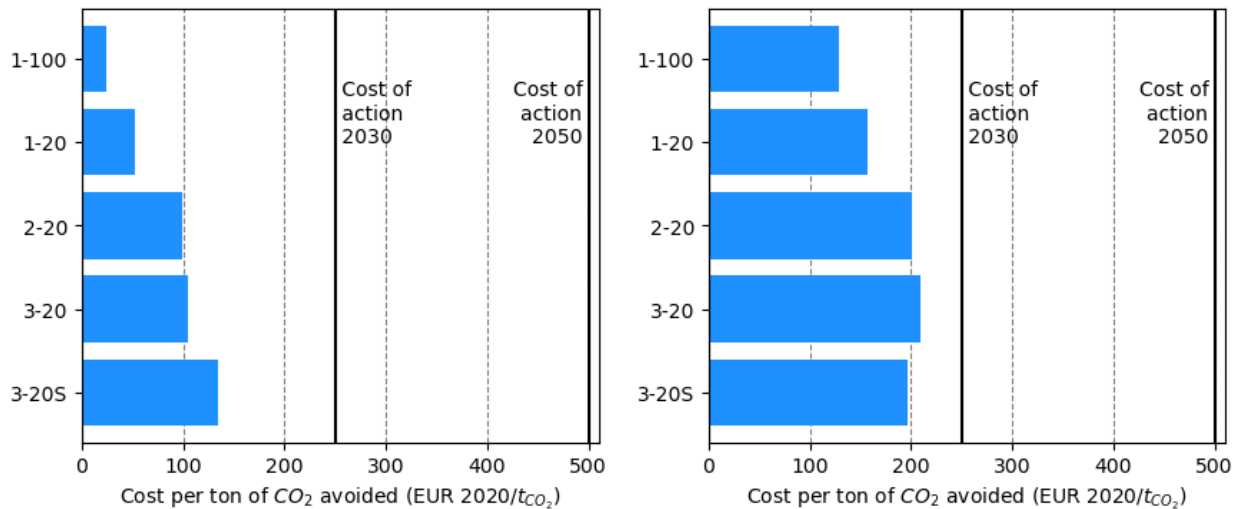


Figure 4-8: Cost of action, amount of subsidies per ton of CO₂ avoided. In case 3-20, biochar is sold at the market price (50 €/kg) and not sequestered. In case 3-20S, biochar is sequestered and not sold.

4.2.5.4 Sensitivity Analysis

To determine the main uncertainties of the techno-economic analysis, a sensitivity analysis is presented in Figure 4-9 and Figure 4-10 for cases 1-20 and 3-20 respectively. Multiple parameters were varied by $\pm 50\%$: the fixed capital investment (FCI), the selling market price of hydrogen, heat and biochar, the costs of electricity, biomass, catalysts and adsorbent and the number of operators.

By evaluating various cost estimation methods, van Amsterdam found that the results can differ hugely from one method to another [51]. Thus the 30% accuracy expected in such method could increase a lot. This inaccuracy can somehow be decreased with the amount of equipment in a so-called damping effect.

In the case 1-20, the main parameters affecting the cost is the hydrogen selling price (the main product of the plant) and the biomass cost. The FCI, electricity cost and heat selling have a lower impact. If the hydrogen could be sold at 4€/kg (higher than the minimum selling price of hydrogen) the facility does not require public subsidies.

In the case 3-20, the hydrogen selling price has less impact because this case produces less hydrogen. The main parameters are the biomass cost and the heat selling price. The biochar selling price is the third main parameter. FCI, H₂ selling price and electricity have a similar and lower impact.

It is important to put the biomass cost into perspective. The variation considered ($\pm 50\%$) is certainly overestimated. In contrary with natural gas the cost of wood energy products is almost constant [35].

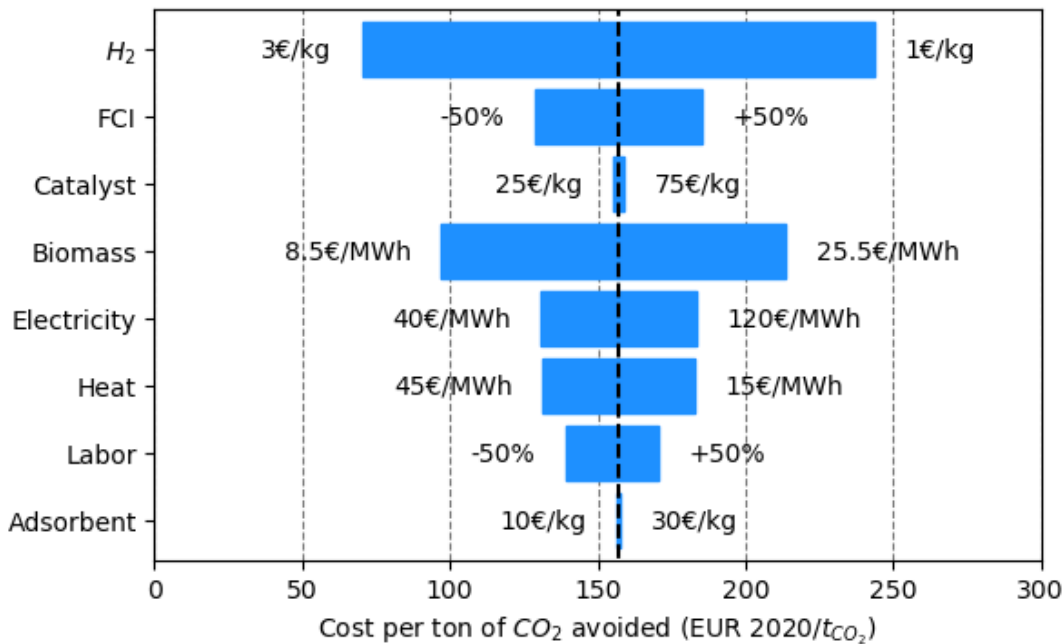


Figure 4-9: Sensitivity analysis on case 1-20 ($\pm 50\%$, market price heat 30€/MWh, H_2 2€/kg).

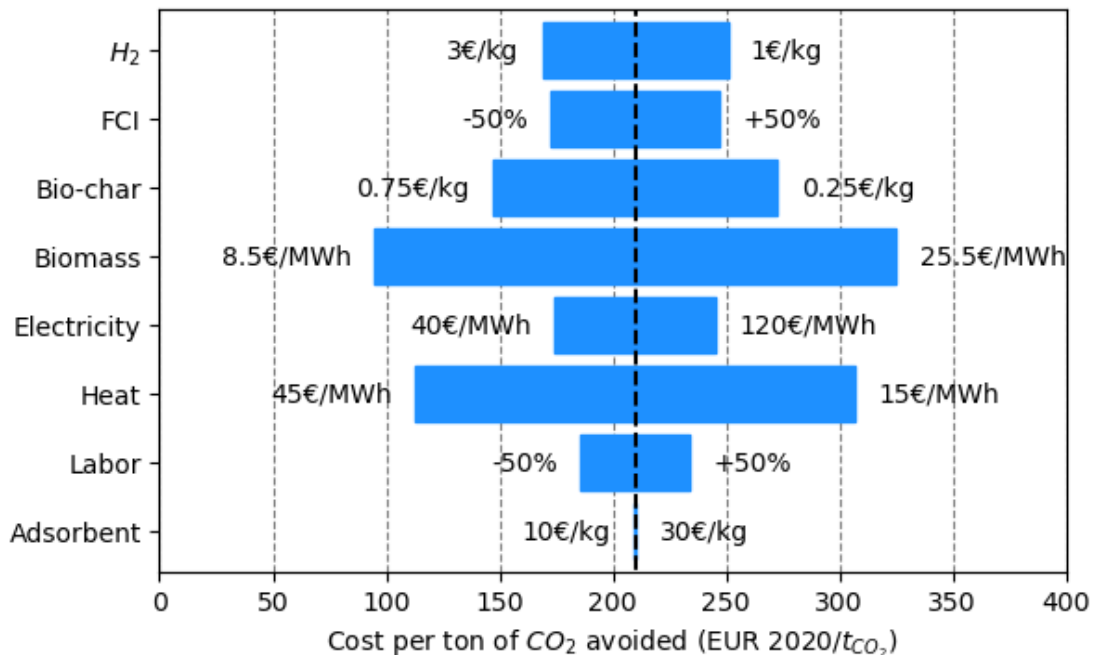


Figure 4-10: Sensitivity analysis on case 3-20 ($\pm 50\%$, market price heat 30€/MWh, H_2 2€/kg).

4.2.6 Conclusion

This article presented a detailed techno-economic analysis of three processes of hydrogen production from biomass. A life cycle assessment was also conducted to evaluate the environmental impacts.

The market prices of hydrogen, heat and biochar are too low to make these processes profitable. Additional subsidies are required. We evaluate this cost between 120 and 210 € per ton of CO₂ avoided by reference to steam methane reforming and the average global warming potential of heat networks in France. This cost could decrease if the market price of natural gas increases in the long term. Other impacts resulting from LCA show less impact on ozone depletion layer, consumption of fossil fuels. The acidification, eutrophication, ecotoxicity and toxicity potential are higher because of electricity consumption or wastes generated by TC processes. More detailed data on emissions are required to confirm this trend. A carbon-negative process is also proposed and evaluated on a techno-economic basis. These processes are in the targets of the “cost of action” to mitigate global warming.

A higher hydrogen selling price could decrease the level of required subsidies. At 4 €/kg, the scenario 1-20 becomes profitable by itself with no subsidy. This hydrogen could be used for small consumer industries or captive H₂-vehicle fleet.

4.2.7 Fundings

This work was funded by the French PIA project “Lorraine Université d’Excellence” (reference ANR-15-IDEX-04-LUE) and by the Hy-C-GREEN project (Europe-FEDER and Grand-Est province).

4.2.8 References

- [1] IPCC. Summary for Policymakers. In: Climate Change 2021: The Physical Science Basis. Contribution of Working Group I to the Sixth Assessment Report of the Intergovernmental Panel on Climate Change. Cambridge University Press; 2021.
- [2] The Future of Hydrogen. IEA; 2019.
- [3] RTE. Bilan électrique 2020. RTE; 2021.
- [4] Howarth RW, Jacobson MZ. How green is blue hydrogen? Energy Science & Engineering 2021;9:1676–87. <https://doi.org/10.1002/ese3.956>.
- [5] David M, Ocampo-Martínez C, Sánchez-Peña R. Advances in alkaline water electrolyzers: A review. Journal of Energy Storage 2019;23:392–403. <https://doi.org/10.1016/j.est.2019.03.001>.
- [6] Bodineau L, Sacher P. Rendement de la chaîne hydrogène. ADEME; 2020.
- [7] Spath P, Aden A, Eggeman T, Ringer M, Wallace B, Jechura J. Biomass to Hydrogen Production Detailed Design and Economics Utilizing the Battelle Columbus Laboratory Indirectly-Heated Gasifier. 2005. <https://doi.org/10.2172/15016221>.
- [8] Demol R, Dufour A, Rogaume Y, Mauviel G. Production of purified H₂, heat and bio-char from wood: comparison between gasification and auto-thermal pyrolysis based on advanced process modeling. Submitted 2021.
- [9] Shahabuddin M, Krishna BB, Bhaskar T, Perkins G. Advances in the thermo-chemical production of hydrogen from biomass and residual wastes: Summary of recent techno-economic analyses. Bioresource Technology 2020;299:122557. <https://doi.org/10.1016/j.biortech.2019.122557>.
- [10] Iwasaki W. A consideration of the economic efficiency of hydrogen production from biomass. International Journal of Hydrogen Energy 2003;6.
- [11] Lv P, Wu C, Ma L, Yuan Z. A study on the economic efficiency of hydrogen production from biomass residues in China. Renewable Energy 2008;33:1874–9. <https://doi.org/10.1016/j.renene.2007.11.002>.
- [12] Parks GD, Curry-Nkansah M, Hughes E, Sterzinger G. Hydrogen Production Cost Estimate Using Biomass Gasification: Independent Review 2011:52.
- [13] Sara HR, Enrico B, Mauro V, Andrea DC, Vincenzo N. Techno-economic Analysis of Hydrogen Production Using Biomass Gasification -A Small Scale Power Plant Study. Energy Procedia 2016;101:806–13. <https://doi.org/10.1016/j.egypro.2016.11.102>.
- [14] Sentis L, Rep M, Barisano D, Bocci E, Sara Rajabi H, Pallozzi V, et al. Techno-economic analysis of UNIFHY hydrogen production system (No. SP1-JTI-FCH.2011.2.3). 2016.
- [15] Salkuyeh YK, Saville BA, MacLean HL. Techno-economic analysis and life cycle assessment of hydrogen production from different biomass gasification processes. International Journal of Hydrogen Energy 2018;43:9514–28. <https://doi.org/10.1016/j.ijhydene.2018.04.024>.

- [16] Valente A, Iribarren D, Dufour J. Life cycle assessment of hydrogen energy systems: a review of methodological choices. *The International Journal of Life Cycle Assessment* 2017;22:346–63. <https://doi.org/10.1007/s11367-016-1156-z>.
- [17] Valente A, Iribarren D, Dufour J. Harmonised life-cycle global warming impact of renewable hydrogen. *Journal of Cleaner Production* 2017;149:762–72. <https://doi.org/10.1016/j.jclepro.2017.02.163>.
- [18] Valente A, Iribarren D, Dufour J. Harmonising the cumulative energy demand of renewable hydrogen for robust comparative life-cycle studies. *Journal of Cleaner Production* 2018;175:384–93. <https://doi.org/10.1016/j.jclepro.2017.12.069>.
- [19] Valente A, Iribarren D, Dufour J. Harmonising methodological choices in life cycle assessment of hydrogen: A focus on acidification and renewable hydrogen. *International Journal of Hydrogen Energy* 2019;44:19426–33. <https://doi.org/10.1016/j.ijhydene.2018.03.101>.
- [20] Koroneos C, Dompros A, Roumbas G. Hydrogen production via biomass gasification—A life cycle assessment approach. *Chemical Engineering and Processing: Process Intensification* 2008;47:1261–8. <https://doi.org/10.1016/j.cep.2007.04.003>.
- [21] Tock L, Maréchal F. Co-production of hydrogen and electricity from lignocellulosic biomass: Process design and thermo-economic optimization. *Energy* 2012;45:339–49. <https://doi.org/10.1016/j.energy.2012.01.056>.
- [22] Moreno J, Dufour J. Life cycle assessment of hydrogen production from biomass gasification. Evaluation of different Spanish feedstocks. *International Journal of Hydrogen Energy* 2013;38:7616–22. <https://doi.org/10.1016/j.ijhydene.2012.11.076>.
- [23] Susmozas A, Iribarren D, Dufour J. Life-cycle performance of indirect biomass gasification as a green alternative to steam methane reforming for hydrogen production. *International Journal of Hydrogen Energy* 2013;38:9961–72. <https://doi.org/10.1016/j.ijhydene.2013.06.012>.
- [24] Iribarren D, Susmozas A, Petrakopoulou F, Dufour J. Environmental and exergetic evaluation of hydrogen production via lignocellulosic biomass gasification. *Journal of Cleaner Production* 2014;69:165–75. <https://doi.org/10.1016/j.jclepro.2014.01.068>.
- [25] Muresan M, Cormos CC, Agachi PS. Comparative life cycle analysis for gasification-based hydrogen production systems. *Journal of Renewable and Sustainable Energy* 2014;6:013131. <https://doi.org/10.1063/1.4864658>.
- [26] Valente A, Iribarren D, Gálvez-Martos J-L, Dufour J. Robust eco-efficiency assessment of hydrogen from biomass gasification as an alternative to conventional hydrogen: A life-cycle study with and without external costs. *Science of The Total Environment* 2019;650:1465–75. <https://doi.org/10.1016/j.scitotenv.2018.09.089>.
- [27] Pelletier C, Rogaume Y, Dieckhoff L, Bardeau G, Pons M-N, Dufour A. Effect of combustion technology and biogenic CO₂ impact factor on global warming potential of wood-to-heat chains. *Applied Energy* 2019;235:1381–8. <https://doi.org/10.1016/j.apenergy.2018.11.060>.
- [28] Pelletier C. Analyse environnementale et économique des filières bois-énergie n.d.:203.

- [29] Peters MS, Timmerhaus KD, West RE. Plant design and economics for chemical engineers. fifth edition. McGraw-Hill New York; 2004.
- [30] Turton R, Bailie RC, Whiting WB, Shaeiwitz JA. Analysis, Synthesis and Design of Chemical Processes. Pearson Education; 2008.
- [31] 2019 Chemical Engineering Plant Cost Index Annual Average. Chemical Engineering n.d. <https://www.chemengonline.com/2019-chemical-engineering-plant-cost-index-annual-average/?printmode=1> (accessed April 8, 2020).
- [32] ECB euro reference exchange rate: US dollar (USD). European Central Bank n.d. https://www.ecb.europa.eu/stats/policy_and_exchange_rates/euro_reference_exchange_rates/html/eurofxref-graph-usd.en.html (accessed April 8, 2020).
- [33] Regionjob.com. 2021. <http://regionsjob.com> (accessed September 27, 2021).
- [34] Pôle emploi. Estimation du coût d'un salarié 2021. <http://entreprise.pole-emploi.fr/cout-salarie/> (accessed September 27, 2021).
- [35] CIBE. Prix du bois-énergie. CIBE 2021. <https://cibe.fr/prix-du-bois-energie/> (accessed September 27, 2021).
- [36] Yordanova S, Migette J-C. Enquête sur les prix des combustibles bois pour le chauffage industriel et collectif en 2017-2018. 2017.
- [37] ADEME. Hydrogène : analyse des potentiels industriels et économiques en France. 2019.
- [38] Philibert C. Perspectives on a Hydrogen Strategy for the European Union n.d.:43.
- [39] Bessarabov D, Wang H, Li H, Zhao N. PEM Electrolysis for Hydrogen Production: Principles and Applications. CRC Press; 2016.
- [40] Surla K. Hydrogène 2019.
- [41] Bilan énergétique de la France pour 2019. Le service des données et études statistiques (SDES); 2021.
- [42] Baddour FG, Snowden-Swan L, Super JD, Van Allsburg KM. Estimating Precommercial Heterogeneous Catalyst Price: A Simple Step-Based Method. Org Process Res Dev 2018;22:1599–605. <https://doi.org/10.1021/acs.oprd.8b00245>.
- [43] Ramírez-Santos ÁA, Bozorg M, Addis B, Piccialli V, Castel C, Favre E. Optimization of multistage membrane gas separation processes. Example of application to CO₂ capture from blast furnace gas. Journal of Membrane Science 2018;566:346–66. <https://doi.org/10.1016/j.memsci.2018.08.024>.
- [44] Swanson RM, Platon A, Satrio JA, Brown RC. Techno-economic analysis of biomass-to-liquids production based on gasification. Fuel 2010;89:S11–9. <https://doi.org/10.1016/j.fuel.2010.07.027>.
- [45] Coûts et rentabilité des énergies renouvelables en France métropolitaine : Éolien terrestre, biomasse, solaire photovoltaïque. 2014.
- [46] Tools and Data CML. Leiden University n.d. <https://www.universiteitleiden.nl/en/science/environmental-sciences/tools-and-data> (accessed October 19, 2021).

- [47] IRENA. Green hydrogen cost reduction: Scaling up electrolyzers to meet the 1.5C climate goal 2020:106.
- [48] Dufour A. Geological Sequestration of Biomass Char to Mitigate Climate Change. *Environmental Science & Technology* 2013;130829114030003. <https://doi.org/10.1021/es4036418>.
- [49] Petit S, Moure G. Les réseaux de chaleur et de froid. Chiffres clés, analyses et évolution. Résultat de l'enquête annuelle - édition 2019. 2019.
- [50] Quinet A. La valeur de l'action pour le climat. Une valeur tutélaire du carbone pour évaluer les investissements et les politiques publiques. France Stratégie; 2019.
- [51] van Amsterdam MF. Factorial Techniques applied in Chemical Plant Cost Estimation: A Comparative Study based on Literature and Cases. Delft University of Technology, 2018.
- [52] Aden A, Ruth M, Ibsen K, Jechura J, Neeves K, Sheehan J, et al. Lignocellulosic Biomass to Ethanol Process Design and Economics Utilizing Co-Current Dilute Acid Prehydrolysis and Enzymatic Hydrolysis for Corn Stover. 2002. <https://doi.org/10.2172/15001119>.
- [53] Sethi V. Sorbent-based Oxygen Production for Energy Systems. 2017.
- [54] Loh HP, Loyns J, White CW. Process Equipment Cost Estimation, Final Report 2002:78.
- [55] Tijmensen MJA, Faaij APC, Hamelinck CN. Exploration of the possibilities for production of Fischer Tropsch liquids and power via biomass gasification. *Biomass and Bioenergy* 2002;24.
- [56] Biegler LT, Grossmann IE, Westerberg AW. Systematic methods for chemical process design 1997.
- [57] Liu G, Larson ED, Williams RH, Kreutz TG, Guo X. Making Fischer–Tropsch Fuels and Electricity from Coal and Biomass: Performance and Cost Analysis. *Energy Fuels* 2011;25:415–37. <https://doi.org/10.1021/ef101184e>.
- [58] Kreutz T, Williams R, Consonni S, Chiesa P. Co-production of hydrogen, electricity and CO from coal with commercially ready technology. Part B: Economic analysis. *International Journal of Hydrogen Energy* 2005;30:769–84. <https://doi.org/10.1016/j.ijhydene.2004.08.001>.
- [59] Hamelinck C, Faaij A, Denul H, Boerrigter H. Production of FT transportation fuels from biomass; technical options, process analysis and optimisation, and development potential. *Energy* 2004;29:1743–71. <https://doi.org/10.1016/j.energy.2004.01.002>.
- [60] Meerman JC, Ramírez A, Turkenburg WC, Faaij APC. Performance of simulated flexible integrated gasification polygeneration facilities, Part B: Economic evaluation. *Renewable and Sustainable Energy Reviews* 2012;16:6083–102. <https://doi.org/10.1016/j.rser.2012.06.030>.
- [61] Mussatti DC, Srivastava R, Hemmer PM, Strait R. EPA Air Pollution Control Cost Manual, sixth edition. Research Triangle Park, North Carolina: US Environmental Protection Agency; 2002.

4.2.9 Supplementary material

4.2.9.1 Transport cost

According to Yordanova and Migette [36], the delivery cost (DC) of biomass in a 27 t-moving floor truck can be estimated by:

$$DC[\text{€}/t] = \left(\frac{\frac{174.8}{nr} + 0.66 \cdot km + 22.3 \cdot dl}{27} \right) \cdot fc$$

Assuming 1h for loading, 0.33 h for unloading and 10 h of work per day. nr is the number of rotation per day, km the round trip distance in km, dl the delivery time assuming a 53 km/h mean velocity. fc is the woodchip specific factor evaluated to 1.15.

The actual wet biomass transported depend on the humidity rate and could be estimated with the following relation between the total weight of wet biomass delivered and the humidity rate in a 27 t-moving floor truck.

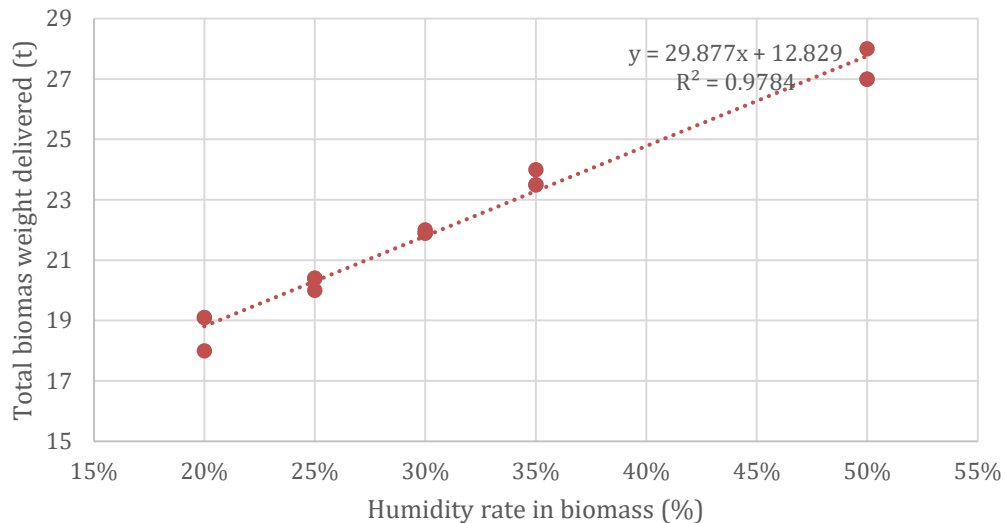


Figure S4-1: Relation between biomass humidity and weight delivered in 27 t-moving floor truck [36].

4.2.9.2 Equipment cost

Table S4-1 presents the source cost of the main equipment used in this techno-economic assessment. Due to the variety of estimates and sources (purchased cost of equipment or final cost delivered installed), this table gives a fixed capital investment factor FCIF to evaluate the final cost that takes into account all direct and indirect costs.

Table S4-1: Equipment cost data.

Device	Year cost	Base cost		Base capacity			n	FCIF factor	Ref.	Note
AREA A										
Truck scale	2000	0.034	MDOL	1	scale	0.6	3.16	[52]		
Forklift	2000	0.018	MDOL	1	forklift	1	1.69	[52]		
Belt conveyor	2002	Abacus: 0.40 m width					4.0 ^a	[29]		
Storage on concrete slab	2000	0.451	MDOL	7056	t	1	2.89	[52]		
Screw conveyor	2002	Abacus: 0.23 m width					4.0 ^a	[29]		
Rotary dryer	2002	Abacus: rotary dryer, flue gas, direct					4.0 ^a	[29]		
AREA B										
VSA oxygen	2014	2.48	MDOL	2500	Nm ³ /h (O ₂)	0.7	1.56	[53]	³	
Pump	1998	Abacus					5.0 ^b	[54]		
AREA C										
Biomass receiving hopper	2007	0.072	MDOL	288	t/day	0.6	4.3 ^c	[44]	⁴	
Gasifier directly heated	2000	3.24	MDOL	69.54	MWth LHV	0.7	2.11 ^d	[55]	⁵	

³ VPSA system (550°C, adsorbent perovskite), exponent: hypothesis based on PSA H₂ estimations, includes air blower, adsorber/desorber vessel, sorbent and vacuum pump. Fixed capital investment 3.872 M\$, total equipment cost 2.48 M\$. Assume \$₂₀₁₄.

⁴Cost 0.5019 M\$2007 for 7 equipment. Installation factor 2.486 (Swanson et al.) plus 1.26 for indirect cost (Peters et al. 2004). Installation factor adjusted to 3.02 (only one equipment), n=0.6 assumed.

⁵Maximum size 105 MW, TPS technology (Termiska Processer with dolomite tar cracker, direct airblown gasifier), based on first generation BIG/CC installations, taken from Faaij (1998).

Ash storage vessel	2007	0.1428	MDOL	119	t/day	0.6	4.3 ^c	[44]	⁶
AREA D									
Cyclone	2002	Abacus: steel multicyclone				5.0 ^b	[29]		
Partial oxidation unit	1968					6.38	[56]	⁷	
Steam generator	2002	Abacus: U-tube stainless steel				5.0 ^b	[29]		
Syngas cooler	2002	Abacus: U-tube stainless steel				5.0 ^b	[29]		
Authothermal steam reformer	2007	93.66	MDOL	31000	kmol/h (syngas)	0.9	1.79 ^e	[57]	⁸
HT & LT shift reactor	2002	39.8	MDOL	1377	MWth daf basis	0.67	1.0	[58]	⁹
Venturi scrubber	2002	Abacus: Ventury scrubber (low energy)				5.0 ^b	[29]		
Wet dynamic scrubber	2002	Abacus: wet dynamic scrubber				5.0 ^b	[29]		
AREA E									
Dissolved air flotation unit	2019	0.062	MDOL	100	m ³ /h	0.6	5.0 ^b		¹⁰
Activated carbon filter	2002	Abacus: vertical column, carbon steel				5.0 ^b	[29]		
AREA F									
Knock-out	2002	0.130	MDOL	160764	kg/h (outlet)	0.6	2.47	[7]	¹¹
Compressor	2000	12	MDOL	13.2	MWe	0.85	2.11 ^d	[55]	
	1993	0.0007	MDOL	1	kWmech	1	2.1	[59]	
	2007	6	MDOL	10	MWe	0.67	1.52	[58]	
	2007	6.31	MDOL	10	MWe	0.67	1.32	[57]	

⁶Cost 0.1428 M\$2007. Installation factor 3.06 (Swanson et al.) plus 1.26 for indirect cost (Peters et al. 2004)

⁷Guthrie method for furnace, MPF = 1.35 (Reformer, carbon steel up to 500 psig), MF=2.72. Multiplied by 2.077 for indirect costs

$$BC[\$1968] = 100000 \left(\frac{S}{S_0} \right)^{0.83}$$

$$IC[\$1968] = BC * (MPF + MF - 1)$$

⁸Authothermal reformer, reference of ATR SFA Pacific, max unit capacity 31000 kmol/h

⁹39.8 M\$₂₀₀₂ for a 2-stage WGS system including heat recovery processing all syngas from a Texaco-type coal gasifier 1377 MWth input BOP, indirects and contingency included, costs from Agahi + Lozza and Chiesa for coal gasification

¹⁰Vendor quote, stainless steel, FCI factor assumed 5.0 and n=0.6

¹¹Pre-PSA knock-out #1 drum 129 979\$2002 for 354 424 lb/h outlet flow

Membrane	2017	$C_0 \left(\frac{Area}{A_0} \right)^{0.70} \left(\frac{Pressure}{P_0} \right)^{0.875} + Area \cdot C_m$ $C_0 = 0.28 \text{ M€}, A_0 = 2000 \text{ m}^2, P_0 = 55 \text{ bar},$ $C_m = 40 \text{ €/m}^2$					1.31	[43]	
Vacuum pump	2017	1.5	kDOL	1	kWe	1	1.31	[43]	
PSA H ₂	1993	23	MDOL	9600	kmol/h (feed)	0.7	1.69	[59]	¹²
	2002	7.1	MDOL	1058.4	kmol/h (purge)	0.74	1 ^f	[58]	¹³
	2002	4.86	MDOL	6468	kg/h (H ₂ prod)	0.6	2.47	[7]	¹⁴
	2008	12	MEUR	16616	kmol/h (H ₂)	0.65	2.28	[60]	¹⁵
AREA G									
Air blower							5.0 ^b		¹⁶
Gas boiler	1998	0.33102	MDOL				5.0 ^b	[54]	¹⁷
Fabric filter	2002	Abacus: 230°C continuous carbon steel					5.0 ^b	[29]	
Flue gas stack	2000	$869.5 \cdot D^{1.16} \cdot H$					2.16	[61]	

^aLang factor for solid [29].

^bLang factor for fluid [29].

^cLang factor for solid-fluid [29].

^dInstalled cost factor = 1.33, other investments costs factor evaluated to 0.66 according to Tijmensen et al. 2002 (including engineering, building interests, project contingency, fees/overheads/profits, start-up cost).

^eLiu et al. (2011) BOP (%) = $0.8867 / (\text{MW}_{\text{HHV_biomass}}^{0.2096})$

^fIncludes installation, apportioned BOP and general facilities, engineering, and process/project contingencies. Other costs such as owners fees, royalties, start-up and pre-production costs, initial inventory, working capital, spare parts, and land are not included.

¹²PSA units (excluding the recycle compressor) cost 23 M\$US₁₉₉₃ for 9600 kmol feed/h. overall installation factor 1.69 (auxiliary equipment and installation labour, engineering and contingencies).

¹³Costs from Middleton; PSA bed size and cost are assumed to scale with purge gas flow rather than with H₂ flow (e.g., as used in Hallale and Liu). PSA unit recovering 85% of hydrogen in a shifted syngas ? (Larson et al.)

¹⁴Based on Schendel et al. (1983) and Leiby (1994) on H₂ production rate \$0.168/SCFD of H₂ (standard cubic feet per day)

¹⁵From Arienti et al., 2008 Sensitivity investment cost on H₂ purity, based case 99.5% H₂ => 100%, 99.0% => 97.8% of base case cost, 99.9% => 101.7% of base case cost

¹⁶Vendor quote

¹⁷Furnace (gas or oil fired vertical cylindrical type for low heat duty range moderate temperature with long contact time. Walls of the furnace are refractory lined

4.2.9.3 Detailed results CAPEX/OPEX

The detailed equipment costs for each cases are presented in Table S4-2, Table S4-3, Table S4-4 and Table S4-5 for cases 1-100 MW, 1-20MW, 2-20MW and 3-20MW respectively.

Table S4-2: Detailed costs of case 1-100 MW.

Equip. ID	Description	Number of equip.	Equipment Cost*	Final cost**	Cost factor	Source
			*purchase equipment/direct or indirect cost depending on the source	**including all direct and indirect capital costs	= final cost/equipment cost	
AREA A - BIOMASS PRETREATMENT						
A-101	Truck scale	1	45,099 €	142,512 €	3.16	Aden et al. 2002
A-102	Forklift	10	238,758 €	403,502 €	1.69	Aden et al. 2002
A-103	Belt conveyor	1	35,296 €	141,184 €	4.00	Peters et al., 2002 (0.40 m width)
A-104	Storage on concrete slab	1	440,374 €	1,272,682 €	2.89	Aden et al. 2002
A-105	Screw conveyor	1	16,974 €	67,896 €	4.00	Peters et al., 2002 (0.23 m diam)
A-106	Rotary dryer, flue gas direct	5	1,972,283 €	7,889,131 €	4.00	Peters et al., 2002
AREA B - OXIDISING AGENT						
B-101	Air blower VSA	1	included			
B-102	VSA oxygen	1	4,479,944 €	6,996,006 €	1.56	Sethi et al. 2017
B-103	VSA vacump pump	1	included			
B-104	Water pump for steam generation	1	2,945 €	14,727 €	5.00	Loh et al., 2002
AREA C - GASIFICATION						
C-101	Biomass receiving hopper	1	125,932 €	538,991 €	4.28	Swanson et al 2010
C-102	Bed material receiving hopper	1	1,186 €	5,074 €	4.28	Swanson et al 2010
C-103	Gasifier directly heated	1	5,542,004 €	11,693,628 €	2.11	Tijmenssen et al., 2002
C-104	Ash storage vessel	1	26,767 €	115,633 €	4.32	Swanson et al 2010
C-105	Cyclone (carbon steel multicyclone)	1	73,958 €	369,789 €	5.00	Peters et al., 2002
AREA D - SYNGAS CLEANING AND UPGRADING						
D-101	Partial oxydation unit	1	519,219 €	3,311,811 €	6.38	Guthrie method 1968
D-102	Cyclone (carbon steel multicyclone)	1	116,448 €	582,242 €	5.00	Peters et al., 2002
D-103	Steam generator	1	16,696 €	83,480 €	5.00	Peters et al., 2002 (U-tube stainless steel)
D-104	Syngas cooler (heat recovery)	1	18,922 €	94,608 €	5.00	Peters et al., 2002 (U-tube stainless steel)
D-105	Authothermal steam reformer	1	9,587,921 €	15,848,220 €	1.65	Liu et al. 2011
D-106	HT shift reactor	1	9,074,727 €	9,074,727 €	1.00	Kreutz et al., 2005
D-107	Syngas cooler (heat recovery)	included				
D-108	LT shift reactor	included				
D-109	Syngas cooler (heat recovery)	1	9,534 €	47,670 €	5.00	Peters et al., 2002 (U-tube stainless steel)
D-110	Venturi scrubber (low energy)	1	70,282 €	351,411 €	5.00	Peters et al., 2002 (low energy)
D-111	Water scrubber (wet dynamic scrubber)	2	96,415 €	482,076 €	5.00	Peters et al., 2002
D-112	Water pump for scrubber	1	20,763 €	103,817 €	5.00	Loh et al., 2002
AREA E - PROCESS WATER CLEANING						
E-101	Water pump for wastewater	1	22,568 €	112,841 €	5.00	Loh et al., 2002
E-102	Dissolved air flotation (DAF)	1	85,981 €	429,904 €	5.00	Industrial quote
E-103	AC filter	5	145,077 €	725,385 €	5.00	Peters et al., 2002 (abacus) D=2m (CS, 1 atm)
AREA F - SYNGAS COMPRESSION AND HYDROGEN SEPARATION						
F-101	Knock-out water	1	70,157 €	173,288 €	2.47	Spath et al., 2005
F-102	Syngas compressor before membrane	1	- €	- €	0.00	Average value
F-103	Membrane hydrogen	1	- €	- €	0.00	Ramirez-Santos et al., 2018
F-104	Retentate vacuum pump	1	- €	- €	0.00	Ramirez-Santos et al., 2018
F-105	Syngas compressor before PSA	1	7,066,762 €	10,741,478 €	1.52	Average value
F-106	PSA hydrogen	1	6,926,699 €	12,107,870 €	1.75	Average value (Hamelinck et al. 2004, Kreutz et al. 2005, Spath et al. 2005, Meerman et al. 2012)
F-107	Hydrogen final compressor	1	2,381,352 €	3,619,655 €	1.52	Average value
AREA G - HEAT & POWER GENERATION						
G-101	Air blower	3	229,890 €	1,149,450 €	5.00	Industrial quote
G-102	Gas boiler	1	1,277,648 €	6,388,240 €	5.00	Loh et al., 2002
G-103	Heat network exchanger	3	200,852 €	1,004,260 €	5.00	Peters et al., 2002 (U-tube stainless steel)
G-104	Pump heat network	1	13,161 €	65,807 €	5.00	Loh et al., 2002
G-105	Fabric filter (230°C continuous carbon steel)	1	140,025 €	700,125 €	5.00	Peters et al., 2002 (carbon steel)
G-106	Exhaust gas booster	2	438,700 €	2,193,500 €	5.00	Industrial quote
G-107	Flue gas stack	1	46,092 €	99,558 €	2.16	EPA, 2002

TOTAL **51,577,412 €** **99,142,178 €** 1.92

Table S4-3: Detailed costs of case 1-20 MW.

Equip. ID	Description	Number of equip.	Equipment Cost*	Final cost**	Cost factor	Source
*purchase equipment/direct or indirect cost depending on the source **including all direct and indirect capital costs = final cost/equipment cost						
AREA A - BIOMASS PRETREATMENT						
A-101	Truck scale	1	45,099 €	142,512 €	3.16	Aden et al. 2002
A-102	Forklift	2	47,752 €	80,700 €	1.69	Aden et al. 2002
A-103	Belt conveyor	1	35,296 €	141,184 €	4.00	Peters et al., 2002 (0.40 m width)
A-104	Storage on concrete slab	1	88,075 €	254,536 €	2.89	Aden et al. 2002
A-105	Screw conveyor	1	16,974 €	67,896 €	4.00	Peters et al., 2002 (0.23 m diam)
A-106	Rotary dryer, flue gas direct	1	394,457 €	1,577,826 €	4.00	Peters et al., 2002
AREA B - OXIDISING AGENT						
B-101	Air blower VSA	1	included		1.56	Sethi et al. 2017
B-102	VSA oxygen	1	1,452,090 €	2,267,624 €		
B-103	VSA vacump pump	1	included			
B-104	Water pump for steam generation	1	2,438 €	12,191 €	5.00	Loh et al., 2002
AREA C - GASIFICATION						
C-101	Biomass receiving hopper	1	47,946 €	205,210 €	4.28	Swanson et al 2010
C-102	Bed material receiving hopper	1	451 €	1,932 €	4.28	Swanson et al 2010
C-103	Gasifier directly heated	1	1,796,337 €	3,790,271 €	2.11	Tijmenssen et al., 2002
C-104	Ash storage vessel	1	10,192 €	44,028 €	4.32	Swanson et al 2010
C-105	Cyclone (carbon steel multicyclone)	1	15,121 €	75,603 €	5.00	Peters et al., 2002
AREA D - SYNGAS CLEANING AND UPGRADING						
D-101	Partial oxydation unit	1	136,523 €	870,804 €	6.38	Guthrie method 1968
D-102	Cyclone (carbon steel multicyclone)	1	21,443 €	107,216 €	5.00	Peters et al., 2002
D-103	Steam generator	1	5,539 €	27,695 €	5.00	Peters et al., 2002 (U-tube stainless steel)
D-104	Syngas cooler (heat recovery)	1	6,243 €	31,214 €	5.00	Peters et al., 2002 (U-tube stainless steel)
D-105	Authothermal steam reformer	1	2,253,041 €	4,025,090 €	1.79	Liu et al. 2011
D-106	HT shift reactor	1	3,086,908 €	3,086,908 €	1.00	Kreutz et al., 2005
D-107	Syngas cooler (heat recovery)	1	included			
D-108	LT shift reactor	1	included			
D-109	Syngas cooler (heat recovery)	1	3,166 €	15,830 €	5.00	Peters et al., 2002 (U-tube stainless steel)
D-110	Venturi scrubber (low energy)	1	27,643 €	138,214 €	5.00	Peters et al., 2002 (low energy)
D-111	Water scrubber (wet dynamic scrubber)	1	26,595 €	132,977 €	5.00	Peters et al., 2002
D-112	Water pump for scrubber	1	4,287 €	21,434 €	5.00	Loh et al., 2002
AREA E - PROCESS WATER CLEANING						
E-101	Water pump for wastewater	1	4,433 €	22,165 €	5.00	Loh et al., 2002
E-102	Dissolved air flotation (DAF)	1	32,725 €	163,626 €	5.00	Industrial quote
E-103	AC filter	1	28,995 €	144,973 €	5.00	Peters et al., 2002 (abacus) D=2m (CS, 1 atm)
AREA F - SYNGAS COMPRESSION AND HYDROGEN SEPARATION						
F-101	Knock-out water	1	26,717 €	65,991 €	2.47	Spath et al., 2005
F-102	Syngas compressor before membrane	1	- €	- €	0.00	Average value
F-103	Membrane hydrogen	1	- €	- €	0.00	Ramirez-Santos et al., 2018
F-104	Retentate vacuum pump	1	- €	- €	0.00	Ramirez-Santos et al., 2018
F-105	Syngas compressor before PSA	1	1,858,792 €	2,825,364 €	1.52	Average value
F-106	PSA hydrogen	1	2,324,819 €	4,063,783 €		Average value (Hamelinck et al. 2004, Kreutz et al. 2005, Spath et al. 2005, Meerman et al. 2012)
F-107	Hydrogen final compressor	1	341,567 €	519,182 €	1.52	Average value
AREA G - HEAT & POWER GENERATION						
G-101	Air blower	1	28,750 €	143,750 €	5.00	Industrial quote
G-102	Gas boiler	1	444,267 €	2,221,333 €	5.00	Loh et al., 2002
G-103	Heat network exchanger	1	46,963 €	234,817 €	5.00	Peters et al., 2002 (U-tube stainless steel)
G-104	Pump heat network	1	3,626 €	18,130 €	5.00	Loh et al., 2002
G-105	Fabric filter (230°C continuous carbon steel)	1	39,942 €	199,712 €	5.00	Peters et al., 2002 (carbon steel)
G-106	Exhaust gas booster	1	109,675 €	548,375 €	5.00	Industrial quote
G-107	Flue gas stack	1	18,103 €	39,102 €	2.16	EPA, 2002
TOTAL			14,832,988 €	28,329,199 €	1.91	

Table S4-4: Detailed costs of case 2-20 MW.

Equip. ID	Description	Number of equip.	Equipment Cost*	Final cost**	Cost factor	Source
			*purchase equipment/direct or Indirect cost depending on the source	**including all direct and indirect capital costs	=final cost/equipment cost	
AREA A - BIOMASS PRETREATMENT						
A-101	Truck scale	1	45,099 €	142,512 €	3.16	Aden et al. 2002
A-102	Forklift	2	47,752 €	80,700 €	1.69	Aden et al. 2002
A-103	Belt conveyor	1	35,296 €	141,184 €	4.00	Peters et al., 2002 (0.40 m width)
A-104	Storage on concrete slab	1	88,075 €	254,536 €	2.89	Aden et al. 2002
A-105	Screw conveyor	1	16,974 €	67,896 €	4.00	Peters et al., 2002 (0.23 m diam)
A-106	Rotary dryer, flue gas direct	1	394,457 €	1,577,826 €	4.00	Peters et al., 2002
AREA B - OXIDISING AGENT						
B-101	Air blower VSA			included		
B-102	VSA oxygen	1	1,452,090 €	2,267,624 €	1.56	Sethi et al. 2017
B-103	VSA vacump pump			included		
B-104	Water pump for steam generation	1	- €	- €	0.00	Loh et al., 2002
AREA C - GASIFICATION						
C-101	Biomass receiving hopper	1	47,946 €	205,210 €	4.28	Swanson et al 2010
C-102	Bed material receiving hopper	1	451 €	1,932 €	4.28	Swanson et al 2010
C-103	Gasifier directly heated	1	1,796,337 €	3,790,271 €	2.11	Tijmenissen et al., 2002
C-104	Ash storage vessel	1	10,192 €	44,028 €	4.32	Swanson et al 2010
C-105	Cyclone (carbon steel multicyclone)	1	15,121 €	75,603 €	5.00	Peters et al., 2002
AREA D - SYNGAS CLEANING AND UPGRADING						
D-101	Partial oxydation unit	1	136,523 €	870,804 €	6.38	Guthrie method 1968
D-102	Cyclone (carbon steel multicyclone)	1	21,443 €	107,216 €	5.00	Peters et al., 2002
D-103	Steam generator	1	3,050 €	15,249 €	5.00	Peters et al., 2002 (U-tube stainless steel)
D-104	Authothermal steam reformer	1	- €	- €	0.00	Liu et al. 2011
D-105	Syngas cooler (heat recovery)	1	- €	- €	0.00	Peters et al., 2002 (U-tube stainless steel)
D-106	HT shift reactor	1	- €	- €	0.00	Kreutz et al., 2005
D-107	Syngas cooler (heat recovery)			included		
D-108	LT shift reactor			included		
D-109	Syngas cooler (heat recovery)	1	10,669 €	53,343 €	5.00	Peters et al., 2002 (U-tube stainless steel)
D-110	Venturi scrubber (low energy)	1	24,684 €	123,420 €	5.00	Peters et al., 2002 (low energy)
D-111	Water scrubber (wet dynamic scrubber)	1	23,496 €	117,482 €	5.00	Peters et al., 2002
D-112	Water pump for scrubber	1	4,803 €	24,017 €	5.00	Loh et al., 2002
AREA E - PROCESS WATER CLEANING						
E-101	Water pump for wastewater	1	4,988 €	24,940 €	5.00	Loh et al., 2002
E-102	Dissolved air flotation (DAF)	1	36,619 €	183,094 €	5.00	Industrial quote
E-103	AC filter	1	32,407 €	162,033 €	5.00	Peters et al., 2002 (abacus) D=2m (CS, 1 atm)
AREA F - SYNGAS COMPRESSION AND HYDROGEN SEPARATION						
F-101	Knock-out water	1	22,827 €	56,384 €	2.47	Spath et al., 2005
F-102	Syngas compressor before membrane	1	643,886 €	1,147,406 €	1.78	Average value
F-103	Membrane hydrogen	1	75,307 €	98,653 €	1.31	Ramirez-Santos et al., 2018
F-104	Retentate vacuum pump	1	- €	- €	0.00	Ramirez-Santos et al., 2018
F-105	Syngas compressor before PSA	1	787,291 €	1,196,682 €	1.52	Average value
F-106	PSA hydrogen	1	931,763 €	1,628,721 €	1.75	Average value (Hamelinck et al. 2004, Kreutz et al. 2005, Spath et al. 2005, Meerman et al. 2012)
F-107	Hydrogen final compressor	1	171,073 €	260,030 €	1.52	Average value
AREA G - HEAT & POWER GENERATION						
G-101	Air blower	1	76,630 €	383,150 €	5.00	Industrial quote
G-102	Gas boiler	1	681,229 €	3,406,144 €	5.00	Loh et al., 2002
G-103	Heat network exchanger	2	38,495 €	192,477 €	5.00	Peters et al., 2002
G-104	pump heat network	1	5,361 €	26,807 €	5.00	Loh et al., 2002
G-105	Fabric filter (230°C continuous carbon steel)	1	46,632 €	233,161 €	5.00	Peters et al., 2002 (carbon steel)
G-106	Exhaust gas booster (turbo-blower 69-kPa max discharge)	1	219,350 €	1,096,750 €	5.00	Industrial quote
G-107	Flue gas stack	1	20,734 €	44,785 €	2.16	EPA. 2002

TOTAL **7,969,050 €** **20,102,072 €** 2.52

Table S4-5: Detailed costs of case 3-20 MW.

Equip. ID	Description	Number of equip.	Equipment Cost*	Final cost**	Cost factor	Source
*purchase equipment/direct or indirect cost depending on the source **including all direct and indirect capital costs = final cost/equipment cost						
AREA A - BIOMASS PRETREATMENT						
A-101	Truck scale	1	45,099 €	142,512 €	3.16	Aden et al. 2002
A-102	Forklift	2	47,752 €	80,700 €	1.69	Aden et al. 2002
A-103	Belt conveyor	1	35,296 €	141,184 €	4.00	Peters et al., 2002 (0.40 m width)
A-104	Storage on concrete slab	1	88,075 €	254,536 €	2.89	Aden et al. 2002
A-105	Screw conveyor	1	16,974 €	67,896 €	4.00	Peters et al., 2002 (0.23 m diam)
A-106	Rotary dryer, flue gas direct	1	394,457 €	1,577,826 €	4.00	Peters et al., 2002
AREA B - OXIDISING AGENT						
B-101	Air blower VSA	1	included		1.56	Sethi et al. 2017
B-102	VSA oxygen	1	1,060,857 €	1,656,664 €		
B-103	VSA vacump pump	1	included		0.00	Loh et al., 2002
B-104	Water pump for steam generation	1	- €	- €		
AREA C - GASIFICATION						
C-101	Biomass receiving hopper	1	47,946 €	205,210 €	4.28	Swanson et al 2010
C-102	Bed material receiving hopper	1	451 €	1,932 €	4.28	Swanson et al 2010
C-103	Gasifier directly heated	1	1,796,337 €	3,790,271 €	2.11	Tijmenssen et al., 2002
C-104	Ash storage vessel	1	4,349 €	18,789 €	4.32	Swanson et al 2010
C-105	Cyclone (carbon steel multicyclone)	1	12,504 €	62,521 €	5.00	Peters et al., 2002
AREA D - SYNGAS CLEANING AND UPGRADING						
D-101	Partial oxydation unit	1	136,523 €	870,804 €	6.38	Guthrie method 1968
D-102	Cyclone (carbon steel multicyclone)	1	12,504 €	62,521 €	5.00	Peters et al., 2002
D-103	Syngas recycling booster	1	52,924 €	264,620 €	5.00	Average value
D-104	Authothermal steam reformer	1	- €	- €	0.00	Liu et al. 2011
D-105	Syngas cooler (heat recovery)	1	- €	- €	0.00	Peters et al., 2002 (U-tube stainless steel)
D-106	HT shift reactor	1	- €	- €	0.00	Kreutz et al., 2005
D-107	Syngas cooler (heat recovery)	1	included			
D-108	LT shift reactor	1	included			
D-109	Syngas cooler (heat recovery)	1	11,599 €	57,995 €	5.00	Peters et al., 2002 (U-tube stainless steel)
D-110	Venturi scrubber (low energy)	1	18,704 €	93,522 €	5.00	Peters et al., 2002 (low energy)
D-111	Water scrubber (wet dynamic scrubber)	1	17,620 €	88,101 €	5.00	Peters et al., 2002
D-112	Water pump for scrubber	1	3,129 €	15,643 €	5.00	Loh et al., 2002
AREA E - PROCESS WATER CLEANING						
E-101	Water pump for wastewater	1	3,183 €	15,913 €	5.00	Loh et al., 2002
E-102	Dissolved air flotation (DAF)	1	20,654 €	103,271 €	5.00	Industrial quote
E-103	AC filter	1	26,692 €	133,461 €	5.00	Peters et al., 2002 (abacus) D=1m (CS, 1 atm)
AREA F - SYNGAS COMPRESSION AND HYDROGEN SEPARATION						
F-101	Knock-out water	1	19,798 €	48,901 €	2.47	Spath et al., 2005
F-102	Syngas compressor before membrane	1	527,411 €	939,846 €	1.78	Average value
F-103	Membrane hydrogen	1	67,397 €	88,290 €	1.31	Ramirez-Santos et al., 2018
F-104	Retentate vacuum pump	1	65,629 €	85,973 €	1.31	Ramirez-Santos et al., 2018
F-105	Syngas compressor before PSA	1	475,880 €	723,337 €	1.52	Average value
F-106	PSA hydrogen	1	556,833 €	973,345 €	1.75	Average value (Hamelinck et al. 2004, Kreutz et al. 2005, Spath et al. 2005, Meerman et al. 2012)
F-107	Hydrogen final compressor	1	110,180 €	167,474 €	1.52	Average value
AREA G - HEAT & POWER GENERATION						
G-101	Air blower	1	76,630 €	383,150 €	5.00	Industrial quote
G-102	Gas boiler	1	707,915 €	3,539,576 €	5.00	Loh et al., 2002
G-103	Heat network exchanger	2	39,173 €	195,867 €	5.00	Peters et al., 2002
G-104	pump heat network	1	5,361 €	26,807 €	5.00	Loh et al., 2002
G-105	Fabric filter (230°C continuous carbon steel)	1	47,273 €	236,366 €	5.00	Peters et al., 2002 (carbon steel)
G-106	Exhaust gas booster (turbo-blower 69-kPa max discharge)	1	219,350 €	1,096,750 €	5.00	Industrial quote
G-107	Flue gas stack	1	20,980 €	45,316 €	2.16	EPA, 2002
TOTAL						
6,793,440 €						
18,256,892 €						
2.69						

TOTAL 6,793,440 € 18,256,892 € 2.69

4.2.9.4 Life cycle inventories

4.2.9.4.1 Woodchips

Figure S4-2 presents the network of the Ecoinvent assembly for wood chips production (*Wood chips, wet, measured as dry mass {Europe without Switzerland}/market for/Cut-off, U*). The transport from the woodchip preparation site to the plant is accounted with the assembly for freight transport (*Transport, freight, lorry, unspecified {RER}/market for transport, freight, lorry, unspecified/Cut-off, U*).

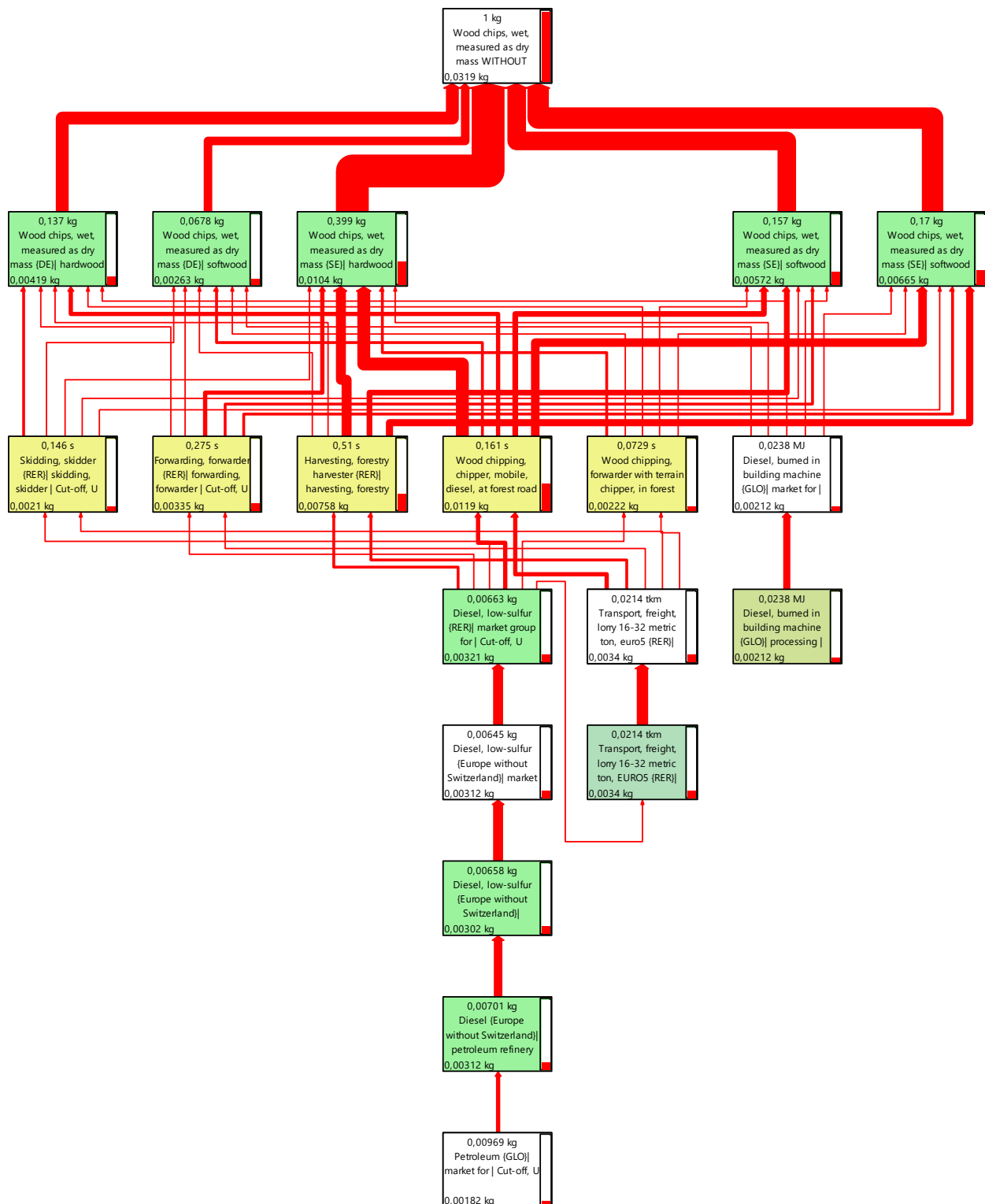


Figure S4-2: Network of fossil carbon dioxide produced from wood chips production (from Ecoinvent).

4.2.9.4.2 Main input and output flows of the gasification plant per functional unit

Table S4-6 present the life cycle inventories of the thermochemical scenarios. All the materials are not included because of a lack of data in Ecoinvent: VSA adsorbent, catalysts for reformer and water gas-shift, membrane.

Table S4-6: Life cycle inventory of thermos-chemical (TC) processes, from Demol et al. 2021.

	CASE	1	2	3
INPUTS				
From the technosphere				
Wood chips, dry	kg.UF ⁻¹	13.0	31.6	56.0
Electricity	kWh.UF ⁻¹	7.57	15.12	20.55
Process water	kg.UF ⁻¹	10.9	16.0	0
Bed material make-up	kg.UF ⁻¹	9.07E-03	2.21E-02	3.92E-02
AC for water cleaning	kg.UF ⁻¹	2.23E-04	1.61E-02	4.99E-02
NaOH	kg.UF ⁻¹	9.77E-02	2.38E-01	4.22E-01
Flocculant	L.UF ⁻¹	1.08E-02	2.63E-02	4.68E-02
Coagulant	L.UF ⁻¹	1.08E-02	2.63E-02	4.68E-02
PSA H ₂ adsorbent AC	kg.UF ⁻¹	2.17E-04	1.70E-04	1.27E-04
PSA H ₂ adsorbent Ze	kg.UF ⁻¹	1.73E-04	1.34E-04	9.85E-05
Natural gas	Nm ³ .UF ⁻¹	1.68E-03	4.08E-03	7.24E-03
Nitrogen	Nm ³ .UF ⁻¹	2.09E-03	5.10E-03	9.04E-03
From the environment				
Air	kg.UF ⁻¹	86.5	262.1	401.3
OUTPUTS				
Products				
Hydrogen	kg.UF ⁻¹	1	1	1
Heat	kWh.UF ⁻¹	19.9	101.8	158.0
Bio-char	kg.UF ⁻¹	0	0	6.16
Wastes to treatment				
Waste in inert landfill	kg.UF ⁻¹	2.13E-01	5.30E-01	3.15E-01
Emissions to water				
Water after AC filter	kg.UF ⁻¹	7.83E+00	2.39E+01	1.51E+01
Emissions to air				
CO ₂ (fossil)	kg.UF ⁻¹	3.59E-03	8.73E-03	1.55E-02
Flue gas	kg.UF ⁻¹	6.38E+01	1.94E+02	3.45E+02
CO	kg.UF ⁻¹	1.23E-01	3.90E-01	2.10E-01
CO ₂ (biogenic)	kg.UF ⁻¹	2.33E+01	5.64E+01	8.72E+01
N ₂	kg.UF ⁻¹	2.63E+01	1.03E+02	1.97E+02
Ar	kg.UF ⁻¹	6.78E-01	1.65E+00	1.24E+00
O ₂	kg.UF ⁻¹	4.58E+00	1.20E-01	2.24E+01
H ₂ O	kg.UF ⁻¹	8.93E+00	2.03E+01	3.71E+01
Naphthalene	kg.UF ⁻¹	1.64E-07	5.20E-07	2.80E-07
Acenaphthylene	kg.UF ⁻¹	1.53E-08	4.87E-08	2.63E-08
Phenanthrene	kg.UF ⁻¹	1.53E-08	4.87E-08	2.63E-08
Anthracene	kg.UF ⁻¹	1.53E-08	4.87E-08	2.63E-08
Pyrene	kg.UF ⁻¹	1.53E-08	4.87E-08	2.63E-08
SO ₂	kg.UF ⁻¹	5.12E-03	1.26E-02	1.48E-02
COV total	kg.UF ⁻¹	1.10E-02	3.44E-02	2.09E-02

4.2.9.4.3 Steam Methane Reforming Susmozas et al. (2013)

Table S4-7 presents the life cycle inventory of the steam-reforming scenario. Steam-reforming catalyst and water gas-shift catalysts are not included due to lack in Ecoinvent database.

Table S4-7: Life cycle inventory of steam methane reforming (SMR), from [23].

	CASE	SMR
INPUTS		
From the technosphere		
Natural gas feedstock	kg.UF ⁻¹	3.18
Natural gas	MJ.UF ⁻¹	8.12
Reaction and makeup water	kg.UF ⁻¹	16.88
Electricity	kWh.UF ⁻¹	1.882
From the environment		
Air	kg.UF ⁻¹	21.68
OUTPUTS		
Products		
Hydrogen	kg.UF ⁻¹	1
Wastes to treatment		
Catalyst to landfill	kg.UF ⁻¹	3.61E-06
Catalyst to landfill	kg.UF ⁻¹	8.83E-05
Emissions to water		
Wastewater	kg.UF ⁻¹	5.69E+00
Emissions to air		
CO ₂ (fossil)	kg.UF ⁻¹	8.48
N ₂	kg.UF ⁻¹	16.63
O ₂	kg.UF ⁻¹	0.66
H ₂ O	kg.UF ⁻¹	8.93

4.2.9.5 LCA results

Table S4-8 presents the detailed impacts results for the case 1-20. Table S4-9 presents the impacts of the different scenarios investigated.

Table S4-8: Detailed impacts results for case 1-20.

Method: CML-IA baseline V3.05 / EU25									
Impact category	Unit	Waste	Woodchips	Transport	Water treatment	Electricity	Other	Total	
Abiotic depletion	ADP	kg Sb eq	0.00E+00	4.86E-07	6.70E-08	5.97E-07	9.51E-07	3.18E-08	2.13E-06
Abiotic depletion (fossil fuels)	ADPf	MJ	0.00E+00	4.19E+00	3.61E-01	1.47E+00	2.84E+00	1.37E-01	9.00E+00
Global warming (GWP100a)	GWP100	kg CO ₂ eq	2.39E-03	2.98E-01	2.34E-02	1.15E-01	2.79E-01	8.54E-03	7.25E-01
Ozone layer depletion (ODP)	ODP	kg CFC-11 eq	0.00E+00	5.05E-08	4.39E-09	5.68E-08	4.59E-07	3.57E-09	5.74E-07
Human toxicity	HTTP	kg 1,4-DB eq	3.28E-04	7.20E-02	8.39E-03	6.72E-02	3.46E-01	5.49E-03	4.99E-01
Fresh water aquatic ecotox.	FAETP	kg 1,4-DB eq	1.46E-06	4.15E-02	2.29E-03	4.90E-02	2.60E-01	5.37E-03	3.58E-01
Marine aquatic ecotoxicity	MAETP	kg 1,4-DB eq	1.75E-05	7.99E+01	6.59E+00	1.70E+02	4.58E+02	1.43E+01	7.29E+02
Terrestrial ecotoxicity	TETP	kg 1,4-DB eq	4.14E-10	2.43E-03	3.35E-05	3.06E-04	4.06E-03	5.10E-05	6.88E-03
Photochemical oxidation	POFP	kg C ₂ H ₄ eq	2.37E-03	3.20E-04	4.06E-06	2.25E-05	5.56E-05	2.27E-06	2.77E-03
Acidification	AP	kg SO ₂ eq	4.09E-03	1.10E-03	1.01E-04	5.67E-04	1.39E-03	4.90E-05	7.30E-03
Eutrophication	EP	kg PO ₄ ³⁻ eq	7.33E+00	2.87E-04	2.42E-05	2.70E-04	5.91E-04	2.39E-05	7.33E+00

Table S4-9: Detailed impacts results for the comparison of all cases.

Method: CML-IA baseline V3.05 / EU25							
Impact category		Unit	SMR	TC1-100	TC1-20	TC2-20	TC3-20
Abiotic depletion	ADP	kg Sb eq	6.83E-07	2.27E-06	2.13E-06	1.61E-06	1.73E-06
Abiotic depletion (fossil fuels)	ADPf	MJ	1.35E+02	9.72E+00	9.00E+00	7.91E+00	8.03E+00
Global warming (GWP100a)	GWP100	kg CO ₂ eq	1.03E+01	7.72E-01	7.25E-01	6.20E-01	6.31E-01
Ozone layer depletion (ODP)	ODP	kg CFC-11 eq	1.47E-06	5.83E-07	5.74E-07	4.53E-07	3.96E-07
Human toxicity	HTTP	kg 1,4-DB eq	2.55E-01	5.16E-01	4.99E-01	4.01E-01	3.69E-01
Fresh water aquatic ecotox.	FAETP	kg 1,4-DB eq	1.33E-01	3.63E-01	3.58E-01	2.82E-01	2.61E-01
Marine aquatic ecotoxicity	MAETP	kg 1,4-DB eq	3.69E+02	7.42E+02	7.29E+02	5.38E+02	5.67E+02
Terrestrial ecotoxicity	TETP	kg 1,4-DB eq	1.33E-03	6.95E-03	6.88E-03	6.03E-03	5.28E-03
Photochemical oxidation	POFP	kg C ₂ H ₄ eq	3.68E-04	2.78E-03	2.77E-03	3.49E-03	1.36E-03
Acidification	AP	kg SO ₂ eq	4.65E-03	7.50E-03	7.30E-03	6.91E-03	5.66E-03
Eutrophication	EP	kg PO ₄ ³⁻ eq	8.52E-04	7.33E+00	7.33E+00	1.21E+01	1.26E+01

CHAPITRE 5 CONCLUSION ET PERSPECTIVES

5.1 Conclusions des travaux menés

Ces travaux ont pu explorer différents aspects des procédés de pyrogazéification de biomasse en vue de produire un vecteur énergétique d'intérêt : l'hydrogène renouvelable.

Des efforts particuliers ont été portés à la chaîne de traitement du gaz de synthèse obtenu. En particulier, dans le chapitre 2 un modèle cinétique détaillé d'oxydation partielle (POX) a été développé et validé sur des données expérimentales obtenues sur des unités pilotes. Une réduction de la quantité totale de goudrons de 60 à 90% a été obtenue selon la quantité d'air ajoutée. Outre la capacité prédictive qu'offre ce modèle cinétique sur la formation d'espèces minoritaires (HAP), la rapidité de l'obtention de la solution permet le couplage entre ce modèle cinétique détaillé et un logiciel de modélisation de procédés tel qu'Aspen Plus®. On peut donc non seulement simuler avec précision la composition du flux de gaz sortant de ce POX, mais aussi la prendre facilement en considération dans les opérations avales (filtration, lavage du gaz...) ce qui permet finalement de mieux appréhender la composition des effluents solides, liquides et gazeux de ce type de procédés.

Le chapitre 3 propose une modélisation détaillée sur Aspen Plus® de trois voies de production d'hydrogène, de chaleur et de bio-char issu de produits secondaires de l'industrie sylvicole. Compte tenu de la dispersion géographique des ressources utilisées et de la nécessité de disposer d'un exutoire de l'excédent de chaleur produite, des unités de petites tailles ont été visées (20 MW_{PCI}, biomasse). Un effort particulier a été porté pour associer des données expérimentales à la modélisation de l'ensemble de la chaîne de traitement. Les bilans matière et énergie détaillés obtenus ont permis d'évaluer l'efficacité énergétique globale de ces procédés (de 76 à 80%) et leurs rendements en hydrogène, chaleur et bio-char. Une estimation des besoins en utilités et consommables est aussi proposée.

L'ensemble des données issues de la modélisation des scénarios de valorisation envisagés permet de réaliser une analyse technico-économique présentée dans le chapitre 4 ainsi qu'une analyse de cycle de vie comparative de ces différentes options. En l'état actuel des prix de marché, un soutien financier est nécessaire pour garantir la faisabilité économique de ce type de procédés. Néanmoins,

il s'agit de procédés générateurs de vecteurs énergétiques très faiblement carbonés : 0,62-0,73 kg_{CO2e}/kg_{H2} pour les scénarios visés contre 10,3 kg_{CO2e}/kg_{H2} pour le procédé de référence de reformage du gaz naturel. Cette valorisation d'une ressource locale renouvelable est également pourvoyeuse d'emplois locaux non-délocalisables et contribue à l'amélioration de la balance commerciale du pays (substitution du gaz naturel importé par des déchets de la sylviculture française). Ces différents éléments pourraient justifier la mise en place d'un soutien financier des pouvoirs publics. Nous avons évalué ce soutien en termes d'euros par tonne de CO₂ évité pour prendre en compte la décarbonation. L'amélioration de la balance commerciale ou la création d'emplois non délocalisables ne sont à ce stade pas quantifiées. On aboutit alors à un soutien de l'ordre de 120 à 210 €/tonne de CO₂ évité dans les conditions actuelles de marché. Ceci est comparable au soutien à apporter à d'autres technologies renouvelables. Il faut remarquer que ce soutien pourrait être ramené à zéro si le prix de production de l'H₂ devient supérieur à 4 €/kg avec le reformage de gaz naturel.

Il est à noter que la co-production de bio-char (scénario 3) peut s'avérer très prometteuse pour sa capacité à séquestrer du carbone sous forme stable (-2.63 kg_{CO2e}/kg_{H2}). Sous cette hypothèse et en prenant en compte la capacité à stocker ce bio-char dans des sols agricoles ou fortement anthroposés, ce procédé serait alors considéré comme négatif en carbone permettant alors de contribuer à la diminution des émissions nationales de gaz à effet de serre pour minimiser les impacts du changement climatique.

5.2 Perspectives

Nous proposons ici quelques perspectives pour la poursuite de ces travaux.

Le scénario 3 de production d'hydrogène, chaleur et bio-char est innovant puisqu'il combine la production de bio-char par une pyrolyse autotherme avec une oxydation partielle des gaz de pyrolyse. La réalisation d'essais sur un pilote pourrait confirmer le potentiel de ce type de procédé particulièrement intéressant pour sa capacité à séquestrer du dioxyde de carbone atmosphérique (par l'intermédiaire de la photosynthèse) dans un bio-char.

Par ailleurs, la séparation de l'hydrogène est une étape cruciale dans la faisabilité technique et économique des procédés proposés. D'après nos connaissances, il n'existe pas de données

disponibles dans la littérature sur la possibilité technique de séparer l'hydrogène d'un syngaz de gazéification par un procédé PSA ou membranaire. En outre, il faudrait déterminer les quantités maximales admissibles de certaines espèces telles que les HAP ou certains composés soufrés connus par ailleurs pour leurs effets néfastes sur les catalyseurs.

L'atteinte de très hauts niveaux de pureté (99.9+%_{vol}) en sortie de PSA nécessite un gaz en entrée du procédé de séparation déjà riche en hydrogène (de l'ordre de 70%_{vol}). Une étude pourrait être menée pour déterminer les puretés atteintes avec une composition en entrée inférieure.

Un procédé hybride combinant membrane et PSA a été proposé. Une autre piste de recherche concerne l'optimisation de ce type d'architecture pour déterminer le nombre et l'enchaînement des étages de séparation, les niveaux de pression, les recyclages éventuels et la nature des matériaux utilisés (type de membrane et d'adsorbant).

Afin d'obtenir un syngaz riche en hydrogène et non-dilué dans l'azote nous avons choisi d'utiliser de la vapeur et de l'oxygène pur comme agents oxydants. La production d'oxygène pure s'avère relativement couteuse. Une alternative consisterait à utiliser l'oxygène produit lors de l'électrolyse de l'eau et habituellement rejeté à l'atmosphère. Ce couplage gazéifieur-électrolyseur propose un système intégré destiné à produire de l'hydrogène (électrolyse et gazéification) ainsi que d'autres vecteurs énergétiques et notamment la chaleur (gazéification et chaleur résiduelle issue de l'électrolyse). Afin de garantir la production d'un hydrogène renouvelable, l'électrolyseur ne doit fonctionner que lors de pics de productions d'électricité renouvelable (solaire, éolien) ou lors de creux de consommation (la nuit notamment). Ce système peut s'avérer très complexe en associant un procédé de gazéification fonctionnant en continu avec une production intermittente d'oxygène (et d'hydrogène) par l'électrolyseur.

Afin de valoriser d'autres ressources, il pourrait aussi être envisagé de produire un gaz de synthèse issu de déchets de bois faiblement pollués et de combustible solide de récupération (CSR). L'utilisation de telles ressources pourraient potentiellement rendre plus complexe la chaîne de traitement du syngaz.

ANNEXE A – RÉSULTATS DÉTAILLÉS DE LA SIMULATION DE PROCÉDÉ

Cette annexe présente les résultats détaillés des bilans matière et énergie obtenus lors de la simulation des 3 scénarios de valorisation du chapitre 3.

A-1 Cas 1-20

	D17	D19	D20	E01	E02	E04	F01	F02	F03	F04	F05	F06	F07	F08	F09	F10	F11	F12	F13	F14	F16	G01	G02	G03	G04	G05	G06	G07		
Total Flow kg/hr	44600	3114	3114	42328	42328	2244	7233	7233	7233	7233	7233	7571	338	287	287	287	287	287	6946	285	9797	9797	16744	16744	18291	18288	18288			
Temperature C	30	40	122	25	25	64	34	155	30	150	30	151	30	30	30	92	30	92	30	15	34	15	44	800	384	110	110	131		
Pressure bar	1.00	2.00	2.00	1.01	1.01	1.01	1.00	2.92	2.92	8.55	8.55	24.99	25.00	24.95	24.95	41.79	41.79	70.00	70.00	1.30	1.00	1.01	1.30	1.01	1.01	1.01	1.20			
Enthalpy MW	-196.3	-13.8	-11.8	-188.5	-188.5	-9.9	-16.3	-15.9	-16.3	-15.9	-16.3	-15.9	-16.3	0.0	0.0	0.1	0.0	0.1	0.0	-16.3	-1.3	0.0	0.1	-16.3	-18.6	-25.7	-25.7	-25.6		
Energy MW	4.0	0.1	2.1	0.0	0.0	0.1	16.4	16.8	16.4	16.8	16.4	16.8	29.8	13.5	11.4	11.5	11.4	11.5	11.4	4.9	0.0	0.0	0.1	4.9	2.6	2.4	2.4	2.5		
Mass Flow kg/hr																														
C																														
COV																												1.206	1.206	1.376
COV-MET																												0.381	0.381	0.434
Mass Flow kg/hr																														
SOOT																												0.19	0.19	0.19

A-2 Cas 2-20

	A01	A03	A04	A05	B01	B02	B03	B04	B05	B07	B08	C01	C02	C03	C04	C07	C08	D01	D02	D03	D11	D13	D17	D19	E01	E02		
Total Flow kg/hr	6189	6189	4641	4641	14987	14987	12884	12884	2103	1887	1887	4641	7880	7828	1351	1887	52	752	8570	8565	8565	5725	53973	1887	51134	51134		
Temperature C	15	15	88.61	88.61	15	58.33	58.19	126	58.33	15	15.01	88.61	819	819	58.33	450	819	58.33	1188	1213	180	30	26.69	40	25	25		
Pressure bar	1.013	1.013	1.013	1.013	1.013	1.5	0.6	1.013	1.5	1.013	2	1.013	1.013	1.008	1.5	2	1.013	1.5	1.013	1.008	1.006	1.005	1.005	2	1.013	2		
Enthalpy MW	-16.08	-16.08	-8.986	-8.986	-0.043	0.138	0.121	0.371	0.017	-8.43	-8.43	-8.986	-15.57	-15.56	0.011	-6.599	-0.012	0.006	-15.53	-15.53	-20.17	-10.22	-237.7	-8.367	-227.7	-227.7		
Energy MW	21.31	21.31	21.51	21.51	-0.04	0.14	0.12	0.37	0.02	-0.03	-0.03	21.51	23.09	23.10	0.01	1.81	-0.01	0.01	23.00	22.99	18.35	15.65	2.70	0.04	0.00	0.00		
Mass Flow kg/hr																												
H2													183.8	183.8					175.1	175.1	175.1	175.1	175.1	0.029		5E-05	5E-05	
CO													1213	1213					2179	2179	2179	2179	2179	0.43		4E-04	4E-04	
CO2													3251	3251					2861	2861	2861	2848	2848	20.02		6.284	6.284	
N2					11322	11322	11322	11322					7.427	7.427					7.426	7.426	7.426	7.425	7.425	1E-03		1E-06	1E-06	
AR					194.3	194.3			194.3				124.8	124.8	124.8				69.48	194.3	194.3	194.3	194.3	0.056		9E-04	9E-04	
O2					3471	3471	1562	1562	1909				50.62	50.62	1226				682.5	2E-06	2E-06	2E-06	2E-06	4E-10				
H2O	2476	2476	928.3	928.3					1887	1887	928.3	2455	2455		1887			2979	2979	2979	160.6	53945	1887	51128	51128			
CH4													238.9	238.9					143.1	143.1	143.1	143	143	0.041		4E-04	4E-04	
C2H2													16.45	16.45					10.73	10.73	10.73	10.65	10.65	0.09		0.01	0.01	
C2H4													17.71	17.71					1.544	1.544	1.544	1.543	1.543	0.001		3E-05	3E-05	
C2H6													19.01	19.01					0.055	0.055	0.055	0.055	0.055	2E-05		3E-07	3E-07	
C3H4													25.32	25.32					0.036	0.036	0.036	0.014	0.023			0.001	0.001	
C3H6													26.59	26.59					0.008	0.008	0.008	0.008	0.008	9E-06		9E-08	9E-08	
BENZENE													93.35	93.35					3.967	3.967	3.967	3.967	3.967					
TOLUENE													19.42	19.42					0.031	0.031	0.031	0.03	0.03	0.001				
OXYLENE													0.557	0.557					2E-05	2E-05	2E-05	2E-05	2E-05	2E-06				
PXYLENE													0.557	0.557					2E-05	2E-05	2E-05	2E-05	2E-05	2E-06				
ETHYNYLB																			0.064	0.064	0.064	0.061	0.061	0.003				
STYRENE																		0.003	0.003	0.003	0.003	0.003	1E-04					
PHENOL													6.683	6.683					0.003	0.003	0.003	3E-05	3E-05	0.003				
GUAIACOL																		5E-09	5E-09	5E-09	5E-09	5E-09	5E-09					
XYLENOL													0.446	0.446														
CRESOL													0.705	0.705					2E-05	2E-05	2E-05	2E-05	2E-05	2E-05				
INDENE													10.58	10.58					0.004	0.004	0.004	0.002	0.001					
INDANE													0.1	0.1					3E-07	3E-07	3E-07	9E-08	2E-07					
MINDENE																		4E-05	4E-05	4E-05	4E-05	1E-05	3E-05					
1MNAPHT													3.713	3.713					2E-05	2E-05	2E-05	4E-06	2E-05					
2MNAPHT													1.114	1.114														
DIPHENYL													2.228	2.228					0.003	0.003	0.003	1E-03	0.002					
NAPHTHA													31.82	31.82					2.108	2.108	2.108	0.885	1.223					
ACENA-YL													8.057	8.057					2.512	2.512	2.512	0.226	2.286					
ACENA-EN													0.252	0.252					0.001	0.001	0.001	3E-05	0.001					
FLUORENE													2.896	2.896					6E-07	6E-07	6E-07	6E-07	6E-07					
PHENANTH													6.572	6.572					0.199	0.199	0.199	0.01	0.189					
ANTHRACE													2.636	2.636					0.024	0.024	0.024	0.024	0.024					
FLTHN													2.413	2.413					1.924	1.924	1.924	1.924	1.924					
PYRENE													2.116	2.116					0.468	0.468	0.468	0.468	0.468					
BAANTHRA																		0.009	0.009	0.009	0.009	0.009						
CHRYSENE																		0.002	0.002	0.002	0.002	0.002						
BAPYR																		0.002	0.002	0.002	0.002	0.002						
BKFLTHN																		0.009	0.009	0.009	0.009	0.009						
NH3																		2E-09	2E-09	2E-09		4E-15						
NO																		2E-10	2E-10	2E-10	2E-10	2E-10						
N2O																		4E-12										
NO2																		6E-18										
HCN																		3E-09	3E-09	3E-09	1E-09	2E-09						
HCL													0.764	0.764					0.764	0.764	0.764	3E-15	3E-17					
H2S													0.789	0.789					0.789	0.789	0.789	0.786	0.016					
SO2																							0.013	0.013				

	E04	F01	F02	F03	F04	F05	F06	F07	F08	F09	F10	F11	F12	F13	F14	F16	F17	F18	F19	F20	F21	F22	G01	G02	G03	G04	G05	G06	G07	
Total Flow kg/hr	2816	2138	2138	2138	2138	2138	2209	71	118	118	118	118	118	2021	161	5565	5565	5565	5565	3426	15859	15859	21305	21305	22853	22850	22850			
Temperature C	61.4	29.21	152.3	30	153.5	30	153.8	30	30	30	91.68	30	91.69	30	16.2	30	30	120.3	30	120.3	30	30	15	44.45	800	329.8	109.9	109.9	131.4	
Pressure bar	1.013	1	2.924	2.924	8.55	8.55	25	25	24.95	24.95	41.79	41.79	70	70	1.3	1.005	2.241	2.241	5	5	5	1.013	1.3	1.013	1.013	1.012	1.2			
Enthalpy MW	-12.4	-4.681	-4.544	-4.681	-4.543	-4.682	-4.544	-4.683	0.002	0.003	0.032	0.003	0.033	0.003	-4.691	-0.714	-9.607	-9.411	-9.608	-9.412	-9.61	-4.929	-0.046	0.086	-14.63	-17.9	-24.99	-24.99	-24.84	
Energy MW	0.14	6.59	6.73	6.59	6.73	6.59	6.73	9.39	2.81	4.69	4.72	4.69	4.72	4.69	1.89	0.00	15.55	15.74	15.55	15.74	15.55	8.96	-0.04	0.09	5.83	2.56	2.36	2.36	2.51	
Mass Flow kg/hr																														
C																														
COV																											0.989	0.989	1.159	
COV-MET																											0.312	0.312	0.366	
Mass Flow kg/hr																														
SOOT																												0.156	0.156	0.156

A-3 Cas 3-20

	E04	F01	F02	F03	F04	F05	F06	F07	F08	F09	F10	F11	F12	F13	F14	F16	F17	F18	F19	F20	F21	F22	G01	G02	G03	G04	G05	G06	G07	
Total Flow kg/hr	1003	909	909	909	909	909	924	15	66	66	66	66	66	843	152	4389	4389	4389	4389	4389	3480	17036	17036	21358	21358	22906	22903	22900		
Temperature C	64.27	106	257.4	30	155.9	30	156.1	30	30	91.68	30	91.69	30	16.51	33.2	33.2	123.9	30	119.9	30	30	15	44.45	800	327.9	109.9	109.9	131.3		
Pressure bar	1.013	1	2.924	2.924	8.55	8.55	25	25	24.95	24.95	41.79	41.79	70	70	1.3	1.003	1.003	2.237	2.237	4.99	4.99	5	1.013	1.3	1.013	1.013	1.013	1.012	1.2	
Enthalpy MW	-4.414	-1.905	-1.821	-1.946	-1.878	-1.946	-1.878	-1.947	3E-04	0.002	0.018	0.002	0.018	0.002	-1.95	-0.677	-6.977	-6.823	-6.983	-6.831	-6.984	-5.039	-0.049	0.092	-12.59	-15.89	-22.98	-22.98	-22.8	
Energy MW	0.05	3.52	3.60	3.48	3.54	3.48	3.54	4.08	0.61	2.64	2.66	2.64	2.66	2.64	0.83	0.00	14.18	14.33	14.17	14.32	14.17	10.69	-0.05	0.09	5.91	2.61	2.41	2.41	2.56	
Mass Flow kg/hr																														
C																														
COV																												0.883	0.883	1.053
COV-MET																												0.279	0.279	0.332
Mass Flow kg/hr																														
SOOT																												0.139	0.139	0.139

ANNEXE B – MODÉLISATION PSA

Cette annexe présente l'avancement de travaux effectués sur la modélisation numérique d'un PSA destiné à séparer l'hydrogène d'un syngaz de gazéification.

Design and modelling of a hybrid process for the separation of hydrogen from biomass gasification syngas

Demol R., Mougel A.

1. Introduction

The biomass gasification process produces gas mainly composed of H₂, CO, CO₂, CH₄. The standard technology used for hydrogen separation is pressure swing adsorption (PSA). However, the composition of hydrogen in the syngas is too low to produce high purity hydrogen (99.9%) in one stage PSA. This concentration should reach at least 70% vol [1]. Another technology that can be used for hydrogen separation is membrane [2]. PSA is a cyclic process whereas membrane process is continuous. To separate hydrogen from syngas, a multistage process is investigated numerically. For the simulation of the PSA, there are several possible approaches: (i) a black box model, i.e. a splitter using outlet purity and recovery rate from industrial data, (ii) a shortcut PSA model [3] considering a batch equilibrium model, or (iii) a complete dynamic PSA model [4], which gives more accurate results. The optimization of a hybrid process composed of membrane and short-cut model PSA has already been studied for a biogas (80% H₂) [5]. However, the syngas produced from biomass gasification is less concentrated in H₂. In this study, a complete PSA model is developed on Matlab® software. The pseudo-steady state solution obtained from the operating condition can be coupled with an existing membrane model software [6]. The final goal is to determine the optimal separation architecture to produce hydrogen from a low-concentrated syngas.

2. Material and methods

a. Pressure swing adsorption

The PSA process cyclic adsorption process based on the variation of pressure during the operation. The pressure is highest during the adsorption stage, to promote adsorption. As for the lowest pressure, it is reached during the purge, to promote desorption, and thus regenerate the adsorbent. To switch from one pressure to the other, there are compression/decompression steps. These 4 steps constitute a PSA cycle and are explained below. In this study, a Skarstrom cycle [7] is modeled with pressurization using the product. In practice, PSA processes set up several columns simultaneously to ensure continuous production.

- I. Adsorption: this step takes place at high pressure. The species having the highest affinity with the adsorbent are adsorbed. The compound the least adsorbed, in this case hydrogen, is concentrated throughout the column.
- II. Depressurization: the column goes from high pressure to low pressure to desorb the adsorbed compounds.
- III. Purge: at low pressure, purge is done. The valves on both sides of the column are opened and part of the product is sent into the column to further desorb the adsorbed compounds and push the desorbed gas at the outlet.
- IV. Pressurization: the column is pressurized with the product up to the high pressure level in countercurrent. This pressurization with the product allows not to overload the adsorbent with impurities in order to prepare the adsorption phase.

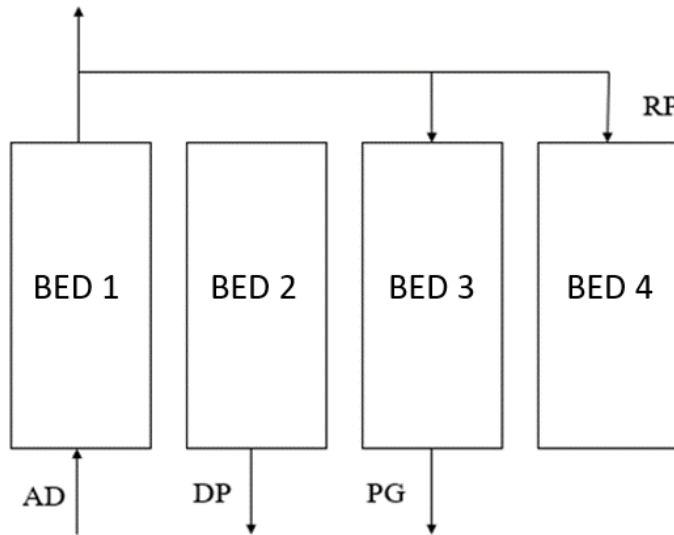


Figure 1: Four-step PSA cycle: AD = Adsorption, DP = Depressurization, PG = Purge, RP = re-pressurization

The profile of concentrations and adsorbed quantities will of course change with each cycle, but a cyclic steady state can be obtained, which corresponds to the state from which the profiles and the state of the column will not change during the following cycles. The choice of adsorbents was made to obtain hydrogen at high pressure. Indeed, the goal is to separate the hydrogen, by choosing an adsorbent on which the hydrogen is not highly adsorbed, it is possible to recover the hydrogen directly during the adsorption phase, and thus at high pressure. This avoids recompressing our product for later use or storage and reduces costs.

b. Model equations

Before developing a mathematical model of PSA, it is necessary to determine the equations governing the flow. For this study, the following assumptions are made:

- Isothermal process
- 1D-Model
- Ideal gas law
- The adsorption equilibrium is represented by the extended Langmuir isotherm.
- The adsorption rate is approximated by a linear driving force (LDF).

The following equations are used for the purge and adsorption steps. Concerning the pressurization and depressurization steps, the assumptions will be explained later.

The mass balance for each compound is calculated using the following equation:

$$\frac{\partial c_i}{\partial t} = -\frac{1}{\varepsilon} \frac{\partial u c_i}{\partial z} - \frac{(1-\varepsilon)}{\varepsilon} \rho_s \frac{\partial q_i}{\partial t} + \frac{\partial}{\partial t} \left(D_{z,i} \frac{\partial c}{\partial z} \right) \quad (1)$$

and the overall mass balance is then calculated by:

$$\frac{\partial c_{gT}}{\partial t} = -\frac{1}{\varepsilon} \frac{\partial u c_{gT}}{\partial z} - \frac{(1-\varepsilon)}{\varepsilon} \rho_s \sum \frac{\partial q_i}{\partial t} \quad (2)$$

In order to calculate the adsorption rate in the adsorbent for each compound, the linear driving force model (LDF) with a constant transfer coefficient was used. The coefficients are reported in Appendix C.

$$\frac{\partial q_i}{\partial t} = \omega_i (q_i^* - q_i) \quad (3)$$

Adsorption equilibrium is estimated by the Langmuir model, according to the following equation:

$$q_i^* = \frac{q_{mi} B_i P_i}{1 + \sum_{i=1}^n B_i P_i} \quad (4)$$

Velocity is calculated for adsorption and purge steps by considering the independence of time on total concentration. Therefore, relation (2) becomes:

$$\frac{\partial u}{\partial z} = -\frac{u}{c_{gT}} \frac{\partial c_{gT}}{\partial z} - \frac{(1-\varepsilon)}{\varepsilon} \rho_s \sum \frac{\partial q_i}{\partial t} \quad (5)$$

Finally, Ergun's equation is used to calculate the pressure drop within the column.

$$\frac{\partial p}{\partial z} = -\frac{150\mu}{d_p^2} \left(\frac{1-\varepsilon}{\varepsilon} \right)^2 u - \frac{1.75}{d_p} \left(\frac{1-\varepsilon}{\varepsilon} \right) \rho u^2 \quad (6)$$

c. Resolution algorithm

To simulate this process, a single column was simulated considering that all columns would have the same behavior. The goal of the algorithm is to reach a pseudo-cyclic steady state: the outlet flow must remain the between two consecutive cycle. To reach this solution, the equations were discretized in space and time as explained in Appendix A. For the adsorption and purge steps, concentrations and adsorbed quantities were solved using the implicit Euler method. Then pressure and velocity were solved simultaneously with a Newton-Raphson method. The concentrations and adsorbed quantities are therefore solved using the velocity and pressure fields of the previous time, then the new velocity and pressure fields are calculated using the concentrations and adsorbed quantities obtained. A schematic representation of this algorithm is presented below.

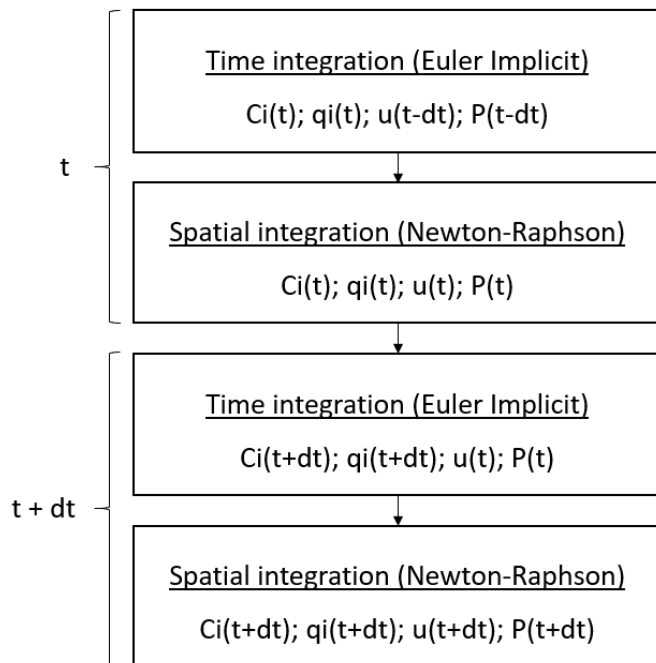


Figure 2: Resolution algorithm

It is noticeable that the equations describing the PSA are stiff differential equations. This makes it difficult to solve them numerically by usual and explicit methods (such as ode functions in Matlab). The choice of the solving method by implicit Euler allows then to obtain a much more stable solution.

Boundary conditions for each step are given below in Table 1.

Table 1: Boundary conditions of PSA process

Adsorption (co-current)	
Z=0	Z=L
$P = P_{feed}$ $c_i = y_i \cdot c_{feed}$ $u = u_{feed}$	$P = P_{exit}$ $\frac{\partial c_i}{\partial z} = 0$ $\frac{\partial u}{\partial z} = 0$
Purge (counter-current)	
Z=0	Z=L
$P = P_{exit,purge}$ $\frac{\partial c_i}{\partial z} = 0$ $\frac{\partial u}{\partial z} = 0$	$P = P_{purge}$ $c_i = y_i \cdot c_{purge}$ $u = u_{purge}$

The pressurization and depressurization steps are not simulated. For the depressurization step, it is assumed that the column changes from high pressure to low pressure instantaneously and that the molar fractions are conserved. Concerning the adsorbed quantities, the value at the end of adsorption is compared to $q_{i,P=P_{low}}^*$ for each point of the space. If the value of $q_{i,P=P_{ads}}$ is higher than $q_{i,P=P_{low}}^*$ then the value of $q_{i,P=P_{low}}$ is set to $q_{i,P=P_{low}}^*$. Otherwise, the value of q_i stays the same.

The pressurization is supposed instantaneous from low to high pressure. The incoming flow is the H₂ enriched product. For all compounds other than H₂, it is then considered that the adsorbed quantities remain the same as those obtained at the end of the purge stage. For hydrogen, the adsorbent is considered to be saturated ($q_{H_2,P=P_{ads}} = q_{H_2,P=P_{low}}^*$). Finally, the concentrations of each specie is the sum of the specie quantity at the end of the purge step plus the quantity from the product to reach the adsorption pressure.

The cycles continue until the cyclic steady state is reached. To know if this state is reached, the maximum adsorbed quantities are compared for each cycle. The cyclic steady state is then reached when this maximum adsorbed quantity no longer varies.

d. Aspen Plus®-Matlab® coupling

As mentioned previously, the goal of this project is to use the PSA model on Matlab® and the membrane software MEMSIC [6] in Aspen Plus® flowsheet. However, this coupling between Matlab and Aspen Plus® is not straightforward. This section gives some information on the coupling method between the two software. As shown in Figure 3, a Fortran subroutine is used to connect the two programs.

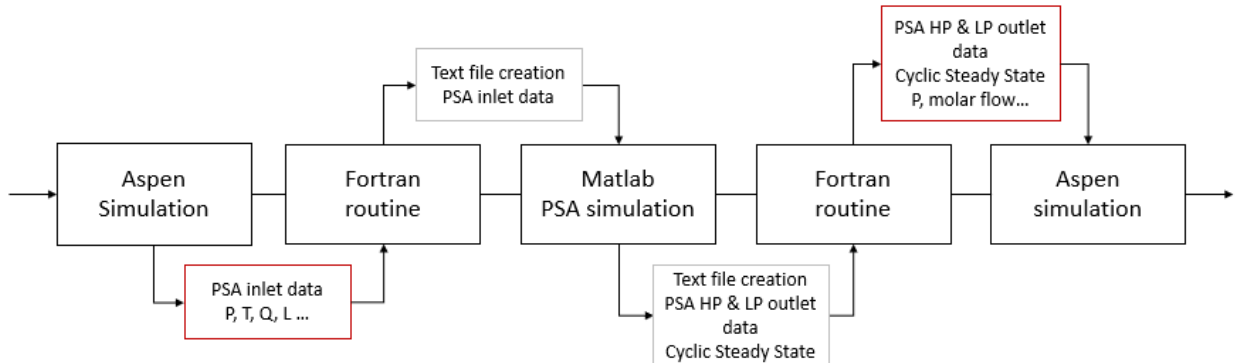


Figure 3: Schematic representation of the Aspen/MATLAB coupling.

The data from the Aspen Plus® simulation are collected with the Fortran routine. This program creates a text file containing these data used as input file data in the Matlab® program. The program then runs the Matlab® script to simulate the PSA until the cyclic steady state is reached. The solution is written in a file read by Fortran program to link with Aspen Plus® simulation. Once this is done, the Aspen Plus® simulation can continue.

3. Results and discussion

a. Model validation

Modeling the dynamic adsorption have to be validated by experimental data. The breakthrough curves of each component were compared to experimental curves [8]. These curves are the result of an adsorption on three different configurations (activated carbon bed; zeolite 5A bed; layered bed (AC: Z5A = 7:3)) in a 1-meter column at 6.5 bar. The feed composition is: 38% v H₂, 50% v

CO_2 , 1% v CH_4 , 1% v CO , 10% v N_2 at the adsorption pressure, a flow rate of flow 5 SLPM and a temperature of 295K. All the specifications are shown in the Table 2.

Table 2: Experimental conditions for breakthrough curves

Feed flow rate (SLPM)	5
Feed temperature (K)	295
Feed pressure (bar)	6.5
Feed composition	38% v H_2 , 50% v CO_2 , 1% v CH_4 , 1% v CO , 10% v N_2
Bed length (m)	1
Bed internal diameter (m)	0.035
Adsorbent density ρ_s (kg/m^3)	AC: 850, Z5A: 1160
Bed porosity ε	AC: 0.433, Z5A: 0.357
Particle diameter d_p (mm)	AC: 2.3, Z5A: 3.14

Figure 4(a) shows the breakthrough curve on an activated carbon bed, under the conditions described above. The predictive model and the experimental point match well. The figure shows that the hydrogen comes out first and that the N_2 is rather badly adsorbed, and quickly decreases the H_2 outlet concentration. Finally, CO_2 comes out last when the adsorbent is saturated. Figure 4(b) shows the results with Zeolite 5A. The experimental points and the predictive model are quite distant. Indeed, it is quite noticeable that the CO_2 leaves the column experimentally well before what the model predicts. This difference between the model and the experimental points is also present on the layered bed, composed of activated carbon and Zeolite 5A.

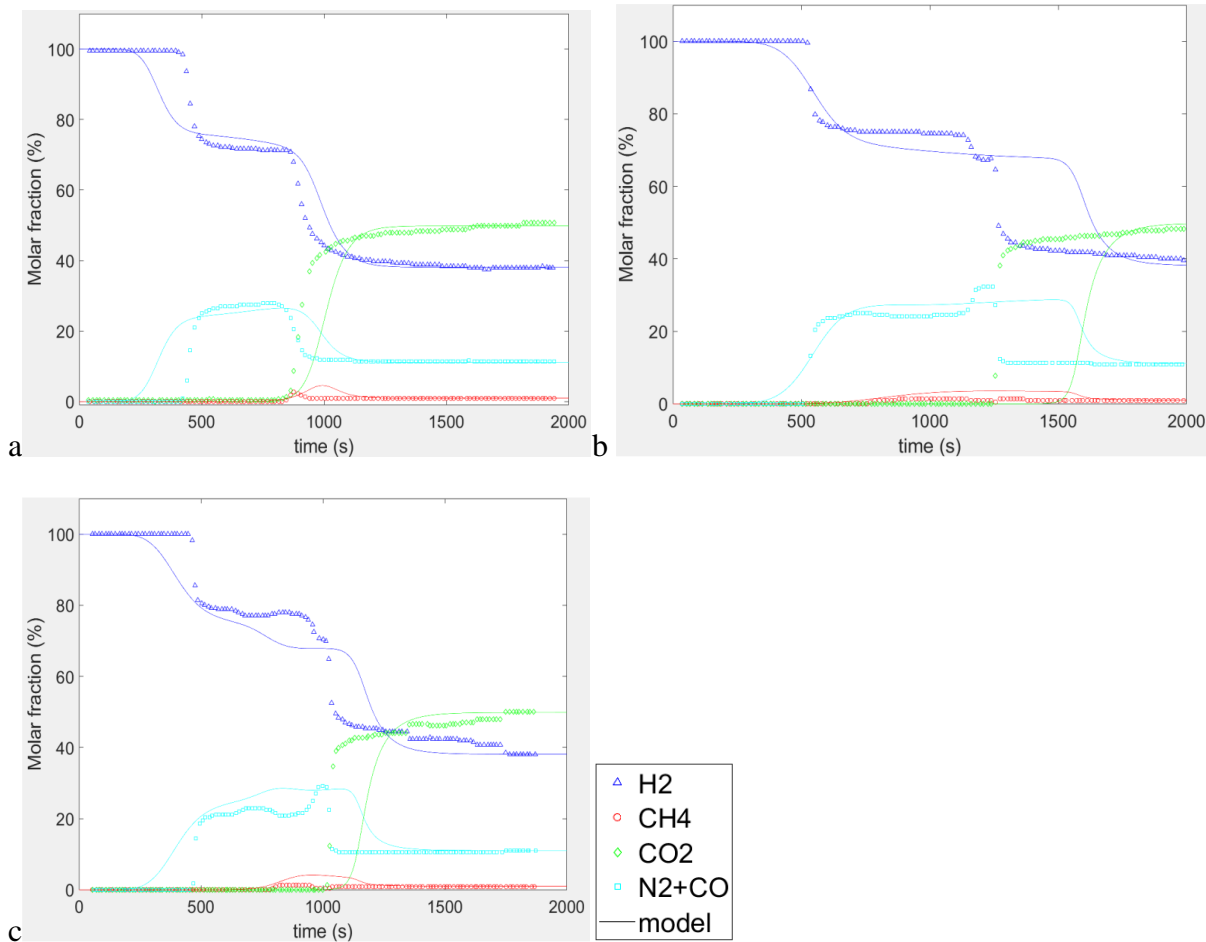


Figure 4: Comparison of experimental curves and mathematical model (a) activated carbon bed, (b) zeolite 5A bed, (c) layered bed

It is important to note that the model is isothermal. However, the experimental data [8] reports a rather large and abrupt temperature increase (55K) due to the strong adsorption affinity of CO₂ on zeolite 5A. Figure 5 shows the influence of temperature on the breakthrough curves. Indeed, an increase of 50K significantly modifies residence time of each species. It is therefore envisaged to improve the model in the future to consider the non-isothermal behavior and to account for these rapid temperature changes due to the adsorption of certain species. Considering the gap between the experimental points and the model due to the hypothesis of an isothermal process, it is appropriate to consider that the established model partially responds to the modeling of a PSA and this model will therefore be used thereafter until it is improved.

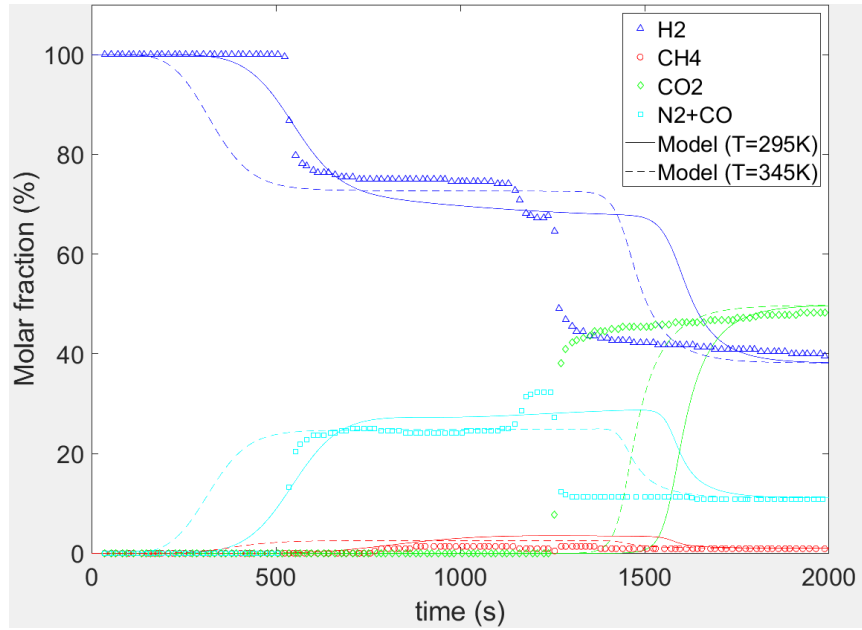


Figure 5: Comparison of mathematical model at $T = 295\text{K}$ and $T = 345\text{K}$.

Figure 8(a) (Appendix D) shows the time evolution of concentrations, adsorbed quantities, velocity and pressure profiles within the column during the adsorption phase. Figure 8(a) corresponds to an activated carbon bed, under the conditions presented in Table 2. The adsorption time is 500s. The evolution of the pressure within the column reveals that the pressure drop along the bed is quite low. The variation in velocity is a little more important, it is therefore not recommended to assume a constant velocity during the adsorption phase.

The incoming flow is quite rich in CO_2 which is very well adsorbed in both adsorbents. Figure 8(b) shows that the affinity between Zeolite 5A and CO_2 is very important. However, in both cases, N_2 adsorbs rather poorly. The PSA does not therefore allow an optimal separation between H_2 and N_2 . This reinforces the idea of associating this PSA with a membrane module that could allow this separation.

b. Application on a gasification syngas

In this part the results are obtained after reaching the cyclic steady state, i.e., when the column remains in the same state for two consecutive cycles. Figure 6 shows the evolution of the total quantity adsorbed as a function of time. The simulated bed is an activated carbon bed. It is then visible that the cyclic steady state is reached after 7 cycles.

The inlet flow considered for this application is a typical flow obtained after O₂/Steam gasification of biomass. The simulation conditions are presented in Table 3.

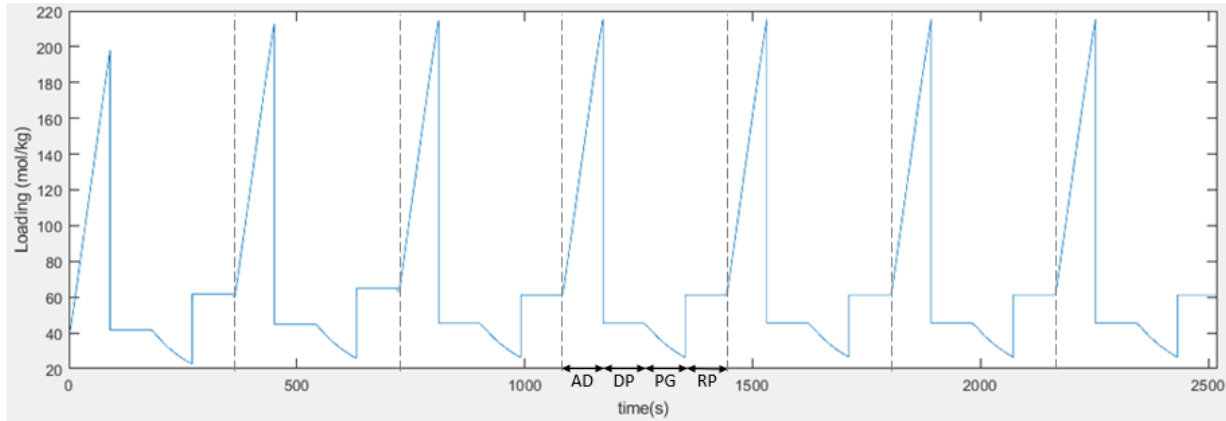


Figure 6: Total loading at successive cycles.

Table 3: Simulations parameters

Feed velocity (m/s)	$0.6 v_{f-mf}$
Feed temperature (K)	295
Feed pressure (bar)	20
Desorption pressure (bar)	1.3
Feed composition	40%v H ₂ , 32%v CO ₂ , 7%v CH ₄ , 19%v CO, 2%v N ₂
Bed length (m)	1
Adsorbent density ρ_s (kg/m ³)	AC: 850, Z5A: 1160
Bed porosity ϵ	AC: 0.433, Z5A: 0.357
Particle diameter d_p (mm)	AC: 2.3, Z5A: 3.14
Adsorption time t_{ads} (s)	90
Total cycle time t_{cycle} (s)	360

The most important criteria to quantify the separation of hydrogen in PSA are the purity and the recovery. The purity of the PSA outlet is the most important element as it determines the future use of the hydrogen obtained. The purer the hydrogen obtained, the more valuable it will be. However, the recovery rate is also very important. It is the ratio between the hydrogen flow leaving the column at

high pressure and the hydrogen flow entering the column. In the case studied, this outgoing stream is not the stream coming out of the adsorption phase, because this stream is partly used to purge and pressurize the column. It is then interesting to study the variation of the duplet (H_2 purity; H_2 recovery) for each bed considered, by varying the size of the bed (which is equivalent to varying the mass of adsorbent used).

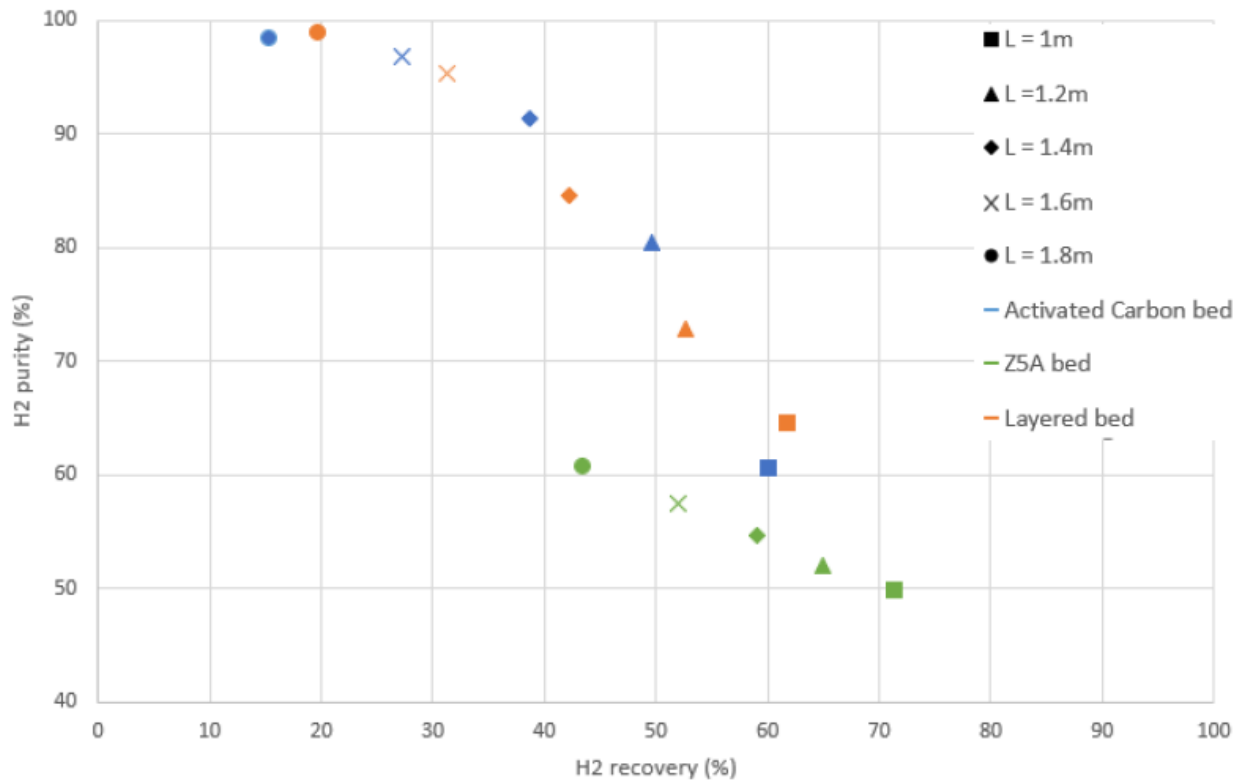


Figure 7: Evolution of the duplet (H_2 purity; H_2 recovery) for each bed and for 5 different lengths.

Figure 7 shows that the increase in purity results in a decrease in recovery, and inversely, for each bed. It is also noteworthy that Zeolite 5A does not offer significant purities, regardless of bed size. This is explained by the fact that this adsorbent retains mainly CO_2 , and retains less the other gases, as can be seen in Figure 8(b) (Appendix D). As a consequence, the adsorbent quickly becomes saturated with CO_2 , which is a major gas in the feed stream, and the purge only removes a small part of this adsorbed CO_2 . During the cycles, this CO_2 remains adsorbed, and the separation is no longer optimal. Concerning the layered bed and the activated carbon bed, the duplets are quite close, it is however represented that the layered bed allows to obtain slightly more important

recoveries at almost equal compositions, especially for high bed lengths. In addition, these two beds make it possible to reach a purity of 98%, but for much too low recovery values. It is therefore necessary to use several separation stages, to obtain the desired purity values, while having an acceptable recovery.

4. Conclusions

This study has allowed the realization of a functional PSA model whose experimental validation is acceptable in view of the hypotheses made. In addition, this model provides a steady-state cyclic solution from a biomass gas, and therefore can be coupled to a steady-state separation process. Results obtained with the model using a feed with low H₂ purity show that a single PSA is not sufficient to achieve very high purity levels while having acceptable recovery rates. It is therefore necessary to have several separation stages and to couple this PSA with a membrane module. Multi-stage separation architectures had to be tested on Aspen Plus®. However, the coupling between Aspen Plus® and Matlab® has been successfully implemented. Finally, it is possible to improve the developed model by removing the hypothesis of an isothermal model and thus adding the calculation of temperature. This new model should correspond better to the experimental values and give more accurate results. It would also be interesting to add the cost equations to determine and compare the CAPEX of the different separation architectures.

5. Appendix

Notations

c_i	Gas phase concentration of component i (mol/m ³)
c_{gT}	Total gas phase concentration (mol/m ³)
d_p	Particle diameter (m)
$D_{z,i}$	Axial dispersion coefficient (m ² /s)
ε	Bed porosity
P	Pressure (Pa)
Q	Volume flowrate (SLPM)
q_i	Particle adsorbed concentration (mol/kg)
q_i^*	Adsorbed concentration in equilibrium (mol/kg)
ρ_s	Adsorbent density (kg/m ³)
t	Time (s)
t_{ads}	Adsorption time (s)
t_{cycle}	Total cycle time (s)
u	Superficial velocity (m/s)
v_{f-mf}	maximum fluidization velocity (m/s)
μ	gas mixture viscosity (kg/m/s)
ω_i	LDF coefficient (1/s)
y_i	Molar fraction of component i
z	Axial position (m)

A. Numerical discretization

Spatial integrations are approximated by backward approximation

$$\frac{dc_i}{dx} \Big|_k = -\frac{1}{\varepsilon} \frac{u_{(k)} \cdot c_{i(k)} - u_{(k-1)} \cdot c_{i(k-1)}}{dx} - \frac{1-\varepsilon}{\varepsilon} \rho_s \omega_i (q_{i(k)}^* - q_{i(k)})$$

$$\frac{dq_i}{dt} \Big|_k = \omega_i (q_{i(k)}^* - q_{i(k)})$$

The velocity is then solved with the Newton-Raphson method:

Where:

$$f(u) = \begin{pmatrix} f_1(u_1, \dots, u_n) \\ \vdots \\ f_n(u_1, \dots, u_n) \end{pmatrix}$$

$$f_k(u) = \frac{u_{(k)} - u_{(k-1)}}{dx} - \frac{u_{(k)}}{c_{gT}} \frac{c_{gT(k)} - c_{gT(k-1)}}{dx} - \frac{1-\varepsilon}{\varepsilon} \rho_s \sum_{i=1}^n \omega_i (q_{i(k)}^* - q_{i(k)}) = 0$$

$$f(u) = \begin{pmatrix} \frac{\partial f_1}{\partial u_1} & \dots & \frac{\partial f_1}{\partial u_n} \\ \vdots & \ddots & \vdots \\ \frac{\partial f_n}{\partial u_1} & \dots & \frac{\partial f_n}{\partial u_n} \end{pmatrix}$$

And:

$$u^{i+1} = u^i - J^{-1} f$$

First approximation is made by u ($t-dt$), and $u(t)$ is calculated at each time.

The same method is used for pressure simultaneously for adsorption and purge steps.

B. Diffusivity and viscosity calculation [9]

Diffusivity:

$$D_{z,i} = \frac{D_{m,i}}{\varepsilon} (20 + 0.5 \cdot Sc \cdot Re) = \frac{D_{m,i}}{\varepsilon} \left(20 + 0.5 \cdot \frac{u \varepsilon d_p}{D_{m,i}} \right) = 20 \frac{D_{m,i}}{\varepsilon} + 0.5 u d_p$$

$$D_{m,i} = \frac{1 - y_i}{\sum_{x=j}^n \frac{y_i}{D_{i,x}}}$$

$$D_{i,j} = \frac{T^{1.5}}{p \sigma_{i,j}^2 \Omega_D} \left(\frac{1}{M_i} + \frac{1}{M_j} \right)^{0.5} \cdot 0.0018583$$

$$\sigma_{i,j} = \frac{\sigma_i + \sigma_j}{2}$$

$$\Omega_D = \left(44.54 \left(\frac{k_B T}{\varepsilon_{i,j}} \right)^{-4.909} + 1.911 \left(\frac{k_B T}{\varepsilon_{i,j}} \right)^{-1.575} \right)^{0.1}$$

$$\varepsilon_{i,j} = (\varepsilon_i \varepsilon_j)^{0.5}$$

Parameters for each component are presented below.

	σ (Å)	ε/k (K)
H ₂	2.915	38.0
N ₂	3.667	99.8
CO	3.590	110
CO ₂	3.996	190
CH ₄	3.780	154

Viscosity

$$\mu_{mix} = \sum_{\alpha=1}^n \frac{x_\alpha \mu_\alpha}{\sum_\beta x_\beta \Phi_{\alpha\beta}}$$

Where:

$$\Phi_{\alpha\beta} = \frac{1}{\sqrt{8}} \left(1 + \frac{M_\alpha}{M_\beta} \right)^{1/2} \left[1 + \left(\frac{\mu_\alpha}{\mu_\beta} \right)^{1/2} + \left(\frac{M_\alpha}{M_\beta} \right)^{1/4} \right]^2$$

C. Langmuir adsorption isotherm parameters

Table 4: Langmuir adsorption isotherm parameters [4].

	k_1 (mol.kg ⁻¹)	k_2 (mol.kg ⁻¹ .K ⁻¹)	k_3 (bar ⁻¹)	k_4 (K)	ω_i
Activated Carbon					
H ₂	16.943	-0.021	6.248e-5	1229	0.7
N ₂	1.6441	-0.00073	0.0545	326	0.099
CO	33.85	-0.09072	2.311e-4	1751	0.063
CO ₂	28.797	-0.07	0.01	1030	0.0135
CH ₄	23.86	-0.05621	3.478e-3	1159	0.147
Zeolite 5A					
H ₂	4.314	-0.0106	0.002515	458	0.7
N ₂	4.8133	-0.00668	6.0507e-4	1531	0.099
CO	11.8454	-0.0313	0.0202	763	0.063
CO ₂	10.03	-0.01858	1.5781	207	0.0135
CH ₄	5.833	-0.01192	6.0507e-4	1731	0.147

D. Time profiles of concentrations, adsorbed quantities, pressure and velocity along the column

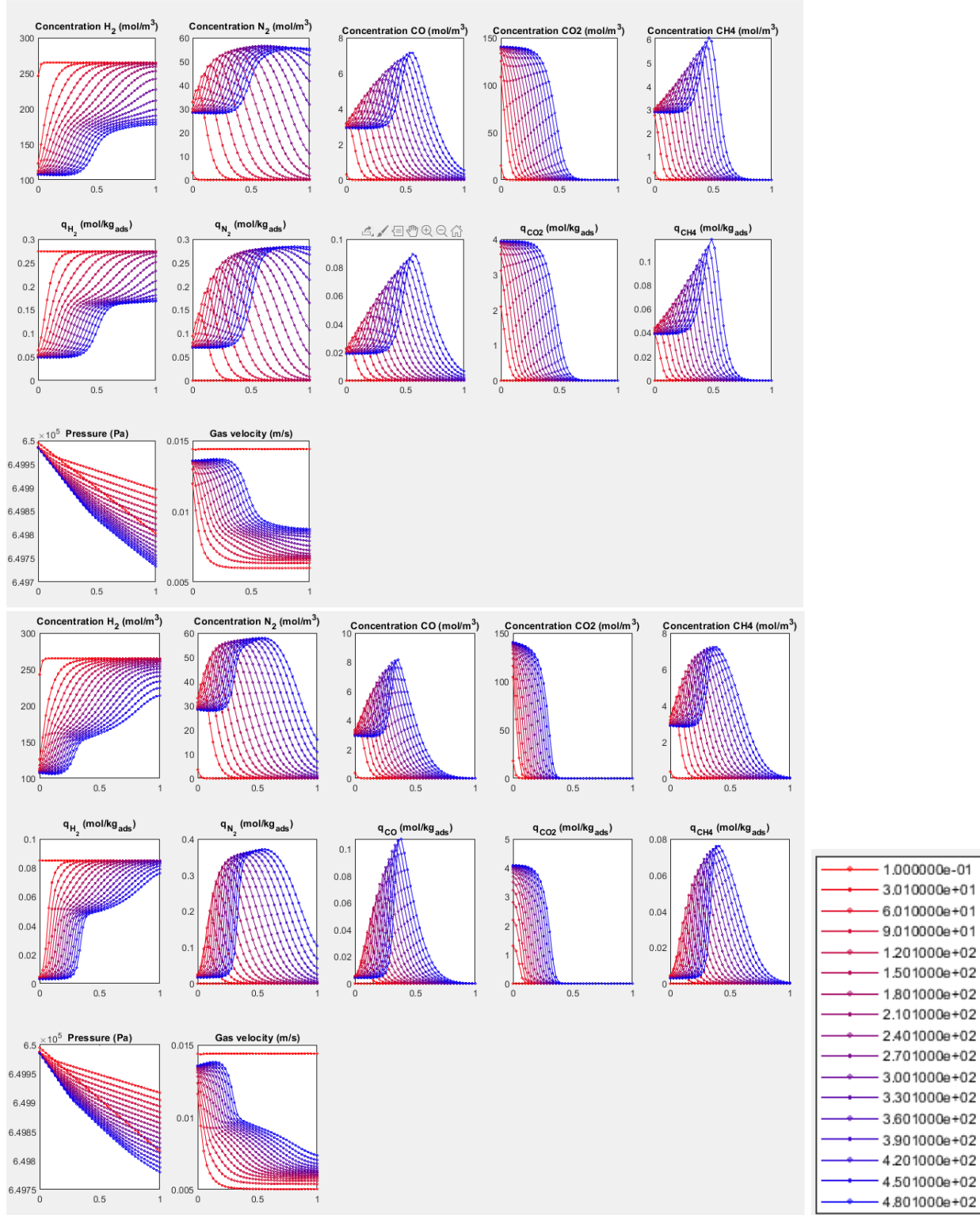


Figure 8: (a) Activated Carbon (b) Zeolite 5A

6. References

- [1] Spath P, Aden A, Eggeman T, Ringer M, Wallace B, Jechura J. Biomass to Hydrogen Production Detailed Design and Economics Utilizing the Battelle Columbus Laboratory Indirectly-Heated Gasifier. 2005. <https://doi.org/10.2172/15016221>.
- [2] Yin H, Yip ACK. A Review on the Production and Purification of Biomass-Derived Hydrogen Using Emerging Membrane Technologies. *Catalysts* 2017;7:297. <https://doi.org/10.3390/catal7100297>.
- [3] Chung Y, Na B-K, Song HK. Short-cut evaluation of pressure swing adsorption systems. *Computers & Chemical Engineering* 1998;22:S637–40. [https://doi.org/10.1016/S0098-1354\(98\)00113-6](https://doi.org/10.1016/S0098-1354(98)00113-6).
- [4] Golmakani A, Fatemi S, Tamnanloo J. Investigating PSA, VSA, and TSA methods in SMR unit of refineries for hydrogen production with fuel cell specification. *Separation and Purification Technology* 2017;176:73–91. <https://doi.org/10.1016/j.seppur.2016.11.030>.
- [5] Ohs B, Falkenberg M, Wessling M. Optimizing hybrid membrane-pressure swing adsorption processes for biogenic hydrogen recovery. *Chemical Engineering Journal* 2019;364:452–61. <https://doi.org/10.1016/j.cej.2019.01.136>.
- [6] Bounaceur R, Berger E, Pfister M, Ramirez Santos AA, Favre E. Rigorous variable permeability modelling and process simulation for the design of polymeric membrane gas separation units: MEMSIC simulation tool. *Journal of Membrane Science* 2017;523:77–91. <https://doi.org/10.1016/j.memsci.2016.09.011>.
- [7] Skarstrom CW. Method and apparatus for fractionating gaseous mixtures by adsorption. US2944627A, 1960.
- [8] Ahn S, You Y-W, Lee D-G, Kim K-H, Oh M, Lee C-H. Layered two- and four-bed PSA processes for H₂ recovery from coal gas. *Chemical Engineering Science* 2012;68:413–23. <https://doi.org/10.1016/j.ces.2011.09.053>.
- [9] Bird RB, Stewart WE, Lightfoot EN. *Transport phenomena*. second edition. 2007.